Synthesis and Study of Fluorescent Molecular Dyes

Thomas P. L. Winstanley

Doctor of Philosophy

School of Chemistry
Newcastle University

July 2013

Dedication

This thesis is dedicated to my parents who have supported me throughout my life and the not inconsiderable time that I have spent at Newcastle University.

Thank you Mum and Dad.

Abstract

Uses for fluorescent dyes are diverse and increasingly important with compounds having many uses in medicinal, chemical and physical fields - amongst others. The creation of new fluorescent dyes helps to push the boundaries of molecular photonics alongside the further study of the underlying principles involved in the systems. This thesis concentrates largely on the synthesis and characterisation aspects of novel fluorescent dyes, though the analysis of the resultant photophysical data also features prominently.

Chapter 1 is an introduction to fluorescence from some of the more basic principles involved in the field. A discussion and comparison of intrinsic and extrinsic fluorescent dyes is followed by a brief discussion of a series of examples of fluorescent molecular sensors. As bodipy dyes feature heavily throughout the thesis the second half of the introduction is focused solely on this topic. This half of the chapter centres around the synthetic approaches towards bodipy, modifications to the bodipy core and the resulting photophysics. Photo-induced electron transfer and fluorescence energy transfer is introduced from basic principles along with selected literature examples that demonstrate these processes in systems that incorporate bodipy.

Chapter 2 discusses the synthesis and photophysics of a new class of fluorescent dyes based on a highly substituted terephthalate core. The initial aim of the chapter was to create fluorescent systems based on a xanthene core, this was found to be non-fluorescent. As such attention was turned towards a terephthalate intermediate which demonstrated strong and highly red shifted fluorescence in solution, as well as solid state fluorescence.

A meso-perfluorinated phenyl ring causes a marked increase in fluorescence quantum yield, along with a pronounced red-shift, relative to the equivalent meso-phenyl variant. This observation lead to a series of F_n-aryl (n = 1,2,3,5) bodipy dyes being synthesised. **Chapter 3** subsequently investigates the relationship between the number and position of fluorine atoms on the aryl moiety, and the resultant photophysical measurements. High fluorescence quantum yields were observed with ortho-substitution of fluorine atoms, a trend that was mirrored with the fluorescence lifetime. Mono-ortho fluorine substitution

of the aryl group was also found to make the bodipy prochiral pathing the way towards axially chiral bodipy compounds.

Chapter 4 follows on from chapter 4 by taking prochiral bodipy compounds to there chiral conclusion. In this chapter several synthetic approaches towards axially chiral (AxC) bodipy compounds are discussed. Included in these synthetic approaches is a completely novel route towards asymmetric bodipy cores thus AxC-bodipy compounds. This chapter represents the first examples of AxC bodipy compounds to exist with future developments in the field aimed at enhanced fluorescence sensing in chiral media and facile enantiomeric determination via circularly-polarised fluorescence measurements.

Chapter 5 is an in-depth experimental section where the synthesis and characterisation of each compound is detailed. Also provided are the details for each chemical used, purification and drying methods for each solvent used and techniques used for proper characterisation of all of the compounds.

Acknoweldgements

I would firstly like to thank my two supervisors Prof. Andrew Benniston and Prof. Anthony Harriman who agreed to take me on as a PhD student.

Without the help, advice and friendship of the members of the Molecular Photonics Laboratory my time as a PhD student would have been both dull and much more difficult. I would particularly like to thank Dr. Ruth Ryan and Dr. Sophie Clift who have been and always will be amongst the best of my friends. Also all of the other group members over the years: Victoria, Vindhya, Songjie, Dan Bai, Xiaoyan, Rashid, Ion, Dima, Sylvia and Irena.

I was lucky to work at Newcastle University as there is a network of helpful, knowledgeable and friendly people. There are numerous people who should be thanked particularly Dr. Mike Hall who is a good friend and has been very generous with his time – always going out of his way to help me in any way that he can.

Dr. Corinne Wills and Prof. William MacFarlane deserve special praise as they constantly maintain the NMR suite. They are also always there to help plan and execute NMR experiments that are out of the ordinary.

Dr. Ross Harrington and Dr.Ulrich Baisch also derserve singling out too as between them they ran the crystallography suite hence all of my X-ray crystal structures.

Other work collegues include Reinner Lerrick, Dr. Lee Higham and Dr. Simon Doherty who have either worked along side me or advised me in one form or another during the past 4 years.

On occasion I have relied on external sources for measurements, as such I would like to thank Swansea Mass Spec department, Dr. Karen Haggerty, Prof. Helge Lemmetyinen and Prof. Nikolai V. Tkachenko.

Life is nothing without the friends around you, of whom I have plenty in Newcastle who have supported me and kept me going: Jonathan Pate, Manuel Arbelairas, Arne Ficks, Ricardo, Francesca, Maria Morcillo, Dave Molyneux, Nico Ward, Marta Omedes Pujol, Manuel Classic, Luke Dixon, Laura Davies, Jenny Wallis, James Flemming, Connor Sibbald, Pedro, Paul Middleton, James Watson, Lynsey Cotterill, Sam Bhatt, Janneke Bins, Matthais Kunz, Alex Davies, Steph D’Arcy, Andy Ross, Georgia Ross, Pete Hunt, Sukhi Johal,

Nichola Hellewell, Clare Recks, Hazzard Rose, Matthais Kunz, Rose Simnett, Miguel Angel Galindo, Steph Galindo, plus Ollie Galindo, and the other cohorts of people in Newcastle.

Finally I would like to thank my parents and family: Ellie, Ollie, Grandma Jess, Grandma Marie, Chris James, Dom Phoenix, Vanessa Bridge, Tom Gater and all my uncles, aunties and cousins. I would also like to pay a special mention to my grandfathers who sadly did not live to see me achieve my PhD. I hope that I continue to make them proud as they will always have had a defining influence in my life.

‘No problem can withstand the assault of sustained thinking.’

- ***Voltaire - French wit, writer and philosopher.***

(1694 – 1778)

List of publications

Mohammed A. H. Alamiry, Andrew C. Benniston, Jerry Hagon, Thomas P. L. Winstanley, Helge Lemmetyinen and Nikolai V. Tkachenko; ‘The Fluorine Effect: Photophysical Properties of Borondipyrromethene Dyes Appended at the Meso Position with Fluorinated Aryl Groups’; *RSC Advances*; **2012**, 2, 4944–4950

Andrew C. Benniston, Thomas P. L. Winstanley, Helge Lemmetyinen, Nikolai V. Tkachenko, Ross W. Harrington, and Corinne Wills; ‘Large Stokes Shift Fluorescent Dyes Based on a Highly Substituted Terephthalic Acid Core’; *Org. Lett.*; **2012**, Vol. 14, No. 6 1374–1377

Table of Contents

A	Acceptor
AA	Amino acid
Acr	Acrylate
Ar	Aryl
BBN	Borabicyclo[3.3.1]nonane
BINAP	2,2'-bis(diphenylphosphino)-1,1'-binaphthyl
BINOL	1,1'-Bi-2-naphthol
Bodipy	Boron Dipyrromethene
br	Broad
Calc.	Calculated
CD	Circular dichroism
COSY	Correlation spectroscopy
CPL	Circularly polarised luminescence
CV	Cyclic voltammogram
D	Donor
DBA	Dibenzylideneacetone
DBU	1,8-Diazabicycloundec-7-ene
DCM	Dichloromethane
DDQ	2,3-Dichloro-5,6-dicyano-1,4-benzoquinone
DFI	2,2-difluoro-1,3-dimethylimidazolidine
DFT	Density functional theory
DMF	N,N-Dimethylformamide
DMSO	Dimethylsulfoxide
D-PeT	Donor excited photo-induced electron transfer
E_A	Energy of activation
EDG	Electron donating group
Eq	Equivalents
EtOAc	Ethyl acetate
EWG	Electron withdrawing group
FC	Friedel-Crafts
Flu	Fluorescence
FRET	Förster resonance energy transfer
FTMS	Fourier-transform mass spectrum

HMBC	Heteronuclear multiple bond correlation
HMQC	Heteronuclear multiple-quantum correlation
HOMO	Highest occupied molecular orbital
HPLC	High-performance liquid chromatography
HSQC	Heteronuclear single quantum coherence
hv	wavelength of light
ICT	Intramolecular charge transfer
IR	Infrared
ISC	Inter-system corssing
K_{NR}	Rate of non-radiative radiation
KOAc	Potassium acetate
K_{RAD}	Rate of radiative radiation
LUMO	Lowest unoccupied molecular orbital
M^+	Positive molecular ion peak
MChx	Methyl cyclohexane
MP	Melting point
MS	Mass spectrum
NAPDH	Nicotinamide adenine dinucleotide phosphate (reduced)
NFSI	trimethyl(trifluoromethyl)silane and N-fluorobenzene-sulfonimide
nIR	Near infrared
NMR	Nuclear magnetic resonance
nUV	Near ultraviolet
PDT	Photo-dynamic therapy
PeT	Photo-induced electron transfer
PhBod	Meso-phenyl bodipy
ppm	Parts per million
RBF	Round bottomeed flask
RET	Resonance energy transfer
RF	Retention factor
RT	Room temperature
S.D.	Standard deviation
S_0	Ground state

S_1	Excited singlet state
SCE	Standard calomel electrode
SS	Stokes Shift
Terpy	Terpyridine
TFA	Trifluoroacetic acid
THF	Tetrahydrofuran
TLC	Thin layer chromatography
TOF-MS	Time-of-flight mass spectrometry
TPP	Meso-tetraphenylporphyrin
VT	Variable temperature
ε	Molar absorption coefficient
λabs	Wavelength of absorption
λem	Wavelength of emission
τ	Fluorescence lifetime
φ_F	Fluorescenece quantum yield

List of figures

Chapter 1

Chapter 2

Chapter 3

List of tables

Chapter 1

Chapter 2

Chapter 3

List of schemes

Chapter 1

Chapter 2

Chapter 1. Introduction

Two separate areas are discussed over three chapters within this thesis. The design and synthesis of large Stokes shift dyes based on a xanthene core is discussed in chapter 2. Though the original target compound of the overall synthesis was not as promising as first thought, some of the intermediate structures turned out to be much more interesting. Chapter 3 explores the effects of fluorine substitution on the spectroscopic properties of difluoroboradiaza-s-indacene (bodipy) compounds the results of which set up the following chapter. Chapter 4 demonstrates new methods to synthesise asymmetric bodipy compounds which in turn is employed to create the first examples of axially chiral bodipy compounds. Each chapter has a separate introduction in which the individual research area is discussed.

As bodipy compounds feature heavily throughout the thesis the introduction will be presented in two halves. The first of which deals with fluorescence from basic principles and the second of which provides a much more detailed overview into the chemistry of bodipy compounds.

1.1 Origins of luminescence

Luminescence is the emission of light from any compound and occurs in two forms: fluorescence and phosphorescence, which are determined by the nature of the excited state. For excited singlet states (for example S_1) the electron undergoes no change in its spin upon excitation. As a result there is a rapid spin-allowed de-excitation of the electron via the release of a photon – fluorescence, with lifetimes typically around 1 – 20 ns.

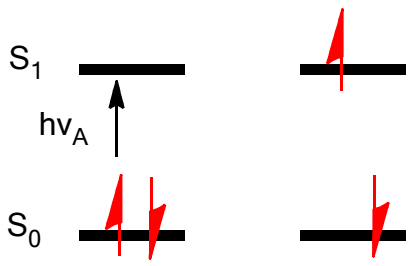

Figure 1 Excitation of a compound to the first excited singlet state. Where hv_A is the wavelength of light absorbed by the compound.

Phosphorescence on the other hand sees the S_1 electron, still in the excited singlet state, spin-flip to a separate excited state known as the triplet excited state (T_1). The transition of the electron back down to the ground state is much slower for phosphorescence as the process is spin forbidden (10^{-3}-10^{0} s^{-1}).

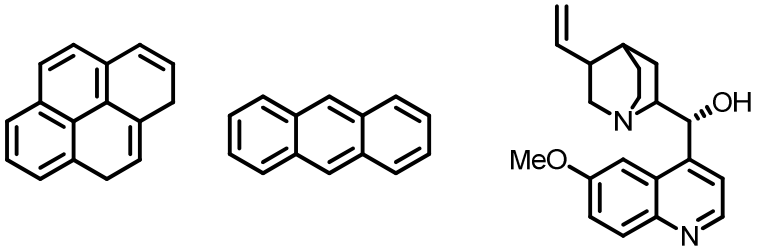

Figure 2 Fluorescent aromatic compounds: pyrene (left), anthracene (middle) and quinine (right).

Fluorescence is typically observed in molecules which exhibit some aromaticity such as pyrene, anthracene and quinine (Figure 2). Indeed quinine was first noted for its fluorescent properties as early as 1845 by Sir John Herschel.[1] Notable examples of compounds that contain no conjugation but exhibit fluorescence include cadmium selenide quantum dots and some lanthanide complexes.

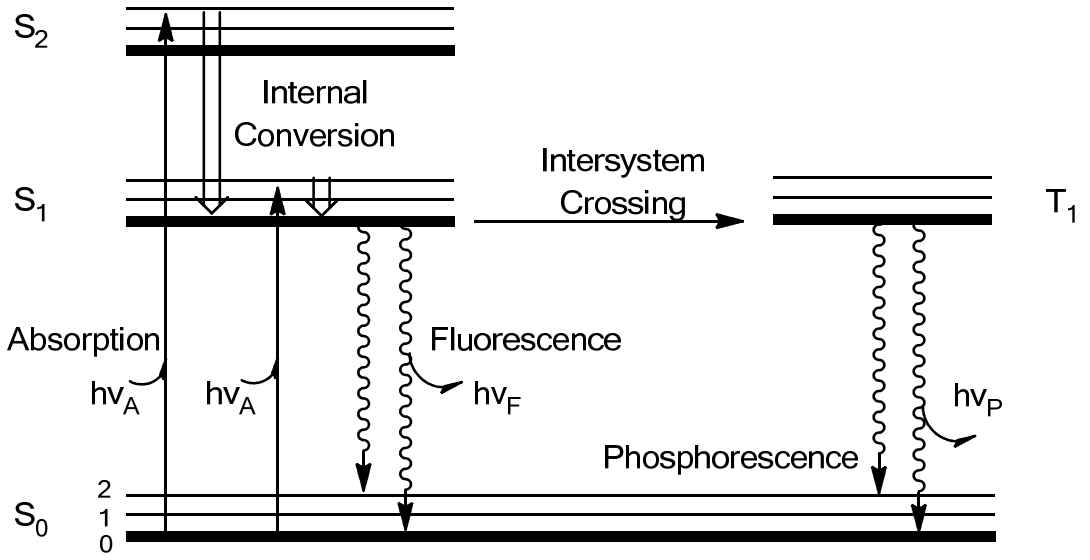

Figure 3 One form of a Jablonski Diagram; the transitions between states are depicted with straight lines, internal conversion by a thick arrow and radiative processes by a wavy arrow. S_N is the singlet energy level, T_1 the triplet excited state, while hv_F and hv_P represent fluorescence and phosphorescence respectively.

The Jablonski diagram (Figure 3) provides a good basic overview of the potential transitions within simple luminescent systems. Light energy is

absorbed by a compound in order to excite an electron into one of the singlet excited states from which point relaxation can occur*. The relaxation can either be radiative (luminescence) or non-radiative, or more usually a combination of the two, which finally results in the repopulation of the S_0 state.

1.2 Characteristics of fluorescence

Below are some characteristics commonly observed in fluorescent molecules as well as brief descriptions of the meaning or importance of these measurements.

1.2.1 Stokes Shift

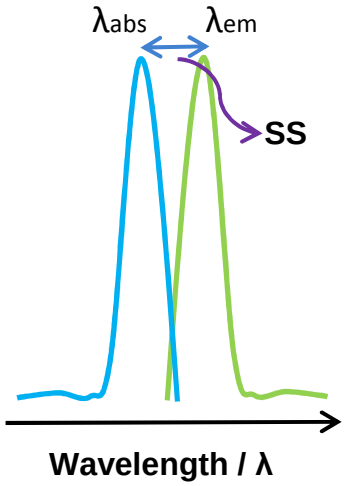

Figure 4 Absorption / emission diagram illustrating a red-shifted emission spectrum and denoting the SS.

In 1852 George Stokes published his paper showing the first recorded experiments revealing, what he modestly called, the Stokes shift.[2] All fluorescent compounds will exhibit a Stokes Shift (SS) to differing degrees. The SS is a measure of the difference in energy between the light absorbed by a compound and that which is emitted. There is commonly a bathochromic shift, equating to a loss of energy, upon emission of light which is commonly caused by the fast decay to the lowest vibrational energy level of the S_1 state. Fluorophores are commonly found to decay to higher vibrational levels of the S_0 thereby losing further energy due to the thermalisation of the excess vibrational energy. There other factors which can determine a SS for a system including: energy transfer and solvent effects.[3]

* NB - Due to the large difference between S_0 and S_1 thermal population of the excited singlet state is not feasible, hence light energy is always used as the route towards excitation.

1.2.2 Emission Spectral Independence of Excitation Wavelength

When a compound absorbs a wavelength of light of energy X and a different higher energy wavelength of energy 2X the observed emission wavelength does not typically differ.

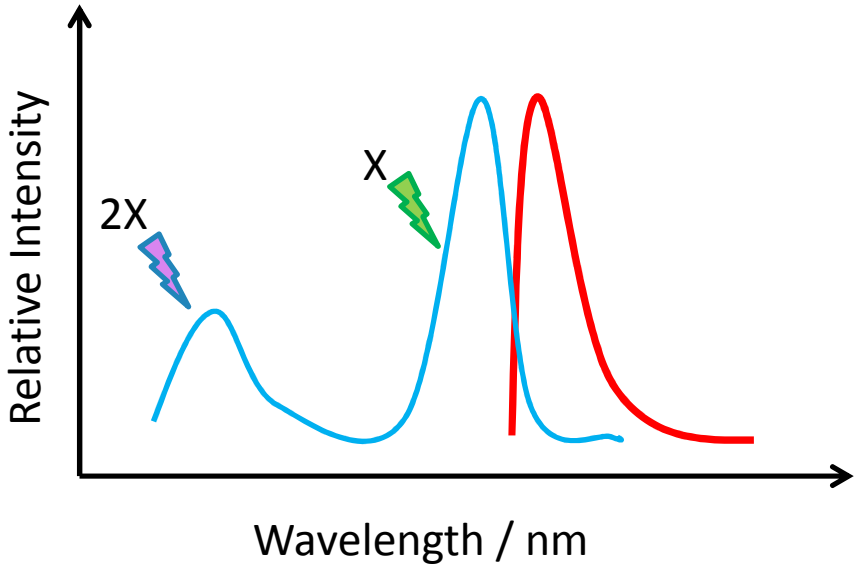

Figure 5 A depiction of Kasha's rule showing a generic absorption / emission spectra, with excitation wavelength 2X situated around the $S_0 – S_2$ absorbance and X situated around the $S_0 – S_1$ absorbance. In spite of differences in the energies of the two excitation wavelengths the observed fluorescence occurs solely from the $S_1 – S_0$ transition.[4]

It is found that upon initial excitation into higher electronic and vibrational levels, any excess energy is dissipated eventually resulting in the population of the S_1 excited state, which duly decays back down to the ground state. The quick relaxation to the S_1 state essentially means that the emission spectrum is independent of the excitation wavelength.

1.2.3 Fluorescence Quantum Yield and Lifetime

The quantum yield and lifetime for a fluorescent system are amongst two of the most important aspects of fluorophores. The quantum yield (Φ_F) is a measure of the efficiency of a fluorescent system, measuring the total number of photons emitted over the total number of photons absorbed. The maximum value of Φ_F is 1 whereby for each photon of light absorbed one is emitted – ideally when designing a molecule one would aim for the highest possible quantum efficiency. The Φ_F for a system relies heavily on the value of the non-radiative rate (k_{NR}) constant, with high k_{NR} values driving the overall Φ_F down.

$$\Phi_F = k_F / \Sigma_i k_i$$

Equation 1 The definition of fluorescence quantum yield in terms of the rates of excited state decay. Where Φ_F = quantum yield; k_F = rate of spontaneous emission of radiation and $\Sigma_i k_i$ = the sum of all types of excited state decay from S_1. $\Sigma_i k_i$ can also be thought of as ($k_F + k_{NR}$) where k_{NR} represents the rate constant for all non-radiative decay processes that occur for that particular system.

The excited state lifetime (τ) is a measure of the average amount of time that a compound remains in its S_1 excited state before returning to S_0. In Equation 2 the lifetime also takes into account the k_{NR} value, were k_{NR} not present for a system the lifetime would then be known as the intrinsic lifetime, which can be calculated by τ / Φ_F.

$$\tau = 1 / (k_F + k_{NR})$$

Equation 2 The excited state lifetime as calculated from the radiative and non-radiative rate constants, where τ = excited state (fluorescence) lifetime.

Both the Φ_F and τ are affected by changes in either the radiative or non-radiative rate constants. For example, a large k_{NR} due to fast rates of internal conversion, could render a compound as being non-fluorescent.

1.3 Fluorophores

The term fluorophore refers to any molecule that exhibits fluorescence. Fluorophores can generally be divided into two different classes: intrinsic (or natural) and extrinsic (typically synthetic). This thesis will be concentrating solely on extrinsic fluorophores, the PhD being mainly synthesis based, though intrinsic fluorophores should be further detailed so as to help create a distinction.

1.3.1 Intrinsic Fluorophores

There are many fluorescent compounds found in nature including aromatic amino acid (AA) residues, flavins and chlorophyll.

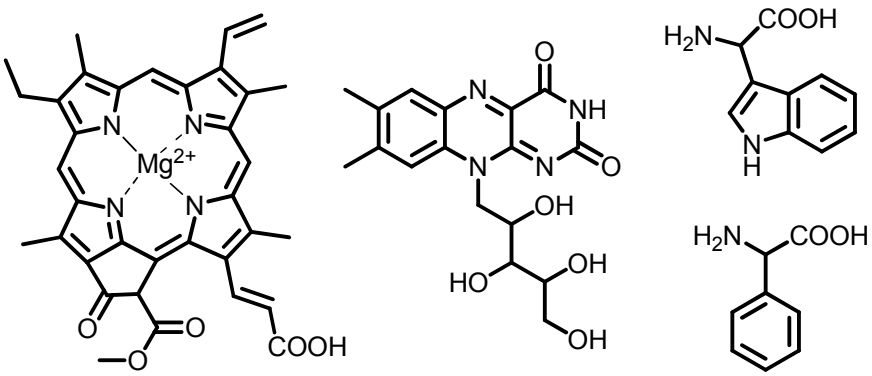

Figure 6 Some examples of intrinsic fluorophores: chlorophyll a (left), riboflavin / vitamin B_2 (centre), tryptophan (top, left), phenylalanine (bottom, left).

The dominant absorption characteristic for most simple intrinsic fluorophores is that they absorb in the UV region of the spectrum. This is typically due to the small amount of conjugation present in such systems. Indeed this is certainly the case with all AA's as shown in Table 1.

Throughout the bodies of animals there are various fluorescent protein compounds which when combined give rise to the phenomenon of auto-fluorescence which is problematic when using fluorescent sensors in vivo. The naturally occurring fluorophore emission can swamp any signal of standard sensing dyes (450 – 600 nm). To circumvent this problem several solutions have been explored for extrinsic dyes such as using dyes with emission in the near infra-red and large SS dyes (described in more detail in chapter 2).[5, 6]

Amino acid	λ_{Abs} / nm	λ_{Em} / nm	Φ_F
Phenylalanine	260	282	0.02
Tyrosine	275	304	0.14
Tryptophan	295	353	0.13

Table 1 Photophysical measurements of the fluorescent amino acids, showing absorption and emission wavelengths in the UV.[7]

1.3.2 Extrinsic Fluorophores

There are primarily three types of extrinsic dyes: nano-scale quantum dots, fluorescent polymers and fluorescent organic dyes.[8, 9] The bulk of the material within this thesis will be addressing the area of fluorescent organic dyes, as such this area is covered in much more detail than the topics of quantum dots and fluorescent polymers.

Organic dyes are molecules which typically have well-defined, wavelength-tunable structures, and are available in a wide range of colours. There are thousands of examples of synthetically designed fluorophores - many of which have been developed based on the make-up of intrinsic fluorescent compounds, and others designed from scratch.

An example of an intrinsic fluorophore which has been mimicked synthetically is that of porphyrin. Porphyrin is an important milestone in chemistry with uses in photodynamic therapy and light capture in dye sensitised solar cells. In nature there exist structures, such as haemoglobin and chlorophyll, which contain the same basic make up of a porphyrin. Indeed these two examples are perhaps amongst the most important molecules on the planet - providing life to plants and animals alike. Porphyrin compounds are comprised of four pyrrole molecules bound together at the 2 and 5 positions to form a macrocyclic polyaromatic system. The synthetic approach towards synthetic porphyrin compounds does differ from the various natural pathways. A typical porphyrin synthesis consists of four condensation reactions between four equivalents of pyrrole and four equivalents of an aldehyde. The benefit of the synthetic approach is that the starting materials are varied and plentiful thereby allowing a multitude of possible porphyrin analogues.[10-21]

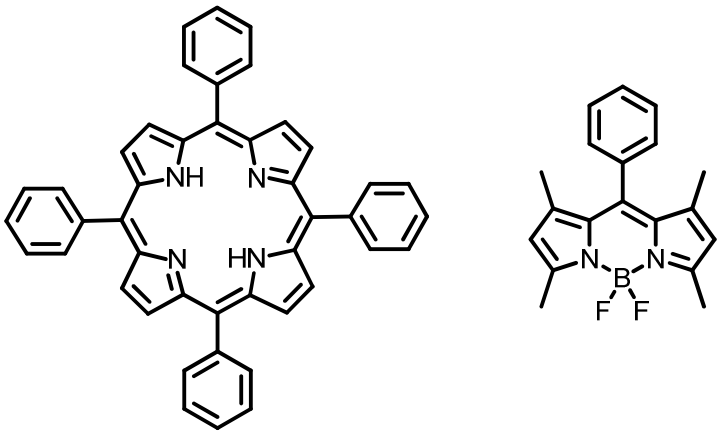

Figure 7 Two synthetic dyes: Meso-tetraphenylporphyrin (TPP, left) which is modelled on naturally occurring compounds, such as chlorophyll and haemoglobin, and 1,3,5,7-tetramethyl(meso-phenyl)bodipy (PhenBOD, right). The bodipy compound is essentially half of a porphyrin molecule with a chelating borondifluoride unit attached. Though the two compounds are related in structure the photophysical measurements of the two groups differ vastly.

The development of porphyrin chemistry lead to the development of other fluorescent dyes which shared similar structural properties with porphyrin, such as bodipy dyes.

	λ_{Abs} / nm[a]	λ_{Em} / nm[a]	Φ_F[a]
Chlorophyll a	666	687	0.32
TPP	417	649, 717	0.11
PhenBOD	503	515	0.71

Table 2 Photophysical measurements for chlorophyll, TPP and PhenBOD demonstrate that in spite of similarities within the structures of each compound the resulting properties are substantially different. [a] Measured in toluene.[22]

Bodipy is often referred to as the ‘little sister’ of porphyrin due to these structural similarities, however the photophysical aspects of bodipy compounds differ greatly from those seen for porphyrin. It is precisely due to the differing chemical and physical properties seen across all extrinsic fluorophores which makes the discovery of new fluorophores a major research goal.

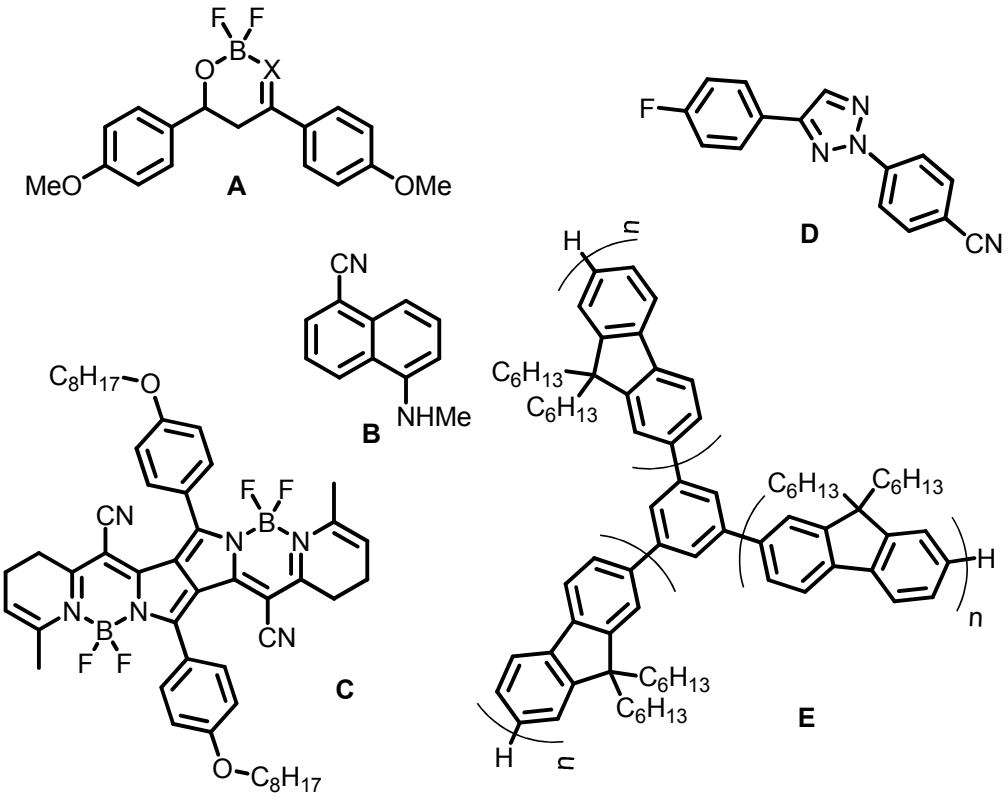

Figure 8 A selection of novel fluorophores that have been recently invented with a range of functions in mind. Where X = N, O and n = 1 – 4.[23-27]

It is possible to see from compounds **A** and **C**, in Figure 8, the influence of BF_2 chelation within newly designed fluorophores. Indeed this chelating motif currently seems to be *en vogue* and BF_2 chelation can be seen in many other novel classes of fluorophores. The presence of a BF_2 group within photonic systems typically brings around positive properties. Boron chelation is found to give rise to large molar extinction coefficients, high fluorescence quantum yields and enhanced photostability.[28, 29]

	λ_{Abs} / nm	λ_{Abs} / nm	Φ_F
A	408	429	0.91
B	346, 389	534	0.15
C	690	712	0.57
D	305	357	0.51
E	360	440	-

*Table 3 Photophysical measurements of the new dyes, that were outlined in Figure 8, show how newly emerging dyes are designed to cover various sections of the electromagnetic spectrum. **A**, **B** and **D** were measured in MeOH while **C** and **E** were measured in $CHCl_3$.*

1.3.3 Uses of Extrinsic Fluorophores

There can be a multitude of different uses for an extrinsic fluorophore depending on the fundamental properties which the compound possesses. Such uses as: lasers (Figure 8, **E**), light harvesting (Figure 7, right), medical applications i.e. PDT, imaging and sensing applications. The list of potential uses and examples for extrinsic is vast, hence only the area of sensing will be introduced as this bears the closest resemblance to the fields being discussed during this thesis.

Provided that a change occurs in an environment there is a good chance that a fluorophore can be employed as a sensor to detect such a change. The design of fluorescent sensors typically takes advantage of certain physical properties of a compound that might differ before and after the change of environment. Temperature, pressure, viscosity, solvent polarity, distance, viscoelasticity, cationic presence and chirality are just some of the parameters that can be detected using fluorescent sensors. In recent years even traces of explosives can be detected using fluorescent polymers.[30]

1.3.3.a Solvent Sensing

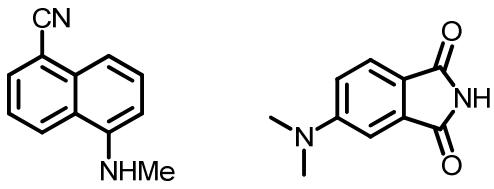

Figure 9 Two solvatochromic molecules which both work in a wide range of environments to accurately provide data of the polarity of solvent media.[25, 31]

Molecules of water within biological microenvironments help to control the structure, function, and dynamics of these biological systems in a unique manner. The use of solvatochromic probes has been a key asset in the exploration of these microenvironments.[32]

Solvatochromic probes are designed so that in differing polar media there is a shift in the emission spectra, which can also be accompanied by a drop in the fluorescence intensity. Solvent probes normally posses a significant dipole moment, indeed typically the larger the dipole moment the more sensitive the probe is to changes in solvent parameters.

The dipole moment of the fluorophore is affected by the differing polarities and properties that are exclusive to each individual solvent. If the dipole moment of S_1 is larger than the dipole moment of S_0 then the rearrangement of the surrounding solvent molecules can bring about a lowering of the energy of the S_1 state prior to the expected radiative decay to S_0. The effect of lowering the energy level of the S_1 is a red shifted emission spectrum, meaning that the polarity of a system can be quantified at a molecular level.[33]

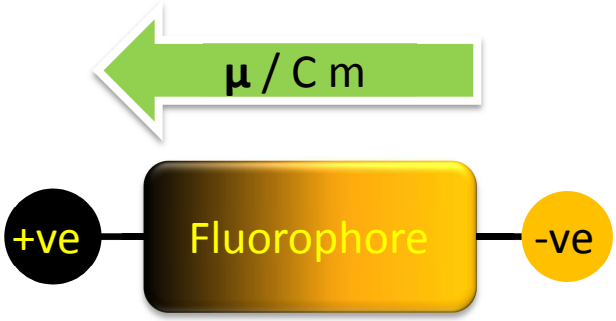

Figure 10 A graphic illustrating a 2D electronic dipole moment of a fluorophore where: +ve and –ve stand for functionalities which express that particular charge (i.e. –ve = NO_2 and +ve = OMe), μ = dipole moment, C m = Coulomb meters unit of measurement.

The two molecules shown in Figure 9 are two examples of solvatochromic probes. Each one possess a large dipole moment across the molecule bought about by the presence of an electron donor and an electronegative functionality being present at opposite sides of the compound. Both systems show a considerable red-shifted emission over 100 nm and around a 70 fold increase in their fluorescence quantum yield when moving from solvents with a high polarity, such as water, to solvents with relatively low polar character such as 1,4-dioxane.[34-37]

1.3.3.b Sensing of Metal Cations and Protons

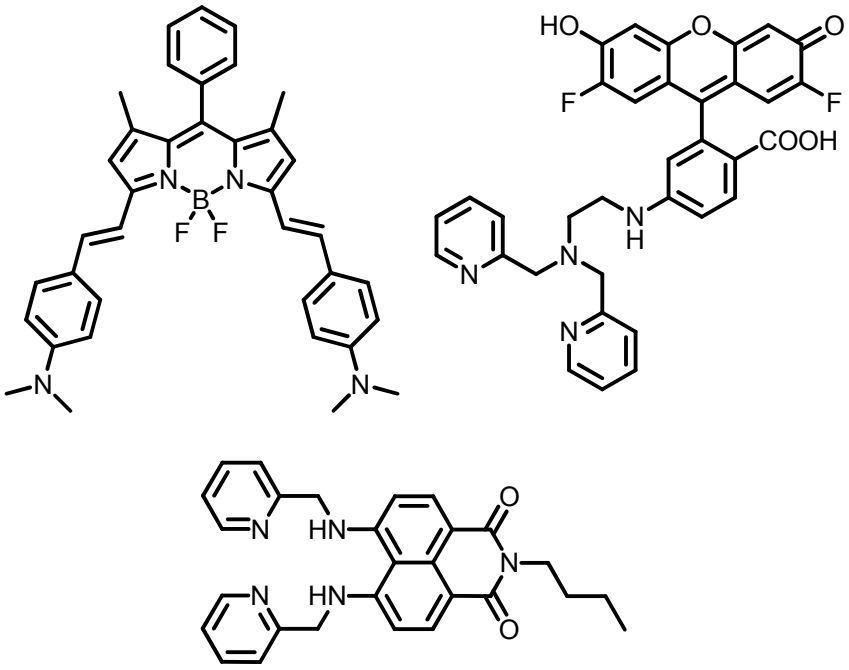

Figure 11 Several probes designed to detect cationic species: protons [pH] (top left), zinc(II) (top right) and copper(II) (bottom).[38-40]

There are several ways of detecting the presence of cationic species, however the main two methods involve the quenching of intramolecular charge transfer (ICT) or photo-induced electron transfer quenching.

The bodipy species shown in Figure 11 is designed to detect protons using the quenching of an ICT state. Protonation of the dimethylaminophenyl groups causes them to become far less effective electron donors than the un-protonated form. With the protonation of the dimethylaminophenyl moieties there is an accompanying hypsochromic shift of both the absorption and emission spectra. It is noted that the absorption and emission spectra of the protonated form resemble that of a distryl-bodipy species – revealing the extent of the effects of protonation at the amino section.

The sensing of metal cations has many different applications whether it be tracing their presence within bodies or monitoring levels of pollution. When detecting metal cations a number of other parameters must be taken into account notably the size and composition of the metal ion.

While protons can be sensed using monodentate ligands metal ions typically require chelating groups in order to better aid detection. As such it is easy to

identify metal ion sensors as they mostly contain poly-dentate moieties, often macrocyclic in nature.

The ratiometric N-butyl-4,5-di[(pyridin-2-ylmethyl)amino]-1,8-naphthalimide sensor (Figure 11, bottom) once again relies upon a ICT quenching mechanism to reveal the cation, in this case copper(II). The observed fluorescence for this particular example increases upon metal binding which is something that is rarely seen in ICT cation sensors with precious few examples in existence for copper(II) systems.[41-45]

The fluorescein based sensor (top right, Figure 11) is designed to detect zinc(II) ions. Note that the metal binding site for this compound differs significantly when compared with the N-butyl-4,5-di[(pyridin-2-ylmethyl)amino]-1,8-naphthalimide above. Here we see the use of a tri-dentate N-methyl-1-(pyridin-2-yl)-N-(pyridin-2-ylmethyl)amino group used, which is a typical trap used for zinc(II) binding. With this example a different method of detecting cationic species is seen, with the used of PeT quenching. The free ligand is almost totally non-fluorescent due to photo-induced electron transfer. Upon metal binding the mechanism by which the quenching occurs is lifted and the Φ_F increases dramatically. The increase in Φ_F is measured allowing for the detection of any zinc(II) ions present.

1.3.3.c Viscosity Probes

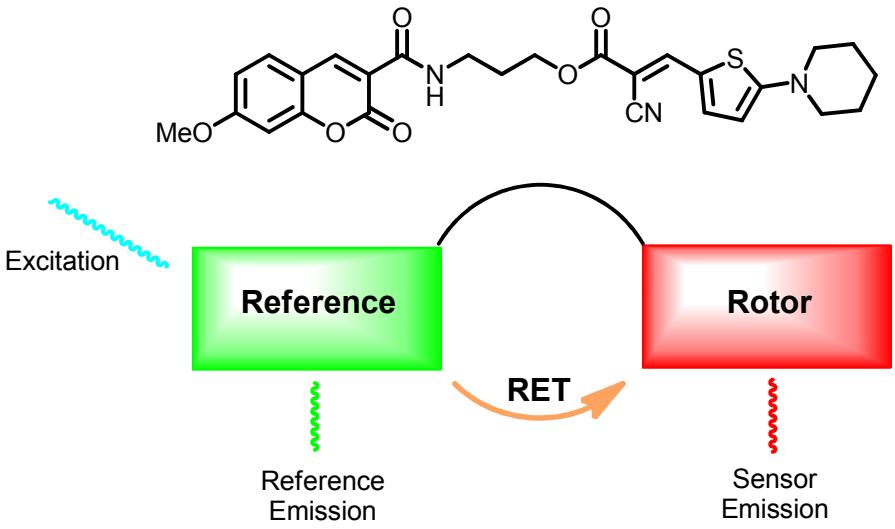

Figure 12 A self-calibrating viscosity probe in which a coumarin has been covalently linked with a molecular rotor (Top). A graphic illustration of the basic functionalities contained within the molecule also showing possible sources of emission.[46]

Measurements of viscosity have applications mainly based in, but not limited to, medicinal applications. Changes to viscosity within the cytoplasm and membranes of cellular environments can point towards a state of disease within that cell, with examples including: cell malignancy, Alzheimer's and diabetes.[47-52] The development of fluorescent viscosity sensors is largely driven by the large sample sizes required for the alternative techniques.[53]

The concept behind the designs of most viscosity probes is typically based around the use of a molecular rotor. Molecular rotors are devices that normally consist of two sections of a compound that freely rotate about a central axis. These sections are large enough for collisions with the surrounding media to interfere with the free rotation. The molecular systems are such that the rate or freedom of rotation has a direct correlation with the quantity of fluorescence observed. With previous examples of sensors the design features a compound with one section that signals where something exists. Yet in the case of viscosity a frame of reference needs to be established in order to accurately measure the environment. For a functional probe the problem of calibration needs to be addressed though dyes exist, dyes such as the series recently designed by Theodorakis *et al*.

Theodorakis developed a dual dye viscosity probe that included a molecular rotor and an internal reference fluorophore (Figure 12). The second viscosity independent dye gives a constant emission against which the fluorescence measurements of the rotor dye can be checked. The ratio of the rotor and reference emissions serves as the internal calibration emission.

The wavelength of light used in for this compound is around 355 nm which would excite only the reference (donor) dye. If the system were placed in a solution with a low viscosity and excited then the sole observable emission wavelength should be that of the donor. There is also a constant flow of energy from the coumarin reference dye to the rotor (acceptor) via resonance energy transfer (RET). The RET has the effect of exciting the rotor, though depending on the viscosity the emission may not be visible. Increasing the fluorescence has the effect of impeding the rotary movement, which in this case would lead to an increase in observable fluorescence from the acceptor.[54-56]

As bodipy compounds feature heavily throughout this thesis, half of the introductory chapter is dedicated to this topic in order to better illustrate the importance of this particular dye.

Boron dipyrromethene dyes, or bodipy for short, have been subjected to an intense development over recent years.[57] This development is because bodipy has inherently desirable fundamental properties such as high fluorescence quantum yield (Φ_{Flu} usually ca. 0.6), high molar extinction coefficients (usually >70,000 M^{-1} cm^{-1}), low inter-system crossing to the triplet excited state, bodipy is robust both chemically, thermally and photo-chemically - in a wide range of solvents, sharp absorption and emission maxima, as well as the ability to easily manipulate the chromophore via synthetic modification.[58, 59]

1.4 Discovery and Structure.

In the late 1960's Alfred Triebs and co-workers first synthesised bodipy when following on from work aimed at complexing dipyrromethenes with transition metals.[60] The group noticed that, during their attempts to synthesise acylated pyrroles, a highly fluorescent compound was created. After further investigation they discovered that the fluorescent product occurred due to a boron chelation to the acid-catalysed condensation product of two pyrroles (Scheme 1).

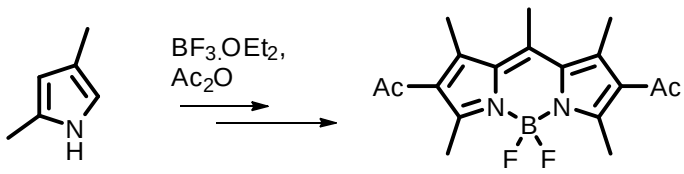

Scheme 1 The original synthetic route used to synthesise bodipy by Triebs et al.

Most bodipy molecules are based on a common 4,4-difluoro-4-bora-3a,4a-diaza-*s*-indacene core with the acronym bodipy arises from the compound class –BOron DIPYrromethene.

1.5 Synthetic Approaches to Bodipy Molecules.

The synthesis of bodipy molecules has not changed too much since its initial discovery by Treibs and co-workers. Bodipy is typically made in a 'one-pot' synthesis, via the condensation reaction of two pyrroles with either an aldehyde, acid chloride, or acid anhydride in the presence of a catalytic quantity of

acid.This condensation reaction yields an intermediate dipyrromethane compound which, in the case of aldehydes, is then oxidised to a ‘dipyrrin core’, typically using DDQ or other mild oxidants. If an acid chloride is used the dipyrrin core is formed without the need of an oxidation step.

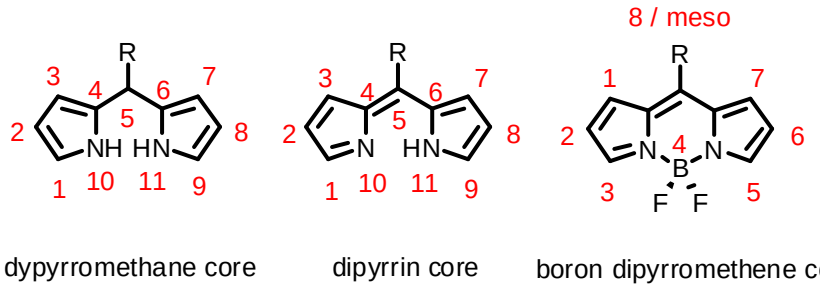

Figure 13 Numbering scheme for bodipy and the intermediate structures. The numbering scheme of bodipy highlights the areas where of the core where further substitution can take place.

Upon formation of the dypyrrin core the addition of excess base followed by a source of BF_2 ($BF_3.OEt_2$) leads to the deprotonation of the dipyrrin and chelation of the BF_2 unit to give bodipy.

Typical yields for the ‘one-pot’ synthesis of bodipy range from 15 to 30% however with the isolation and purification of each intermediate the yields obtained can be quantitative. Furthermore due to the wide array of aldehydes, acid chlorides, acid anhydrides and pyrroles available the range of bodipy molecules available is vast.

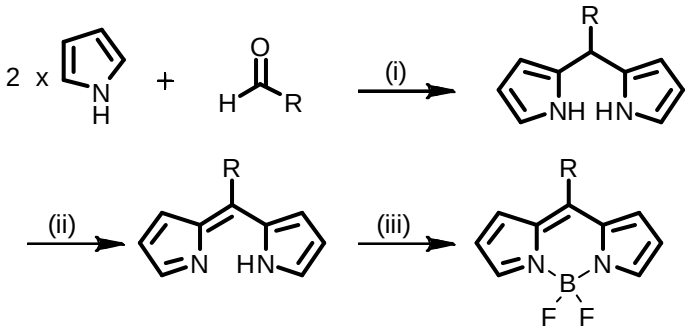

Scheme 2 The typical modern ‘one-pot’ synthesis of bodipy compounds using pyrrole and an aldehyde starting material. (i) DCM, TFA; (ii) DDQ; (iii) $^{i}Pr_2NEt$, $BF_3.OEt_2$

Synthesis of bodipy molecules is also possible using a pyrrole with an aldehyde substituent plus one equivalent of a second pyrrole. This allows for the creation of unsymmetrical bodipy molecules, though does not allow for flexibility with

regards to substitution at the meso carbon, which in this case must always be a proton.

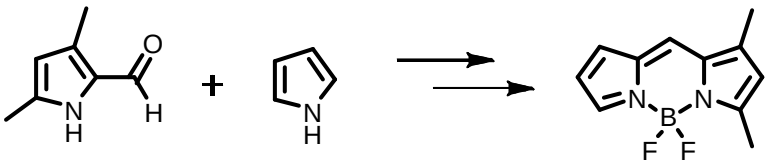

Scheme 3 One of many possible routes towards asymmetric bodipy cores, in this example the aldehyde functionality can be found pre-connected to one of the two equivalents of pyrrole.

In 2008 Burgess *et al* discovered a synthesis of bodipy which does not rely on the addition of a second equivalent of pyrrole.[61] As with the synthesis of the unsymmetrical bodipy (Scheme 3), Burgess' synthesis involves the use of a pyrrole-2-carbaldehyde. This pyrrole is then treated with $POCl_3$ which forms a dipyrromethenium cation with a dichlorophosphate counterion. This intermediate can be transformed to the equivalent bodipy with the addition of excess base and $BF_3.OEt_2$ (Scheme 4).

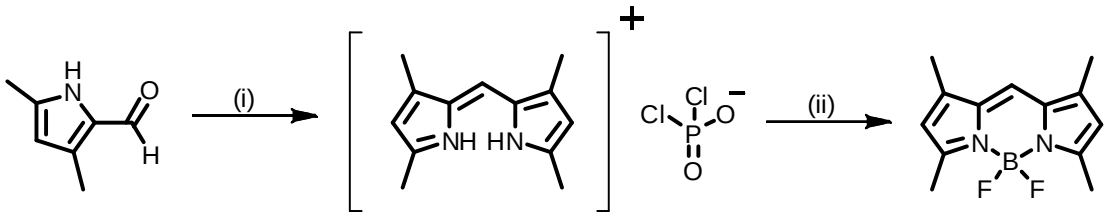

Scheme 4 Burgess' synthesis of bodipy using $POCl_3$. (i) $POCl_3$, DCM; (ii) Et_3N, $BF_3.OEt_2$. Percentage yield = 92%.

As with the synthesis of the unsymmetrical bodipy the $POCl_3$ route does not allow for functionality at the meso-position of the bodipy. The Burgess synthesis also requires the presence of an aldehyde moiety on the pyrrole which limits the possible starting materials. Percentage yields for the Burgess synthesis do vary depending on the starting pyrrole, however for more simple starting materials the yields are very high.

The structural flexibility enabled by the various synthetic approaches allows for the chromophore of the bodipy molecule to be tuned to absorb and emit in specific regions of the spectrum from near UV (nUV) to near IR (nIR) emitters.[62, 63]

Near UV emitter

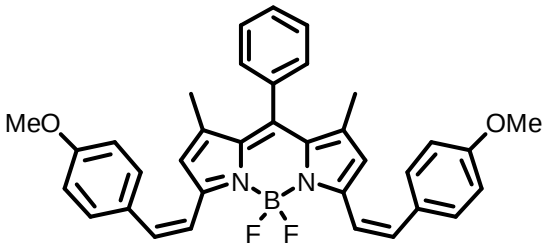

Near IR emitter

Figure 14 Two bodipy compounds with absorption and emission at the two extremes of the visible light spectrum (nUV) λ_{Abs} – 399 nm, λ_{em} – 444 nm; compound (nIR) λ_{Abs} (S_0 – S_1) 640 nm, λ_{em} – 655 nm.

1.6 **Aza-bodipy**

Changing the meso carbon in the bodipy fluorophore for a nitrogen atom leads to a new class of derivatives called the aza-bodipys. Azadipyrromethene was first discovered in the 1940's but it was not until 1993 when boron was chelated to the azadipyrromethene that azabodipy came into being. [64-66]

There are two recognised synthetic routes towards these compounds both of which begin with a chalcone which can be treated with either nitromethane and a base, or a source of cyanide and a base.

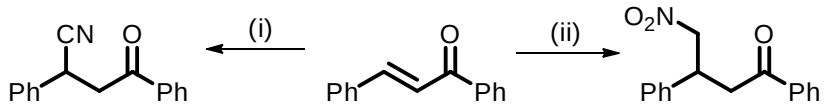

Scheme 5 The two synthetic routes of aza-bodipy starting materials from a chalcone. (i) CN^-, base; (ii) $MeNO_2$, base.

Both intermediates can then be reacted with ammonium acetate, or similar sources of nitrogen, to form intermediate pyrroles. These intermediate pyrroles themselves react with another molar equivalent of pyrrole to form the desired azadipyrromethene product. If this reaction is performed in an alcohol, typically ^{t}BuOH, then the azadipyrromethene intermediate precipitates out of solution and can be filtered, collected and taken to the next synthetic step without the need for further purification. The azadipyrromethene can then undergo the boron chelation reaction similar to that seen for the bodipy compounds.

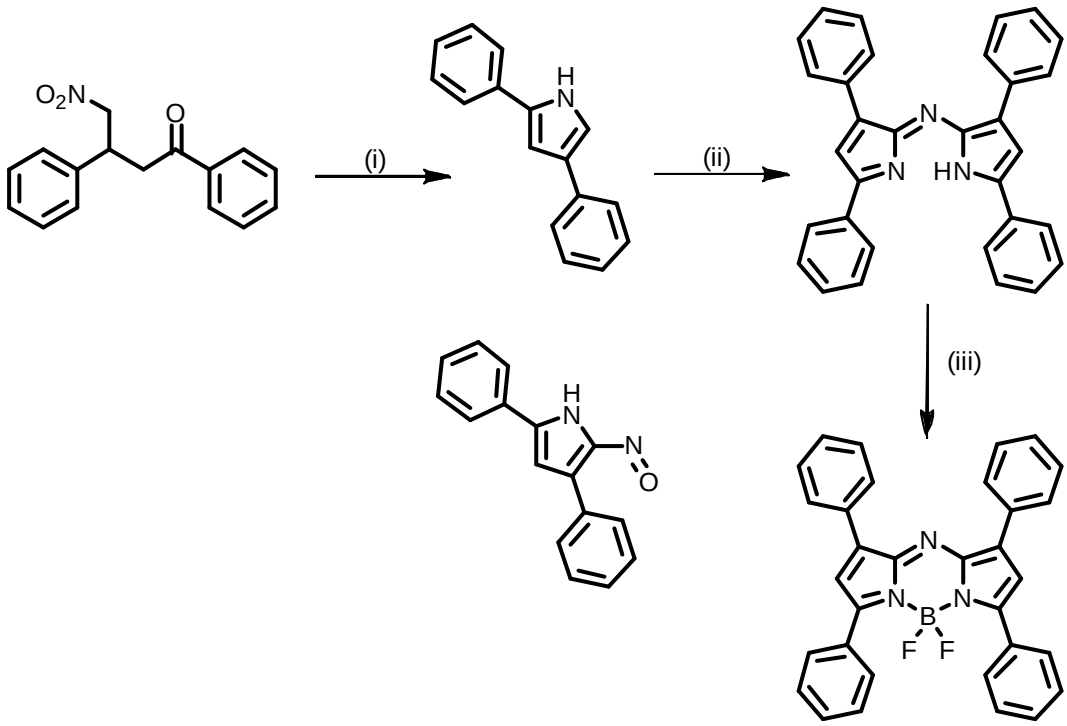

Scheme 6 Synthesis of aza-bodipy molecules from the 5-nitrosopyrroles. (i) NH_4OAc, ^tBuOH; (ii) H^+; (iii) $BF_3.OEt_2$, base.

As the azabodipy compounds have to incorporate a lot of aromaticity into their structure it is no surprise that they are heavily red-shifted, with the absorption and emission maxima often exceeding 650 nm.[67] The exact wavelength strongly depends on the nature of the aryl groups attached. While *para*-electron donating groups attached to the 5-aryl ring cause red-shift as well as increasing the molar absorption coefficient, para-electron donating groups attached to the 3-aryl ring have a more subtle red-shift.

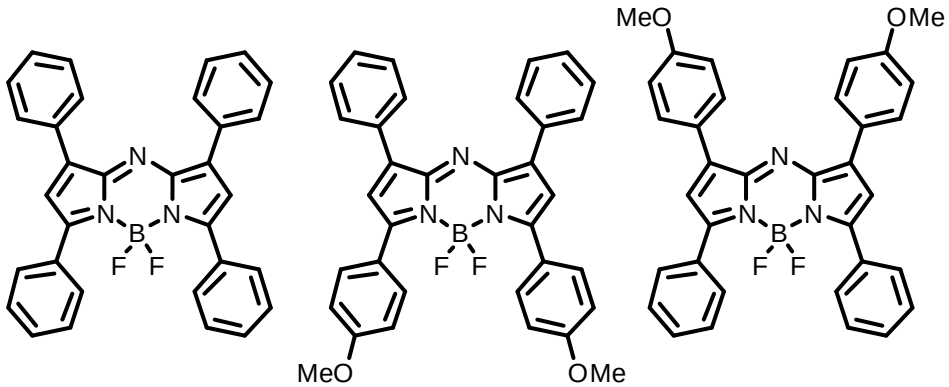

Figure 15 A selection of azabodipy compounds with differing absorption and emission wavelengths due to the composition of the substituent groups attached to the core. (left) λ_{Abs} – 650 nm, λ_{em} – 672 nm; (middle) λ_{Abs} 688 nm, λ_{em} – 715 nm. (right) λ_{Abs} – 664 nm, λ_{em} – 695 nm.[68]

The quantum yield of fluorescence (Φ_F) for aza-bodipy molecules does vary, with typical values lying around Φ_F = 0.3 in chloroform. The compounds do have very large molar absorption coefficients, much higher than those seen for the N-substituted porphyrin systems.

The combination of the large absorption coefficient combined with the NIR absorption and make aza-bodipy compounds ideal candidates as either photosensitizers or fluorescent probes within cells. Azabodipy compounds are also more resistant to photo-bleaching than the meso-carbon bodipy analogues, which allows for them to be continuously irradiated when inside a cell without appreciable degredation. This allows for 'video' footage of dye aggregation within cells to be monitored with a high degree of detail.[69]

1.7 **Modification of Bodipy.**

Many of the properties of bodipy molecules can be altered due to substitution at different regions of the bodipy. There are three main sections which are typically available to change on a basic bodipy unit: the dipyrromethene core, boron centre, and meso substituent. Substitution at these positions cause very different effects, even if similar groups are introduced.

1.7.1 ***Modification of the Dipyrromethene Core.***

1.7.1.a *Switching the Pyrroles*

There are two possible routes used to create differences at the core of the bodipy molecule. The first of these is by simple exchange of the pyrroles used to create the compound, for example using 2,4-dimethylpyrrole instead of pyrrole. The resulting bodipy compound would have four additional methyl groups present on the bodipy core. While the inclusion of four methyl groups might not seem too important it has a dramatic effect on the photochemistry observed - with increasing aliphatic groups present on the dipyrromethene core typically causing a substantial red shift (Figure 16).[70] With modifications to the starting pyrroles it is possible to begin to choose the region of absorption and emission of the desired compound.

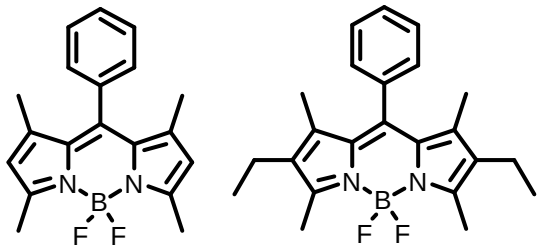

Figure 16 Bodipy compounds created with different pyrrole starting materials. The difference in the core though modest does cause some significant changes in the photophysics of the two compounds: (left) λ_{abs} 500 nm, λ_{em} 510 nm); (right) λ_{abs} 524 nm, λ_{em} 537 nm – both compounds were measured in cyclohexane.

A bathochromic shift is observed in most bodipy systems that have extended conjugation stemming from the pyrrole backbone.[71] The use of halide-substituted pyrroles, which in turn are subject to cross-coupling reactions, give rise to aryl-substituted bodipy compounds, these bodipy compounds typically show an enchanced red-shift for both absorption and emission. This red-shifted absorption allows for bodipy molecules to be used and monitored in vivo as the shift moves the absorption and emission maxima away from the autofluorescence naturally encountered in cells. As a result bodipy compounds have potential applications in medical fluorescence imaging, or as photosensitizers.[72]

The starting pyrroles can also be modified to introduce further functionalisation to bodipy systems. An example of this can be found in the work done by O'Shea *et al.*, where aryl substituents were used which themselves have existing functional groups attached (Scheme 7). In this example the further functionalisation provided by the methoxy substituents in the presence of BBr_3 form O-B bonds, which gives rise to a tetra-chelating bodipy complex. The increased structural rigidity causes a large increase in the fluorescence quantum yield due to a diminished non-radiative rate constant.[73]

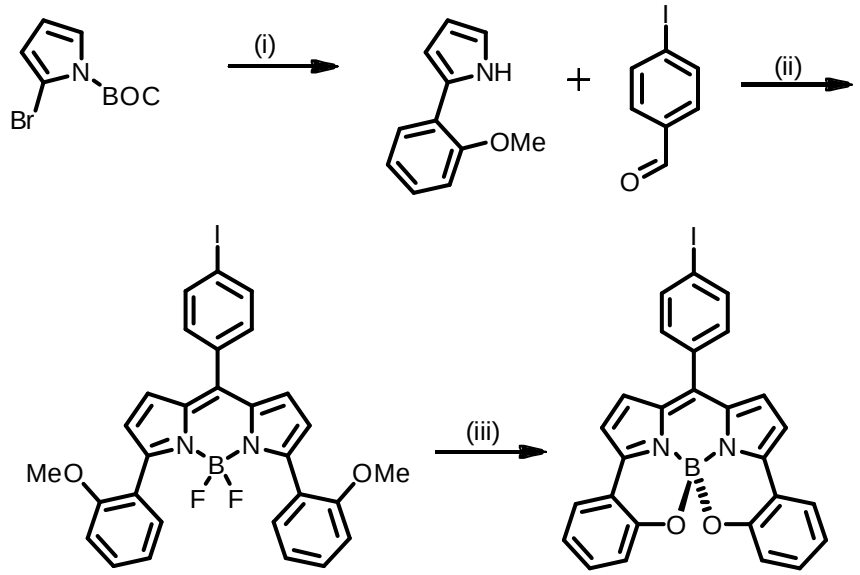

Scheme 7 Modification of starting pyrrole via Suzuki cross-couping to give a bodipy which can be reacted further by a cyclisation of the two methoxy substituents to the boron of the core. (i) 2-MeOPhB(OH)$_2$, Na_2CO_3, 10% $Pd(PPh_3)_4$, toluene, 80^{o}C; NaOMe, MeOH, THF; (ii)TFA, DCM; DDQ; $^iPr_2NEt$, $BF_3.OEt_2$; (iii) BBr_3. Bodipy 1: λ_{abs} 545 nm, λ_{em} 598 nm, ϕ_f 0.08; Bodipy 2: λ_{abs} 500 nm, λ_{em} 510 nm, ϕ_f 0.41.[74, 75]

1.7.1.b *Direct Modification of the Dipyrrin Core.*

The second route available to change the core of the bodipy is modification of the bodipy core directly, which is perhaps the most dynamic route available to alter the properties of the compound. Thanks to its robust nature bodipy can survive many harsh reaction conditions, hence can easily be functionalised. Typical functionalisations include the Knoevenagel condensation reaction - which gives an expansion of the conjugation, bromination - allowing for cross-coupling reactions, direct palladium-mediated functionalisations, oxidations, nitrations, sulfonations and chlorination of the dipyrromethane intermediate.[76-79] Provided the bodipy core survives the reaction intact it is possible to perform most common reactions. Direct modification of the bodipy core does carry many advantages when compared with modifying the starting pyrroles, yet convergent synthesis - using pre-modified pyrroles, is preferable due to the relatively low yielding bodipy reaction.

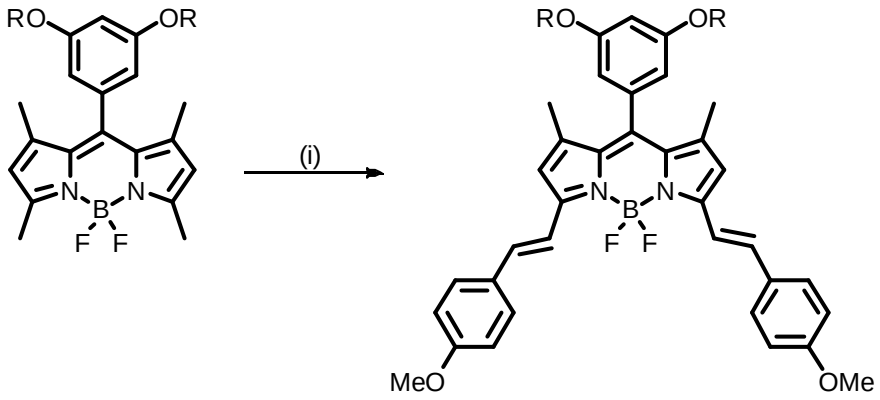

Scheme 8 Knoevenagel reaction at the 3,5 position of the bodipy. (i) p-anisaldehyde, AcOH / piperidine, benzene, reflux with Dean-Stark apparatus.[80]

The hydrogens on the 3 and 5 carbons are acidic enough to subject to a condensation reaction between the bodipy and an aromatic aldehyde.

The Knoevenagel reaction provides a simple route to extend the conjugation present within a bodipy system without subjecting the bodipy to harsh conditions, or the use of expensive catalysts. It is also possible to introduce some functionality that allows for the styryl derivatives to be used in sensing applications.[81] Strangely the quantum yield is not affected by the introduction of the styryl groups. It would be expected for longer chains to increase the non-radiative rate constant, however quantum yields are observed which do not seem to follow a defined trend.

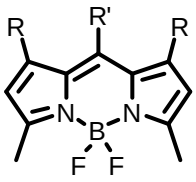

1, 2

1 & 3 - R = H, R' = Ph
2 & 4 - R = Me, R' = C_6F_5

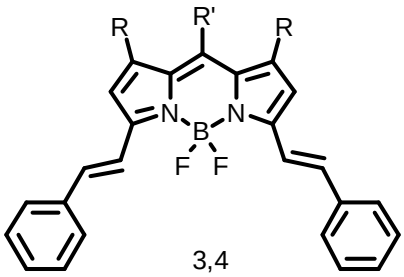

3,4

Compound	MeCN	Hexane	THF	DCM
1	0.17	0.29	0.25	-
2	-	-	-	0.99
3	0.84	0.70	0.83	-
4	-	-	-	0.60

Figure 17 Comparison of the quantum yields of fluorescence for styryl substituted bodipy versus non-substituted.[82-84]

Figure 17 shows ϕ_{Flu} for two different sets of bodipy compounds. Comparisons of ϕ_{Flu} for both sets shows that there is no obvious link between the inclusion of extended conjugation and ϕ_{Flu}. Compound **4** shows a drop in ϕ_{Flu}, relative to compound **2**, which would be expected when adding steric bulk at the 3a nd 5 positions. Whereas compounds **1** and **3** show the exact opposite.

1.7.1.c *Palladium Cross Coupling Reactions at the Bodipy Core.*

Palladium catalysed reactions are one of the cornerstones of modern day chemistry with the 2010 Nobel Prize being awarded to three of the fathers of this particular field: Heck, Negeshi and Suzuki. As such it should not come as a surprise that the desire to expand bodipy chromophores in ever more imaginative directions has lead to the widespread use of cross-coupling reactions during syntheses.

In order for these reactions to work the bodipy compounds need the correct functionality, which often leads to the need for: chlorination, bromination, and iodination of the bodipy compound.

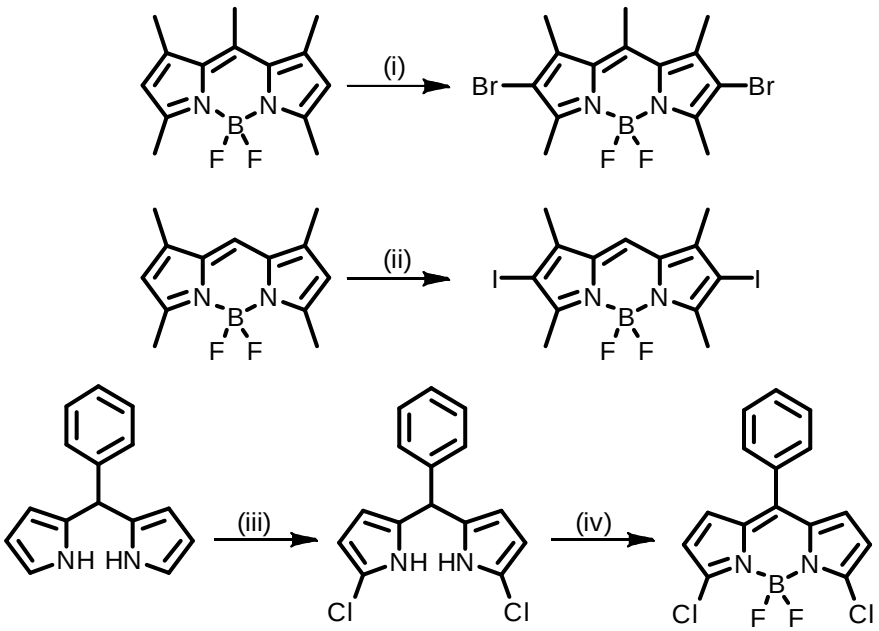

Scheme 9 Synthetic routes to halogenated bodipy compounds, which is typically are required step before the bodipy undergoes a palladium cross-coupling reaction. (i) Br_2, DCM; (ii) I_2, HIO_3, H_2O, EtOH, Δ; (iii) NCS, THF, -78°C; (iv) p-chloranil, $BF_3.OEt_2$, Et_3N.[72, 85]

While bromination and iodination of bodipy is usually fairly straightforward the chlorination is more complex. To prepare chlorine substituted bodipy compounds the chlorination step must take place before the bodipy is formed. This can be done either by chlorinating the dipyrromethane intermediate, for which you have to isolate the intermediate, alternatively you can chlorinate the starting pyrrole – which also allows for unsymmetrical bodipy molecules.[86]

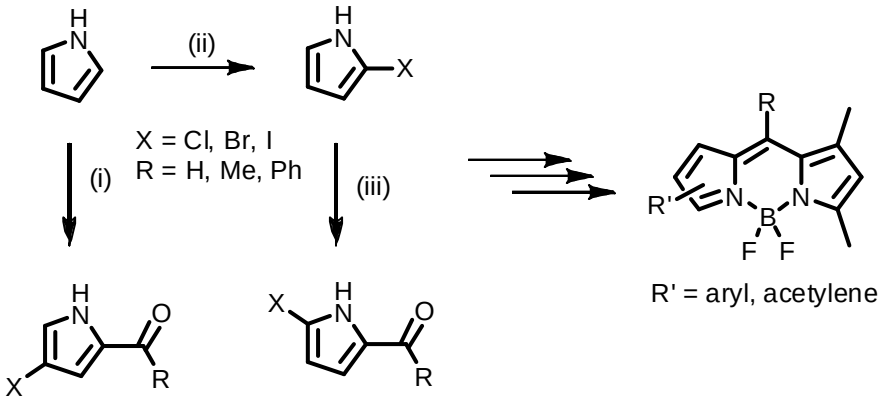

Scheme 10 A versatile monofunctionalisation of pyrroles leading to unsymmetrical bodipys. (i) Toluene, Δ, pyrrolidine, Cl_2, NaOH; (ii) NXS, THF – where X = Cl, Br, I i.e. NBS – 'one-pot' reaction with the next step; (iii) Acylating agent – prepared via a Vilsmeier reaction beforehand.[87]

Once the bodipy has been halogenated, or alternatively has appropriate functionalisation such as terminal-alkyne, boronic acids etc, cross-coupling reactions can be undertaken.

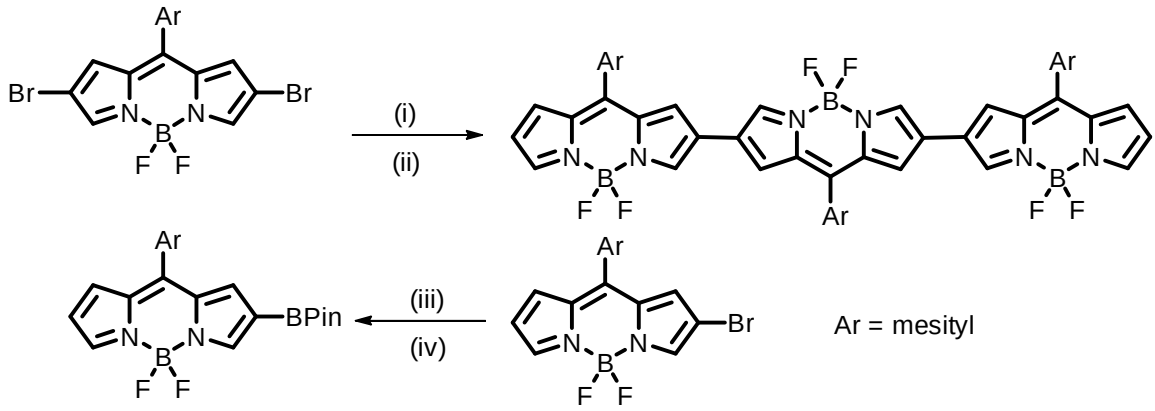

Scheme 11 Suzuki-Miyaura reactions on an bodipy with an α-unsubstituted pyrrin core. (i) $Pd_2(dba)_3$, $CHCl_3$, $^tBu_3P$, HBF_4; (ii) $CsCO_3$, THF, H_2O; (iii) $Pd_2(dba)_3$, $CHCl_3$, X-Phos, B_2Pin_2 (iv) KOAc, dioxane, Δ.

The resulting products typically have extended conjugation and give dispersed fluorescence emission maxima. The ability to select mono- and di-substituted compounds also aids the ability to tune the bodipy emission.[88, 89] As described in Scheme 11 it is also now possible to perform cross coupling reactions on α-unsubstituted bodipy thanks to the ability to regioselectively halogenate the starting material.[90]

1.7.2 ***Modification of Bodipy at the Boron Centre***

The next aspect of the bodipy which can be manipulated is the boron centre. The BF_2 can either be modified directly, or alternatively a pre-modified boron unit can be introduced.

1.7.2.a *Alteration of the BF_2 Unit via the Introduction of Aryl Substituents*

Substitution of one or more of the BF_2 fluorines allows for expansion of the chromophore via inclusion of aryl groups, the addition of functional moieties, or chelation to alkoxide.

Though there are limits to the reactions which can take place at the boron centre as it is susceptible to substitution of the core fluorine atoms under particularly harsh conditions.[91, 92]

Aryl groups can be introduced to the boron centre via the use of aryl-Grignard reagents in ether. It is possible to selectively mono-substitute at the boron centre by performing the reaction at a low temperature, typically 0^{o}C.[93] The same reaction can also be performed at room temperature to give the equivalent di-substituted bodipy. Alternatively the use of aryl-lithium reagents can give the di-substituted bodipy – though thermal control cannot be exercised as the reaction is too fast.

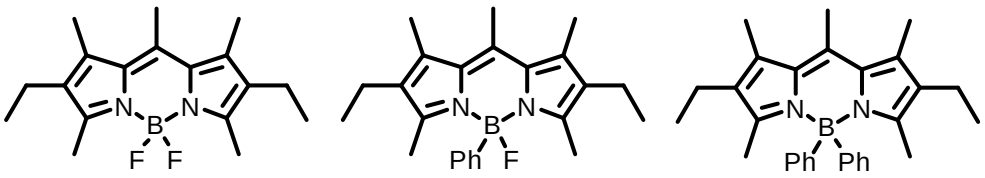

Figure 18 Absorption, emission and fluorescence quantum yield values for bodipy compounds with increasing aryl substitution at the boron centre:(left) - λ_{abs} 517 nm, λ_{em} 538 nm, ϕ_f – 0.83, (centre) - λ_{abs} 524 nm, λ_{em} 543 nm, ϕ_f – 0.90, (right)- λ_{abs} 513 nm, λ_{em} 548 nm, ϕ_f – 0.91.

As with the Knoevenagel condensation at the methyl groups on the bodipy core, expansion of the conjugation at the boron centre typically leads to a red-shifted emission, though effects on the absorption vary as seen in Figure 18. While the substitution of one phenyl ring onto the boron causes a moderate red-shift for both absorption and emission, the di-substituted boron centre sees no shift in the absorption but instead a larger Stokes shift.

In terms of the scale of the redshift the effects of the expansion of the chormaphore off the boron centre are not as pronounced as similar expansions off the bodipy core (Figure 19). Whereas the red-shift resulting from aryl-substituted boron is around 7 nm for the mono-substituted compound, the red-shift seen from direct covalent linkage between core and aryl group is often >40 nm.[94] Calculations performed on bodipy compounds routinely show a lack of HOMO character on the boron centre, which could explain the limited red-shift upon arylation of the boron core.

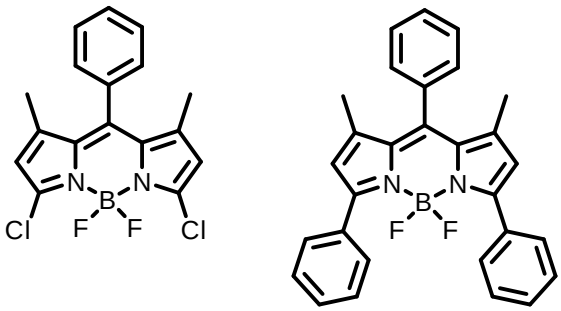

Figure 19 Chlorinated bodipy (left) - λ_{abs} 508 nm, λ_{em} 519 nm, ϕ_f – 0.27; 3,5-diphenyl bodipy (right) - λ_{abs} 547 nm, λ_{em} 582 nm, ϕ_f – 0.21.

The newly substituted aryl groups can be selected to absorb at higher energy wavelengths than bodipy compounds typically would. This wavelength depends on the absorption profile of the aryl group which is being introduced. This can be advantageous in energy transfer cassettes (discussed later) as it can provide a route to link together multiple chromophores.

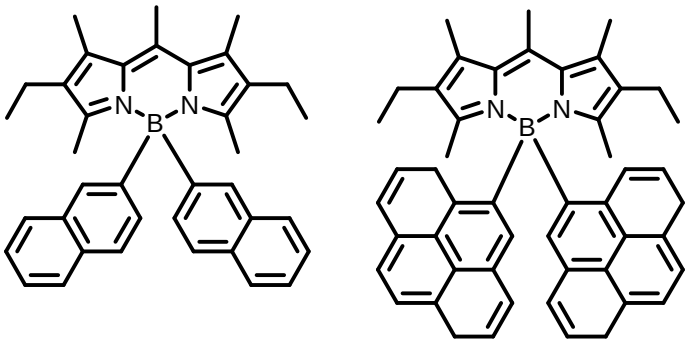

Figure 20 Substitution of different aryl-groups onto the boron centre of the bodipy. Di-napthyl bodipy – $\lambda_{abs\text{-}aryl}$ 270 – 305 nm; di-anthracene bodipy – $\lambda_{abs\text{-}aryl}$ 230 – 317 nm.

1.7.2.b *Alteration of the BF_2 Unit via the Introduction of Alkyl Substituents*

The addition of alkyl groups to the bodipy core can be achieved using the same route as for the addition of aryl groups. Grignard reagents can be used to either mono or di-alkylate the boron centre thus replacing one or both fluorine atoms.

The introduction of alkyl groups is also possible via a different approach. This route does not rely on the substitution of the BF_2 fluorines, instead the dipyrromethane is isolated and treated with the appropriate dialkylborane compound. This approach is limited by the availability of the starting material, though the complexation step can result in much better yields, compared with the fluorine substitution (between 30% and 90%) and hence is a more cost-efficient method to produce alkyl bodipy compounds.[95]

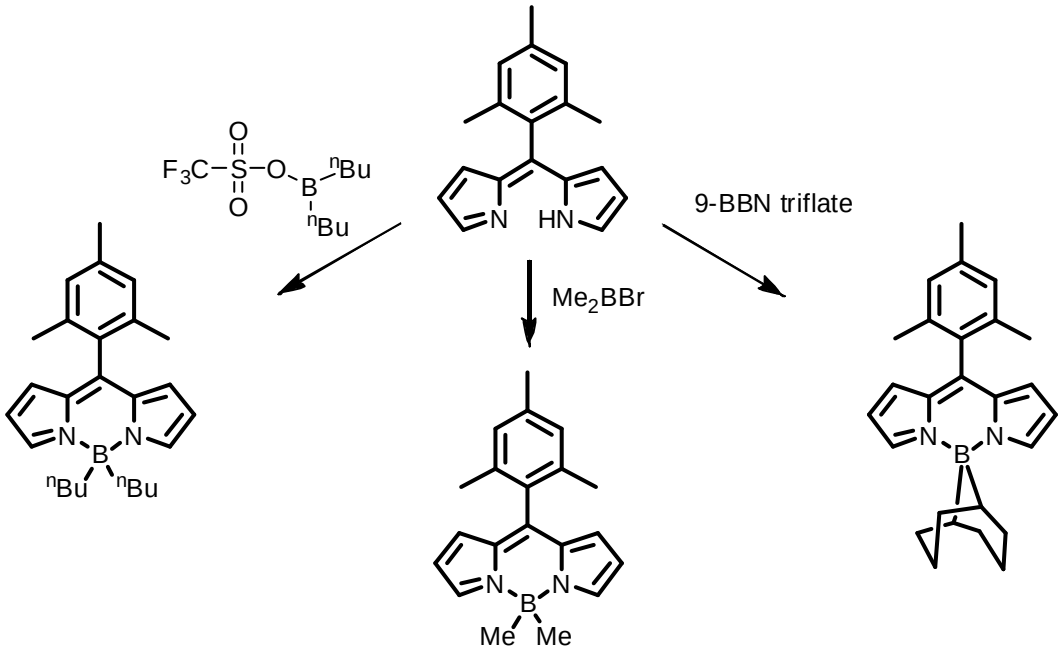

Scheme 12 Complexation of alkyl-boranes to dipyrrin to form bodipy compounds with a pre-substituted boron centre.

A trend is observed whereby increasing the steric bulk of the alkyl chains attached to the boron cause a decrease in the quantum yield of the system. This decrease is most likely due to an increase in the rate of non-radiative decay caused by an increase in flexibility within the fluorophore.

1.7.2.c *Alteration of the BF_2 Unit via the Introduction of Alkoxyl Substituents*

Addition of alkoxy moieties to the boron centre has been achieved in two different synthetic manners. The first alkoxy-boron compound to be synthesised (Scheme 13) involved the treatment of a bodipy with sodium methoxide in methanol and gives both the mono and di-substituted 4-methoxysubstituted bodipy in good yields. The longer that the reaction is refluxed the more of the di-substituted product is formed giving some control over the final product.[96]

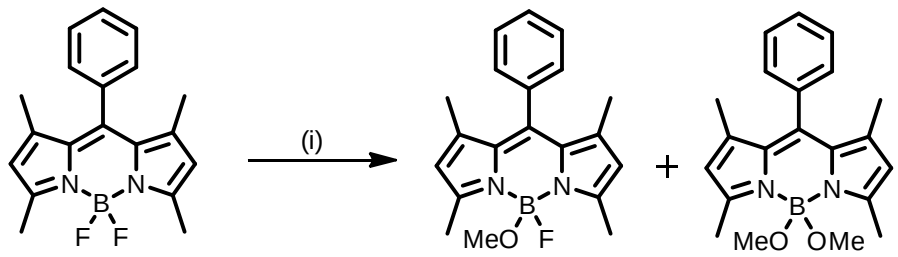

Scheme 13 Substitution of F for OMe on a bodipy boron centre. (i) NaOMe, MeOH, reflux.

The photophysical properties of the alkoxy-bodipy compounds, both mono and di-substituted, are almost identical to that of the starting bodipy compound. The

only difference between the two is the solubility in water, which is increased for the alkoxy-bodipy compounds.

It is also possible to substitute alkoxy groups into the boron centre using the lewis acid $AlCl_3$. It is thought that the $AlCl_3$ activates the B-F bonds, hence facilitating the nucleophilic-substitution of the fluorine atoms with the alcohols. Unlike the previous example it is not possible to attain the mono-substituted product, instead the di-substituted product is isolated exclusively.

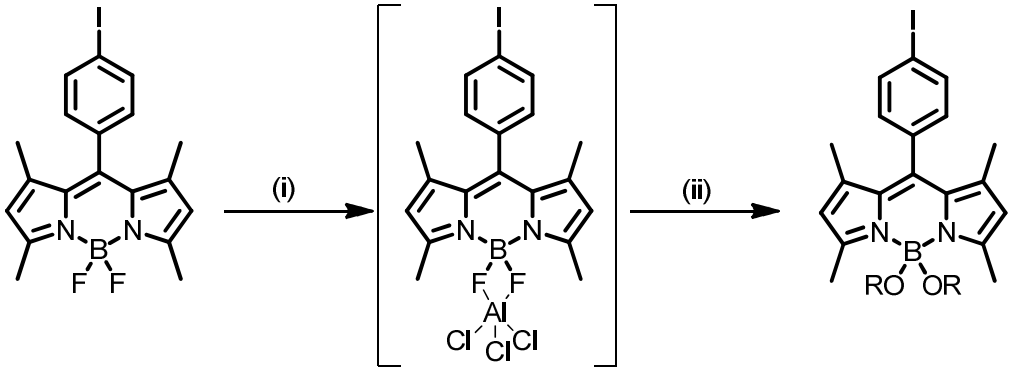

Scheme 14 The proposed intermediate structure when bodipy is reacted with $AlCl_3$. (i) $AlCl_3$ or $GaCl_3$, DCM; (ii) ROH.

The use of chelating alcohols such as bisnapthol or 1,2-dihydroxybenzene has been probed using the above synthesis as well as the substitution of aryloxy compounds. The chelating and aryloxy alcohols do lead to significant changes to the photophysics of the resulting bodipy, unlike the alkoxy-bodipy compounds.

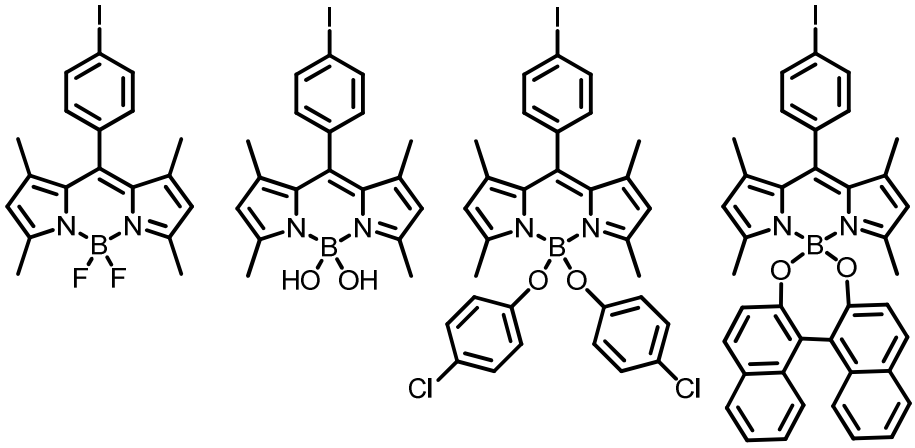

Figure 21 Photophysical measurements of a fluorine substituted bodipy compound (left) vs equivalent hydroxyl/aryloxy-bodipy substituted compounds. Di-fluoro bodipy - λ_{abs} 504 nm, λ_{em} 516 nm, ϕ_f – 0.002, Di-hydroxy bodipy - λ_{abs} 504 nm, λ_{em} 517 nm, ϕ_f – 0.54, Di-(p-chlorophenyl) bodipy - λ_{abs} 506 nm, λ_{em} 520 nm, ϕ_f – 0.065, Di-BINOL bodipy - λ_{abs} 506 nm, λ_{em} 516 nm, ϕ_f – 0.002.[97]

Whereas hydroxyl groups groups cause little changes to the photophysics, monodentate and bidentate-aryloxy cause a large drop in the fluorescence quantum yield as well as modest bathochromic shifts in the absorption and emission spectra. One interesting difference from this trend is found when 4-nitrophenol is introduced onto the boron. In this instance an increased quantum yield (ϕ_{Flu} – 0.71) and lifetime (τ - 4.1 ns vs 3.1 ns for the diflouro-iodophenyl bodipy shown in Figure 21).

One other route towards substitution at the boron centre which is worth mentioning is depicted in Scheme 7. The 3,5-orthomethoxyphenyl substituted bodipy core can be treated with BBr_3, which causes the cyclisation of the bodipy core to the aryl substituents via a demethylation reaction. The photophysical changes bought about by this transformation are stark with the fully cyclised product showing a much higher quantum yield compared with the starting material, as well as a heavily red-shifted absorption and emission spectra.

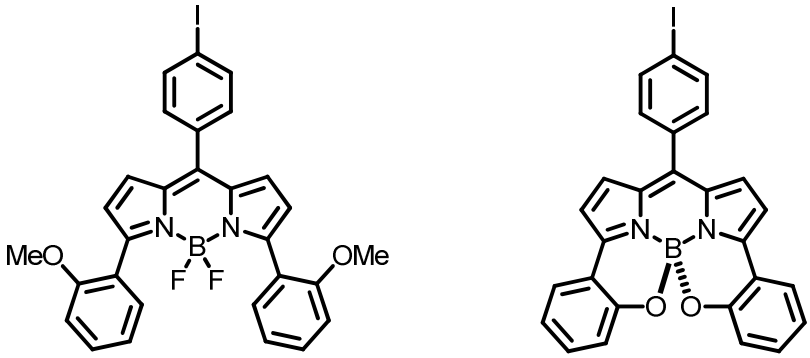

Figure 22 Cyclisation of the 3,5-methoxy aryl substituents onto a boron centre. (left) - λ_{abs} 550 nm, λ_{em} 597 nm, ϕ_f – 0.07, (right) - λ_{abs} 630 nm, λ_{em} 654 nm, ϕ_f – 0.41.

The cyclised product shows a bathochromic shift of 57 nm from the original bodipy, most probably due to the phenyl substituents being rigidly constrained closer to planarity with the dipyrromethene core – thus effectively extending the conjugation. The cyclised product also demonstrates a pronounced increase in fluorescence quantum yield as the aryl substituents can no longer dissipate energy by spinning. Interestingly the resulting cyclised bodipy compound exhibits helical chirality, something which until now has not been further examined within this system or those which are similar.

1.7.2.d *Arriving at Aryl, Alkys and Aryloxy Bodipy Compounds via Cl-Bodipy.*

A new class of bodipy compounds, Cl-bodipy, has recently been published by Thompson *et al.* which provides a high yielding intermediate capable of facile boron substitution by using BCl_3 to form the bodipy core.[98] The creation of this intermediate allows for a more facile approach to the three previously discussed classes of boron substituted bodipy compounds, with the chlorine atoms much easier to displace than their fluorine counterparts.

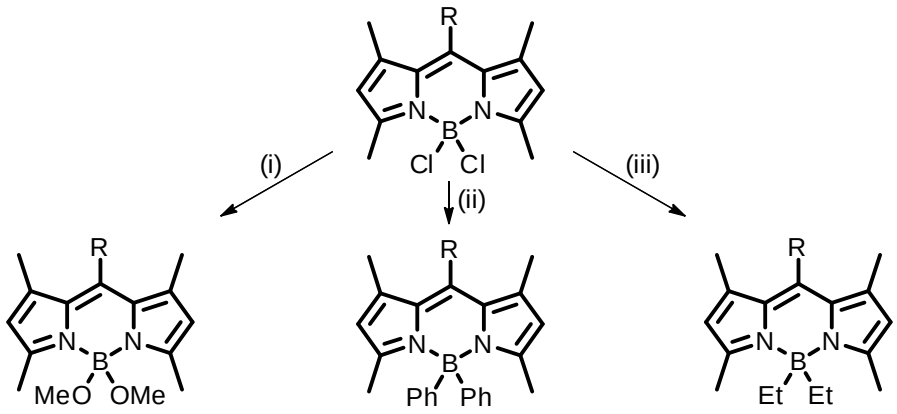

Scheme 15 Cl-bodipy allows access to alkoxy-, aryl- and alkyl-bodipy compounds. (i) NaOMe, MeOH; (ii) PhLi, THF; (iii) EtMgBr, Et_2O.

1.7.3 ***Functionalisation Off the Meso Carbon.***

One final part of bodipy, which can be exploited in order to further allow for a higher diversity of products is via functionalization of the meso carbon. As with the dipyrromethene core much of the functionalisation at the meso position can be introduced in the starting materials, in this case the aldehyde / acid chloride instead of the pyrroles.

Thanks to the decades of research into porphyrin systems the synthesis of dipyrrin ligands is well known.[99-101] Since dipyrromethene is, to all intents and purposes, half of a porphyrin, most of the chemistry which was applicable to porphyrins can also be used on bodipy compounds.

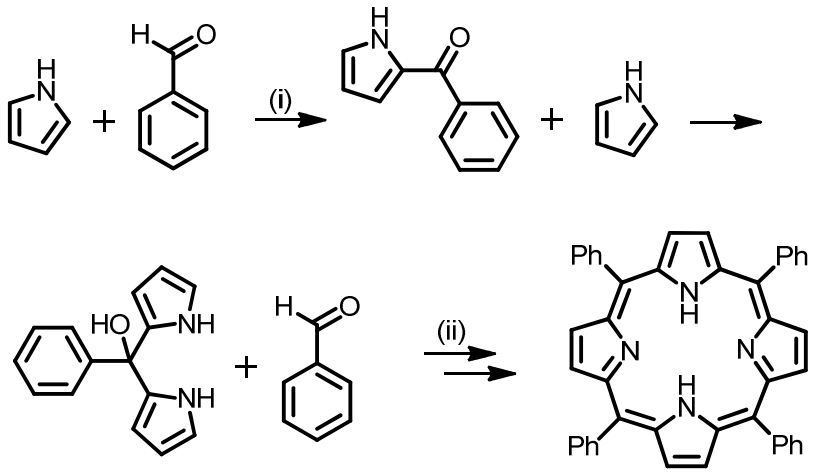

Scheme 16 Synthesis of porphyrin compounds, highlighting the similarity between porphyrin and bodipy syntheses. (i) H^+, (ii) DDQ.

As mentioned earlier the synthesis of bodipy compounds occurs via a condensation reaction between an aldehyde or acid chloride and two equivalents of pyrrole. One of the main advantages of this method, as it pertains to the aldehyde / acid chloride moiety, is the sheer quantity of available starting materials. Furthermore, as with the dipyrrin core, there is also the possibility to further functionalise the meso substituent after the bodipy synthesis – as such the meso group is commonly used as a synthetic handle towards more complex compounds.

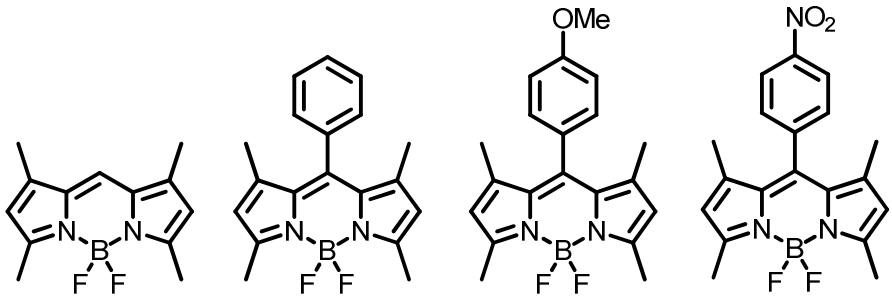

Figure 23 Effects of electronic changes on aromatic meso substituents. Unsubstituted bodipy (far left) - λ_{abs} 503 nm, λ_{em} 516 nm, ϕ_f – 0.80, Stokes shift – 13 nm. Phenyl bodipy (middle left) - λ_{abs} 500 nm, λ_{em} 520 nm, ϕ_f – 0.36, Stokes shift – 20 nm. Methoxy bodipy (middle right) - λ_{abs} 500 nm, λ_{em} 519 nm, ϕ_f – 0.38, Stokes shift – 19 nm. Nitro bodipy (far right) - λ_{abs} 500 nm, λ_{em} 527 nm, ϕ_f – 0.01, Stokes shift – 27 nm. All compounds were measured in DCM.

Unfunctionalised aryl and alkyl meso-substituents tend not to have a large impact upon the photophysical properties of the bodipy fluorophore. (Figure 23).[102, 103] The introduction of aryl meso-groups typically results in an increased Stokes shift, due to slightly red-shifted emission, and a drop in quantum yield - due to an increase in k_{NR}. The red-shifted emission results firstly from the

increase in conjugation present and can also be altered by the electronic contribution from the substituents present on the phenyl ring. While ‘neutral’ and electron withdrawing groups cause a bathochromic shift, electron donating groups can cause the opposite effect.[104]

It is also possible to add halogenated-alkyl groups into the meso position which in turn allows for functionality to be substituted on the chromophore at a later time.

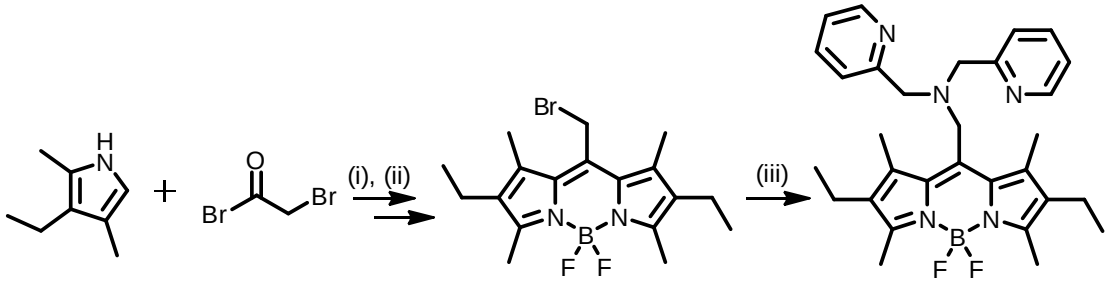

Scheme 17 Synthesis of a zinc sensor via the introduction of a meso-(bis[pyridine-2-ylmethyl]amine) . (i) DCM, TFA; (ii) Et_3N, $BF_3.OEt_2$; (iii) THF, bis(pyridin-2-ylmethyl)amine, Δ.

The product formed from the above reaction between bromo-acetylbromide and 2,4-dimethyl-3-ethylpyrrole is a detector for zinc ions, and is one of many examples of meso-substituted bodipy compounds being used as PeT fluorescence sensors.[105]

1.8 **The use of functional bodipy compounds**

Due to the vast flexibility of bodipy synthesis there are a plethora of potential applications available such as: energy transfer cassettes, fluorescence labelling, nIR emitters, laser dyes, sensors, sensitisers in solar cells, and as support structures for reactive intermediates.[73, 82, 93, 106-115]

1.8.1 ***Photo-induced Electron Transfer***

A large area of research interest in bodipy chemistry involves the evolution of sensors to detect: changes in pH, metal ions, dangerous gases, or to monitor processes on a cellular level. Each of these uses required a mechanism for detection, specifically physical or chemical process, that can be used advantageously, which causes a large change in photophysical properties specific to the target. Photo-induced electron transfer (PeT) helps to provide a

mechanism whereby certain changes to chemical environments can be detected via an emission gradient.

The use of PeT for sensing devices is one of the most common examples of a functional bodipy. PeT is a phenomenon where an excited electron from a donor transfers to an acceptor down an energy gradient. In photochemistry PeT is typically used as a mechanism to quench the excited state. Although excited state (fluorescence) lifetimes are typically very fast, for bodipy compounds it is ca. 3 ns, the speed of PeT is much faster – often <1 ps. As a result, if given the option, a system will undergo PeT quenching of the excited state, in effect turning the fluorescence 'off'. [116-119]

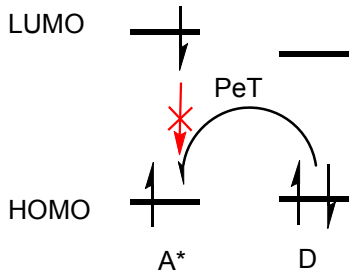

Figure 24 Photo-induced electron transfer PeT, where a lone pair of electrons (typically attached in close proximity to the fluorophore) quenches fluorescence of the excited state.

Scheme 17 shows a system which is used as an on / off fluorescent zinc ion sensor. In this system the lone pair of electrons on the amine attached to the bodipy core will readily PeT quench the excited state. Yet once zinc has been chelated to the system the lone pair is bound to the zinc ion, effectively dropping the HOMO energy level and this prevents PeT quenching which in turn turns the fluorescence 'on'.

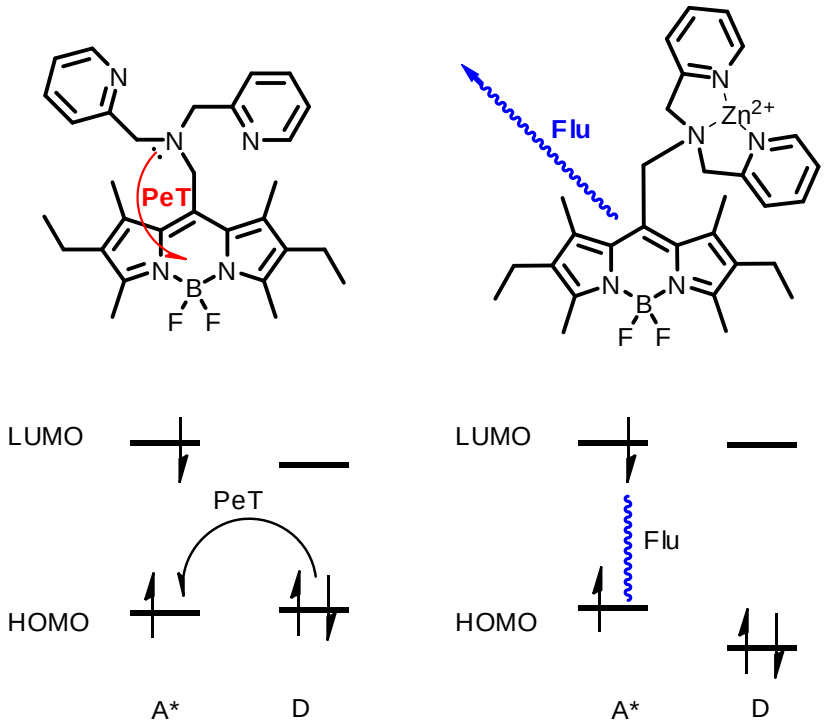

Figure 25 Fluorescent 'on' / 'off' zinc sensor. (left) - λ_{abs} 491 nm, λ_{em} 509 nm, ϕ_{Flu} – 0.077; (right) - λ_{abs} 491 nm, λ_{em} 511 nm, ϕ_{Flu} – 0.857. Measured in DMSO.

1.8.1.a *Donor-excited photo-induced electron transfer*

The para-nitrophenyl bodipy shown in Figure 23 exhibits a ϕ_{Flu} that is much lower than those similar bodipy compounds also present in the same figure.

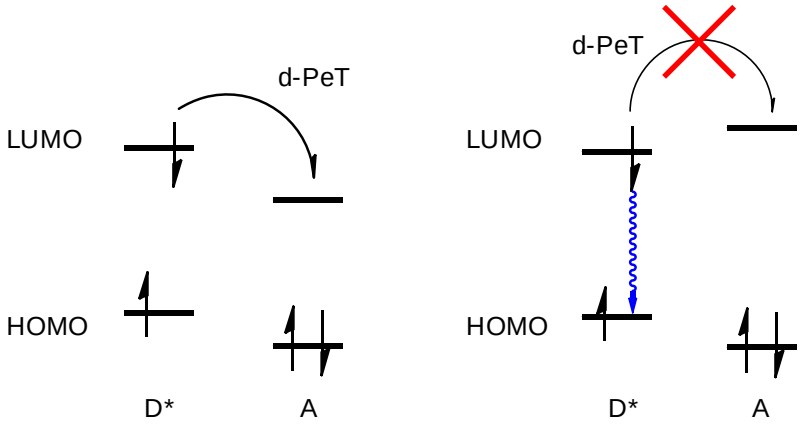

Figure 26 Donor-excited photo-induced electron transfer (left).

The presence of a meso-nitrophenyl group causes the electron transfer from the excited bodipy to the electron deficient phenyl moiety.[120] This can be known as donor-excited PeT or d-PeT, where effectively the electron deficient phenyl group becomes the acceptor and the bodipy core the donor (usually it is the other way around). Indeed it is possible to tune the HOMO and LUMO energy levels within a system to prevent d-PeT if that is not desirable.[121]

Work has been done by Nagano *et al.* to use rational principles to design effective bodipy sensors designed to detect NO in a range of pH environments. A diaminophenyl bodipy was synthesised which would PeT quench the bodipy excited state. This system would then cyclise when in contact with NO (Figure 27, compound **c** below) lowering the HOMO of the aryl moiety thus causing the fluorophore to fluoresce.

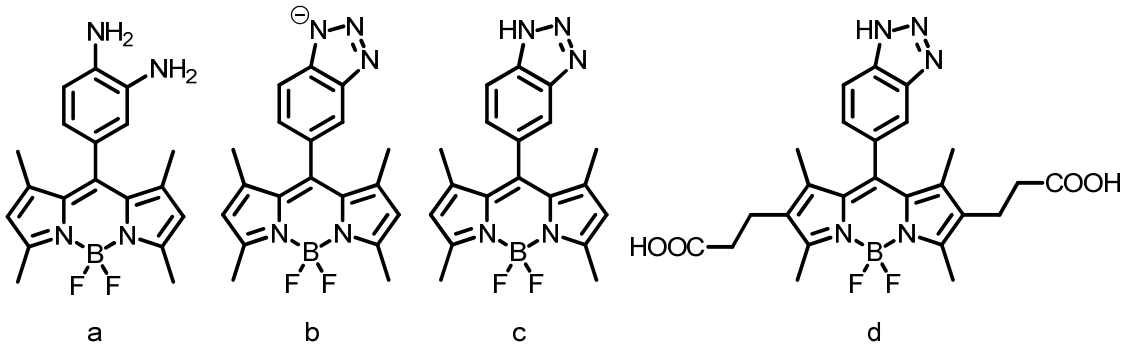

*Figure 27 Diamino-substituted aryl bodipy compounds. Compound **a** - λ_{abs} 496 nm, λ_{em} 505 nm, ϕ_f – 0.001; Compound **c** - λ_{abs} 498 nm, λ_{em} 507 nm, ϕ_f – 0.40; Compound **d** - λ_{abs} 521 nm, λ_{em} 537 nm, ϕ_f – 0.74. Measured in a 0.1 M phosphate buffer (1% DMSO co-solvent).*

Compound **a** was made and tested, proving that there was indeed a distinctive ‘on’ / ‘off’ effect in the presence of NO. Yet upon further examination it was found that the fluorophore failed to exhibit the same effect in the basic conditions in which it was to be used. It was found that the triazole group was deprotonated in this environment, this raised the aryl HOMO energy level (Figure 28), thus causing a quenching of fluorescence.

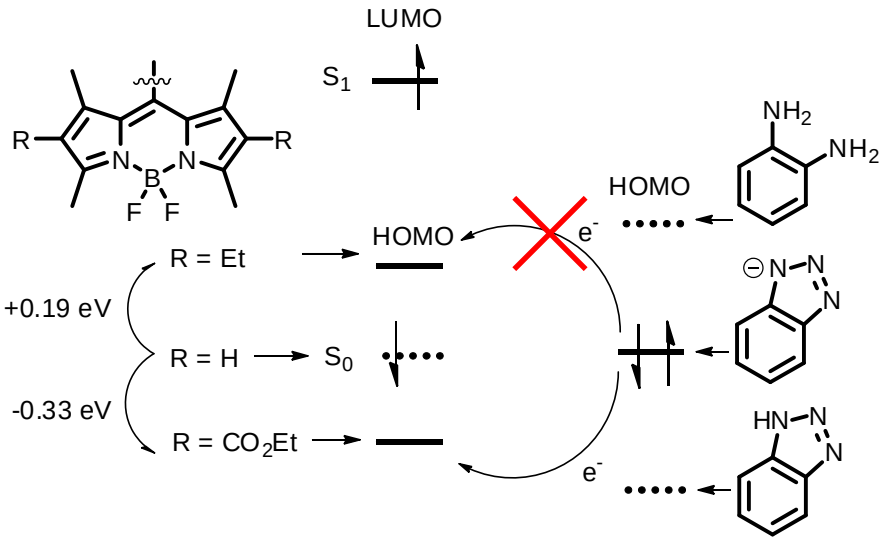

Figure 28 Manipulating the HOMO energy levels within simple systems to perfect ON / OFF response of NO detection in a pH independent environment.[104]

The problem was eventually resolved by creating a bodipy core with a higher energy HOMO – by including alkyl groups at the 2 and 4 positions. This prevented the deprotonation from quenching fluorescene, allowing the sensor to be used in environments with varying pH.

1.8.2 ***Energy Transfer***

1.8.2.a *Förster Resonance Energy Transfer*

Förster resonance energy transfer (FRET) is a mechanism for transferring a photon between singlet (S_1) excited states 'through-space' via non-radiative dipole coupling; i.e., the two molecules do not have to be linked directly via conjugation. The process of energy transfer can take place over a relatively large distance, sometimes >150 Å.[122, 123]

$$k_F = \frac{(8.8 \times 10^{-25}) K^2 \Phi_f}{n^4 \tau_F r^6} J_F$$

Equation 3 The equation for the Förster resonance energy transfer with in a system. Where: k_f - rate constant; K – orientation factor; Φ_f – quantum yield of the donor; J_F – overlap intergral; n – refractive index of the solvent; τ_F – fluorescence lifetime of the donor S1 state; r – distance dependence.

FRET efficiency depends on several factors such as the distance between the two luminophores (Figure 29), the angle of the dipole moment on each

luminophore, the refractive index of the solvent (if applicable) and the spectral overlap of the emission wavelength of the donor dye and the absorbance wavelength of the acceptor dye. It is important that all of these factors are kept constant in order that measurements can be made on individual aspects of FRET in the molecule.

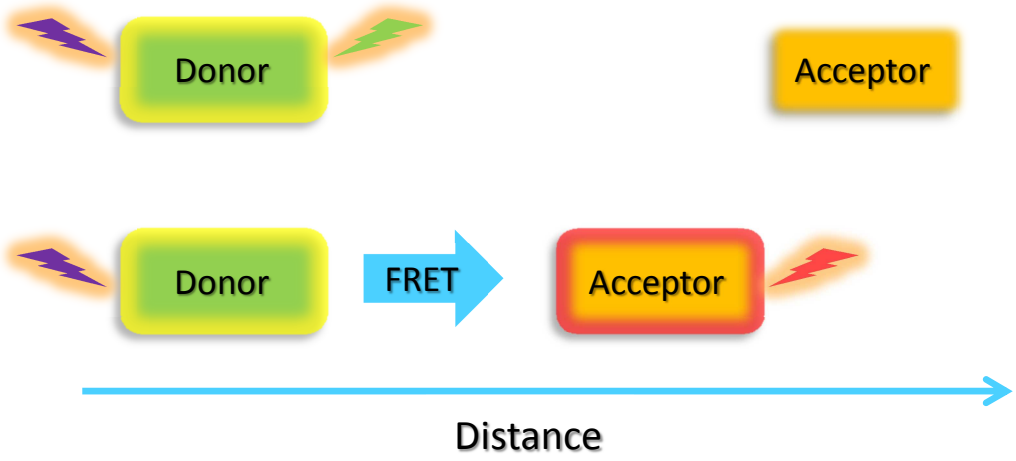

Figure 29 A depiction of the distance dependence exhibited by energy transfer systems. If the distance separating the acceptor and donor fluorophore is too great then FRET does not occur. Depending on the efficiency of the system if the acceptor can be moved closer to the donor then FRET can occur and fluorescence from the acceptor fluorophore can be observed.

The distance that both fluorophores are from each other is perhaps the most crucial of all the dependences of FRET. The further that the donor–acceptor pair are from each other (r), the less FRET takes place. The relationship between the k_F and r is $1 / r^6$, meaning that any increase in the distance between donor and acceptor, will greatly affect the rates of energy transfer within the system. This particular facet of FRET can be used to make so called 'molecular rulers', whereby a donor and acceptor fluorophores can be held rigidly within a larger molecule and the distance between the two calculated using value of k_F. The use of molecular rulers is particularly relevant to work using DNA where by the lengths of strands of DNA can accurately be measured, even to a <30 nm distance.[124]

In order for FRET to occur the dyes that are combined in the array must have an acceptable overlap integral J_F. J_F is a measure of the extent that the normalised fluorescence emission of the donor and the absorbance of the acceptor overlap.

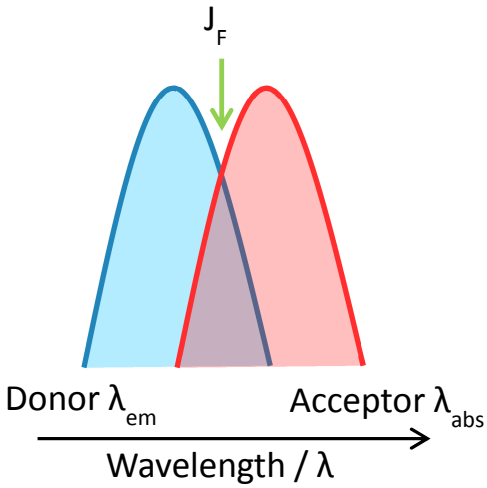

Figure 30 The overlap integral between the emission spectra of a donor dye (blue) and the absorbance of an acceptor dye (red). Where J_F denoted the overlap integral of the two dyes.

J_F is a thermodynamic factor that increases with the molar absorbance coefficient (ε) of the dyes involved. Compounds showing a small Stokes shift but large ε will give a high J_F and a fast rate of energy migration.

Another aspect of FRET is the need for the acceptor and donor dyes to adopt the correct orientation so that the dipoles of each dye can interact, or the orientation factor, K. This term accounts for the mutual alignment of the transition dipoles on the donor and acceptor. K is at a maximum for parallel orientations and approaches zero for orthogonal geometries. The larger the orientation factor, the more FRET will occur.

An understanding of the principals behind energy transfer can lead to a number of molecular devices such as: probes for receptor / ligand interactions, monitoring the spatial distribution and assembly of proteins or distribution and transport of lipids, light harvesting arrays, and cascade systems.[125-130]

1.8.2.b *Energy Transfer Cassettes*

A reoccurring problem in the field of organic dyes is the relatively small Stokes shift found which means that they tend not to be favourable for use in flow cytometry. A solution to this is offered whereby ‘antenna’ light harvesting moieties are attached to the bodipy core, in positions that do not affect the π-system of the bodipy, such as off the boron centre.

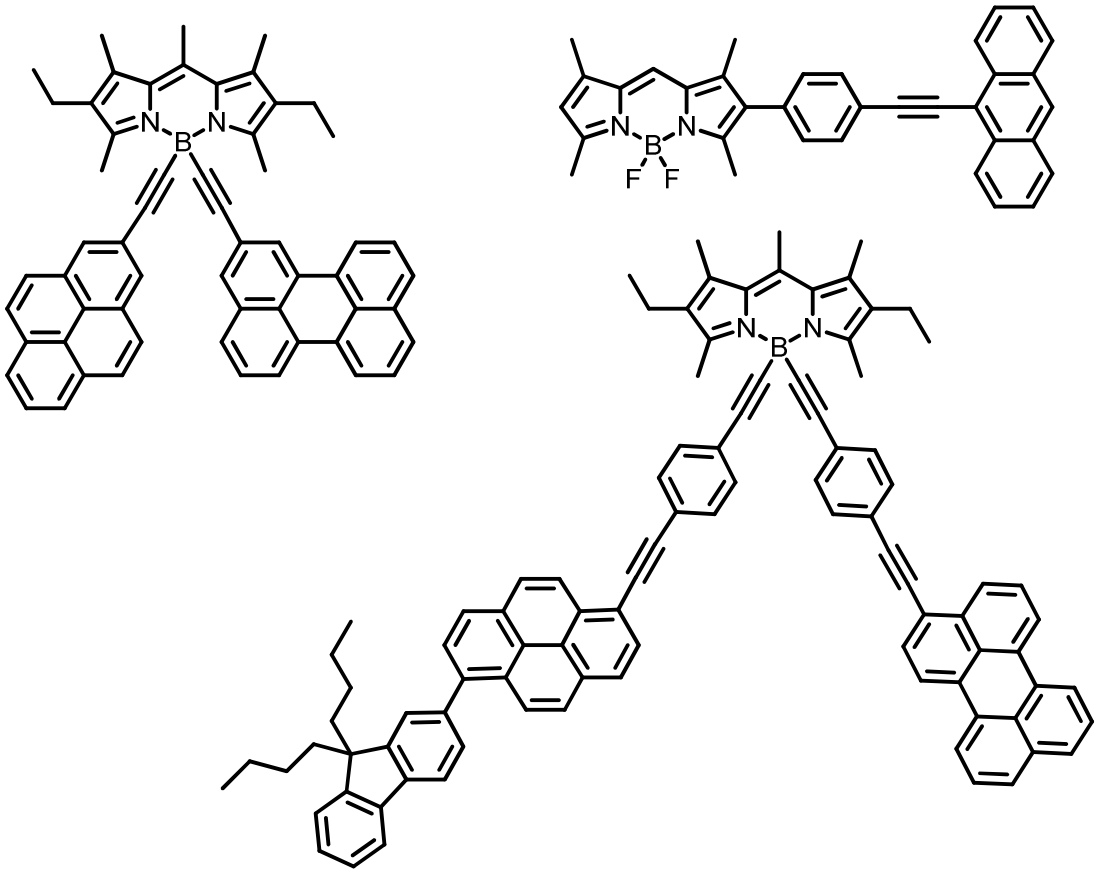

Figure 31 Energy transfer cassettes which incorporate bodipy.[131]

Work performed by Harriman *et al.* saw up to four different complementary donor moieties attached to a single bodipy acceptor (Figure 31, bottom right). In this particular example the appendages, attached to the bodipy terminus, have absorption profiles which absorb at different spectral regions - meaning that each moiety can be independently excited. The energy of the excited donor moiety is then transferred, via an energy gradient (Figure 32), to the bodipy acceptor.

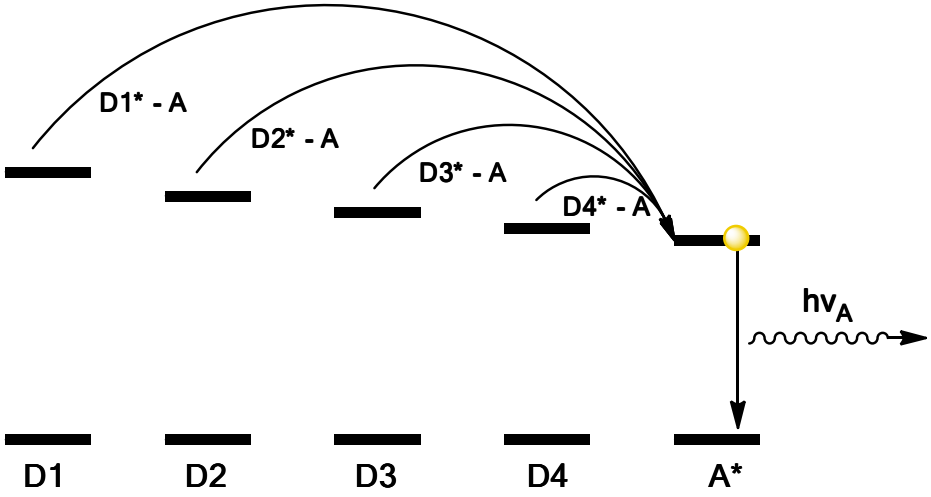

Figure 32 A representation of the energy level gradient within the molecular cascade system created by Harriman et al. Each donor moiety (D#) can be independently excited and will undergo ultrafast energy transfer to the bodipy acceptor (A) which undergoes a radiative deactivation of the excited state.

The result of this work is a device which effectively has a variable Stokes shift. Also the molecule can collect light of wavelengths between 300 and 550 nm and funnel this light energy to a focal point. Due to the extremely efficient energy transfer which occurs between the donor and acceptor the only wavelength of light which is emitted by the system comes exclusively from the bodipy. Creating systems that can capture light and efficiently transfer energy is of great interest to those aiming to synthesise artificial photosynthetic systems – currently a hot topic.[132]

1.9 **Concluding Remarks**

Despite the original observations of fluorescence occurring as early as 1845 it wasn't until the 1970's when the topic really took off. This is largely due to a lack of affordable and reliable analytical equipment which is required to understand the complexities of such systems.

The development of new fluorophores, while at first heavily modelled on naturally fluorescent compounds, has begun to move towards more inventive extrinsic compounds. The move towards such innovative compounds is largely due to the understanding of the intricacies of the area. Such an understanding is indeed a reason why continued focus on the fundamentals of fluorescence should continue alongside the more glamorous arm of applications.

By understanding the complexities of photonic systems it is then possible to apply and knowledge rendered towards novel applications of fluorescent compounds.

Bodipy dyes are infinitely flexible photonic dyes capable of being honed to accommodate many different functions. As such bodipy has received a lot of attention over the past 10 years and is likely to be further developed well into the future.

Synthetically bodipy is easy to arrive at and it can be edited in a plethora of different directions. In the following chapters bodipy is addressed in a systematic study in order to ascertain the effects of multiple fluorine substitution at the meso-aryl moiety and also in initial incursions into chiral bodipy compounds with a view to chiral sensing.

1.10 **References**

1. J. Herchel, *Phil.Trans. R. Soc. London*, 1845, **135**, 143-145.
2. G. Stokes, *Phil. Trans. R. Soc. London*, 1852, **142**, 463-562.
3. J. Lakowicz, *Principles of Fluorescence Spectroscopy*, Kluwer Academic / Plenum Publishers, London.
4. M. Kasha, *Disc. Faraday Soc.*, 1950, **9**, 14-19.
5. R. Thompson, *Topics in Fluorescence Spectroscopy*, Springer, 1994
6. J. Lakowicz, *Probe Design and Chemical Sensing*, Plenum Press, New York City.
7. A. Demchenko, *Ultra-Violet Spectroscopy of Proteins*, Springer-Verlag, New York, 1981.
8. W.-E. Lee, C.-L. Lee, T. Sakaguchi, M. Fujikid and G. Kwak, *Chem. Commun.*, 2011, **47**, 3526-3528.
9. T. E. Rosson, S. M. Claiborne, J. R. McBride, B. S. Stratton and S. J. Rosenthal, *J. Am. Chem. Soc.*, 2012, **134**, 8006-8009.
10. P. Rothemund, *J. Am. Chem. Soc.*, 1936, **58**, 625-627.
11. A. D. Adler, F. R. Longo, J. D. Finarelli, J. Goldmacher, J. Assour and L. Korsakoff, *J. Org. Chem.*, 1967, **32**, 476-476.
12. J. B. Kim, J. J. Leonard and F. R. Longo, *J. Am. Chem. Soc.*, 1972, **94**, 3986-3992.

13. G. R. Seely and J. S. Connolly, *Fluorescence of Photosynthetic Pigments in Vitro. in Light Emission by Plants and Bacteria*, Academic Press, 1986.
14. H. H. Strain, M. R. Thomas and J. J. Katz, *Biochim. Biophys. Acta*, 1963, **75**, 306-311.
15. M. Yuen, G. Closs, J. Katz, J. Roper, M. Wasielewski and J. Hindman, *Proc. Nat. Acad. Sci. U S A*, 1980, **77**, 5598-5601.
16. S. Ma and X. Lu, *J. Org. Chem.*, 1993, **5**, 1245-1251.
17. J. E. Falk, *Porphyrins and Metalloporphyrins*, Elsevier, New York, 1975.
18. P. D. Beer, M. G. B. Drew and R. J. Jagessar, *Chem. Dalton Trans.*, 1997, **5**, 881-886.
19. R. Wormald, J. Evans, L. Smeeth and K. Henshaw, *Photodynamic Therapy for Neovascular Age-Related Macular Degeneration*, Cochrane Database Syst. Rev., 2007.
20. M. G. Walter, A. B. Rudine and C. C. Wamser, *J. Porphyrins and Phthalocyanines*, 2010, **14**, 759-792.
21. A. Yella, H.-W. Lee, H. N. Tsao, C. Yi, A. K. Chandiran, M. K. Nazeeruddin, E. W.-G. Diau, C.-Y. Yeh, S. M. Zakeeruddin and M. Grätzel, *Science*, 2011, **334**, 629–634.
22. M. A. H. Alamiry, A. C. Benniston, J. Hagon, T. P. L. Winstanley, H. Lemmetyinenb and N. V. Tkachenko, *RSC Adv.*, 2012, **2**, 4944-4950.
23. R. Yoshii, A. Nagai, K. Tanaka and Y. Chujo, *Chem. Eur. J.* , 2013, **19**, 4506-4512.
24. G. Tsiminis, N. A. Montgomery, A. L. Kanibolotsky, A. Ruseckas, I. F. Perepichka, P. J. Skabara, G. A. Turnbull and I. D. W. Samuel, *Semicond. Sci. Technol.*, 2012, **27**, 094005 - 094011.
25. A. Fakhari and S. E. Rokita, *Chem. Commun.,* , 2011, **47**, 4222-4224.
26. W. Yan, Q. Wang, Q. Lin, M. Li, J. L. Petersen, X. Shi and G. M. Fischer, *Chem. Eur. J.*, 2011, **17**, 5011 – 5018.
27. M. Isom-Ki-Krondahl, I. Gçttker-Schnetmann, E. Daltrozzo and A. Zumbusch, *Chem. Eur. J.* , 2009, **15**, 4857-4864.
28. G. Ulrich, R. Ziessel and A. Harriman, *Angew. Chem. Int. Ed.*, 2008, **47**, 1184-1199.
29. M. J. Kwak and Y. Kim, *Bull. Korean Chem. Soc.*, 2009, **30**, 2865-2866.

30. Y. Wang, Y. Yang, G. A. Turnbull and I. D. W. Samuel, *Mol. Cryst. Liquid Cryst.*, 2012, **554**, 103-110.
31. M. Sameiro and T. Gonçalves, *Chem. Rev.* , 2009, **109**, 190-212.
32. N. Nandi, K. Bhattacharyya and B. Bagchi, *Chem. Rev.*, 2000, **100**, 2013-2046.
33. R. W. Sinkeldam, N. J. Greco and Y. Tor, *Chem. Rev.*, 2010, **110**, 2579-2619.
34. G. Saroja, B. Ramachandram, S. Saha and A. Samanta, *J. Phys. Chem. B*, 1999, **103**, 2906-2911.
35. T. Soujanya, T. S. R. Krishna and A. Samanta, *J. Phys. Chem.*, 1992, **96**, 8544-8548.
36. G. Saroja, T. Soujanya, B. Ramachandram and A. Samanta, *J. Fluoresc.*, 1998, **8**, 405-410.
37. D. Mandal, S. Sen, D. Sukul, K. Bhattacharyya, A. K. Mandal, R. Banerjee and S. Roy, *J. Phys. Chem. B*, 2002, **106**, 10741-10747.
38. T. Hirano, K. Kikuchi, Y. Urano and T. Nagano, *J. Am. Chem. Soc.*, 2002, **124**, 6555-6562.
39. Z. Xu, Y. Xiao, X. Qian, J. Cui and D. Cui, *Org. Lett.*, 2005, **7**, 889-892.
40. E. Deniz, G. C. Isbasar, O. A. Bozdemir, L. T. Yildirim, A. Siemiarczuk and E. U. Akkaya, *Org. Lett.*, 2008, **10**, 3401-3403.
41. P. Ghosh, P. K. Bharadwaj, S. Mandal and S. Ghosh, *J. Am. Chem. Soc.*, 1996, **118**, 1553-1554.
42. S. Kaur and S. Kumar, *Chem. Commun.*, 2002, 2840-2841.
43. S. Banthia and A. Samanta, *J. of Phys. Chem. B*, 2002, **106**, 5572-5577.
44. B. Ramachandram and A. Samanta, *Chem. Commun.*, 1997, 1037-1038.
45. Y. Zheng, J. Orbulescu, X. Ji, F. M. Andreopoulos, S. M. Pham and R. M. Leblanc, *J. Am. Chem. Soc.*, 2003, **125**, 2680-2686.
46. M. Dakanali, T. H. Do, A. Horn, A. Chongchivivat, T. Jarusreni, D. Lichlyter, G. Guizzunti, M. A. Haidekker and E. A. Theodorakis, *Bioorg. Med. Chem.*, 2012, **20**, 4443-4450.
47. J. S. Goodwin, K. R. Drake, C. L. Remment and K. A. Kenworthy, *Biophys. J.*, 2005, **89**, 1398-1410.
48. M. D. Dibner, K. A. Ireland, L. A. Koerner and D. L. Dexter, *Cancer Res.*, 1985, **45**, 4998-5003.

49. A. M. Aleardi, G. Benard, O. Augereau, M. Malgat, J. C. Talbot, J. P. Mazat, T. Letellier, J. Dachary-Prigent, G. C. Solaini and R. J. Rossignol, *Bioenerg. Biomembr.*, 2005, **37**, 207-225.
50. X. Hou, S. J. Richardson, M.-I. Aguilar and D. H. Small, *Biochemistry*, 2005, **44**, 11618-11627.
51. J. H. Ahn, T. Y. Kim, Y. J. Kim, M. W. Han, T. H. Yoon and J. W. Chung, *Diabetic Medicine*, 2006, **23**, 1339-1343.
52. B. Y. Salazar Vázquez, M. A. Salazar Vázquez, V. C. Venzor, A. C. Negrete, P. Cabrales, J. S. Díaz and M. Intaglietta, *Clinical Hemorheology and Microcirculation*, 2008, **38**, 57-64.
53. S. Wang, A. H. Boss, K. R. Kensey and R. S. Rosenson, *Clinica Chimica Acta*, 2003, **332**, 79-82.
54. M. A. Haidekker, T. P. Brady, D. Lichlyter and E. A. Theodorakis, *J. Am. Chem. Soc.*, 2005, **128**, 398-399.
55. D. Fischer, E. A. Theodorakis and M. A. Haidekker, *Nat. Protoc.*, 2007, **2**, 227-236.
56. H.-J. Yoon, M. Dakanali, D. Lichlyter, W. M. Chang, K. A. Nguyen, M. E. Nipper, M. A. Haidekker and E. A. Theodorakis, *Org. & Biomol. Chem.*, 2011, **9**, 3530-3540.
57. G. Ulrich, R. Ziessel and A. Harriman, *Angew. Chem. Int. Ed.*, 2008, **47**, 1184-1201.
58. A. Loudet and K. Burgess, *Chem. Rev.*, 2007, **107**, 4891-4932.
59. A. Dalla Cort, G. Ercolani, A. L. Iamiceli, L. Mandolini and P. Mencarelli, *J. Am. Chem. Soc.*, 1994, **116**, 7081-7087.
60. A. Treibs and F.-H. Kreuzer, *Liebigs Ann.*, 1968, **718**, 208-223.
61. L. Wu and K. Burgess, *Chem. Commun.*, 2008, 4933-4935.
62. J. Bañuelos, V. Martín, C. F. A. Gómez-Durán, I. J. A. Córdoba, E. Peña-Cabrera, I. García-Moreno, Á. Costela, M. E. Pérez-Ojeda, T. Arbeloa and Í. L. Arbeloa, *Chem. Eur. J.*, 2011, **17**, 7261-7270.
63. Y. Zhao, X. Lv, Y. Liu, J. Liu, Y. Zhang, H. Shi and W. Guo, *J. Mat. Chem.*, 2012, **22**, 11475-11478.
64. M. A. T. Rogers, *J. Chem. Soc. (Resumed)*, 1943, **0**, 590-596.
65. W. H. Davies and M. A. T. Rogers, *J. Chem. Soc. (Resumed)*, 1944, **0**, 126-131.

66. G. Sathyamoorthi, M.-L. Soong, T. W. Ross and J. H. Boyer, *Heteroatom Chem.*, 1993, **4**, 603-608.
67. A. Loudet, R. Bandichhor, L. Wu and K. Burgess, *Tetrahedron*, 2008, **64**, 3642-3654.
68. A. Gorman, J. Killoran, C. O'Shea, T. Kenna, W. M. Gallagher and D. F. O'Shea, *J. Am. Chem. Soc.*, 2004, **126**, 10619-10631.
69. A. Palma, L. A. Alvarez, D. Scholz, D. O. Frimannsson, M. Grossi, S. J. Quinn and D. F. O'Shea, *J. Am. Chem. Soc.*, 2011, **133**, 19618-19621.
70. M. Kollmannsberger, K. Rurack, U. Resch-Genger, W. Rettig and J. Daub, *Chem. Phys. Lett.*, 2000, **329**, 363-369.
71. J. Li, B. Hu, G. Hu, X. Li, P. Lu and Y. Wang, *Org. & Biomol. Chem.*, 2012, **10**, 8848-8859.
72. T. Yogo, Y. Urano, Y. Ishitsuka, F. Maniwa and T. Nagano, *J. Am. Chem. Soc.*, 2005, **127**, 12162-12163.
73. A. Loudet, R. Bandichhor, K. Burgess, A. Palma, S. O. McDonnell, M. J. Hall and D. F. O'Shea, *Org. Lett.,* 2008, **10**, 4771-4774.
74. N. Miyaura, H. Suginome and A. Suzuki, *Tet. Lett.*, 1981, **22**, 127-130.
75. H. Kim, A. Burghart, M. B. Welch, J. Reibenspies and K. Burgess, *Chem. Commun.*, 1999, **0**, 1889-1890.
76. S. Zhu, J. Zhang, G. Vegesna, A. Tiwari, F.-T. Luo, M. Zeller, R. Luck, H. Li, S. Green and H. Liu, *RSC Adv.*, 2012, **2**, 404-407.
77. C. Thivierge, R. Bandichhor and K. Burgess, *Org. Lett.*, 2007, **9**, 2135-2138.
78. J.-H. Ye, G. Wang, C. Huang, Z. Hu, W. Zhang and Y. Zhang, *Synthesis*, 2012, **44**, 104-110.
79. H. J. Wories, J. H. Koek, G. Lodder, J. Lugtenburg, R. Fokkens, O. Driessen and G. R. Mohn, *Rec. Trav. Chim. Pays-Bas*, 1985, **104**, 288-291.
80. O. Buyukcakir, O. A. Bozdemir, S. Kolemen, S. Erbas and E. U. Akkaya, *Org. Lett.*, 2009, **11**, 4644-4647.
81. A. Coskun, E. Deniz and E. U. Akkaya, *Org. Lett.*, 2005, **7**, 5187-5189.
82. K. Rurack, M. Kollmannsberger and J. Daub, *New J. Chem.*, 2001, **25**, 289-292.
83. W. Qin, M. Baruah, M. Van der Auweraer, F. C. De Schryver and N. Boens, *J. Phys. Chem. A*, 2005, **109**, 7371-7384.

84. O. Galangau, C. Dumas-Verdes, R. Meallet-Renault and G. Clavier, *Org & Biomol Chem.*, 2010, **8**, 4546-4553.
85. M.-M. Shi, H.-Z. Chen, J.-Z. Sun, J. Ye and M. Wang, *Chem. Commun.*, 2003, 1710-1711.
86. V. Leen, E. Braeken, K. Luckermans, C. Jackers, M. Van der Auweraer, N. Boens and W. Dehaen, *Chem. Commun.*, 2009, 4515-4517.
87. P. E. Sonnet, *J. Org. Chem.*, 1972, **37**, 925-929.
88. T. Rohand, W. Qin, N. Boens and W. Dehaen, *Eur. J. Org. Chem.*, 2006, **2006**, 4658-4663.
89. S. Yin , V. Leen, C. Jackers , D. Beljonne, B. Van Averbeke, M. Van der Auweraer , N. Boens and W. Dehaen, *Chem. Eur. J.*, 2011, **17**, 13247-13257.
90. Y. Hayashi, S. Yamaguchi, W. Y. Cha, D. Kim and H. Shinokubo, *Org. Lett.*, 2011, **13**, 2992-2995.
91. S. M. Crawford and A. Thompson, *Org. Lett.*, 2010, **12**, 1424-1427.
92. D. A. Smithen, A. E. G. Baker, M. Offman, S. M. Crawford, T. S. Cameron and A. Thompson, *J. Org. Chem.*, 2012, **77**, 3439-3453.
93. C. Goze, G. Ulrich, L. J. Mallon, B. D. Allen, A. Harriman and R. Ziessel, *J. Am. Chem. Soc.y*, 2006, **128**, 10231-10239.
94. L. H. Thoresen, H. Kim, M. B. Welch, A. Burghart and K. Burgess, *Synlett*, 1998, **1998**, 1276-1278.
95. H. L. Kee, C. Kirmaier, L. Yu, P. Thamyongkit, W. J. Youngblood, M. E. Calder, L. Ramos, B. C. Noll, D. F. Bocian, W. R. Scheidt, R. R. Birge, J. S. Lindsey and D. Holten, .*J. Phys. Chem. B*, 2005, **109**, 20433-20443.
96. Y. Gabe, T. Ueno, Y. Urano, H. Kojima and T. Nagano, *Anal Bioanal Chem*, 2006, **386**, 621-626.
97. C. Tahtaoui, C. Thomas, F. Rohmer, P. Klotz, G. Duportail, Y. Mély, D. Bonnet and M. Hibert, *J. Org. Chem.*, 2006, **72**, 269-272.
98. T. Lundrigan, S. M. Crawford, T. S. Cameron and A. Thompson, *Chem. Commun.*, 2012, **48**, 1003-1005.
99. E. D. Sternberg, D. Dolphin and C. Brückner, *Tetrahedron*, 1998, **54**, 4151-4202.
100. R. W. Wagner and J. S. Lindsey, *J. Am. Chem. Soc.*, 1994, **116**, 9759-9760.

101. D. M. Wallace, S. H. Leung, M. O. Senge and K. M. Smith, *J. Org. Chem.*, 1993, **58**, 7245-7257.
102. L. Jiao, C. Yu, J. Li, Z. Wang, M. Wu and E. Hao, *J. Org. Chem.*, 2009, **74**, 7525-7528.
103. J.-H. Olivier, J. Barberá, E. Bahaidarah, A. Harriman and R. Ziessel, *J. Am. Chem. Soc.*, 2012, **134**, 6100-6103.
104. Y. Gabe, Y. Urano, K. Kikuchi, H. Kojima and T. Nagano, *J. Am. Chem. Soc.*, 2004, **126**, 3357-3367.
105. Y. Wu, X. Peng, B. Guo, J. Fan, Z. Zhang, J. Wang, A. Cui and Y. Gao, *Org. & Biomol. Chem.*, 2005, **3**, 1387-1392.
106. C.-W. Wan, A. Burghart, J. Chen, F. Bergström, L. B. Å. Johansson, M. F. Wolford, T. G. Kim, M. R. Topp, R. M. Hochstrasser and K. Burgess, *Chem. Eur. J.*, 2003, **9**, 4430-4441.
107. R. Ziessel, C. Goze, G. Ulrich, M. Césario, P. Retailleau, A. Harriman and J. P. Rostron, *Chem. Eur. J.*, 2005, **11**, 7366-7378.
108. R. E. Pagano, O. C. Martin, H. C. Kang and R. P. Haugland, *J. Cell Biol.*, 1991, **113**.
109. G. Ulrich, S. Goeb, A. De Nicola, P. Retailleau and R. Ziessel, *Synlett*, 2007, **2007**, 1517-1520.
110. I. García-Moreno, D. Zhang, Á. Costela, V. Martín, R. Sastre and Y. Xiao, *J. Appl. Phys*, 2010, **107**, 073105-073101.
111. T. Gareis, C. Huber, O. S. Wolfbeis and J. Daub, *Chem. Commun.*, 1997, 1717-1718.
112. M. Baruah, W. Qin, R. A. L. Vallée, D. Beljonne, T. Rohand, W. Dehaen and N. Boens, *Org. Lett.*, 2005, **7**, 4377-4380.
113. Y. Qian, L. Zhang, S. Ding, X. Deng, C. He, X. E. Zheng, H.-L. Zhu and J. Zhao, *Chem. Sci.*, 2012, **3**, 2920-2923.
114. M. H. Chisholm, K. Choojun, J. C. Gallucci and P. M. Wambua, *Chem. Sci.*, 2012, **3**, 3445-3457.
115. J.-B. Wang, X.-Q. Fang, X. Pan, S.-Y. Dai and Q.-H. Song, *Chem. Asian J.*, 2012, **7**, 696-700.
116. A. Burghart, H. Kim, M. B. Welch, L. H. Thoresen, J. Reibenspies, K. Burgess, F. Bergström and L. B. Å. Johansson, *J. Org. Chem.*, 1999, **64**, 7813-7819.
117. Q.-H. Xu, D. Moses and A. J. Heeger, *Phys. Rev. B*, 2003, **67**, 245417.

118. B. Kraabel, C. H. Lee, D. McBranch, D. Moses, N. S. Sariciftci and A. J. Heeger, *Chem. Phys. Lett.*, 1993, **213**, 389-394.
119. N. S. Sariciftci, L. Smilowitz, A. J. Heeger and F. Wudl, *Science*, 1992, **258**, 1474-1476.
120. T. Ueno, Y. Urano, H. Kojima and T. Nagano, *J. Am. Chem. Soc.*, 2006, **128**, 10640-10641.
121. T. Ueno, Y. Urano, K.-i. Setsukinai, H. Takakusa, H. Kojima, K. Kikuchi, K. Ohkubo, S. Fukuzumi and T. Nagano, *J. Am. Chem. Soc.*, 2004, **126**, 14079-14085.
122. T. Förster, *Intermolecular Energy Migration and Fluorescence. Ann. Phys*, 1948, **2**, 55-75.
123. B. P. Maliwal, S. Raut, R. Fudala, S. D'Auria, V. M. Marzullo, A. Luini, I. Gryczynski and Z. Gryczynski, *J. Biomed. Opt.*, 2012, **17**, 011006-011001.
124. O. Thoumine, E. Saint-Michel, C. Dequidt, J. Falk, R. Rudge, T. Galli, C. Faivre-Sarrailh and D. Choquet, *Biophys. J.*, 2005, **89**, L40-L42.
125. W. Berger, H. Prinz, J. Striessnig, H. Kang, R. Haugland and H. Glossmann, *Biochem.*, 1994, **33**, 1875 - 1883.
126. B. S. Watson, T. L. Hazlett, J. F. Eccleston, C. Davis, D. M. Jameson and A. E. Johnson, *Biochem.*, 1995, **34**, 7904-7912.
127. J. W. Nichols and R. E. Pagano, *J. Bio. Chem.*, 1983, **258**, 5368-5371.
128. A. Ajayaghosh, V. K. Praveen and C. Vijayakumar, *Chem. Soc. Rev.*, 2008, **37**, 109-122.
129. P. G. Wu and L. Brand, *Anal. Biochem.*, 1994, **218**, 1-13.
130. T. Franzl, D. S. Koktysh, T. A. Klar, A. L. Rogach, J. Feldmann and N. Gaponik, *Appl. Phys. Lett.*, 2004, **84**, 2904-2906.
131. R. Ziessel, G. Ulrich and A. Harriman, *New J. Chem.*, 2007, **31**, 496-501.
132. Y. Nakamura, N. Aratani and A. Osuka, *Chem. Soc. Rev.*, 2007, **36**, 831-845.

Chapter 2. An exploration of a New Series of Molecular Fluorophores Based on a Highly Substituted Terephthalate Core.

2.1 Introduction

2.1.1 Fluorescent sensors

Fluorescent compounds are of great interest in many different fields from uses as laser dyes, liquid crystal displays and most prominently in diagnostic applications such as molecular sensors and imaging agents.[1,2]

The success of fluorescent compounds in diagnostic applications lies in the very high sensitivity that can be achieved (using extremely low concentrations of fluorophore), as well as good signal to noise ratios.[3,4] The use of fluorescent dyes in combination with microscopy results in a technique which is completely non-invasive hence dynamic processes can be observed without any interference with the host.

There are a plethora of potential uses of fluorophores, -particularly in medicinal fields- where cell imaging, radical detection and pH measurements are particularly useful.[5,6,7,8]

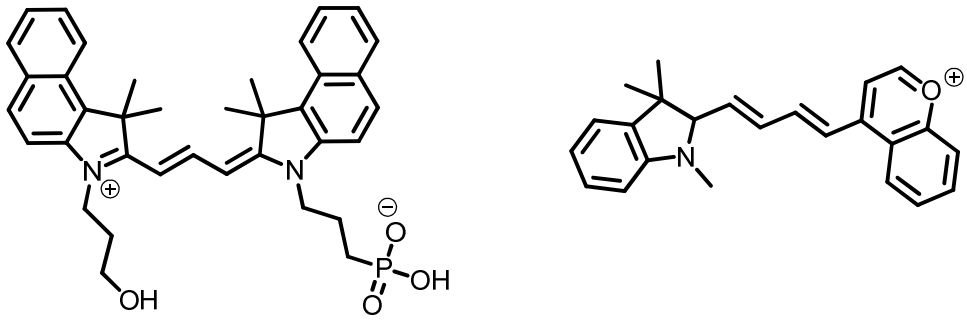

*Figure 1 Dylight NIR fluorescent dyes with a cyanine core (left) and a benzopyrillium core (right)[9].**

Despite having many advantages and potential uses, fluorescent sensors must first overcome the problem of auto-fluorescence in order to be considered as a feasible tool within medicine. Auto-fluorescence is a naturally occurring phenomenon whereby the cell fluoresces when exposed to light. The observed emission typically results from NAPDH and flavins and this can saturate any signal resulting from fluorescent probes, indeed the typical amount of

* *Both compounds are made by Thermo Scientific; http://www.piercenet.com.*

fluorescence observed from a fibroblast cell is equal to around 35,000 molecules of fluorescein.[10,11,12,13] Different options are available in order to get around the problem caused by auto-fluorescence for example: time-gated spectroscopy, lanthanide millisecond emitters, near IR (NIR) emitters, delayed fluorescence, and molecules that have a large Stokes shift (SS) - indeed it is the latter that is the target in this particular chapter.[14,15;16,17]

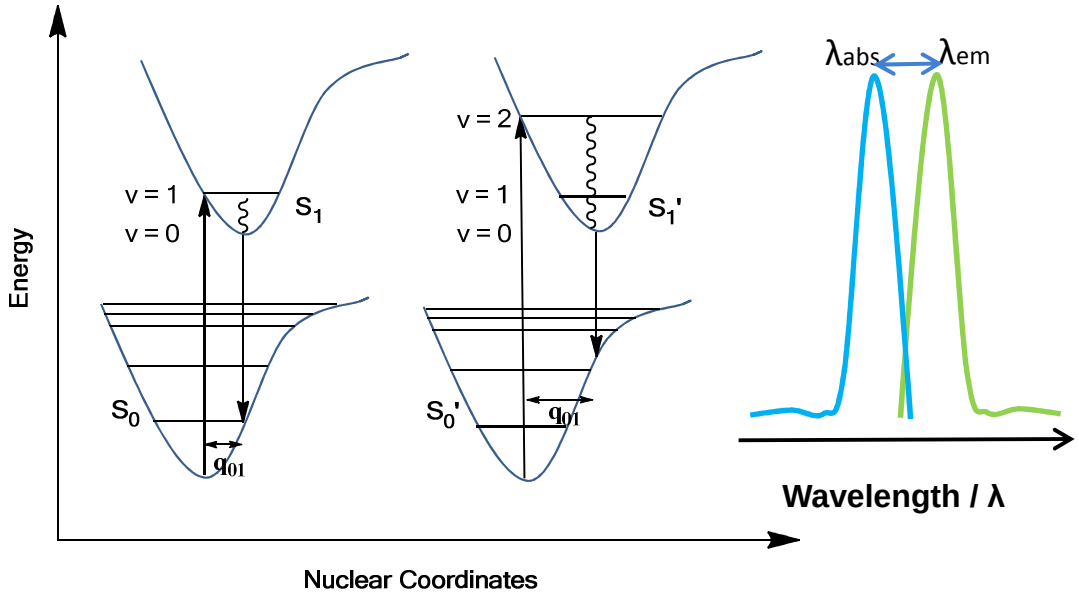

Figure 2 Frank-Condon energy diagram (left) where S_0 = ground state, S_1 = excited singlet state; v = vibronic energy levels and q_{01} = shift in the nuclear coordinates from S_0 to S_1; absorption – emission spectra (right) showing $\Delta_{(\lambda abs-\lambda em)}$ which also happens to be the SS for a compound.

The SS of a compound is a measure of the difference in energies between the absorption and emission of a species ($\Delta_{(\lambda abs-\lambda em)}$). When used as a sensor in-vivo fluorophores with large SS values are preferable. When there is more than one fluorophore (with a small SS) present in a sample the compound has a tendency to self-quench due to energy transfer processes between the individual molecules of dye.

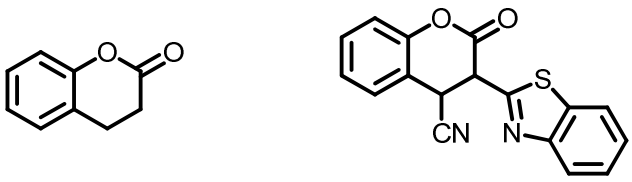

Figure 3 Basic structure of a coumarin compound (left), functionalised coumarin dye with a large SS.[18]

Compounds that are based on a coumarin substructure have been shown to have very large SS and are themselves useful fluorophores.[19,20,21] For a

compound to have a large SS, such as coumarin derivatives, it is important for the ground and emissive state structures to be very different.

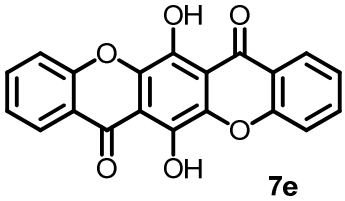

7e

Figure 4 The target compound 6,13-dihydroxy-chromeno- [2,3-b]xanthene-7,14-dione first prepared by Liebermann et al. in 1934.[22]

The discovery of new and innovative molecular dyes is important in advancing the fields of medical imaging. New dyes should ideally be highly fluorescent, easy to make in high yields, and in this case have a large SS.

The following chapter details attempts to synthesise a new class of dyes with a large SS. The inspiration for the work came when reviewing paint pigments synthesised at the beginning of the 20th century where terephthalic acid was substituted and cyclised to form 6,13-dihydroxy-chromeno- [2,3-b]xanthene-7,14-dione units. While the structures of the xanthene compound only bare a vague similarity to coumarin molecules, it was believed that, if fluorescent, there would likely be a large SS arising from any observed emission.

The overall flexibility of the synthesis of the xanthene compounds meant that a wide range of products was available. This would likely allow for control of both photochemical and electrochemical properties as well as the ability to easily synthesise complex compounds. Starting materials for the synthesis are both cheap and readily commercially available, as such the xanthene dyes seem like ideal candidates to pursue. Though the target compound had already been synthesised no photochemical measurements, or any other measurements, existed for these compounds with the exception of melting point values and elemental analysis.

2.2 Synthesis and Characterisation

2.2.1 Synthesis

The total synthesis of the 6,13-dihydroxy-chromeno-[2,3-b]xanthene-7,14-dione is shown in Scheme 1. The synthesis was adapted from the original 19th century prep which did need some modification, mostly on safety grounds and occasionally where modern methods were more efficient.[22, 23]

The 6 step synthesis starts with a simple addition-elimination reaction to introduce bromine to the commercially available diethyl-2,5-dihydroxyterephthalate starting material (Figure 5). Then during the recrystallization this intermediate is oxidised to the quinone analogue via the addition of HNO_3 in excellent yields (90%). After several attempts the procedure was modified increasing the equivalents of HNO_3 from 1 equivalent to 1.2 equivalents thereby enhancing the reaction yields upwards of 99%.

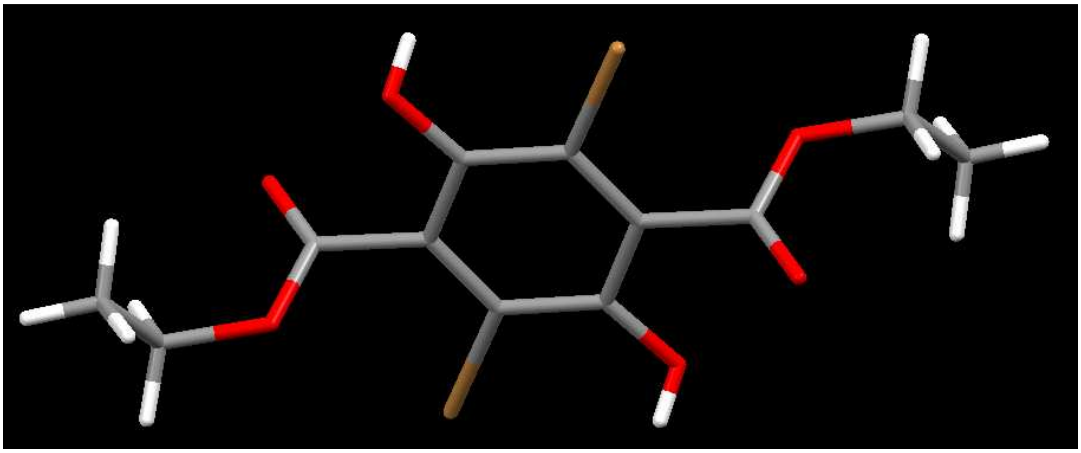

*Figure 5 The dibromohydroquinone intermediate (**2a**) formed after the addition of bromine to starting material **1**, this is subsequently oxidised via the addition HNO_3.*

The substitution of the bromine occurs via an electrophilic addition reaction with an aromatic alcohol to form **3**. The hydroxyl groups of the quinone promote inductive withdrawl facilitating the addition of bromine. Yields for the reactions varied between 66-99% (Table 1), where the excellent yields seen for **3a** and **3e** come when both ortho and meta positions are unsubstituted.

It should be noted at this stage that **3e** was the first compound which was bought through to **7e**, although the products across the synthesis from **5e**-**7e** had many solubility problems meaning that firstly characterisation was hindered, furthermore an insoluble dye cannot be subjected to photophysical

measurements. Indeed it proved that the only solvent capable of dissolving **7e** was nitro-benzene at reflux (211^{o}C) – not particularly pleasant conditions to use. It was thought that the insolubility was caused by the efficient π-stacking of the compound. As such **5e**-**7e** were not investigated any further, instead alternative structures were devised, with the emphasis firmly placed on the prevention of π-stacking in the final compound (**a**-**c**).

Compound	**3a**	**3b**	**3c**	**3d**	**3e**
Yield (%)	66	99	67	75	95

*Table 1 Percentage yields for reactions **3a**-**3e**.*

Depending on which aryl alcohol is used the resulting product varies in purity, forming either an oil or a solid, when worked up. The solid product precipitated during the work up gave a clean NMR spectrum meaning that there was no need for further purification. On the other hand if an oil was formed from the reaction then this was usually impure and often required purification via column chromatography, though this can wait until after the subsequent synthetic step.

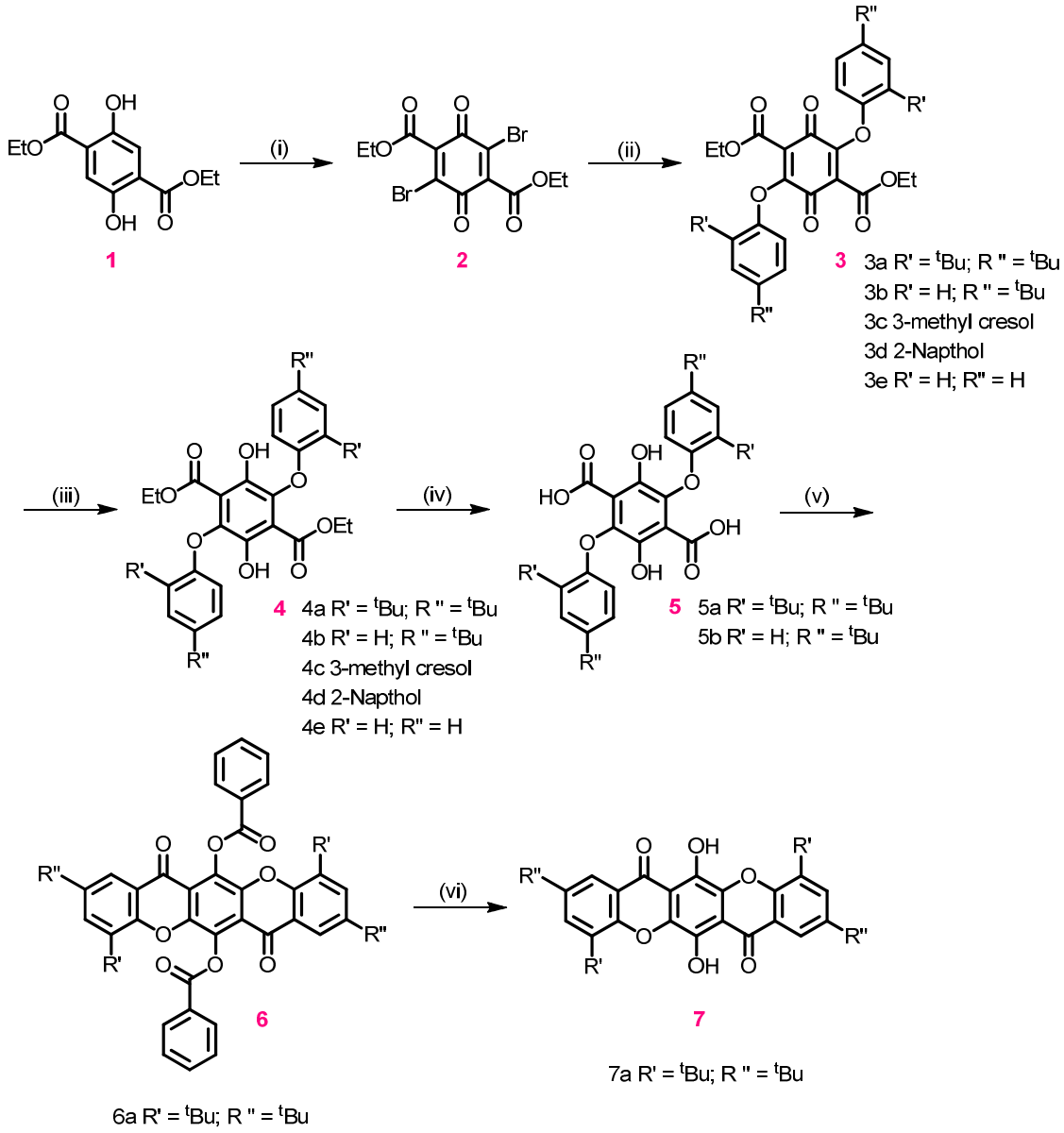

Scheme 1 The synthesis of 6,13-dihydroxy-chromeno-[2,3-b]xanthene-7,14-dione. (i)DCM, Br_2, HNO_3, >99%; (ii) acetone, pyridine, ArOH, Δ; (iii) Zn, AcOH, sonification; (iv) ***5a*** *EtOH, KOH; (iv)* ***5b*** *MeOH, NaOH; (v) Benzoyl chloride, H_2SO_4 cat., Δ; (vi) aniline, Δ.*

The reduction of the quinone to the hydroquinone was achieved using powdered zinc in acetic acid with the reaction agitated in an ultrasonic bath. In the case of some of the more heavily substituted produces i.e. **3a**, precipitation of the product occurs if left in the reaction mixture for a period after the sonication. This allows for the direct filtration of the zinc / product slurry without the need for a separation or further purification. After the filtration the slurry is washed with DCM which readily dissolves the product while leaving the zinc powder behind. For those compounds which did not crash out in the reaction

mixture, as well as those where the starting material was an oil, a separation is required, followed by column chromatography.

Regardless of the work-up method, yields for the reduction reaction typically approached unity, giving a green / yellow fluorescent solid, with the colour not varying in spite of the differing aryl attachments. Compound **4d** was designed to investigate whether increasing extent of the conjugation of the aryl-group causes any photophysical changes upon inclusion. As no obvious differences were observed between **4d** and other equivalent compounds, investigations involving **4d** were halted.

Once reduced the product underwent a carboxylation reaction to form **5**. This reaction was only performed on **4a** and **4b** as these were seen as the best candidates to take forward. The reaction to form **5**, saw varying success with the best yields for **4a** reaching only 25%.

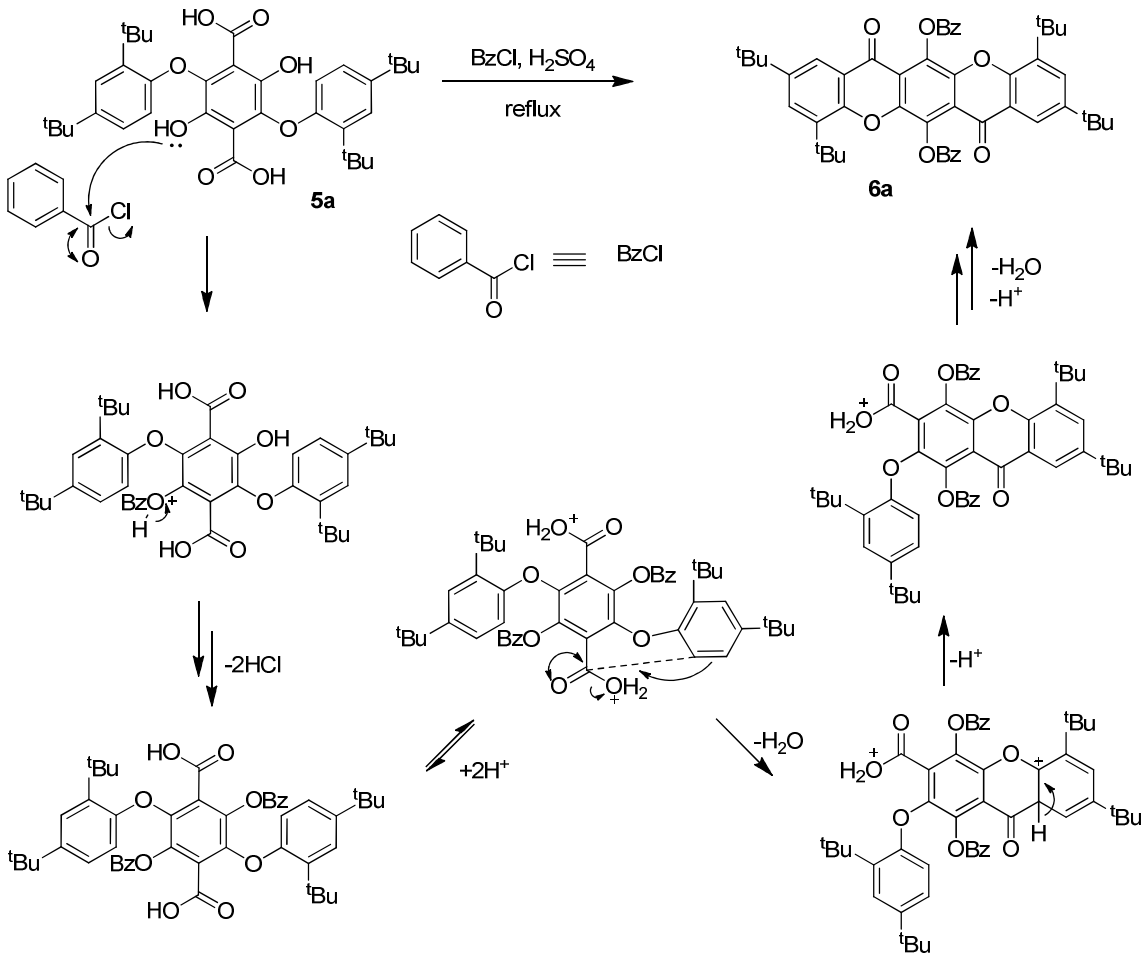

*Scheme 2 Protection of the hydroquinone core of **5a** followed by an intramolecular Friedel-Crafts reaction.*

With the proviso of attaining the most steric bulk possible only **5a** was taken forward through the final two reactions - the first of which was a Friedel-Crafts (FC) cyclisation reaction. The FC reaction was completed in good yields, on several separate occasions to give **6a**, a yellow solid.

The final reaction of the series is a basic deprotection of the benzoyl protected OH groups on **6a** to give **7a** in yields typically >99.9%. **7a** was a red crystalline solid which was readily soluble in a range of solvents, and which formed thin needle-like structures when recrystallized from ethanol. The total yield from **2** to **7a** was around 11.5%, while not ideal across 6 synthetic steps this value is acceptable. The improvement of step (iv) could see the total yield rise as much as four times, hence may be worth optimising.

Once the crystals of the pure compounds had been collected the samples were then subjected to a full characterisation including the following techniques: ^{1}H and ^{13}C NMR spectroscopy, mass spectrometry, melting points and infra-red spectrometry. The crystals themselves were also submitted for X-ray structural analysis. Such a comprehensive characterisation was performed as previously only the melting point and elemental analysis had been reporteed.

2.2.2 Characterisation

2.2.2.a NMR Characterisation

All ^{1}H NMR analysis for compounds **2**-**3** and **5**-**7** gave results which were unremarkable, while the proton NMR for compound **4a** was especially interesting.

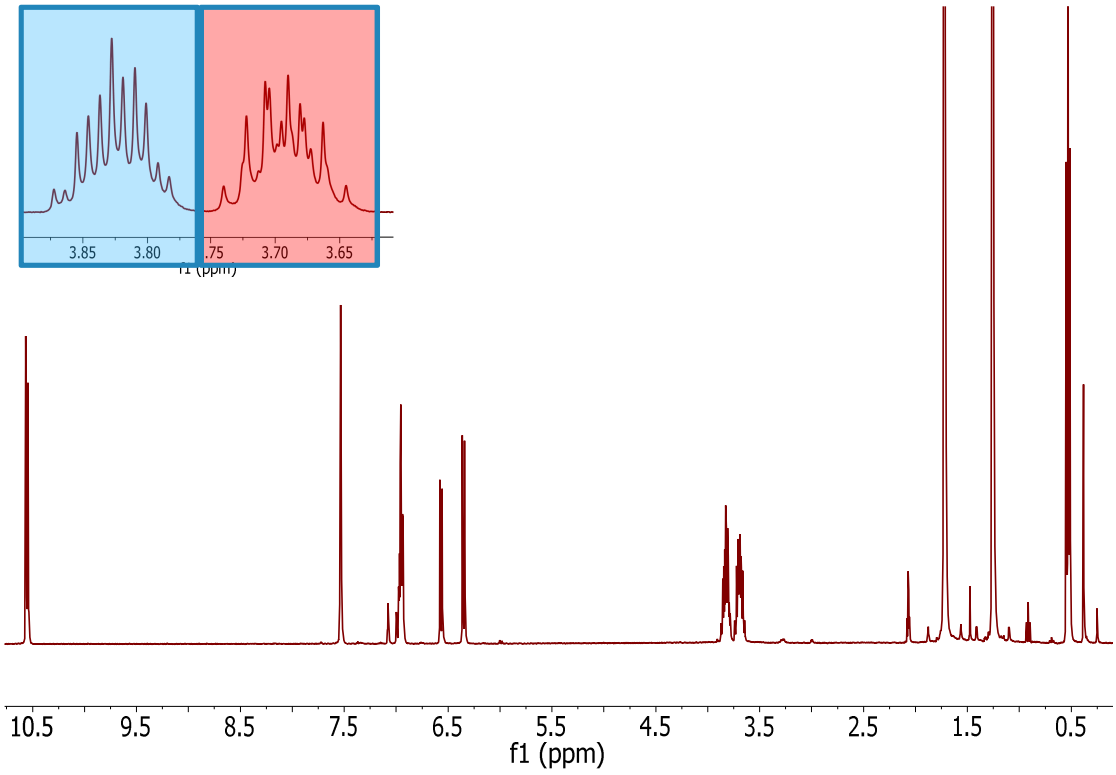

*Figure 6 The ^{1}H NMR spectrum of **4a**, with an expansion of the methylene protons (inset) detailing a complex splitting pattern owing to the inequivalence of the two methylene protons as well as revealing the presence of two isomers (A – Blue; B – Red).*

The proton NMR spectrum revealed that the two methylene protons, found on the ethyl ester moeity of the molecule, were in two different environments. These should typically form a quartet with intensity (i = 4H), instead isomers appeared each with two sets of doublets of quartets (i = 2H). This in turn means that the rotation of groups around the hydroquinone is hindered in **4a**. The hindrance is, likely bought about by the steric bulk of the tertiary butyl groups on the aryloxy section of the molecule, introduced in step (ii) of the synthesis. As a result of this steric bulk, two rotamers are formed in the compound with relative intensities of 1 : 0.8. The different rotamers will hence be referred to as isomers A and B.

Indeed the methylene protons are not the only indication of inequivalence at the ethyl group of the ester. The CH_3 next to the methylene protons, which under normal circumstances would be a triplet, is instead found to be two triplets (Figure 7).

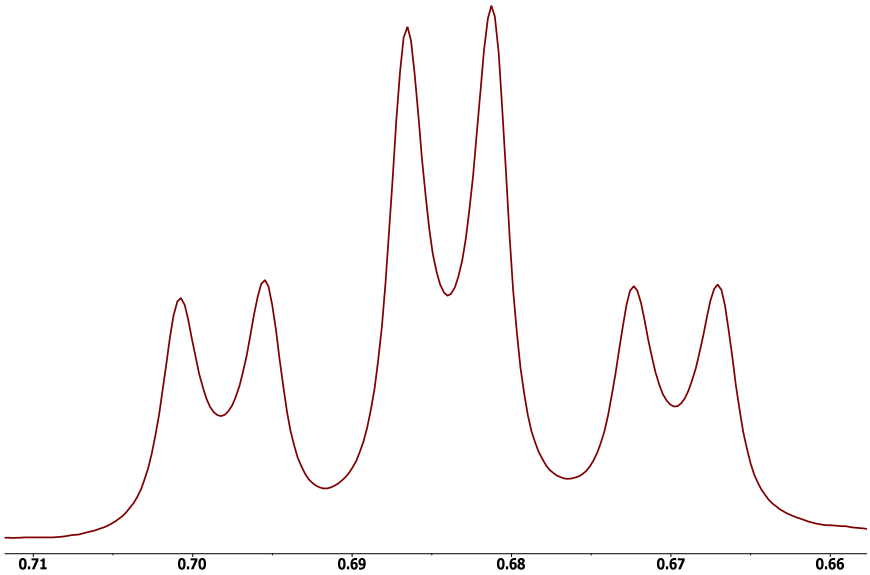

*Figure 7 ^1H NMR spectrum of the ethyl CH_3 groups of **4a** resulting from the inequivalence found in the molecule. Here two triplets exist with ratios or ca. 1 : 0.8.*

The peaks due to the butyl-CH_3 protons are 4 singlets (Figure 8). Comparison of these peaks in the proton NMR s run at different spectrometer frequencies confirms that these are singlets and not doublets.

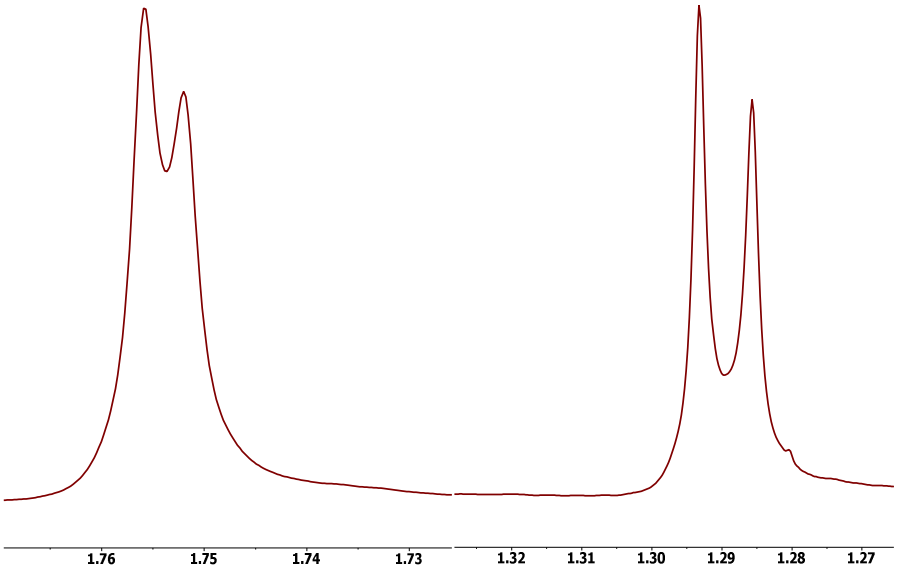

*Figure 8 Ortho and para methyl groups of **4a**, which shows the presence of two different isomers which have an intensity ratio of 1 : 0.8 as with the triplets seen in Figure 7.*

Isomer A has peaks at 1.282 and 1.745 ppm (due to para and ortho ^{t}butyl groups respectively) and Isomer B at 1.275 and 1.741 ppm (due to para and ortho ^{t}butyl groups respectively).

The complicated multiplets, seen inset in Figure 6, around 3.7 and 3.85 ppm (due to OCH_2CH_3) can be simplified by selective decoupling of the triplet at 0.55 ppm (Figure 9).

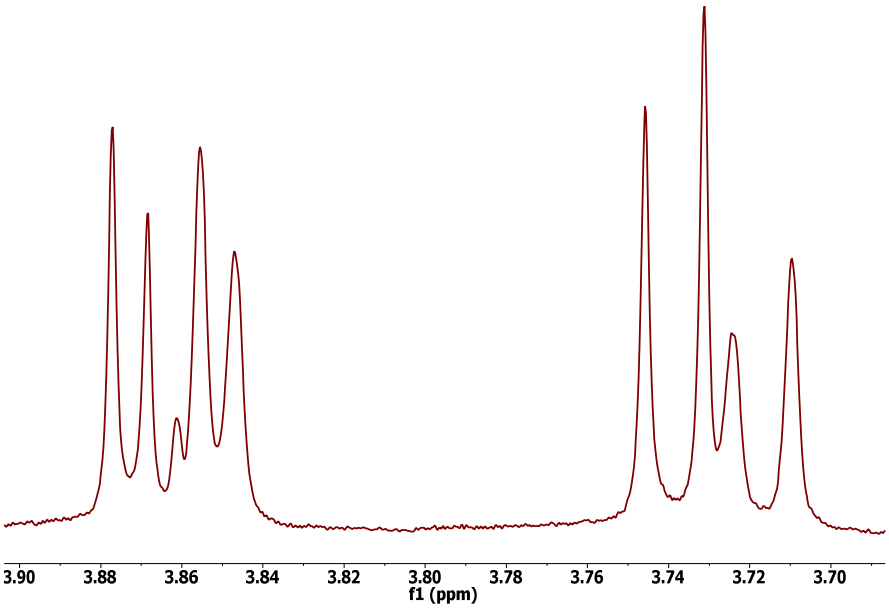

Figure 9 Selectively decoupled ^{1}H NMR spectrum showing doublets due to the methylene protons of the OCH_2CH_3 ester group forming two doublet of doublets.

Upon decoupling of the CH_3 protons the peaks appear as two doublets for each isomer (a small impurity is present at 3.845 ppm).

Two doublets at 3.704 and 3.850 ppm with $^2J_{HH}$ = 10.95 Hz due to Isomer A

Two doublets at 3.719 and 3.842 ppm with $^2J_{HH}$ = 10.76 Hz due to Isomer B

The splitting of these CH_2 groups into doublets confirms the inequivalence of the methylene protons. To ratify that the interpretations of the splitting were accurate a simulated spectra was produced (Figure 10). The simulated spectra confirmed that the two methylene protons were indeed inequivalent.

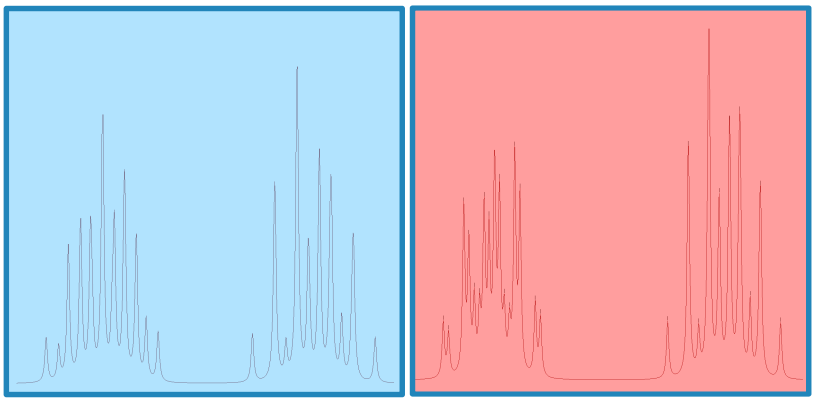

*Figure 10 The simulated spectra showing the splitting of the methylene protons of **4a**, in toluene (left, blue) and d_{10}-o-xylene (right, red).*

The aromatic region of the spectra is also complicated by the presence of the two rotamers. That said it is possible to identify both sets of peaks for each isomer and as a result the associated coupling constants. Figure 11 shows the assignments of both sets of aryl protons along with their coupling constants.

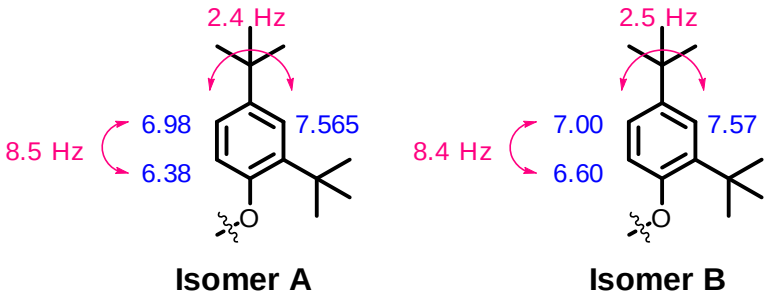

*Figure 11 The assignments of shifts (**blue**) and coupling constants (**pink**) of the aromatic protons of both isomers of **4a**.*

As mentioned before it is the steric restraints which exist that give rise to the two rotamers. A high temperature variable temperature ^{1}H NMR (VT) study was performed in order to establish if there is a thermal barrier which could be overcome. The initial VT study was performed in toluene with measurements

taking place up to 100 ^{o}C, but in this solvent the full coalescence of both sets of peaks was not observed. Due to this *o*-xylene was instead used (b.p = 144 ^{o}C), this allowed a temperature range of -50 to 140 ^{o}C.

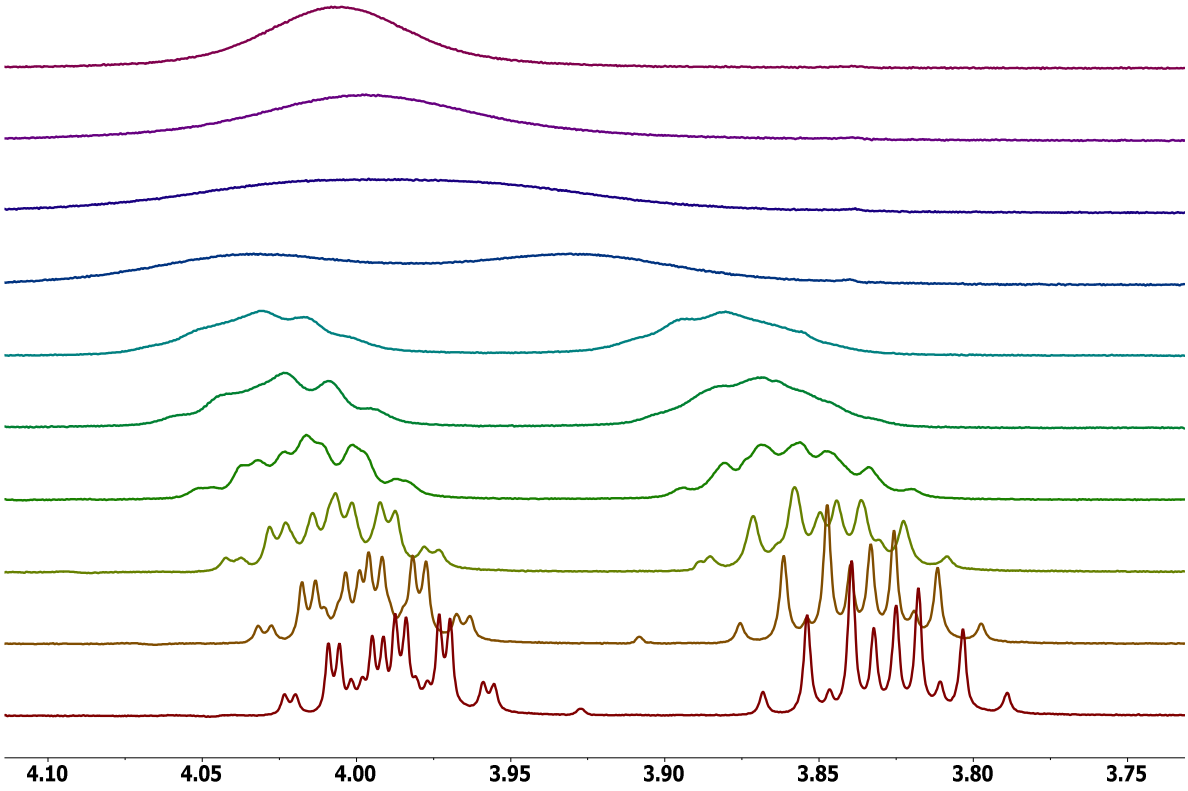

*Figure 12 ^{1}H VT stacked spectra of **4a** detailing the CH_2 region. N.B. the NMR was performed in d_{10}-o-xylene hence the splitting pattern is slightly different than that seen in the simulated spectra. Temperature increases from the bottom trace upwards from 23 to 100 ^{o}C in 20 ^{o}C steps, from this point the temperature increases in 10 ^{o}C steps with the last two measurements taken at 135 and 140 ^{o}C. The whole ^{1}H NMR spectrum can be seen in the experimental section for **4a**.*

It was found that on heating the sample over this range, coalescence was observed in several regions of the spectrum. Once coalescence was observed the sample was allowed to cool and a final measurement was performed at room temperature where the original spectra was observed once again. There exist two exchange processes within the system: the intramolecular exchange of the two CH_2 protons and intramolecular exchange between the two rotamers. To calculate the rate of exchange both of these values must be taken into account.

$k = Ae^{(-E_A/k_bT)}$	$ln\,(k) = -E_A/RT + ln\,(A)$

Equation 1 The Arrhenius equation (left) and the natural log of the Arrhenius equation (right). A – Pre-exponential factor, k – rate constant, E_A – energy of activation, R – gas constant, k_b – Boltzmann constant and T – temperature in Kelvin.

The least-squares fitting of the rates of exchange was plotted, Figure 13. From this plot the activation energy for the system has been calculated from the Arrhenius equation to be 57.6 kJmol^{-1}. This value is surprisingly high showing exchange processes demonstrate a high dependence on temperature. The temperature dependence was seen to be Arrhenius-like giving a straight line from the plot.

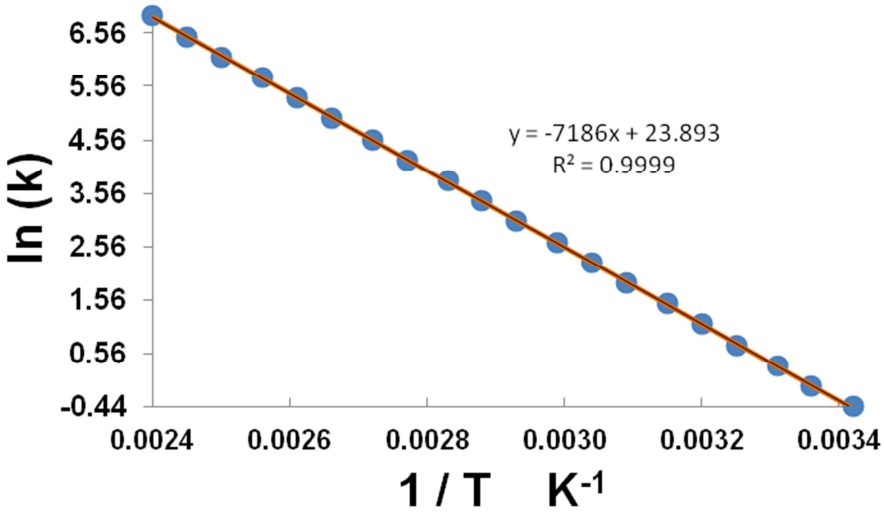

*Figure 13 Arrhenius plot for **4a** in d_{10}-o-xylene, which signals the activation energy required to bring about full rotation of the aryloxy moieties. Where T – temperature and k – rate constant of coalescence.*

The $^{13}C\{^1H\}$ NMR spectrum of **4a** in d_8-toluene is also made more complex by the presence of the two rotamers. That said the impact of the chemical shifts is less pronounced in the ^{13}C NMR spectrum with none of the shift differences for the two isomers varying by ca. 0.04 ppm, making it hard to identify the two isomers. The two isomers can best be seen on spectrometers with larger field strengths, though even in this instance differentiation between the two is difficult to observe.

2.2.2.b X-Ray Crystal Structure Analysis

All compounds were also subjected to an X-Ray crystal structure determination. Though most equivalent compounds gave rise to similar X-ray structures, hence

the following structures will be discussed: **2**, **2a**, **3a**-**7a,** with the exception of **6a** as sufficiently pure crystals of the material could not be grown.

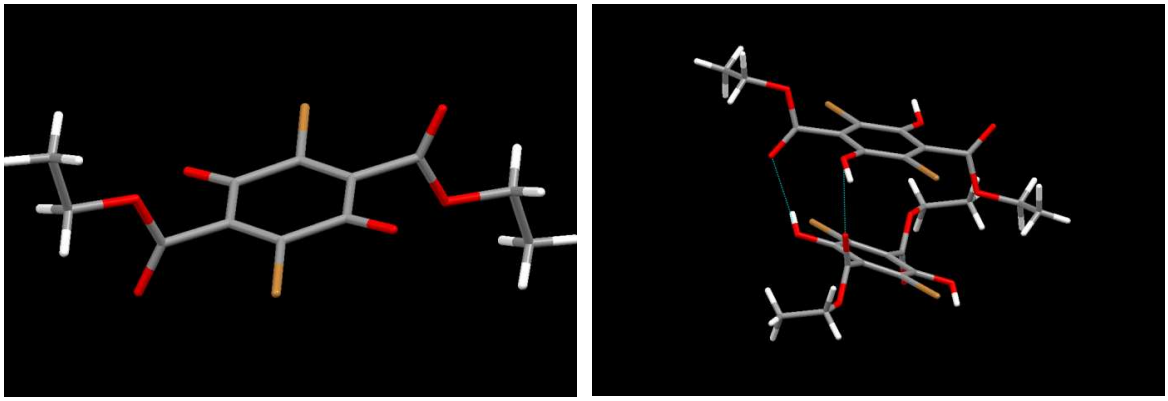

*Figure 14 The crystal structure of **2** (left) shows the two ethyl groups in an anti conformation and has no disorder. The crystal structure for **2a** (right) contains two molecules, the presence of hydroxyl groups should also be noted as it is this reason that HNO_3 is needed – in order to oxidise **2a** to **2**.*

The crystal structures for the series of compounds help to reveal the likely hydrogen bonding networks which exists within the systems. A lot of the hydrogen bonding that is present is related directly to the changes in the quinone / hydroquinone core of the system.

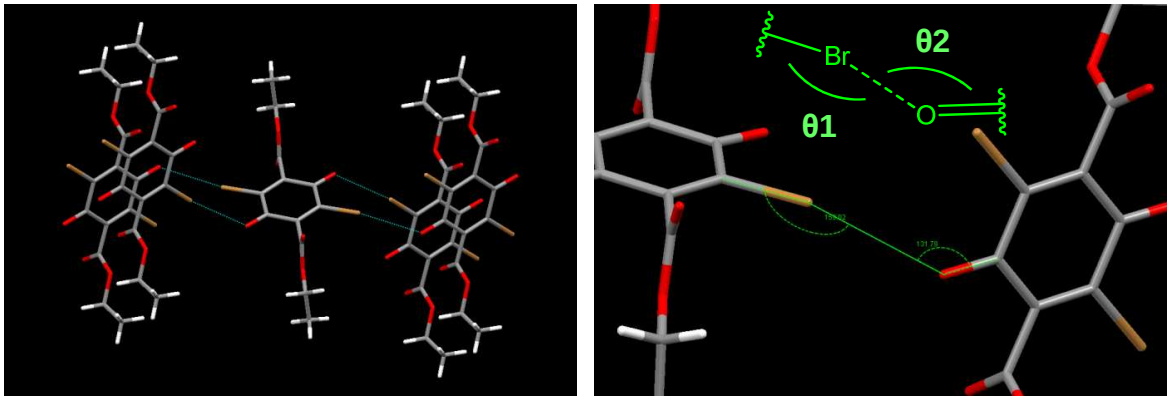

*Figure 15 Crystal packing diagram of **2** (left) that gives evidence of halogen bonding between the two bromine atoms and the oxygen atoms of the quinone core of other molecules within the crystal lattice. The halogen bonding angles (θ1 and θ2 – given in Table 2) for **2** clarified (right).*

For **2** molecular interactions observed between the carbonyl groups of the quinone and the electropositive bromine atoms are halogen bonds. The bond angles and bond length are typical of those found in halogen bonds and not consistent with those seen for hydrogen bonds.[24]

	Bond Length	θ1	θ2
2	3.11 Å	159^{o}	131^{o}
Typical values	3.15 Å [a]	154^{ob}	126^{o} [b]

Table 2 Bond length and angles associated with the halogen bonding. [a] *S.D. ± 0.2 Å* [b] *S.D. ± 2.5*^{o}

It is clear from a comparison between **2** and **2a** that the intermediate dibromohydroquinone has no such halogen bonding networks, with the system reverting to hydrogen bonding between the hydroxy and ester carbonyl groups. Interestingly in the case of **2a** the hydrogen bonging is intermolecular, whereas in all other systems where there is both hydroxy and ester carbonyl groups available bonding is found to be exclusively intramolecular.

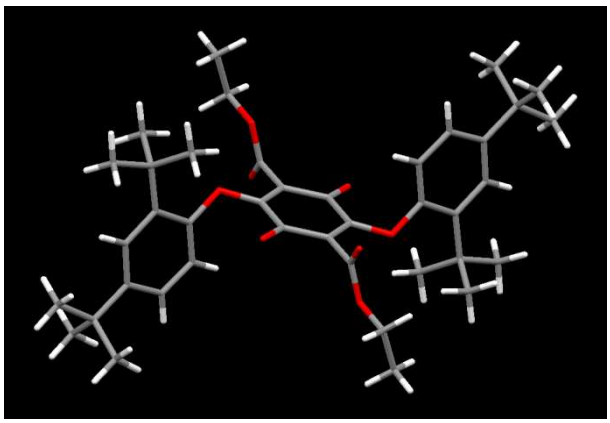

*Figure 16 Crystal structure of **3a** with both ethyl ester and aryloxy groups in an anti-conformation to each other.*

Unsurprisingly for compound **3a** there are no significant weak interactions. The substitution of bromine for the aryl alcohol stops halogen bonding, and with no hydroxy groups present there is no hydrogen bonding either. There is an inversion centre found at the centre of the quinone group which suggest uniformity between the orientation of the two aryloxy substituents. The aryloxy groups themselves adopt an anti-conformation to minimise their energy. It is possible that the presence of the tertiary-butyl groups prevents the free rotation of the aryloxy unit.

The lack of hydrogen bonding in **3a** is very important as it would seem that the introduction of hydrogen bonding, brought about by the reduction of the quinone core, causes the inequivalence seen in the proton NMR spectrum of **4a**.

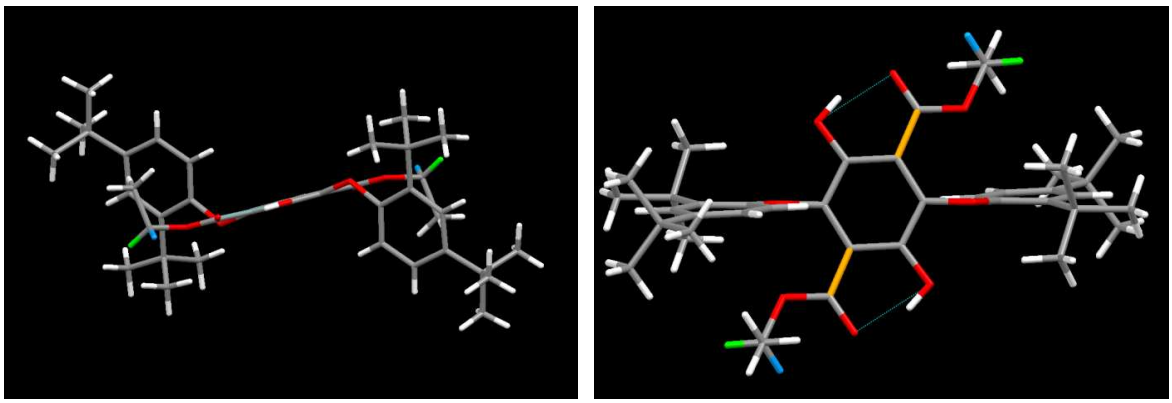

*Figure 17 Crystal structure of **4a** showing the molecule through the plane of the hydroquinone (right) and the molecule from above the hydroquinone. The two methylene protons have been coloured to depict their inequivalence.*

The hydrogen bond visibly changes the orientation of the ester group thereby preventing rotation around the bond connecting the ester with the hydroquinone (shown in orange in Figure 17– right). The system as a whole is more rigid with the hydrogen bonding bringing about the formation of pseudo 6-membered rings at either end of the hydroquinone. The increased rigidity of the system means that the first bond which can undergo free rotation is the O**C-O**CH_2 bond of the ester. It is likely that the full rotation of this bond is heavily restricted by the bulky aryloxy group. As such it is easy to see how both sets of methylene protons are inequivalent to each other. To that end the splitting of the methylene protons, which is observed in the ^{1}H NMR spectrum, is understandable. What is particularly ambiguous is the presence of two isomers in the ^{1}H NMR spectrum and lack there of in the crystal structure. The uniformity which is adopted in the crystal structure is absolute with each molecule appearing in an anti-conformation and no disorder in evidence.

Indeed the identity of the other isomer is not clear. Multiple crystals were examined in order to see whether there was a second isomer present and each measurement resulted in the same structure. It should also be noted that all NMR spectroscopic measurements were carried out on crystals of the compound as well as the precipitate to establish whether the crystallisation process was somehow resulting in crystals of only one isomer. In spite of the large barrier to rotation it is feasible that the molecule shifts to a single isomer upon crystallisation. There was no difference seen in the proton NMR measurements before and after crystallisation of **4a**. Further investigation as to the identity of the two isomers is discussed at a later point.

The unit cell has an inversion centre at the centre of the hydroquinone, similar to that seen for **3a**, a C2 axis and a glide plane, meaning that **4a** has more symmetry than that seen for **3a**. The aryloxy groups both sit out of the plane of the hydroquinone core by 11.5^{o} which is due to the bulk of the ortho-^{t}butyl groups.

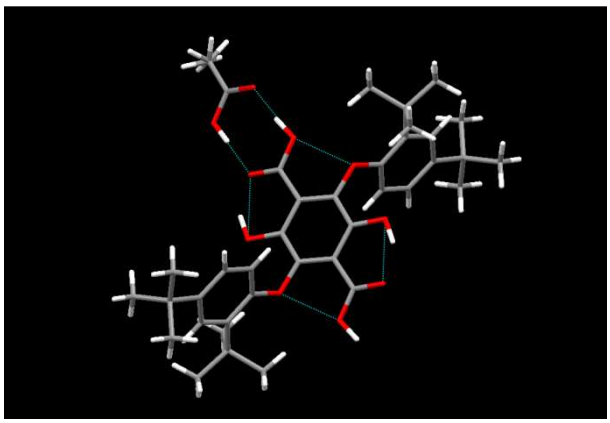

*Figure 18 The X-Ray crystal structure of **5a** has a molecule of acetic acid which associates with the newly formed carboxylate group.*

The presence of a carboxylic acid group in place of the ethyl ester removed all traces of two isomers seen for **4a**, again suggesting that the steric bulk present in the ortho position of the aryloxy substituent created a barrier to rotation. The hydrogen bonding observed between the carbonyl oxygen and the hydroxyl group in **4a** was also present in **5a**. Additional hydrogen bonding was also observed between the oxygen of the aryloxy group and the carboxylic O-H. Also present in the unit cell was a molecule of acetic acid resulting from the recrystallization, which was performed in acetic acid.

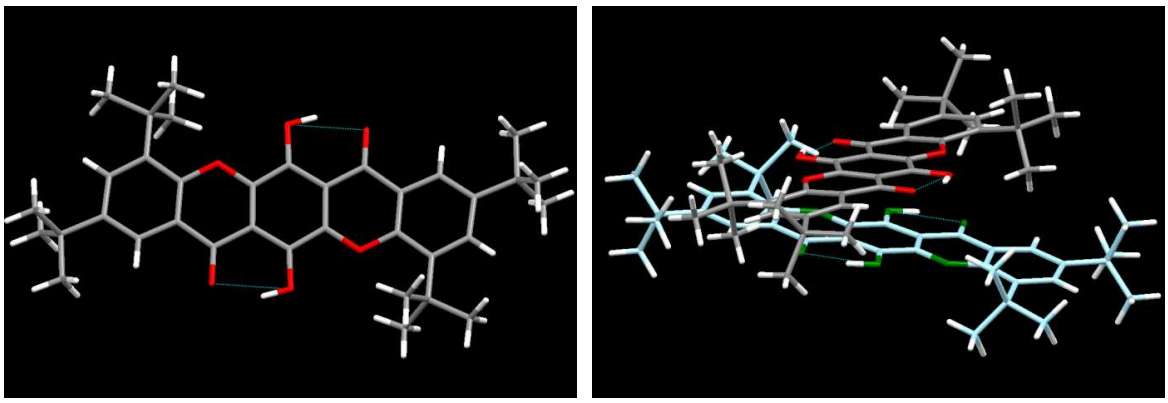

*Figure 19 X-Ray crystal structure of **7a** (left), unit cell for **7a** (right) with one of the two compounds discoloured for clarity. When viewed from above the crystal packing diagram forms a 'T' shape which likely results from π-stacking between the two compounds.*

Though **7e** did not form crystals which were good enough to measure the molecule likely had the same flat core as seen for **7a**. Without the steric bulk bought about by the presence of the ^{t}butyl groups it is easy to see how the individual molecules would have π-stacked thereby making **7e** all but insoluble. Indeed there is some evidence that there is still some π-stacking in **7a**, where the unit cell shows two molecules, slightly offset, criss-crossing over each other to form a 't' shaped dimer. The distance between the two molecules is around 3.6 Å, which is well within the limits of π-stacking. [25]

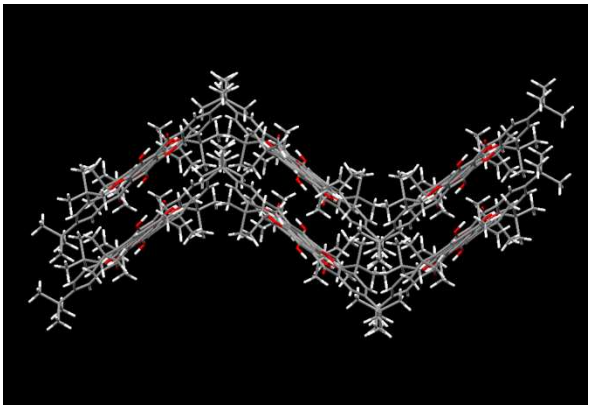

*Figure 20 Crystal packing diagram for **7a** that shows the molecules forming a 'lightening' shaped packing motif.*

There is no intermolecular hydrogen bonding observed in the crystal packing, though there does appear to be some association between some of the C(**CH$_3$**)$_3$ groups and the phenyl ring of the aryloxy substituent.

2.2.2.c Infrared, Mass Spectral and Melting Point Analysis

All Infrared (IR) spectra for the compounds produced similar values, with the carbonyl stretches usually dominating the spectra. The IR spectrum of **7a** was helpful in determining its subsequent oxidation to form **7ox**, with the disappearance of the dominant O-H stretch demonstrating a successful oxidation.

The mass spectra of the compounds mostly showed an [M^{+}] peak where expected. Compounds that contained elements with major isotopes, such as bromine, demonstrated the appropriate isotopic patterns. The exception to this was for the derivatives of compound **4** which all showed the [M-H] mass peak.

Most melting point measurements gave narrow ranges with the exception of the majority of **3** having melting points over 250^{o}C which was the above limit of the equipment.

2.3 Further Investigation of the Barrier to Rotation of Compound 4

2.3.1 Computational Models

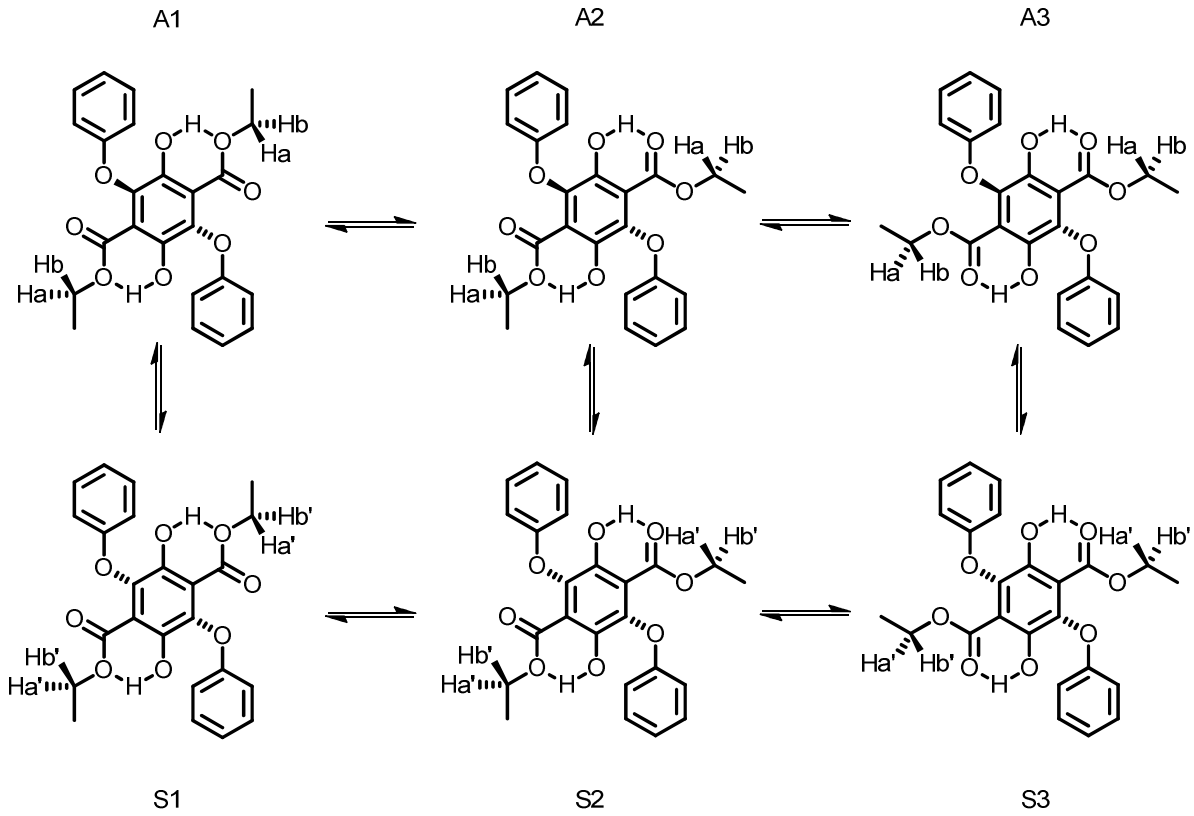

*Figure 21 Possible conformations for **4a** depending on the 'Up-Up' (Syn) and 'Up-Down' (Anti) arrangement of the two aryl groups and the site for intramolecular hydrogen bonding to the ester. The ^{t}butyl groups have been removed for clarity. S = syn and A = anti; for S1 and S3 there is a C2 rotation axis, and for A1 and A3 there is an inversion centre. Both symmetry elements can be found at the centre of the hydroquinone ring.*

One possible explanation for the presence of two isomers is detailed in Figure 21, whereby there exists an exchange process between anti and syn conformations. The switch between anti and syn conformers can be bought about by the breaking of the hydrogen bonding network in the system. This break theoretically would allow the ester group to 'swing' away from the aryloxy group thereby allowing the aryloxy moiety to rotate as the steric inhibition has been removed. That said there is no direct evidence that the proposed exchange reveals the identity of the other isomer as being the syn conformer. Taking the size of the E_A into account one would expect that there would be some evidence of the syn isomer within the crystal structure. The lack of syn isomer in the crystal structure seems to suggest that upon crystallisation there

is some pathway whereby the molecule reorganises to form the anti isomer exclusively, which presumably is the lowest energy form.

There is a difference in the symmetry elements within each of the conformers. While anti has a C2 rotation access located in the centre of the hydroquinone ring, the syn conformation has an inversion centre located in the same position.

To further investigate the barrier to rotation a computational model was analysed to ascertain the relative energetics of **4a**. Initially the structure was subject to a simple MM2 calculation, from here the resulting molecule was forced into both syn and anti-conformations. Once the two conformations had been set up they were then used as starting points for a DFT calculation using B3LYP and the 6-311G++ basis set using the Gaussian 3 program.[26]

It was firstly recognised that the determined X-Ray structure appeared not to be the true energy minimised structure. Indeed strangely the calculations appeared to show that the syn conformer was ca. 5 kJ mol $^{-1}$ more energetically favourable than the anti-conformer. It would be expected that, in a syn conformer, the steric bulk of one aryloxy group would clash with the other thereby causing the syn conformation to be less favourable energetically, hence the computational results are surprising.

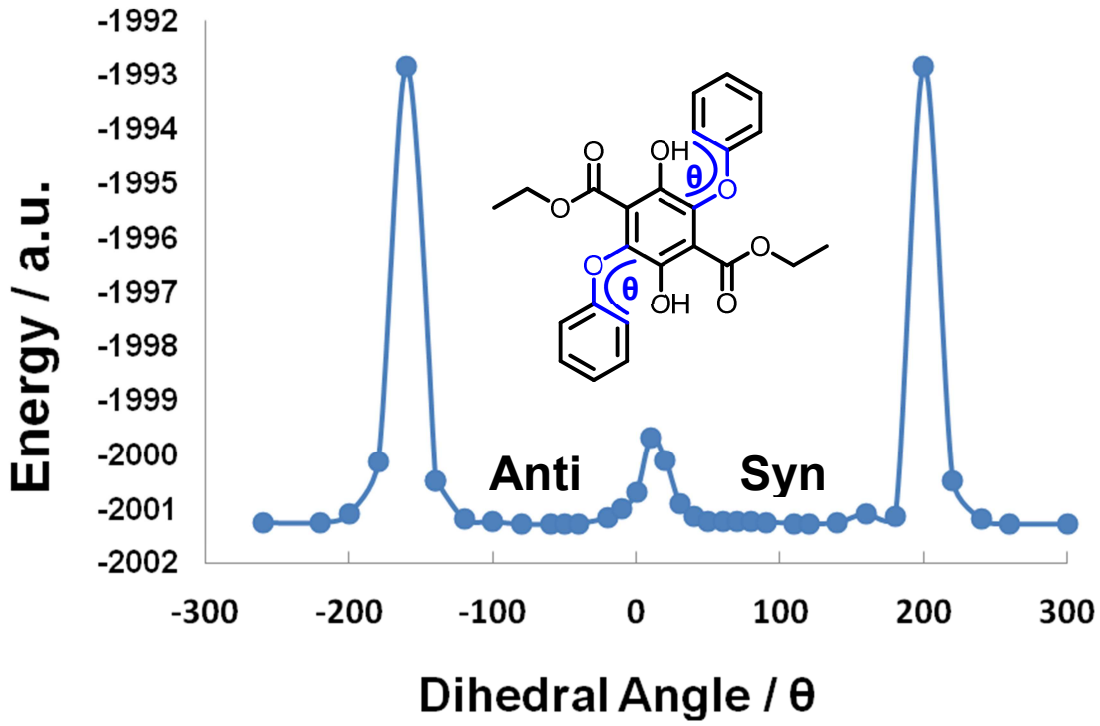

*Figure 22 Calculated energies of the anti and syn conformers for **4a** when the angle is θ changed. The two t-butyl groups on the aryloxy moiety omitted in order to aid clarity.*

In total there were 3 energy-minimised structures which could be identified (Figure 23). For the two lowest energy structures it is possible to see the same hydrogen bonding pattern that is seen in the terephthalate site in the crystal structure of **4a**. The study also suggests that the bulk of the ^{t}butyl group, in combination with the hydrogen bonding and the presence of the ethyl ester, restricted free rotation around the terephthalate core – which ties in with the information rendered from the NMR experiments.

As well as the two aforementioned conformations a third energy minimised structure was highlighted, where the hydrogen bonding in one of the two pseudo-6-membered rings had been broken thus allowing the ester to rotate out of plane with the terephthalate core. The calculated energy for this particular conformer is around 21-25 kJmol^{-1} less stable than the syn and anti-forms and most likely resembles a structure which may be found on the potential energy surface – sitting somewhere in between the anti and syn forms of the molecule.

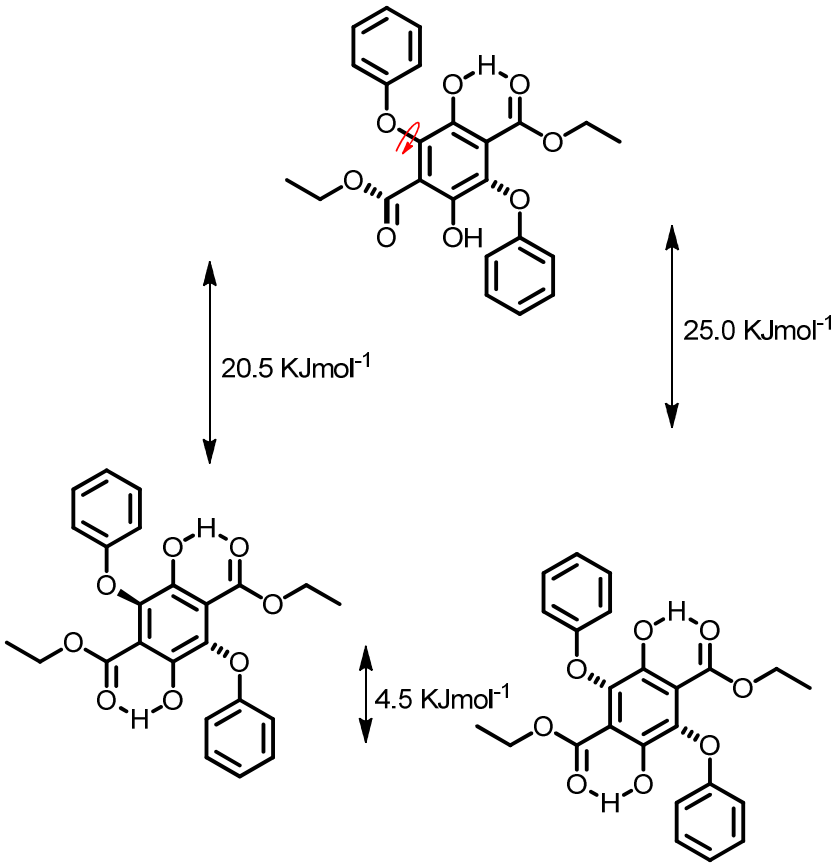

*Figure 23 Computer calculated energy-minimized structures for **4a** using B3LYP and the 6-311G^{++} basis set. NB ^{t}butyl groups have been removed for clarity.*

2.3.2 Subsequent Synthesis of Compounds with Varying Composition of the Ortho-Phenolic Substituent

A further study was carried out in order to determine more of the parameters which lead to restricted rotation around the terephthalate core. Specifically whether there was a size or position of substituent which might lead to the restrictions, and whether the type of group could be varied.

Compound	8	9	10	11	12	13	14	15	16	17
Yield	75	79	54	84	59	91	55	52	52	85

*Table 3 Percentage yields for compounds **8** – **17**, with higher values found where compounds contain no ortho-groups.*

In order to further assess the barrier to rotation a series of further compounds were made. The synthesis of the compounds did not vary much from the described synthetic route used to get to **4**. The yields across the series fell in-or-around those seen for compounds **4a**-**e**, though in the case of **8**-**17** none of the syntheses were optimised.

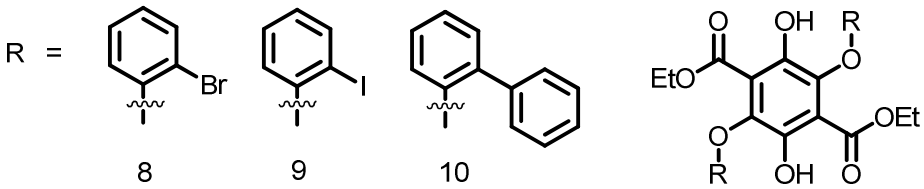

8 9 10

*Series 1 Initial attempts to find groups which caused restricted rotation leading to the presence of two isomers resulted in compounds **8**, **9**, and **10**.*

The first compound to be made was **10**, where an ortho-phenyl group had been introduced onto the aryloxy group. While increasing the steric bulk at the ortho position it was also thought that the extra conjugation might exert some influence over the photophysics of the molecule.

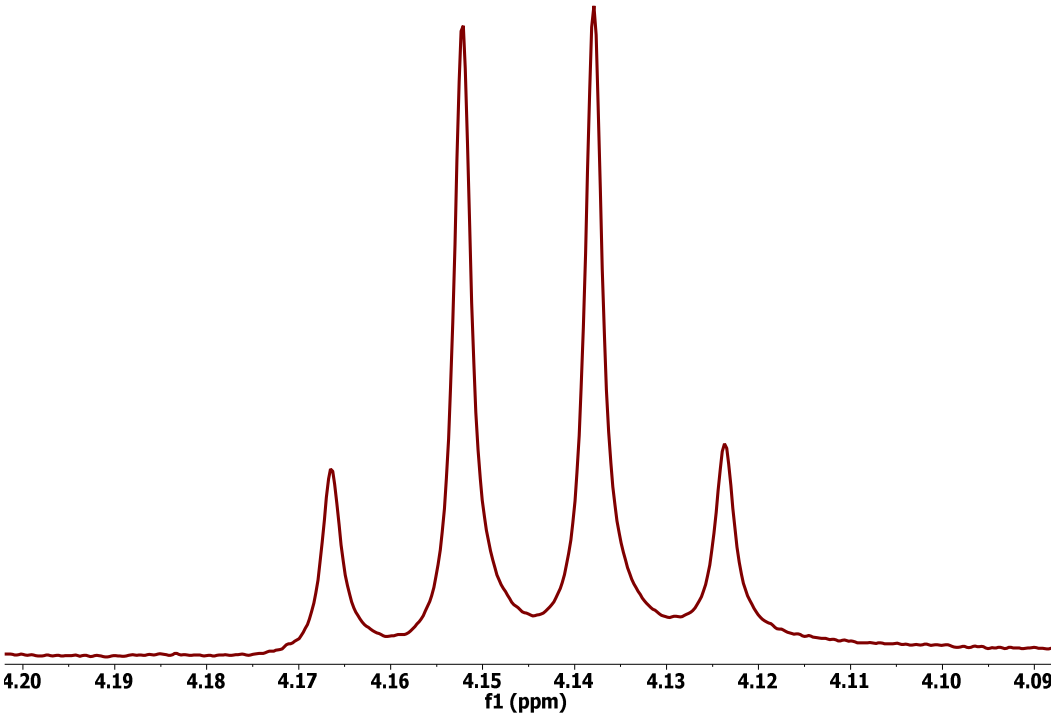

*Figure 24 ^{1}H NMR spectrum of **10** with a zoomed in section detailing the methylene protons (inset).*

The proton NMR spectrum revealed that there were not two conformers present for **10**, nor was there any evidence that the methylene protons were inequivalent. In the case of **10** it is thought that the flat ortho-phenyl group could simply rotate 90^{o} thereby allowing the rotation of the ethyl ester and aryloxy groups. Note that a phenyl group is around the same bulk in two dimensions as a ^{t}butyl group, yet the latter is much larger in the seemingly all important third dimension.

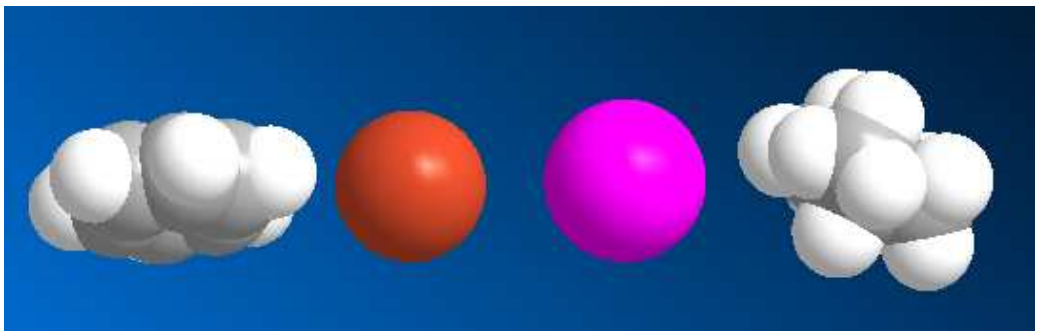

Figure 25 The approximated relative size of benzene, atomic bromine, atomic iodine and 2-methylpropane.

As seen in Figure 25, the size of the bromine, iodine and ^{t}butyl groups increases from left to right, importantly the increase is over each of the three dimensions. Benzene on the other hand, while larger than both atomic bromine and iodine, is flat therefore does not occupy as much space in the third dimension. As such it was hoped that the halogen series might exhibit similar conformations to those seen for **4a**. By replacing the ^{t}butyl group with a halogen series it will also be possible to increase the size of the ortho-substituent in a stepwise manner, while also producing a product which could take advantage of cross coupling reactions to expand off the aryloxy moiety at a subsequent stage.

Proton NMR spectra of compound **8** showed no sign of isotopic splitting of any proton traces within the compound, hence the chlorine derivative was not investigated. Surprisingly the same observations were also made for compound **9**. It seems that the even the steric bulk which is imposed by an iodine atom is not enough to successfully restrict rotation.

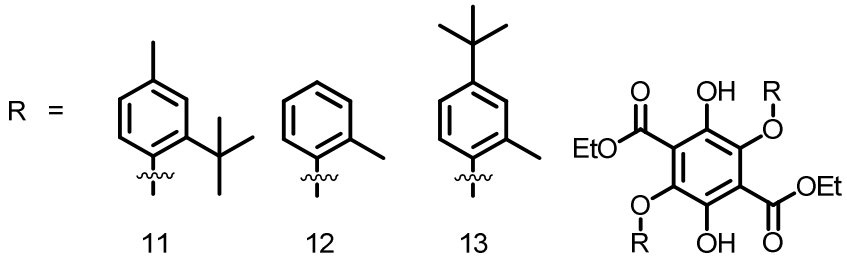

*Series 2 Compounds **11**, **12** and **13** were created to explore whether there is a relationship between bulk in the para-position and the formation of the two conformers.*

Since there was also steric bulk present at the para position of **4a** it was considered prudent to prove that the presence of this bulk did not have an effect on the creation of conformers. While compound **11** has the same steric bulk at

the ortho position as **4a**, it has less steric bulk at the para position. In this instance there is splitting of the methylene protons of **11**.

Compound **12** has little bulk around the aryloxy group, while **13** has dramatically more sterics located at the para position. For both compounds there are no observed conformers showing that steric bulk in the para position has no influence over the restricted rotation seen for compounds such as **11**, hence only bulk at the ortho position can cause CH_2 inequivalence and the presence of isomers.

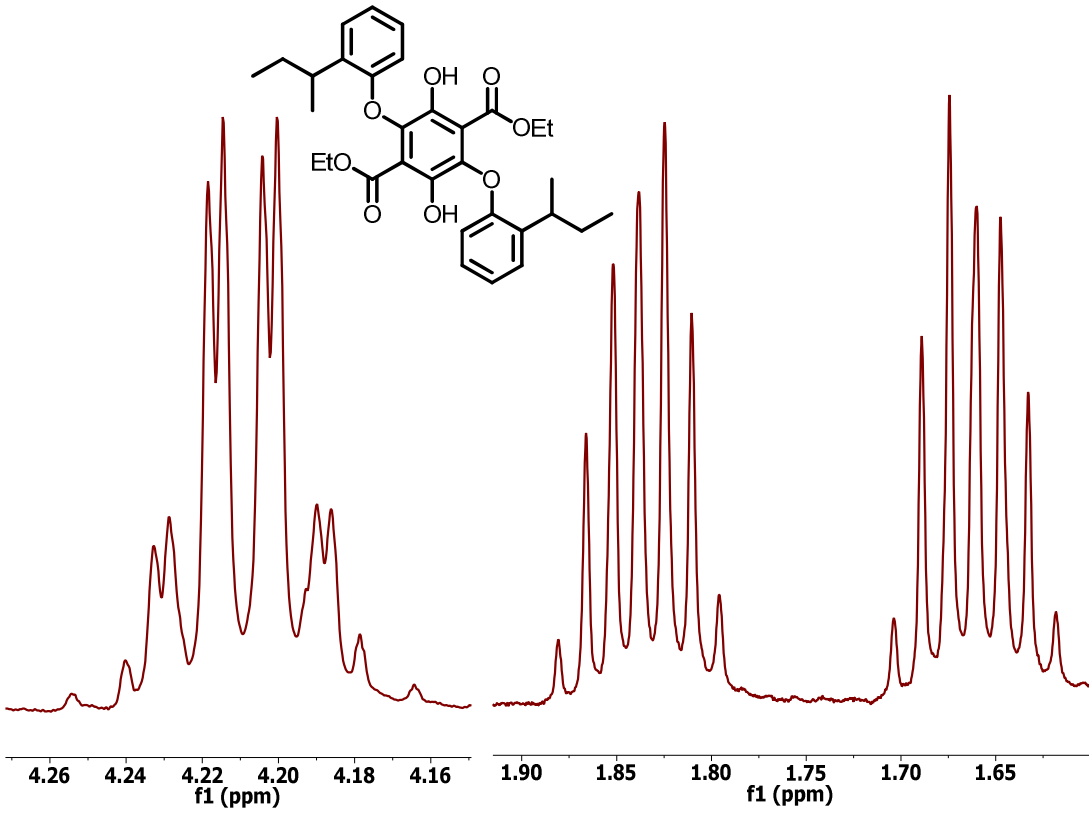

*Figure 26 Compound **14** (inset) and the methylene region of the ^1H NMR of **14** (left) and the CH_2 protons of the sec-butyl group (right).*

The introduction of a 2-sec-butylphenol group was the first result which also showed the presence of two isomers. In this case the 2-sec-butyl group represents a step down in 3 dimensional size relative to ^{t}butyl. The splitting of the two methylene protons was less pronounced than that seen for the ortho-^{t}Bu containing aromatic groups. The observed splitting pattern also differs from that of the ortho-^{t}butyl group, with the sec-butyl splitting resembling two quartets – though the pattern is likely more complex.

The methylene protons of the sec-butyl group were themselves split into two multiplets -most likely two doublet of pentets. The two sets of splitting seen at

4.21 ppm and 1.85-1.65 ppm (Figure 26) confirmed that 2-sec-butyl was large enough to restrict free rotation and create two isomers.

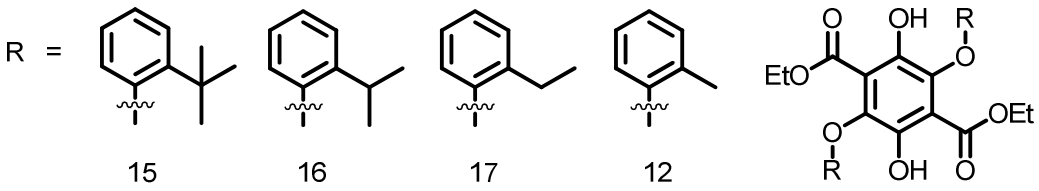

*Series 3 Compounds **15**, **16**, **17** and **12** in order of decreasing bulk at the ortho position.*

Since it had been shown that ^{t}butyl groups restrict aryloxy rotation and that ortho-methyl groups create no such hindrance, there might be an effect observed when the steric bulk is stripped from a ^{t}butyl group in stages. Series 3 shows the transition from ^{t}butyl (**15**) to methyl (**12**) via stepwise removal methyl groups.

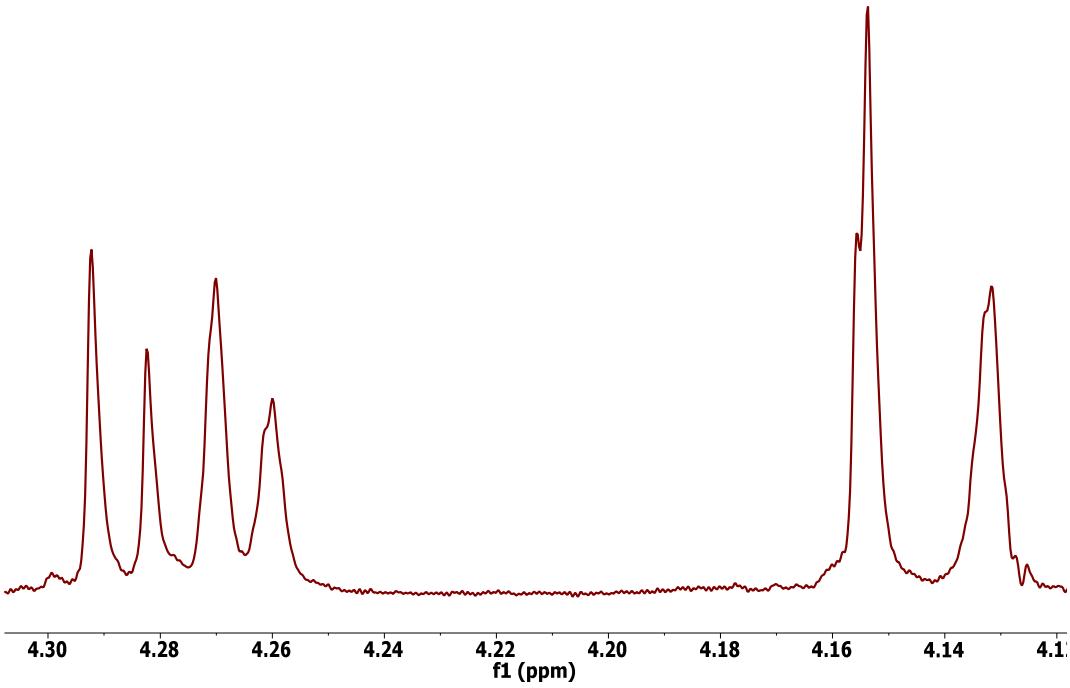

*Figure 27 ^{1}H{Me} NMR spectrum of **15,** where the ethyl CH_3 group was decoupled, showed the presence of two isomers once again. Both isomers were present in different ratios, again approximately 0.8 : 1, as well as the two separate inequivalent protons of the methylene group. In spite of the presence of the two isomers there was no evidence in any crystal structure of **15** as to the identity of this second isomer.*

Iso-propyl groups are similar in dimensions to phenyl rings, by virtue of having much of the steric bulk spread over two planes. While iso-propyl is the same size as ^{t}butyl in two dimensions, the omission of one methyl group causes the ^{i}propyl unit to be much flatter. As such it is thought that the ^{i}propyl group should

fall somewhere between the results seen for phenyl and ^{t}butyl and indeed this is what was observed (Figure 28).

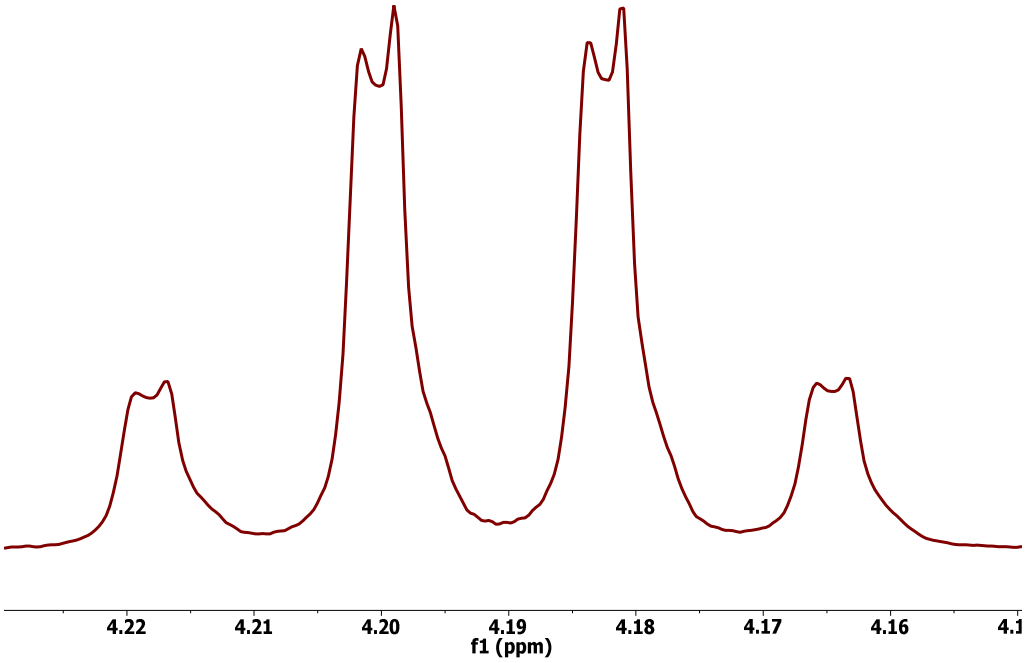

*Figure 28 Methylene region of **16**, showing some a small degree of splitting, confirming that ^{i}propyl groups do indeed limit rotation of the aryloxy groups.*

As shown in Figure 28 **16** still has enough steric bulk to restrict rotation and cause the formation of two conformers.

In the case of **17**, when one further methyl group is stripped, there was no splitting observed so that either the ethyl group did not prevent free rotation in the system, or that any observed splitting had coupling constants which were too small to see in the NMR spectra.

The summary of the supplemental study confirmed that it was possible to use groups other than ^{t}butyl in order to bring about restricted rotation. The groups that caused restricted rotation were all of a similar size and composition to the ^{t}butyl group. With useful boundaries now established, any further research aimed at exploiting the presence of two isomers has a frame of reference to base initial designs on.

2.4 Electrochemistry

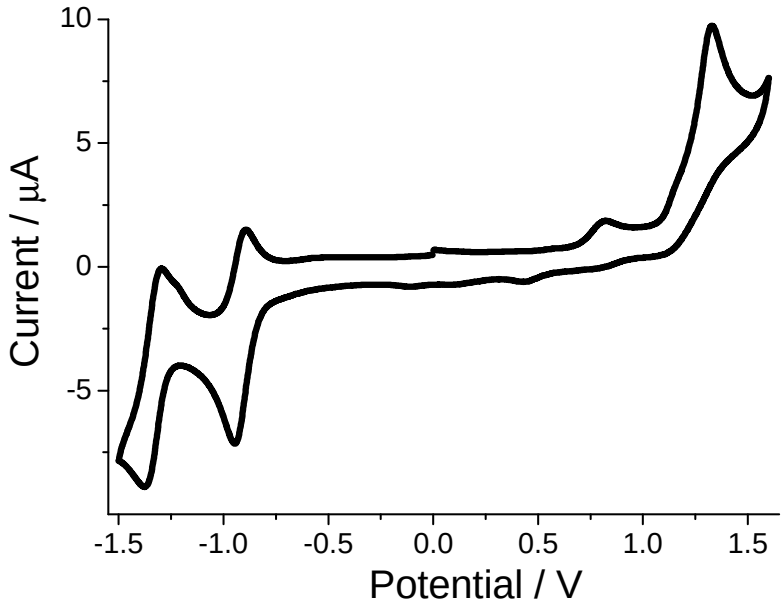

*Figure 29 Cyclic Voltammogram of **7a**; recorded in MeCN, with a glassy carbon electrode, silver wire reference electrode, and platinum counter electrode.*

The final product **7a** was subject to a cyclic voltammogram (CV) in order to investigate the electrochemical properties of the system. At a negative voltage two redox peaks are oberved for **7a**, showing two fully reversible one electron reductions. The first of the two redox peaks ($E_{1/2}$ = -0.92 V; ($E_{1/2}$ = -1.35 V) are most probably related to the hydroquinone of the xanthene core. There was also a one electron non-reversible oxidation peak ($E_{1/2}$ ≈ 1.24 V) which again is likely due to the oxidation of the hydroquinone moeity.

2.5 Photophysical measurements

While en route to synthesise compound **7** it was noticed that **4a**-**e** were highly fluorescent both in the solid state and while in solution. The fluorescence appears to be totally absent from the synthetic precursors **2** and **3a**-**e** suggesting that the presence of a quinone in the system quenches the fluorescent state. The fluorescence quenching of fluorophores by quinones is typically recognised as a photo-induced electron transfer reaction.[27]

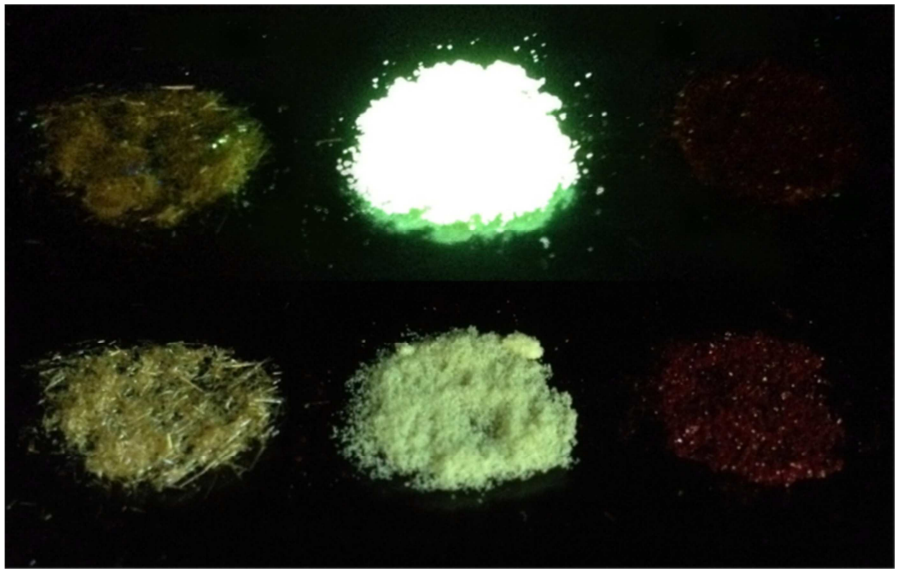

*Figure 30 A picture of compounds **2** (left), **4a** (middle) and **7a** (right) under UV illumination (top) and in daylight (bottom). Clear luminescence is visible from **4a** while all other compounds exhibit no such phenomenon.*

2.5.1 Solid state fluorescence

As mentioned previously, all compounds with structures relating to **4a** were highly fluorescent in the solid state both as crystals and as an amorphous powder. It is thought that the anti-conformation of the aryloxy groups is likely causing a separation between each molecular unit within the crystal lattice. This space prevents the self-quenching which might otherwise occur if the crystal packing had a higher density.[28]

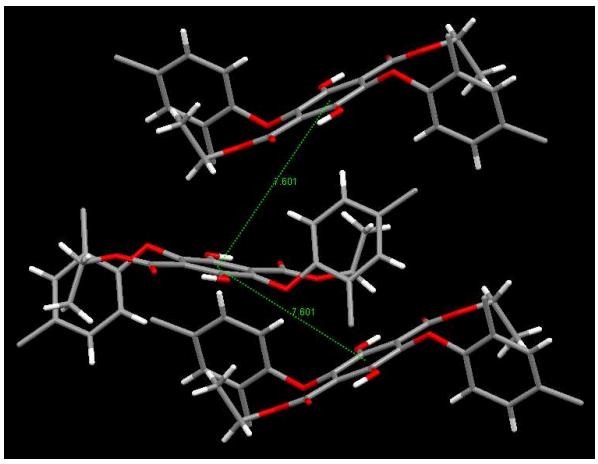

*Figure 31 The distance between each individual molecule of **4a** within the crystal structure, as measured from the S2 centre of one unit to the corresponding S2 centre of each unit. The ^{t}butyl groups have been omitted for clarity.*

As seen in the crystal packing for each structure related to **4**, the terephthalate groups do not appear to undergo any π-stacking. The centroid to centroid distance is typically over 6 Å, with values found at around 7.6 Å for **4a**. The >6 Å separation would be enough to prevent self-quenching according to studies on crystal packing diagrams. [29]

The intermolecular distance may well not be the only reason that solid state fluorescence exists within the system. Dreuw *et al*. noted that, in the commercially available solid state fluorescent Pigment Yellow 101, the presence of an OH group was crucial for solid state fluorescence to be observed.[30] This was found to be due to the stabilising effects of the hydroxyl group on the non-bonding orbitals. The presence of the OH lowered the energies of the n orbitals which prevented any forbidden transitions from taking place – thus promoting solid state fluorescence. The removal of these OH groups was found to cause a large increase in energy of the n orbital meaning that the S_1 corresponded to the forbidden n-π* dark state. Indeed this could suggest why firstly there is fluorescence seen in compound **4a-e** secondly might also suggest why the precursor **3** exhibited no fluorescence.

2.5.2 Absorption Measurements

	λ_{abs} / nm [a]	λ_{flu} / nm [a]	SS / cm^{-1} [b]	ε_{max} / M^{-1} cm^{-1}	Φ_{flu} [c]
4a	402	502	4933.2	13000	0.19

*Table 4 Photophysical measurements for **4a**, measured in MeCN; [a] ± 2 nm, [b] ± 25 cm^{-1}, [c] ± 10%.*

The absorption spectra for **4a** gave a broad absorbance peak with λ_{max} 402 nm and a halfwidth of 49 nm. It is likely that there are several different absorbance peaks which combine to form this peak, with the terephthalate and aryloxy groups both contributing. The absorbance was measured in both toluene and MeCN, with no difference observed between the two solvents. The molar extinction coefficient for **4a** was measured as being 13000 M^{-1} cm^{-1}, a moderate value, roughly a third the size of typical values recorded for coumarin derivatives.[21,31]

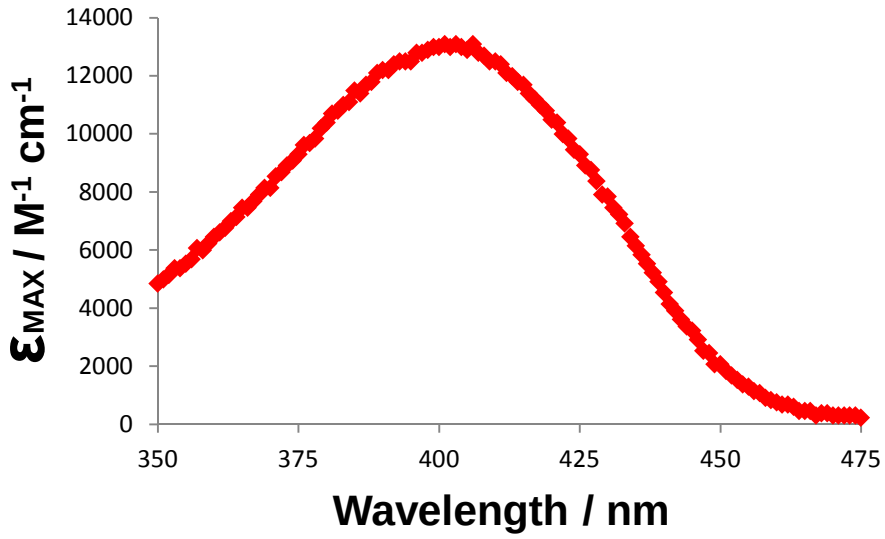

*Figure 32 The broad absorption spectrum for **4a**, measured in MeCN, is typical for analogous compounds.*

The photophysics of **4b**-**e** and **10** was also measured yet it became obvious that changing the aryloxy substituent had little or no effects on any of the photophysical measurements. As such the recorded absorption and emission spectra were all nearly identical for each compound, hence only the results of **4a** shall be discussed.

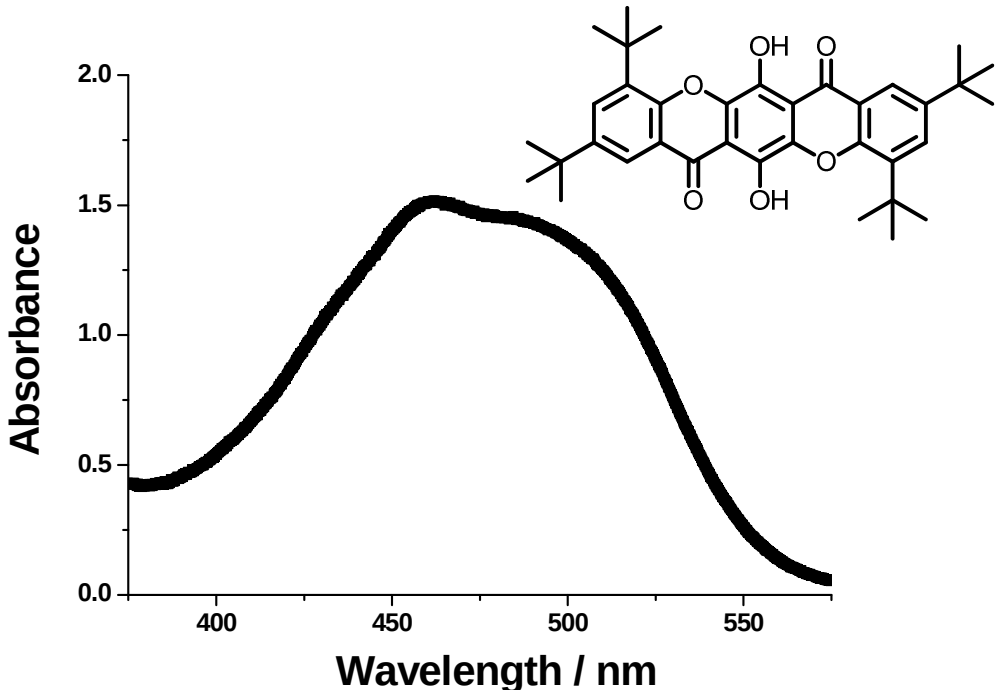

*Figure 33 The absorption spectrum of **7a** measures in MeCN, with a maximum at 461 nm and two shoulder-peaks at 435 and 486 nm.*

The comparison between the intermediate **4a** and the final fully ring-closed product **7a** demonstrated that the ring closing of the system caused a large red-shift. The absorption spectra showed a relatively strong broad absorption peak with the absorption maxima for **7a** found at 461 nm. The absorption showed at least two shoulder peaks at 435 nm and 486 nm. The shoulders suggest that there is more than one part of the compound which can absorb light energy. It is likely that the redshift which is seen in the absorption spectra for **7a** is due to the increased π-conjugation which now spreads across the whole molecule.

Surprisingly there was no fluorescence observed for **7a** in either the solid or solution state. It should be noted that there was still fluorescence observed in the synthetic precursor **6a**. Compound **6a** is a yellow solid which is strongly fluorescent in both solid and solution states.

The colour observed for **7a** is thought to strongly rely on the terephthalate core. Initially it was though that the intramolecular hydrogen bonding network at the terephthalate core was responsible for fluorescence quenching, by aiding the efficient deactivation of the S_1 excited state via enhancement of the rate of non-radiative decay.[32] The two six-membered rings which result from the hydrogen bonding allow for a tautomeric proton switch (Figure 34). Work by Waluk *et al*. showed that, with aromatic alcohols, the photoexcitation of a cyclic hydrogen-

bonded complex can cause a proton transfer, which was found to stabilise an intramolecular charge transfer state. This promotes a quick non-radiative transition to the S_0 thereby quenching fluorescence. [33]

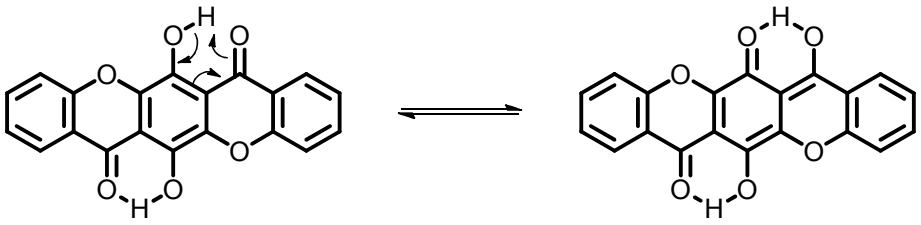

Figure 34 A hypothesised proton shift via a tautomerisation of the hydroxyl proton leading to a pseudo-six membered ring.

The colour of the compound can be seen turning from red to blue in concentrated H_2SO_4. This colour change is reversible, where the addition of a small quantity of water causes the red solid product to precipitate out of solution. It is possible that in extremely strong acids the hydrogen bonding network is disrupted – leading to the colour change from red to blue.

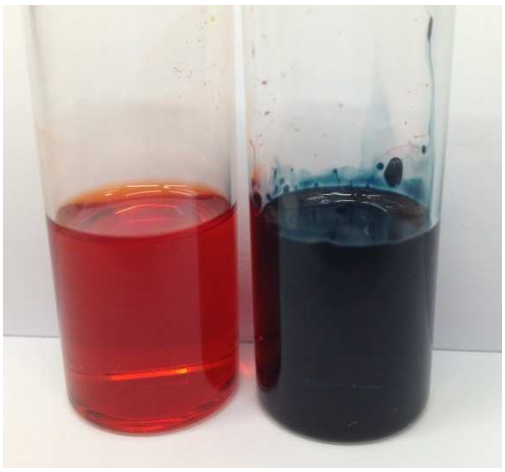

*Figure 35 The colour of **7a** was found to change colour in concentrated acid – here shown in DCM (left) and in concentrated H_2SO_4 (right).*

Other strong acids have also been tested to see if the same colour change can be observed. The only acid which caused any change in the colour was HNO_3, though this is thought to be the oxidation of the hydroquinone moiety to form a quinone. A result which is backed up with the OH protons disappearing from the ^{1}H NMR spectrum as well as a lack of evidence for an O-H stretch in the IR spectrum of the compound.

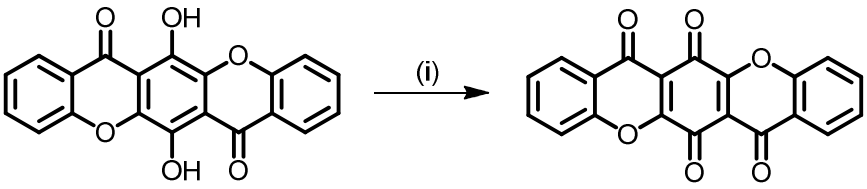

*Scheme 3 Oxidation of **7** to form **18**; (i) HNO_3, DCM.*

The oxidised product was a yellow solid, formed in quantitative yields, which was not fluorescent as either a solid or in solution.

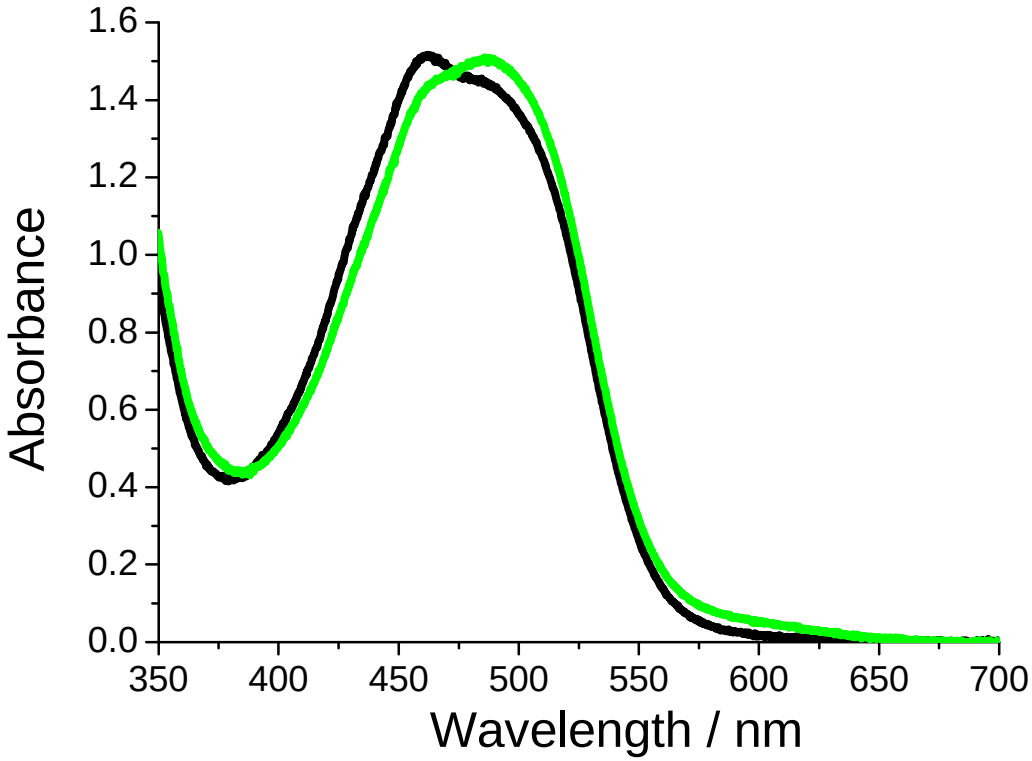

*Figure 36 Absorbance spectra of **7a** at atmospheric pressure (black) and at 550 MPa (green), measured in methylcyclohexane (MeChx).*

The absorbance spectra for **7a** was measured at varying pressure from 0 to 550 MPa to see if pressure had an effect on the system. Increasing the pressure on the system was found to result a bathochromic shift. Absorbance at 461 nm is seen to drop while absorbance at 486 and 600 nm is seen to increase.

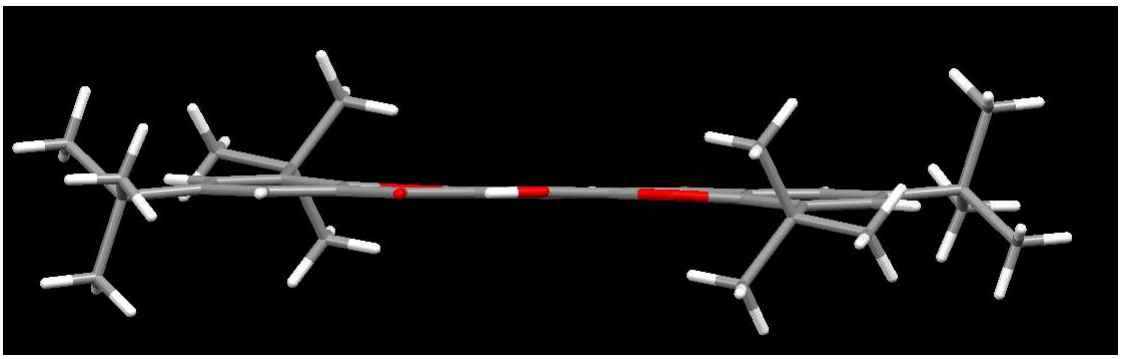

*Figure 37 The xanthene core of **7a** when looking down the H**O-C** bond. Note that there is around a 5^{o} twist in the core at either end revealing that even as a crystalline solid **7a** is not fully planar.*

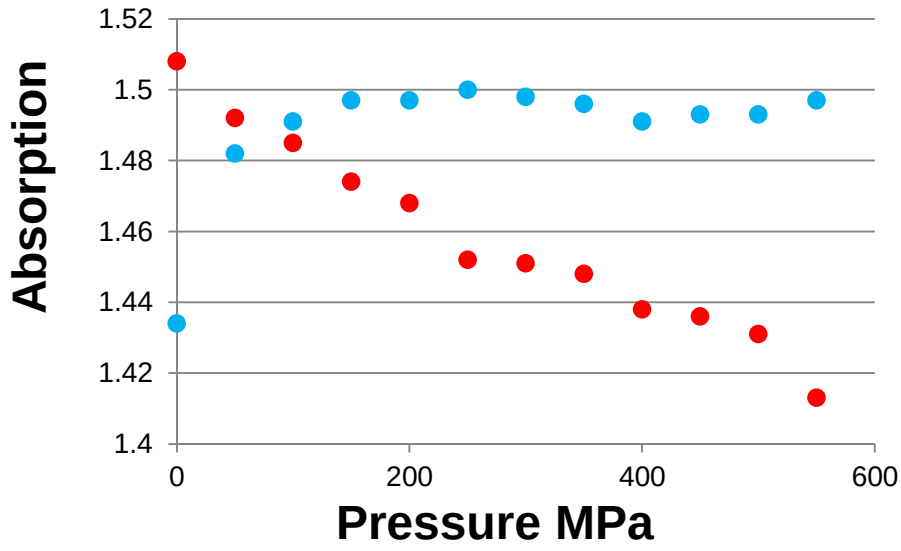

*Figure 38 Absorption of **7a** at 460 nm (**red**) and 490 nm (**blue**) against increasing pressure.*

The absorption at **460**, **490** and **590** nm was plotted against pressure in order to see the effects of pressure on the three areas of the absorption spectra which appear to change. There is an apparent decline in the intensity found at **460** nm while at both **490** and **590** nm the intensity of the absorbance increase. Where the intensity found at **590** nm undergoes a steady increase the intensity found at **490** nm initially increases rapidly after which point it remains roughly constant. The loss in intensity at **460** nm was around 0.095 a.u. while the combined increase in intensity at **490** and **590** nm was nearly equal at 0.099 a.u.

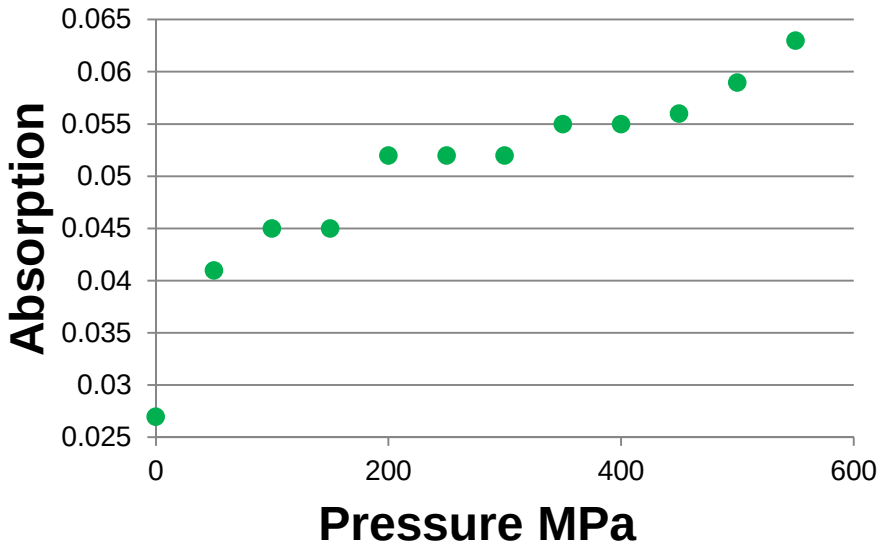

*Figure 39 Absorption of **7a** at 590 nm is shown to increase with increasing pressure with around a 2-fold increase observed from 0 – 550 MPa.*

The change in absorbance can be put down to a change in the molecular structure, where the total space of **7a** is reduced to a minimum. As shown in Figure 37 even in the crystal form the central core of the compound is not flat, with the aryl rings at each end around 5^{o} out of plane. In solution there is likely to be more flexibility in the system therefore it comes as no surprise that increasing the pressure on the system will cause the compound to find ways to minimise the space it occupies, theoretically becoming more planar. The increase in planarity should aid orbital overlap thereby accounting for the observed bathochromic shift.

It should be noted that MeChx undergoes a phase change at around 280 MPa. This shift occurs due to the solvent switching from an axial conformation to the less voluminous equatorial conformation.[34]

2.5.3 Emission Measurements

The fluorescence spectra for **4a** had a broad emission maxima at 502 nm and the spectrum was a mirror image of the absorption spectra. As with the absorption spectra the maxima was not altered by the presence of different aryloxy groups. The fluorescence quantum yield for **4a** was 0.19 suggesting that around 80% of the energy of excitation is lost to non-radiative decay. It is feasible that the non-radiative decay originates due to vibrations associated with the terephthalate intramolecular hydrogen bonding network, as with **7a**, as well

as there being room for flexibility within the system allowing for other forms of non-radiative decay.

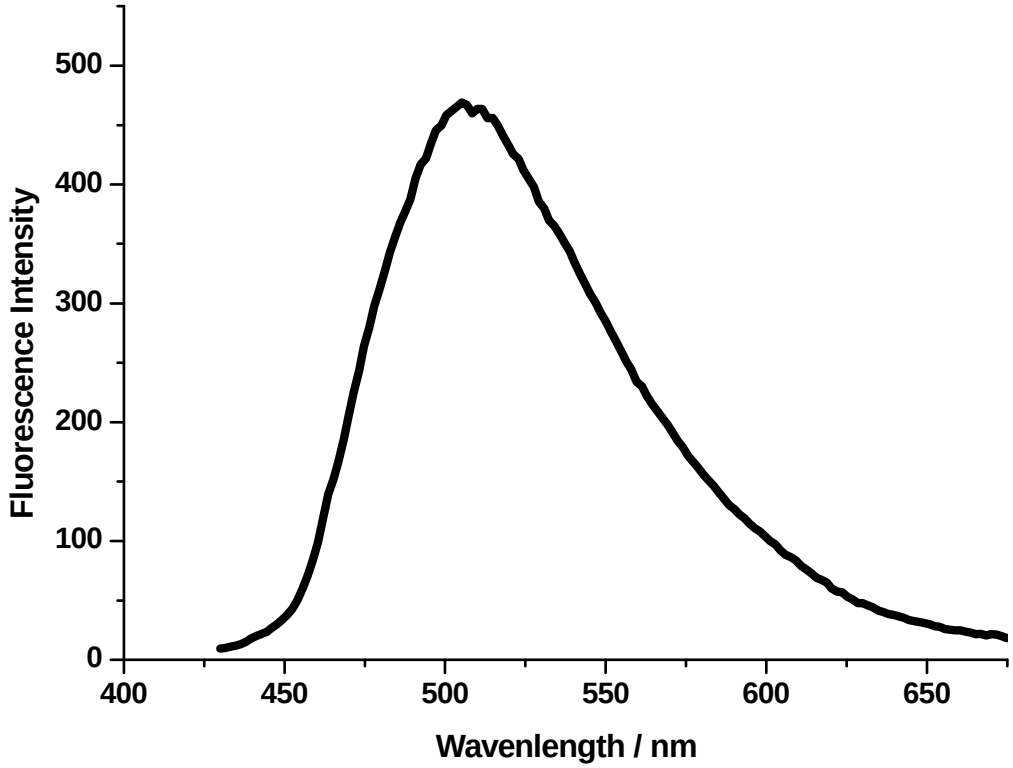

Figure 40 Fluorescence spectrum for 4a, measured in toluene, with a fluorescence maximum at 502 nm.

Evidently there is a large Stokes Shift observed in the case of **4a** in the order of 100 nm. The size of the SS itself implies that there exists a large structural difference between the ground and excited state structures. This is not surprising as the system is far from rigid, something which might explain the modest fluorescence quantum yield.

2.5.4 Lifetime Measurements

The fluorescence half-life of **4a** was measured via single-photon counting. The lifetime was seen to be strictly mono-exponential with a lifetime of 3.3 ns.

τ / ns [d]	k_{RAD} / 10^7 s^{-1}	k_{NR} / 10^8 s^{-1}
3.3	5.8	2.5

*Table 5 Lifetime measurements for **4a**, [d] ± 5%, τ was recorded in toluene.*

The radiative rate constant (k_{RAD}) is found to be 5.8 x 10^7 s^{-1}, which was in good agreement with the value calculated from the modified Strickler-Berg equation (Equation 2) 7.4 x 10^7 s^{-1}.

$$k_{RAD} \approx 3 \times 10^9 . \nu^2 . \varepsilon_{max} . \Delta\nu_{1/2}$$

Equation 2 Modified Strickler-Berg equation, where ν is the peak maximum (cm^{-1}) and $\Delta\nu_{1/2}$ is the peak width at half-height (cm^{-1}) for the fitted spectrum (see experimental).

From the values ascertained from the fluorescence quantum yield and k_{RAD} the value for the rate of non-radiative decay (k_{NR}) for the first excited singlet state was found to be 2.5 x 10^8 s. The value for k_{NR} dominates the quantum yield expression which was expected due to the relatively low value for k_{RAD}.

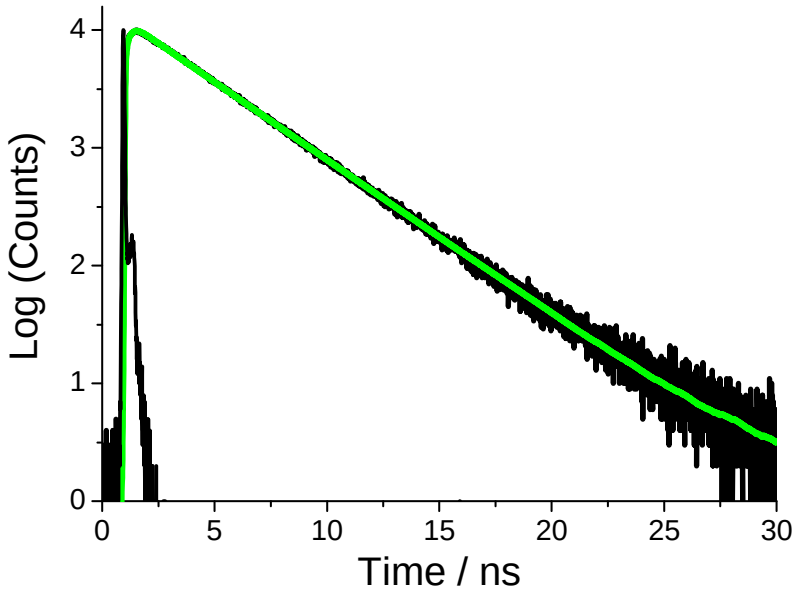

*Figure 41 A mesurement of the fluorescence lifetime of **4a**, recorded in toluene showing a mono-exponential decay of the singlet exctied state.*

2.6 Unsymmetrical aryloxy substitution

With the lack of fluorescence capability shown by **7a** attention turned to **4**. Efforts were made to see if it were possible to have two different aryloxy groups present on the same terephthalate core. If it were possible to introduce two different aryloxy groups which themselves are fluorescent then it should be possible to form donor-acceptor-donor systems or energy transfer cassettes.

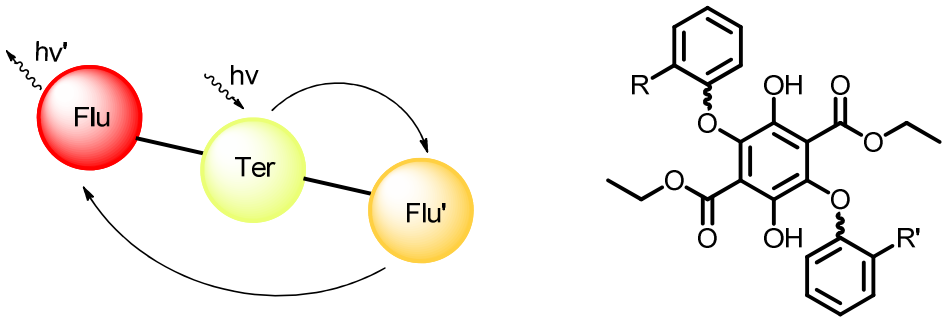

*Figure 42 A generic energy transfer cassette based on a terephthalate core (left) and a chiral version of compound **4** (right) where R≠R' and at least one of either R or R' contain a group which restricts rotation.*

Systems which contained two different aryloxy groups (where at least one aryloxy group had an ortho group which restricted rotation) would also be chiral, meaning that it is potentially possible to synthesise a chiral fluorophore in near quantitative yields on a fairly large scale.

Initially attempts were made to synthesise, isolate and purify the mono-substituted intermediate followed by the subsequent introduction of the second aryloxy group. Preparation of the compound via this method should result in the minimal loss of yield while also being able to make a diverse range of compounds from an initial starting material.

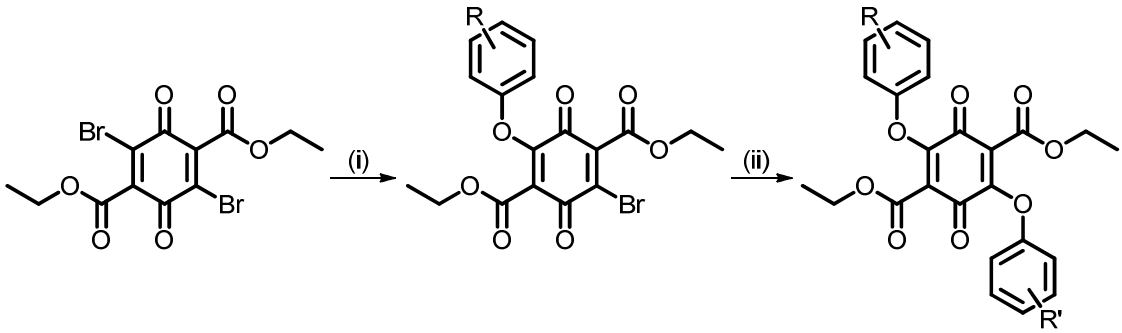

*Scheme 4 The proposed stepwise synthesis of unsymmetrical **3**. (i) acetone, pyridine, 1 equivalent ROH; (ii) acetone, pyridine, 1 equivalent R'OH.*

It proved impossible to isolate the intermediate despite several different attempts, with starting material and disubstituted product continuously isolated. It may well be the case that the first substitution reaction at the terephthalate core activates the ring, thus making the second substitution quicker.

The second synthetic tactic involved less subtlety, in this method both aryloxy groups were introduced at the same step without isolating the intermediate. Though the second method was in many ways similar to the original method described in Scheme 1, the addition of two separate aryloxy groups would lead

to the synthesis of three different products: the two disubstituted symmetrical compounds and the unsymmetrical product thus requiring rigorous purification, which would likely lead to reduced yields.

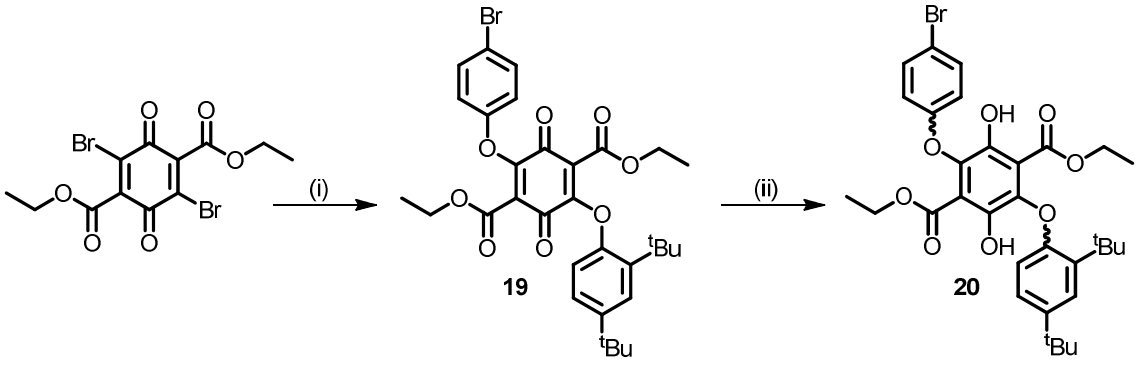

*Scheme 5 Synthesis of a mixed aryloxy quinone intermediate **19** and hydroquinone **20**. (i) pyridine, acetone, 4-bromophenol, 2,4-ditertbutylphenol; (ii) Zn, AcOH.*

Compound **19** was successfully synthesised using the method described above in a modest yield of 39%. As anticipated other side-products were also isolated and characterised, including diethyl 2,5-bis(4-bromophenoxy)-3,6-dioxocyclohexa-1,4-diene-1,4-dicarboxylate 38%. Though diethyl 2,5-bis(2,4-di-tert-butylphenoxy)-3,6-dioxocyclohexa-1,4-diene-1,4-dicarboxylate could not be conclusively identified it is likely that it was present though in low yields ca. 5%. There is certainly a relationship between the size / presence of an ortho group and the yield of product from the reaction – demonstrated by the low overall yield of the 2,4-di^{t}butyl derivative versus the 4-bromo.

The presence of the unsymmetrical product **19** was confirmed via ^{1}H NMR spectrum at which point **19** was reduced to **20**. Once again the reduction step resulted in high yields >99% as was anticipated. The ^{1}H NMR spectrum confirmed the presence of two different aryloxy groups on the terephthalate core showing AB splitting for the 4-bromophenolic moiety as well as signals for the 2,4-di^{t}butylphenoxy group.

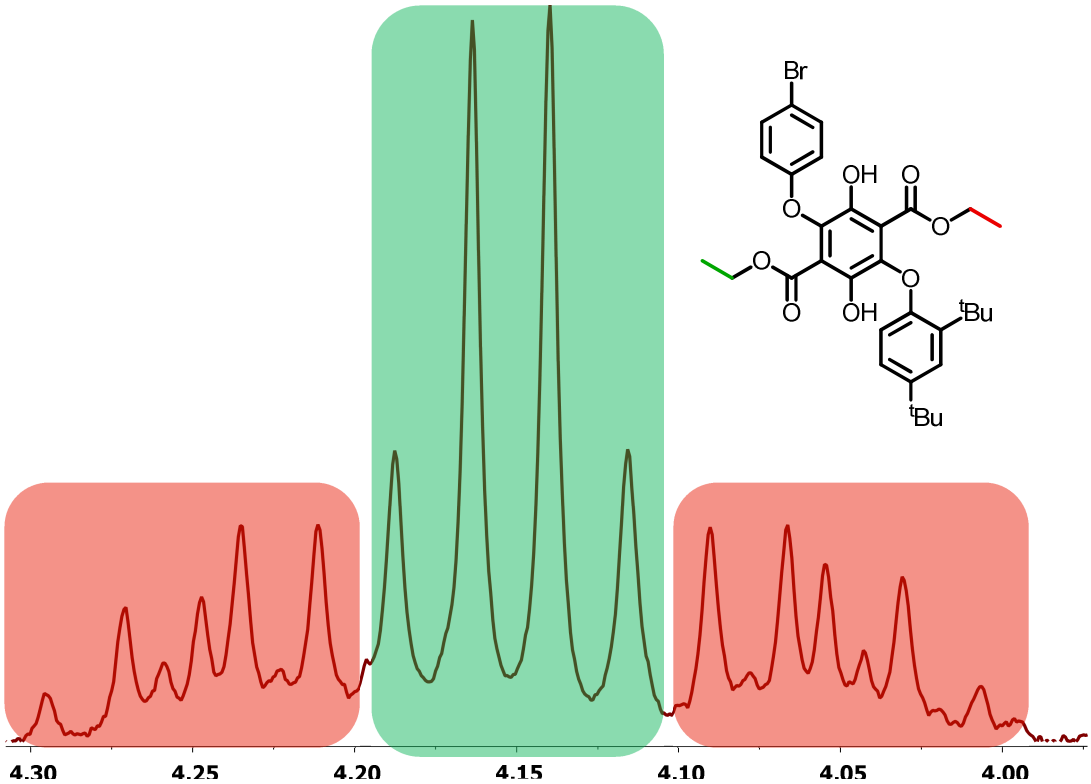

*Figure 43 Methylene region of the proton NMR spectrum of **19** shows the presence of two different environments for each of the two methylene groups. This firstly demonstrates the inequivalence of both **red** and green protons and secondly further demonstrates the inequivalence of each of the **red** protons.*

In the methylene region the presence of two aryloxy groups was also very noticeable. Figure 43 shows both the presence of quartet expected for the methylene protons situated next to the 4-bromophenoxy group (**green**) and two multiplets relating to the inequivalent protons on the ester group next to the ^{t}butyl containing aryloxy group (**red**). It is also useful to note at this stage that though **20** does show the methylene inequivalence, there is no evidence of any presence of rotamers within this system as there is free rotation around the aryloxy group opposite. Simply put compound **20** appears to show evidence that it is indeed a diastereotopic system.

2.7 Substitution of Different Aryloxy Groups on to the Core

Up until now the aryloxy moiety which has been used has been relatively simple. Yet if the terephthalate core were to be used as part of a molecular energy transfer cassette, the other fluorophores should easily be able to be introduced to the system as well as survive the overall synthesis. Several target

compounds were identified (based mostly on price / availability) and their synthesis attempted.

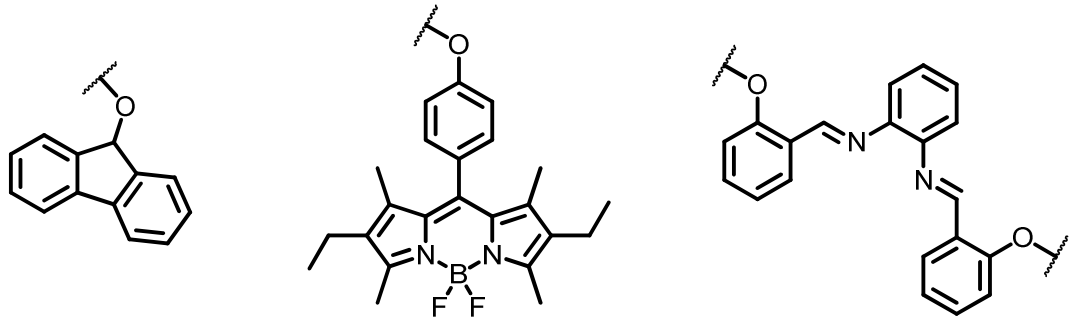

Figure 44 Potential aryloxyl group candidates to be introduced on to a terephthalate core.

Fluorenol (left) is both a cheap reagent to synthesise, has potential photonic applications - such as the ability to photorelease[35] and has the potential to be further functionalised. The addition of fluorenol to terephthalate systems will also show that it is possible to add alkoxyl as well as aryloxyl groups.

Bodipy systems (middle) are currently very popular, highly fluorescent systems which are easy to synthesise and modify. The addition of bodipy to terephthalate groups was aimed at potential energy transfer cassettes, where two different bodipy compounds could both be present on the core at the same time.

Salen complexes are cheap and easy to make, if phenylene-1,2-diamine is used to create the systems then they form complexes which are both solid state fluorescent and can potentially bind to metal centres. One further benefit of introducing salen is that it might be possible to attach one salen ligand to two sites on the same terephalate core, thereby locking the system in the syn conformation.

While experiments with the salen and fluorenol failed, with both yielding starting material, initial reactions with bodipy proved facile yielding the desired product in the very high yields anticipated for the reaction. It is thought that while aryloxyl compounds will react readily even with large steric bulk, the salen compounds were too bulky to react in with **2** under the conditions used. Changing the solvent to one with a higher boiling point might alleviate that particular problem, and as such should be considered as a path to further develop these compounds in the future.

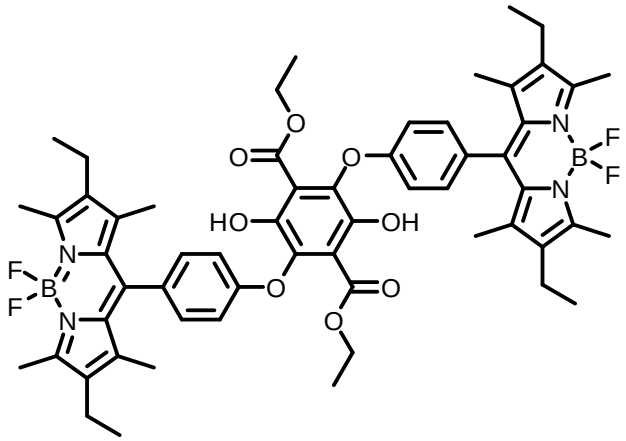

*Figure 45 Compound **21b**, the addition of bodipy as the aryloxylate to form a derivative of compound **4**. The synthesis gave a 60% overall yield. Luminescence was only observed when in the hydroquinone form **21b**, with the quinone form **21a** yielding no observable fluorescence – in theory making the system a crude on/off switch for redox reactions.*

The absorption spectrum for **21b** showed peaks at 380 nm and 400 nm which relates to the S_0-S_2 excitation of bodipy and the S_0-S_1 excitation of the terephthalate group. There is a sharp absorption maxima for the S_0-S_1 excitation for the bodipy at 526 nm, which is typical for bodipy – as is the shoulder peak seen at 498 nm.

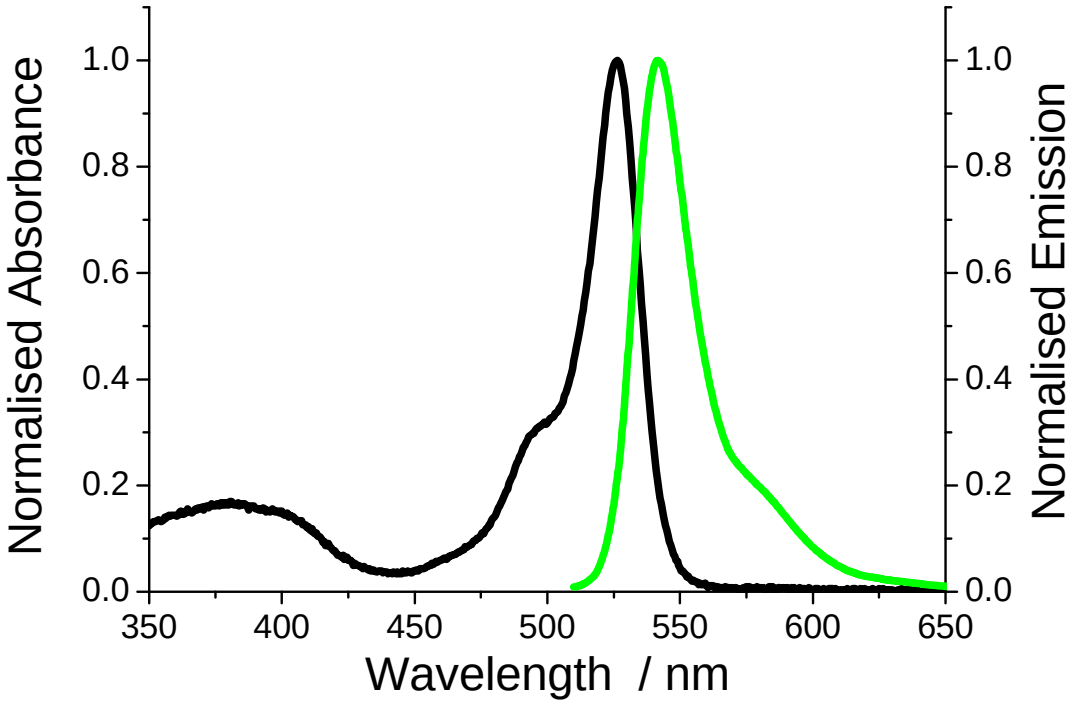

*Figure 46 The absorption (**black**) and emission (**green**) spectra for compound **21b**, measured in toluene.*

The emission spectrum for **21b** is a good mirror image of the absorption with an emission maxima at 541 nm. Both the absorption and emission spectra are red-shifted from similar bodipy derivatives by around 4 nm.[36,37].

2.8 Conclusion and Future Work

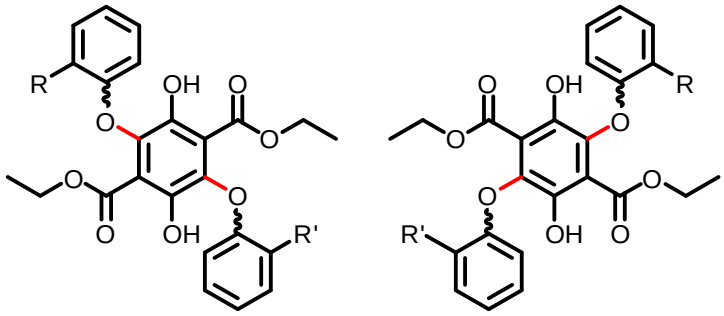

*Figure 47 A generic chiral molecule of **4**, where R and R' have the required steric bulk to prevent rotation around the bond.*

While the target compound showed little promise as a compound with photonic applications, the scope for the intermediate **4** is much larger. Since there is potential chirality within this group of molecules expansion of the system off the positions of the aryloxy groups is something which should be investigated further. Variation at the sites on the aryloxy ring would firstly allow for better separation of the diastereomers which are formed in the reaction as well as better separation of the resulting enantiomers on a chiral column. Secondly the ability to vary the substituents on the aryloxy ring, along with the other groups on the terephthalate core, would allow the ability to tune the fluorophore to chiral surroundings – if chiral sensing were desired.

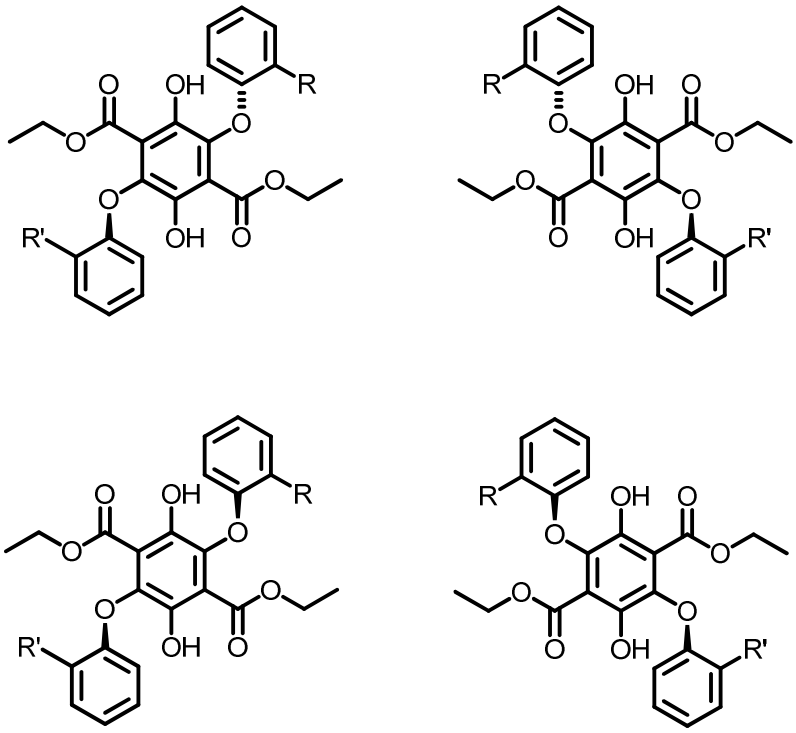

*Figure 48 Diastereomers of chiral **4**: anti (top, left) and syn (bottom, left) with both enantiomers detailed (right, top and bottom).*

To conclude, the synthesis of the desired 6,13-dihydroxy-chromeno[2,3-b]xanthene-7,14-dione via the original synthetic scheme was a success, yielding the desired product in good yields. The effects of π-stacking caused characterisation of the original target molecule to be virtually impossible hence the target was revised to allow for further bulk around the substituents in order to prevent any stacking. A bulky product (**7a**) was synthesised successfully and was fully soluble in a range of organic solvents hence easier to characterise. This particular class of compound did not show any luminescent properties, though reactions at the dihydroxy groups does cause some of the fluorescence to be restored. As such there is also possible scope to use the derivatives of **7** to be used for the sensing of strong alkylating reagents which are commonly associated with nerve agents.[38]

The attention turned from the target molecule to the intermediate **4**, which showed vibrant fluorescence in both solid and solution states. Yields for the derivatives of **4** were excellent, with all compounds exhibiting identical photonic properties.

Compound **4a** revealed the presence of prochirality shown by inequivalent protons on the ester moieties as well as two rotamers: *anti* and *syn*. A

subsequent study to assess the barrier to rotation around the aryloxy-terepthalate (Ar-T) bond was undertaken. This study showed that there is a size and dimensional limit after which the free rotation around the Ar-T bond is compromised.

Systems based around **4a** have been made to be unsymmetrical and therefore chiral which widens the field of possible for these molecules.

2.8.1 7a as a Backbone for Zinc-Bound Ligands

The final compound **7a** was subjected to further experiments to see whether there was any scope for the compound to act as a centre point for ligand attachment.

Theoretically **7a** should bind with metal ions in solution as a result of the two binding sites indicated in Figure 49 (inset). To test if metal binding to the system was feasible a titration was performed where zinc (II) triflate was titrated into a solution of **7a** as the absorption spectra was measured. Initially during the first measurement an excess of zinc (II) triflate was added to **7a**. A redshift was observed upon addition of the metal ion, with the absorption maximum at 461 nm decreasing in intensity, as well as the intensity at 490 and 590 nm increasing, suggesting that there is a binding interaction between **7a** and zinc (II) ions.

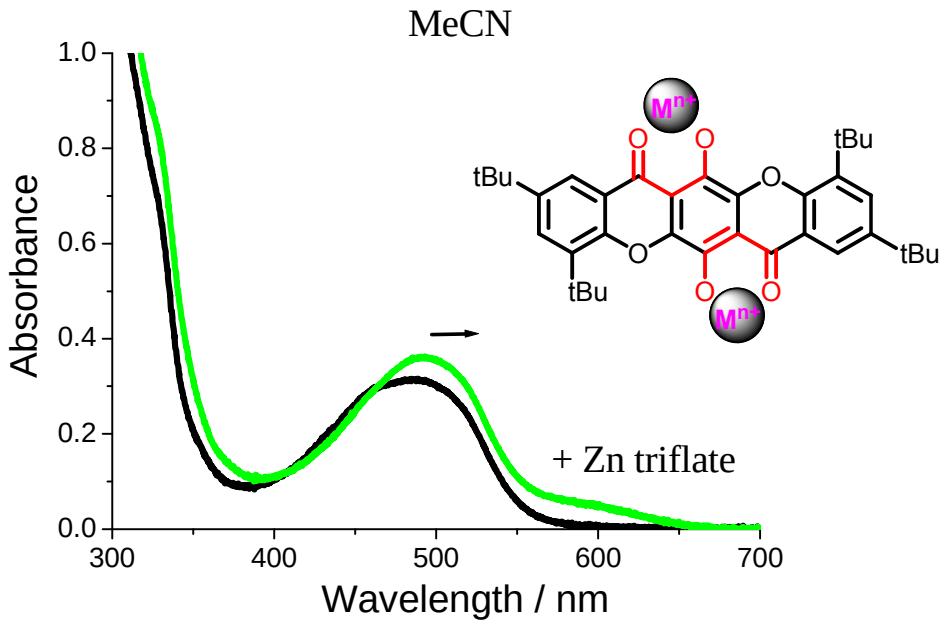

*Figure 49 The absorbance spectra of **7a** shifting before (black) and after (green) a titration of Zn^{2+}; the sites available for metal binding (inset).*

The changes to the absorption spectra were looked at in some more detail by titrating known quantities of zinc triflate to a solution of **7a** (ca. 25% relative to [**7a**]). Absorption measurements were taken at the three wavelengths where changes in intensity were observed (460, 490 and 590 nm).

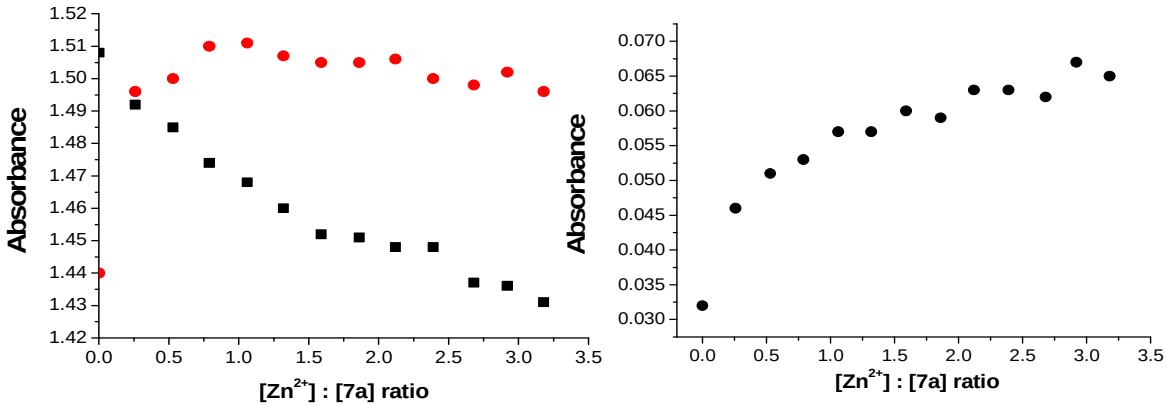

*Figure 50 Absorbance of **7a** at 460 nm (left, **black**), 490 nm (left, **red**) and 590 nm (right) against increasing concentrations of zinc triflate, measured in MeCN.*

Unfortunately the recovery of the compound with the zinc ions bound to the xanthene core was not achieved, though it is thought that the binding was successful.

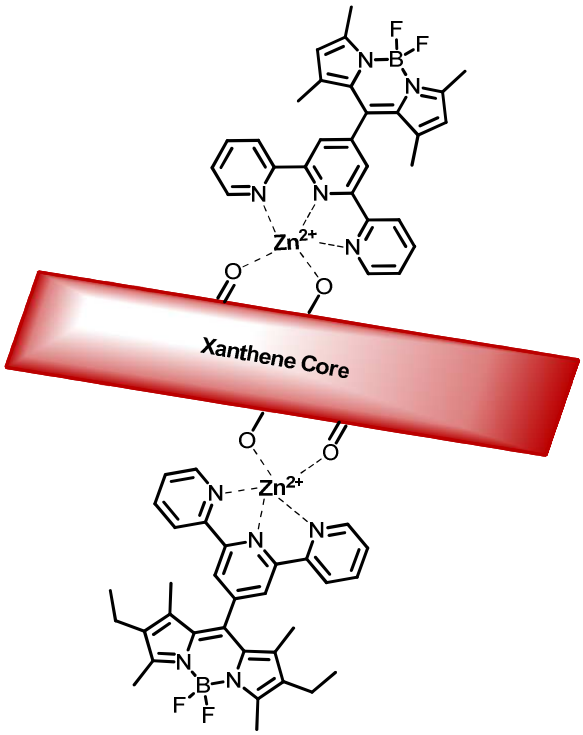

Figure 51 A secondary target molecule incorporating two complementary terpyridine-bodipy units linked to the xanthene core by zinc (II) ions. NB There would likely be one further ligand coordinated around the zinc atom, likely triflate, this has been removed for clarity.

Given more time the aim of the subsidiary project was to bind two terpyridine-linked bodipy units to the xanthene core. Initial attempts to create the terpyridine-bodipy compounds (Bod-Terpy) were successful, as well as isolation of the zinc (II) bound Bod-Terpy.

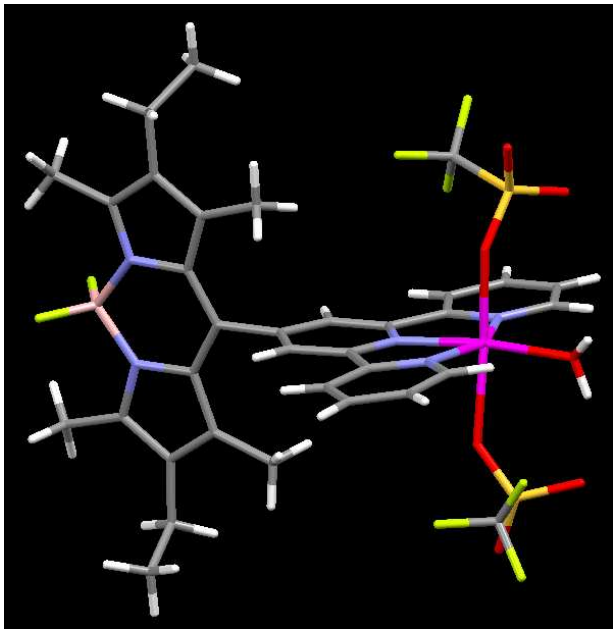

Figure 52 The crystal structure of the isolated zinc-bound Bod-Terpy compound. There are three other ligands present: two triflate and one water.

It proved more difficult than anticipated to introduce two different substituents onto the zinc centre. Various attempts were made to attach different component molecules to the zinc centre with none proving to be successful.

2.9 References

1. R. F. Kubin and A. N. Fletcher, *J. Luminescence*, 1982, **27**, 455-462.
2. Tkachenko, *New Developments in Liquid Crystals*, InTech, 2009.
3. C. McDonagh, C. S. Burke and B. D. MacCraith, *Chem. Rev.*, 2008, **108**, 400-422.
4. X. Cao, W. Lin and L. He, *Org. Lett.*, 2011, **12**, 4716–4719.
5. C. L. Amiot, S. Xu, S. Liang, L. Pan and J. X. Zhao, *Sensors*, 2008, **8**, 3082–3105.
6. F. V. Englich, T. C. Foo, A. C. Richardson, H. Ebendorff-Heidepriem, C. J. Sumby and T. M. Monro, *Sensors*, 2011, **11**, 9560–9572.
7. E. W. Miller, A. E. Albers, A. Pralle, E. Y. Isacoff and C. J. Chang, *J. Am. Chem. Soc.*, 2005, **127**, 16652–16659.
8. S. Andersson-Engels, C. a. Klinteberg, K. Svanberg and S. Svanberg, *Phys. Med. Biol.* , 1997, **42**, 815–824.
9. I. M. Riederer, R. M. Herrero, G. Leuba and B. M. Riederer, *J. Proteometrics*, 2008, **71**, 222 – 230.
10. M. R. El-Gewely, *Biotechnology Annual Review*, Elsevier, 2005.
11. D. L. Taylor, *Applications of Fluorescence in the Biomedical Sciences*, Alan R. Liss Inc., New York, 1986.
12. M. Feller, R. Morris and E. Gruenstein, *J. Histochem. Cytochem.*, 1979, **27**, 1613 – 1622.
13. L. A. Ernst, R. K. Gupta, R. B. Mujumdar and A. S. Waggoner, *Cytometry*, 1989, **10**, 3 – 10
14. J. Wu, Z. Ye, G. Wang, D. Jin, J. Yuan, Y. Guan and J. Piper, *J. Mater. Chem.*, 2009, **19**, 1258–1264.
15. J.-C. G. Bünzli, *Chem. Rev.*, 2010, **110**, 2729–2755.
16. A. C. Benniston, A. Harriman, S. L. Howell, C. A. Sams and Y.-G. Zhi, *Chem. Eur. J.*, 2007, **13**, 4665–4674.
17. K. Rurack, M. Kollmannsberger and J. Daub, *New J. Chem.*, 2001, **25**, 289–292.
18. G. Signore, R. Nifosì, L. Albertazzi, B. Storti and R. Bizzarri, *J. Am. Chem. Soc.*, 2010, **132**, 1276–1288.
19. G. Signore, R. Nifosì, L. Albertazzi, B. Storti and R. Bizzarri, *J. Am. Chem. Soc.*, 2010, **132**, 1276–1288.
20. R. J. V. Trebra and T. H. Koch, *J. Photochem. Photobio. A*, 1987, **41**, 111 – 120.
21. T. Wolff and H. Görner, *Phys. Chem. Chem. Phys.*, 2004, **6**, 368-376.
22. H. Liebermann, G. Lewin, A. Gruhn, E. Gottesmann, K. Schonda and D. Lisser, *Chem. Ber.*, 1934, 156–179.
23. E. Heim, *Chem. Ber.*, 1888, 589 – 604.

24. P. Auffinger, F. A. Hays, E. Westhof and P. S. Ho, *PNAS*, 2004, **101**, 16789 – 16794.

25. M. O. Sinnokrot, E. F. Valeev and C. D. Sherrill, *J. Am. Chem. Soc.* , 2002, **124**, 10887-10893.

26. Gaussian, Inc., Wallingford CT, Editon edn., 2004.

27. D. Gust and T. A. Moore, *Top. Curr. Chem.*, 1991, **159**, 103 – 151.

28. H. Langhals, T. Potrawa, H. Nymth and G. Linti, *Angew. Chem.* , 1989, **101,**, 497–499.

29. H. Langhals, T. Potrawa, H. Nöth and G. Linti, *Angewandte Chemie International Edition in English*, 1989, **28**, 478-480.

30. A. Dreuw, J. Plötner, L. Lorenz, J. Wachtveitl, J. E. Djanhan, J. Brünin, T. Metz, M. Bolte and M. U. Schmidt, *Angew. Chem. Int. Ed.* , 2005, **44**, 7783 –7786

31. G. S. Hammond, C. A. Stout and A. A. Lamola, *J. Am. Chem. Soc.*, 1964, **86**, 3103-3106.

32. R. Englman and J. Jortner, *J. Mol. Phys.*, 1970, **18**, 145 – 164.

33. J. Herbich and J. Waluk, *Phomchem. Photobiol. A: Chem.*, 1994, **80**.

34. V. I. Saranov and L. A. Gribov, *Appl. Spectorsc.*, 1984, **38**, 313-317.

35. P. T. Dragana Zivkovic, University of Basel, 2007.

36. P. Kele, X. Li, M. Link, K. Nagy, A. Herner, K. Lrincz, S. Béni and O. S. Wolfbeis, *Org. Biomol. Chem.*, 2009, **7**, 3486 – 3490.

37. C. Dumas-Verdes, F. Miomandre, E. Lépicier, O. Galangau, T. T. Vu, G. Clavier, R. Méallet-Renault and P. Audebert, *Eur. J. Org. Chem.*, 2010, **13**, 2525 – 2535.

38. W. Chen, S. A. Elfeky, Y. Nonne, L. Male, K. Ahmed, C. Amiable, P. Axe, S. Yamada, T. D. James, S. D. Bull and J. S. Fossey, *Chem. Comm.*, 2011, **47**, 253 - 255.

Chapter 3 – The Fluorine Effect – A systematic Study of Fluorine Atoms Substitution at the Aryl Moiety of Bodipy Molecules

3.1 Introduction

3.1.1 Fluorine: a History in Chemistry

Since 1957 fluorine containing groups have been included into pharmaceuticals, and now approximately 20% of all drugs contain fluorine atoms.[1] While it is quite well understood how fluorine atoms can enhance the metabolic stability of drug molecules, it is not fully understood fluorine affects selectivity at the molecular level.[2]

In spite of fluorine being isolated in 1886 it took a further 80 years for the widespread use of fluorine in laboratories. This breakthrough was due to the development of selective, and more importantly safe, fluorinating agents such as 2,2-difluoro-1,3-dimethylimidazolidine (DFI), trimethyl(trifluoromethyl)silane and N-fluorobenzene-sulfonimide (NFSI).

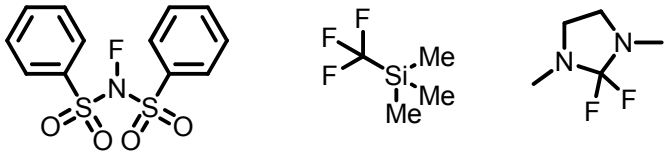

Figure 1 Selectictive fluorinating agents: NFSI, trimethyl(trifluoromethyl)silane and DFI. These new fluorinating agents allowed for the increased incorporation of fluorine into compounds, thus allowing for further studies into the effects of fluorine atoms in such systems.

3.1.2 Properties of Fluorinated Compounds

Fluorine is the most electronegative element in the periodic table and forms very strong C-F bonds, with the added bonus of increasing the strength of adjacent carbon-carbon single bonds. The presence of perfluorinophenyl groups in the meso position of bodipy has also been shown to increase partial charge on the 3 and 5 methyl protons of the bodipy core, thus resulting in a higher reactivity at these positions.[3] The electron deficient nature exhibited by fluorine containing compounds means that they are model candidates for n-type semiconductors. [4,5]

Substituent	σ_I	σ_R
F	0.52	-0.34
Cl	0.47	-0.23
Br	0.44	-0.19
CH_3	0.04	-0.11
CF_3	0.42	0.10
OH	0.29	-0.43
OCF_3	0.39	-0.04

Table 1 Hammett type substitution values for a range of fluorinated groups alongside appropriate comparisons.

The presence of fluorine unsurprisingly causes inductive electron withdrawing effects on surrounding atoms, due to the extreme electronegativity of the fluorine atom. Yet it is also possible for the fluorine to donate electrons via resonance effects (Table 1).[6]

It was originally though that the size difference between fluorine and hydrogen was insignificant, with fluorine believed to be ca. 12.5 % larger than hydrogen. The determination of the size of these two atoms arose from the Pauling van der Waals radii for the atoms, however these figures have now been reassessed. The accepted value for the radius of fluorine is now normally quoted from the calculations of Bondi or Williams and Houpt.[7,8] These values differ from the Pauling values by around 10 %, making fluorine between 22.5 % or 25 % larger than hydrogen (depending on which model is used) which is a significant increase relative to the Pauling models. The revision of the size of fluorine atoms means that they are roughly isosteric with oxygen (Table 2). The steric increase can sometimes be seen in bioisosterism measurements between fluorinated and non-fluorinated drugs – with the increase in size often changing the binding affinity of the receptor to the ligand.[9]

	Pauling	Bondi	Williams and Houpt
H	1.20	1.20	1.15
F	1.35	1.47	1.44
O	1.40	1.52	1.44

Table 2 The atomic radii (Å) of hydrogen, fluorine and oxygen according to three different models: Pauling, Bondi, and Williams-Houpt.

Fluorinated compounds are typically hydrophobic and have negative entropies of aqueous solvation.[10] In spite of the observed hydrophobicity there is some evidence, though it is cause for some debate, that the C-F bond may participate

in hydrogen bonding due to its high dipolarity.[11] Hydrogen bonding between carbon and fluorine atoms can be demonstrated when hexafluorobenzene is co-crystallised with benzene and its hexa-substituted derivatives.[12]

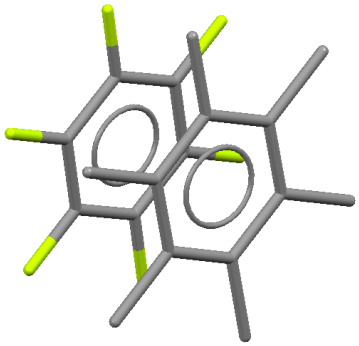

Figure 2 A crystal structure demonstrating the co-crystallisation of hexafluorobenzene with hexamethylbenzene.

Fluorination of aromatic compounds always increases lipophilicity. It is typically found that the addition of fluorine to pharmaceuticals leads to an increased affinity for natural receptors, leading to fluorinated compounds being labelled as 'polar hydrophobic'. It may be possible to use this increased lipophilicity to improve the delivery of bodipy probes across the blood brain barrier.[13]

3.1.3 Effects of Hydrogen being Replaced by Fluorine

The benefits of the inclusion of a fluorine atom or atoms into organic structures are well documented.[2] A good example of the uses of fluorine compounds is in the field of medicinal biosteres, where the replacement of the hydrogen atoms of a hydrophobic compound with fluorine, decreases the metabolic susceptibility of the compound. The decreased rate of metabolism is bought about by blocking the metabolically labile site thus reducing the rate at which the compound undergoes oxidation by enzymes in the liver.[14]

The quantity and substitution pattern of fluorine atoms on an aromatic system is known to heavily influence the energy of the σ and π frameworks.[15, 16] This influence is much more pronounced for the π-systems than for the σ-systems. As an example the exchange of hydrogen atoms with fluorine atoms, on sections of polyaromatic systems which interact with the primary π-conjugated scaffold, can cause a substantial lowering of LUMO energy levels and raising of

HOMO energy levels within the system. The lower-lying LUMO, bought about by the use of fluorine, allows for more efficient electron injection into the system. The reduced HOMO-LUMO energy gap within fluorescent compounds would cause a red-shift in the absorption and emission. As mentioned in the introduction to bodipy red-shifted chromophores have potential applications as endo-cellular sensors, with the red-shifted fluorescence unobscured by autofluorescence.

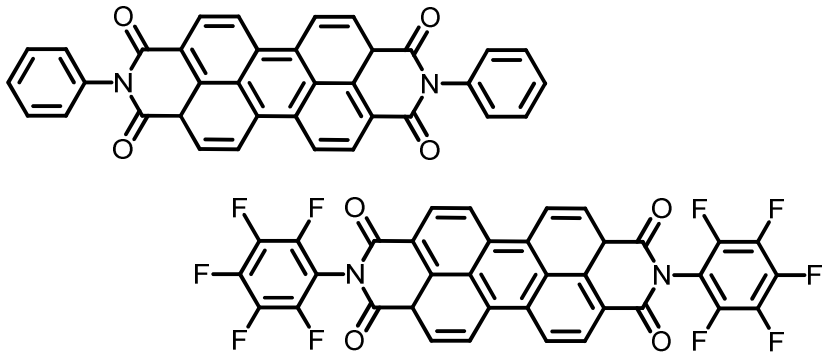

Figure 3 N,N'-diphenyl-3,4,9,10-perylenetetracarboxylic diimide and N,N'-diperfluorophenyl-3,4,9,10-perylenetetracarboxylic diimide. The half-wave reduction potential for N,N'-diperfluorophenyl-3,4,9,10-perylenetetracarboxylic diimide was -0.37 eV (vs SCE), 0.14 eV more positive than that for N,N'-diphenyl-3,4,9,10-perylenetetracarboxylic diimide.

Perfluorination of N,N'-diphenyl-3,4,9,10-perylenetetracarboxylic diimide (Figure 3) has substantial effects on the LUMO energy level as a result of a strong electron withdrawing effect, and the ability for the system to accept two electrons – something that the non-fluorinated system cannot do.[17]

It is also found that in fluorinated conjugated materials, where the HOMO is lowered (relative to similar un-fluorinated derivatives) the systems are less susceptible to oxidative degredation granting further positive effects on the lifetime of the device.[18]

3.1.4 An Outline of the Work Undertaken

There have been various studies into the chemistry of fluorinated compounds looking at their photophysical aspects.[19, 20] The following chapter is a follow on to some of these studies. The driving force behind the work is based on observations made about the quantum yield of perfluoroaryl bodipy compound **23**. Compound **23** was seen to have a quantum yield which was twice that of

the phenyl derivative (difference is solvent dependent), representing a significant improvement in quantum efficiency.

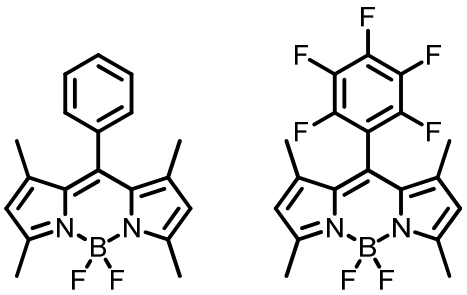

*Figure 4. 4,4'difluoro -8-(phenyl)-3,5,7,9 tetramethyl-4-bora-3a,4a-diaza-s-indacene (compound **22,** left) Φ_f = 0.50 (DCM), and 4,4'difluoro -8-(2,3,4,5,6-pentafluorophenyl)-3,5,7,9 tetramethyl-4-bora-3a,4a-diaza-s-indacene (compound **23,** right) Φ_f = 0.99 (DCM).*

Our intention was to try and better understand the relationship between the quantity and substitution pattern of fluorine atoms on a bodipy core with the observed quantum efficiency observed between **22** and **23**. In particular whether the relationship is based on the electronic effects of fluorine or if a simple sterics argument could be made. As well as the primary aims it would also be possible to test some other properties of fluorinated compounds, such as the relationship between fluorine-substitution at increasing pressure versus the fluorescence intensity.

If understood the inclusion of fluorine atoms within photonic systems may then be rationalised and potentially applied to other fluorescent systems.

To explore the relationship between fluorine substitution and increasing quantum yield a series of fluorinated meso-aryl bodipy compounds was synthesised and tested. The series varied the number and position of fluorine atoms on the meso-aryl moiety.

3.1.5 Synthetic Strategy

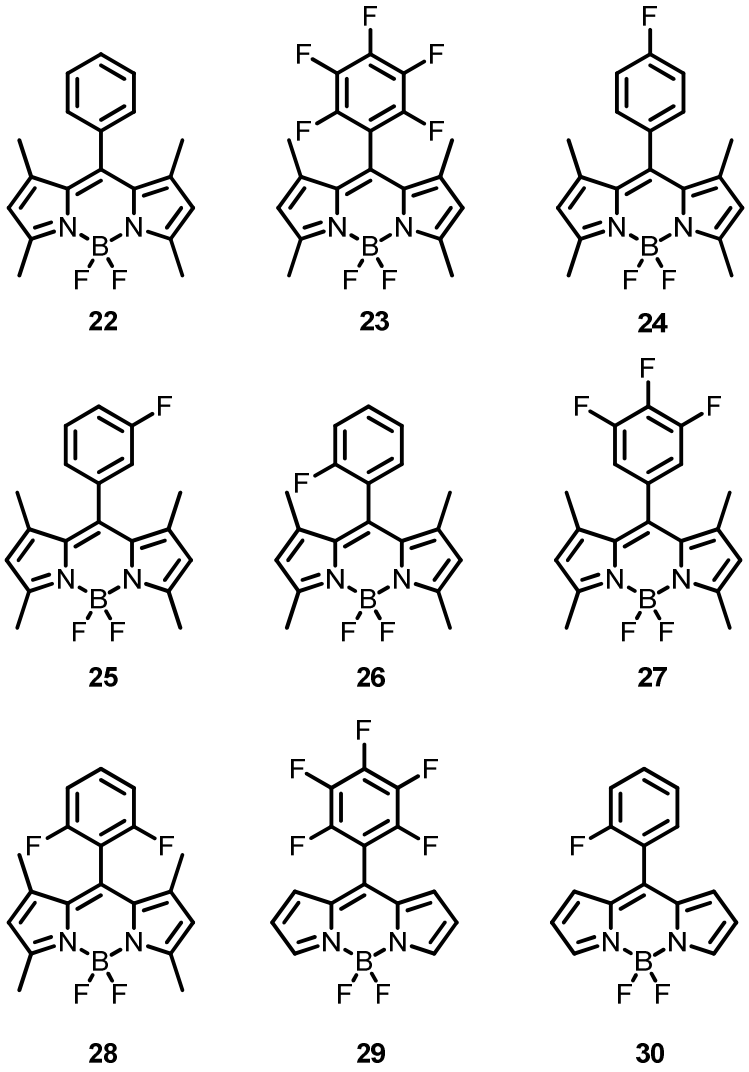

*Figure 5 Numbering scheme for all compounds discussed in this chapter. Initially the pentafluoro derivative (**23**) was made, following the synthesis of **23** more derivatives were made with fluorine substitution of varying position and quantity. Compounds **29** and **30** have a bare core in order to further explore the limits of the steric / electronic effects bought about by fluorine atom substitution.*

To best understand the choices of molecules synthesised in the series it is helpful to break the series up into sub-series in order to address each aspect which is being explored: electronic substitution pattern, electronic quantity, and sterics (with as **29** and **30** control compounds).

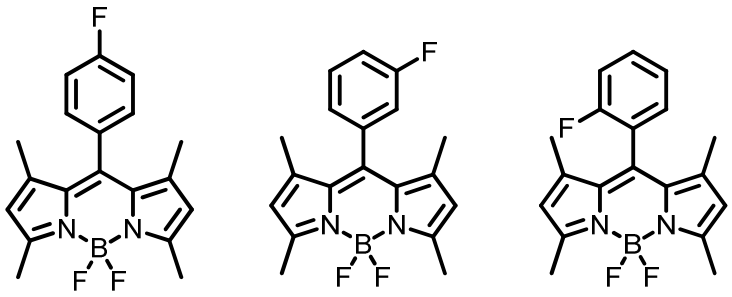

24 25 26

Series 1 Bodipy compounds with single ortho-, meta- and para-fluorine substitutions.

Compounds **24-26** were created in order to ascertain if the positioning of the fluorine atoms on the phenyl ring has any effect on the photophysical properties of the bodipy. As discussed in the introduction to the chapter, proximity to fluorine atoms can have a pronounced effect on the properties observed - due to the highly electron deficient nature of fluorine.

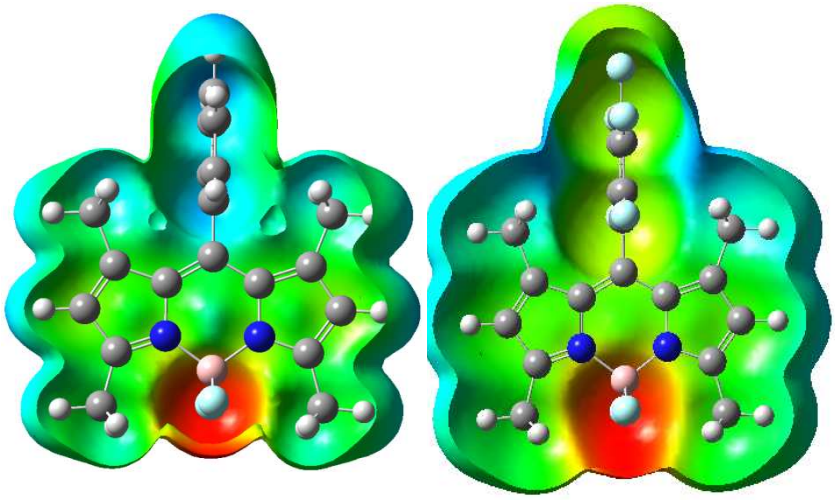

*Figure 6 A computer model showing the electrostatic potential of **23** (left) and **22** (right) mapped onto the isosurface. High electron density is depicted using red while lower electron density is blue.*

In Figure 6 it is possible to see an increase in the electron density at the bond between the penta-aryl group and the meso-carbon relative to the un-fluorinated bodipy (**22**). If the electron-withdrawing nature of fluorine is causing the bodipy to become more rigid, this could explain the rise in the Φ_f from **22** and **23**.

If the reason for the observed increase in fluorescence quantum yield is related to an increased rigidity, due to the proximity of the fluorine atoms to the meso

carbon, then it should be possible to predict the relative size for the Φ_f Series 1. It should be expected that **26** will exhibit the largest increase in quantum yield with **25** following and **24** exhibiting the least electron withdrawing effect of all – in accordance with the Hammett plots of fluorine substitution.

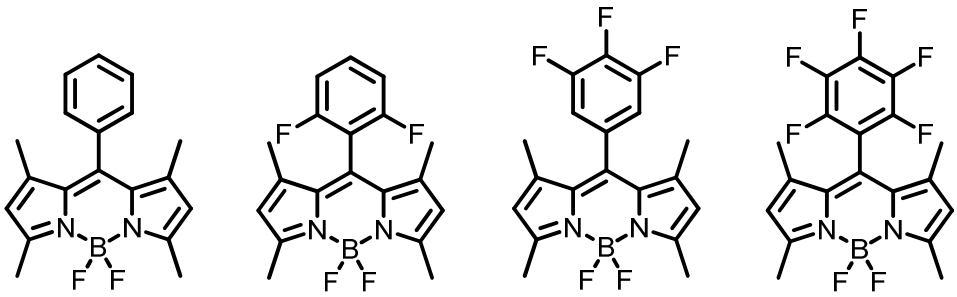

Series 2 Bodipy compounds with increasing numbers of fluorine atoms.

If there is an electronic effect on the spectroscopic measurements then it should be exaggerated by the presence of incremental numbers of fluorine atoms. One may expect a 'stepwise' increase in the fluorescence quantum yield equivalent to the number of fluorine atoms present on the aryl-substituent.

It is possible that both the number of fluorines and the substitution pattern of them both exhibit an effect upon the photophysics.

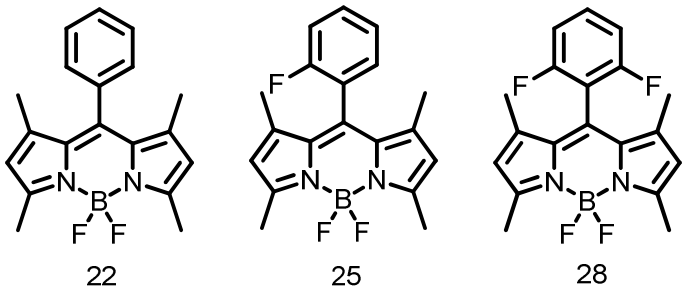

Series 3 Increasing size at the ortho position of the aryl group.

As discussed in the introduction to bodipy compounds may act as molecular rotors, provided that the mechanism for rotation is not sterically hindered. While it is considered that there is not enough room for the phenolic substituent to fully rotate it may well rock back and forth, thus decreasing quantum yield.[21] Indeed if there were full rotation of the phenyl ring then the quantum yield would closely resemble those seen in the derivatives with a totally unsubstituted dipyrrin core.[22] The size difference between fluorine and hydrogen atoms though not

huge could be enough to prevent the ‘rocking’ of the phenolic group. The prevention of rotation should lead to an increased fluorescence quantum yield, a further explanation for the differences between **22** and **23**.

If this is the case one would expect to see increased quantum yields in compounds **26** and **28** relative to **22**. In addition the prevention of rotation in **26** should give rise to a radically different fluorine NMR spectra owing to the two fluorine atoms on the boron centre being in different environments.[23]

If the rotation is hindered upon ortho-substitution it is important to attempt to show that this is due to the presence of fluorine and that it does not occur for hydrogen. Ideally deuterating at the ortho position would be preferable as deuterium is the only entity which is smaller than fluorine and that can be substituted into the system. Deuterium far from being larger than hydrogen might well be smaller depending on the conditions at which the measurement takes place. Hence the substitution of deuterium for hydrogen would not impede rotation while still influencing the fluorine atoms at the BF_2 unit. Unfortunately the acquisition of the appropriate starting material was far too expensive. As such ortho-fluorine is the smallest group that can be introduced with the mono-ortho product **26** having the least steric bulk.

The controls with unsubstituted bodipy cores (**29** and **30**) cannot be directly compared to the other 7 tetra-methyl substituted bodipy using photophysical measurements. This is simply because they are different fluorophores and hence have inherently different properties. Yet it is possible to compare **29** and **30** via NMR, specifically ^{19}F NMR spectroscopy. In theory there should be rotation around the C8-meso bond in both compounds, if there is not then compound **30** should show further splitting of the BF_2 fluorine atoms.

3.2 Synthesis and Characterisation

3.2.1 Synthesis

The compounds shown in Figure 5 were prepared via standard procedures (in the case of **22**-**28**) and a slightly modified procedure in the case of **29** and **30**.[24] The synthesis of all compounds was uncomplicated and produced low yields – typical of most 'one-pot' bodipy syntheses (given in table 3).

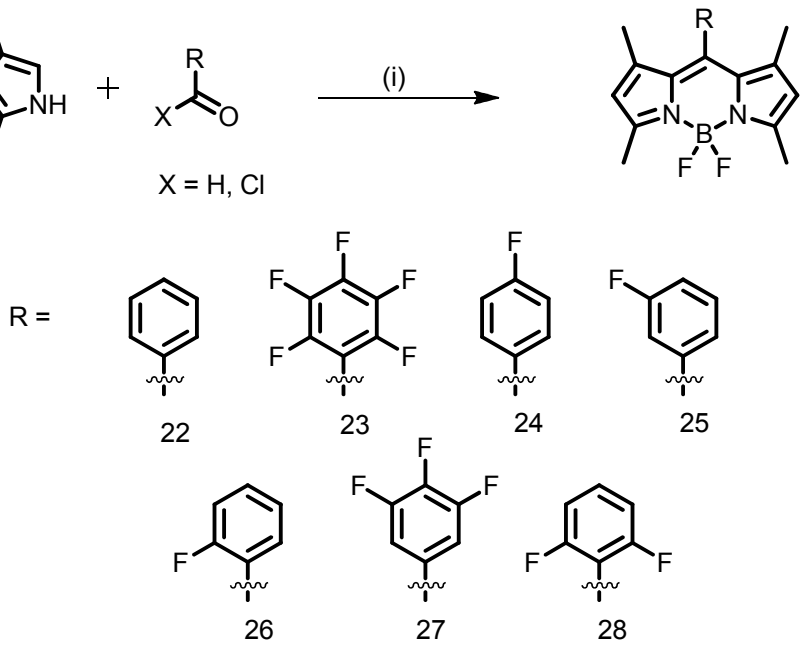

*Scheme 1 The synthesis of the methyl-substituted bodipy compounds **22**-**28**. If X = H: (i) DCM, TFA; DDQ; $^{i}Pr_2NEt$, $BF_3.OEt_2$. If X = Cl: (i) DCM, TFA; $^{i}Pr_2NEt$, $BF_3.OEt_2$.*

The choice between F_n-aryl acid chloride and F_n-aryl aldehyde was simply down to the list of available starting materials. Unsurprisingly the reactions for which the acid chloride was used, gave moderately better yields – presumably as there is one less synthetic step involved.

	22[a]	**23**[a]	**24**[a]	**25**[a]	**26**[a]	**27**[b]	**28**[a]
Yield (%)	15	9	10	11	15	25	10

*Table 3 Total yields from the syntheses of compounds **22**-**28**. [a] – aldehyde starting material; [b] – acid chloride starting material.*

The electron-withdrawing aspect of fluorine causes increased reactivity at the carbonyl carbon of the aldehyde – by way of increasing the partial positive charge on the carbon thereby giving rise to promoted attack of nucleophilic

groups. It might therefore be expected for the percentage yields to give rise to a trend whereby the yield increases with the presence of more fluorine atoms. However there is no appreciable trend in yield when compared with the quantity of fluorine atoms.

The synthesis of **29** and **30** differs from the typical preparation as unsubstituted pyrrole is used in a large excess at the beginning. This excess pyrrole is distilled off and the dipyrromethane intermediate is isolated. The intermediate was then dissolved in DCM and reacted in the same way as the methyl-substituted dipyrromethane variant, undergoing oxidation followed by boron chelation. Both pyrrole derivatives were synthesised in typical yields:

	29	30
Yield (%)	11	10

*Table 4 Total yields for the reactions forming **29** and **30** using a 'one-pot' method.*

It is possible to perform the reaction in 'one-pot' without isolating the intermediate product, however the 'one-pot' method causes difficulties with the work up and purification. The TFA present in the reaction mixture causes the pyrrole to polymerise forming polypyrrole.[25] Polypyrrole can cause blockages at the top of chromatography columns which is problematic. Any remaining pyrrole can degrade on the column – unless a basic solid-phase is used, thus wasting significant quantities of pyrrole.

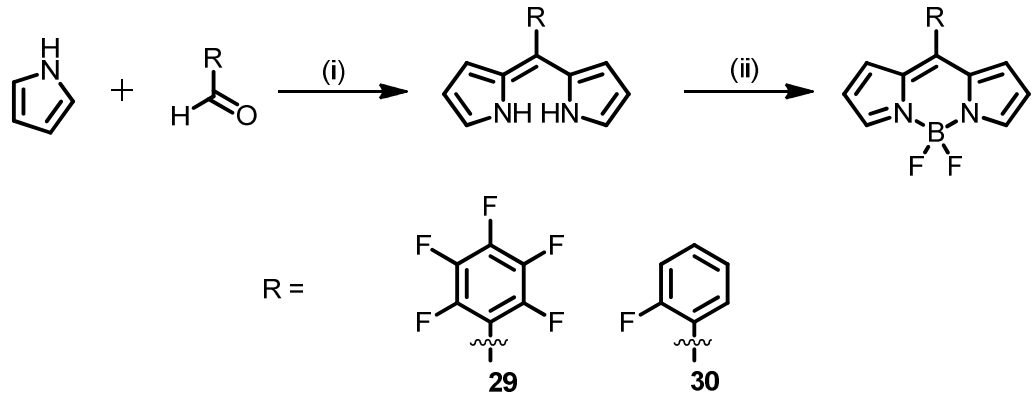

Scheme 2 Synthesis of unsubstituted bodipy compounds. (i) excess pyrrole, TFA; (ii) DCM, DDQ; $^{i}Pr_2NEt$, $BF_3.OEt_2$.

Upon synthesis all compounds were firstly rigorously purified to remove any trace impurities which might show up in the photophysical analysis. The purification was two-fold firstly the crude material was passed through a

standard silica column to remove the bulk of the impurities. Secondly the purified material was subjected to several crystallisations via slow-vapour diffusion – typically by dissolving the bodipy in DCM and using petrol to form the crystals.

Once the crystals of the pure bodipy compound had been collected the samples were then subjected to a full characterisation including the following techniques: ^{1}H, ^{13}C, ^{11}B, ^{19}F NMR spectroscopies, mass spectrometry, melting points and IR spectrometry.

3.2.2 Characterisation of Compounds 22 – 28

3.2.2.a NMR Characterisation

Whilst the ^{1}H and ^{11}B NMR measurements were all quite mundane, with the exception of **26**, the ^{13}C and ^{19}F NMR were more complex than expected.

All measurements of the ^{11}B NMR gave similar results, a triplet at ca. -0.20 ppm with a 32 Hz B-F splitting, which is typical for the boron NMR spectrum of bodipy compounds. Meaning that the differing substitution patterns of the fluorine atoms at the meso positions does not have an effect on the electronics at the boron centre. The similarity in shifts did not come as a surprise as there is little or no electronic contribution at the boron centre from the HOMO orbital.

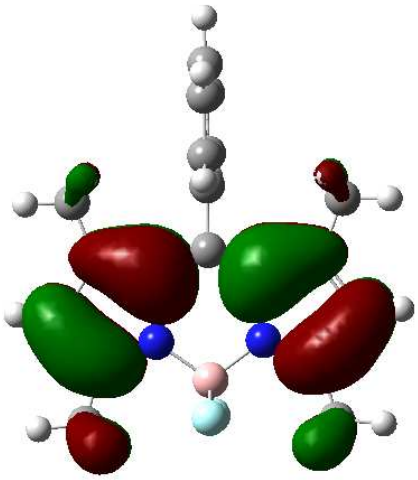

*Figure 7 HOMO of **22** calculated using 6-311G^{++} that shows the lack of orbital contribution at the boron centre of the bodipy core.*

For all compounds the coupling constant seen in the boron spectra equated to those seen in the fluorine in the ^{19}F spectra of the equivalent compounds.

Though the proton NMR spectrum was fairly ordinary it is worth mentioning about the splitting patterns observed in the protons in the aromatic region. As fluorine is spin ½ it causes the splitting of surrounding atoms in the same way that a proton might.

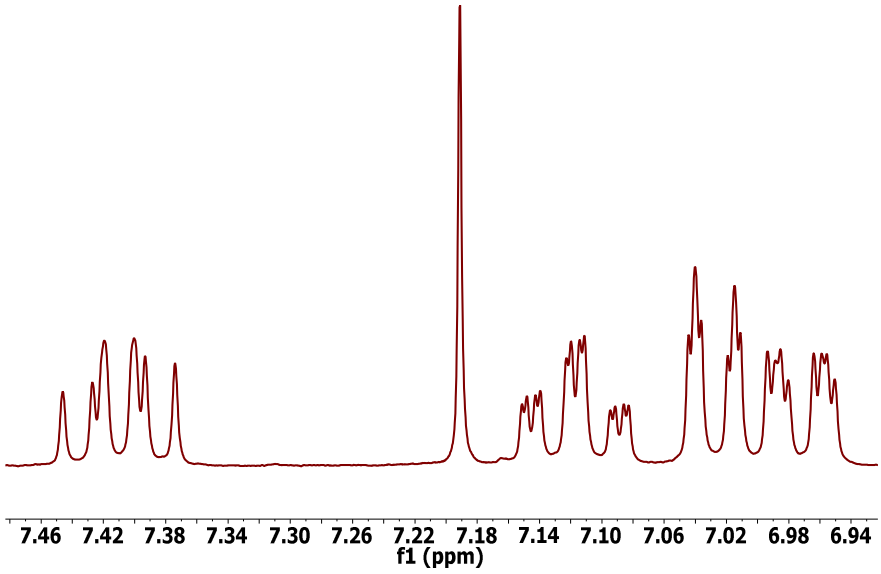

*Figure 8 ^{1}H NMR spectrum of the aryl region of **25**, showing a splitting pattern which is much more complicated than might be expected for a meta-substituted aryl bodipy.*

As seen in Figure 8 when fluorine is present on an aryl bodipy moiety the splitting pattern differs from the value expected if the fluorine were an NMR inactive group. The difference in splitting patterns from the expected patterns can make the assignment of peaks much more complex, even in the case of **24**. The presence of a para-fluorine atom causes the aryl protons of **24** to become an AA'BB'X system greatly complicating the spectra.[26] Where one would normally see a two sets of doublets in para-substituted aromatic systems, here a complex set of multiplets is observed.

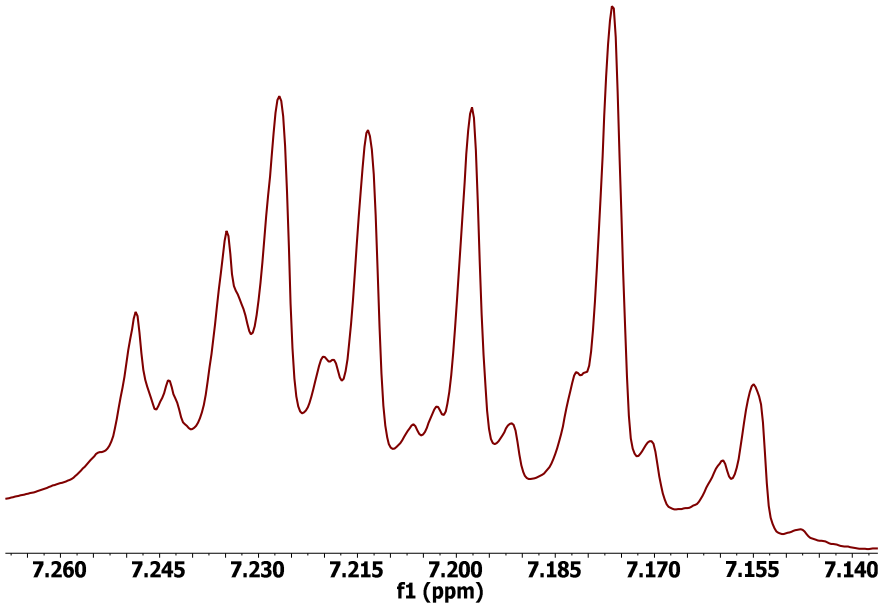

*Figure 9 ^{1}H NMR spectra of the aryl region of **24**, with extra splitting owing to ^{19}F-^{1}H splitting.*

^{13}C NMR spectra are typically run as proton decoupled spectra. As the NMR machines which were accessible only had two probes it was not possible to decouple the C-F splitting at the same time as the C-H splitting. As a result the carbon NMR spectra were much more complex than anticipated. Once again the fluorine atoms on each aromatic ring would cause splitting of each carbon which it is attached to as well as further splitting to adjacent carbon atoms with this splitting decreasing the further the carbon is from the fluorine.[27]

$J_{C1\text{-}F}$ = 245.0 Hz
$J_{C2\text{-}F}$ = 21.0
$J_{C3\text{-}F}$ = 7.7
$J_{C4\text{-}F}$ = 3.3

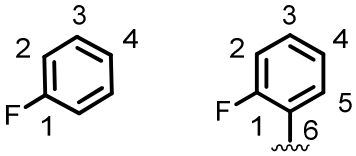

Figure 10 Coupling constants between F and C on a phenyl ring (left) and the effect of ortho-disubstitution upon a phenyl ring, where all 6 carbon atoms of the ring are inequivalent (right).

The complexity is further increased if the molecule is substituted at another position of the ring as this would make each of the six phenyl carbons inequivalent, with the exception of para-substitution.

In the case of multiple fluorine substitution around the ring each inequivalent fluorine acts separately splitting the carbon atoms of the ring. If there are multiple fluorine atoms on a ring it becomes more difficult to discern where the

peaks are as further splitting causes the loss of peak height. The further loss of peak height is not helped by the weak signal to noise ratio of ^{13}C NMR.

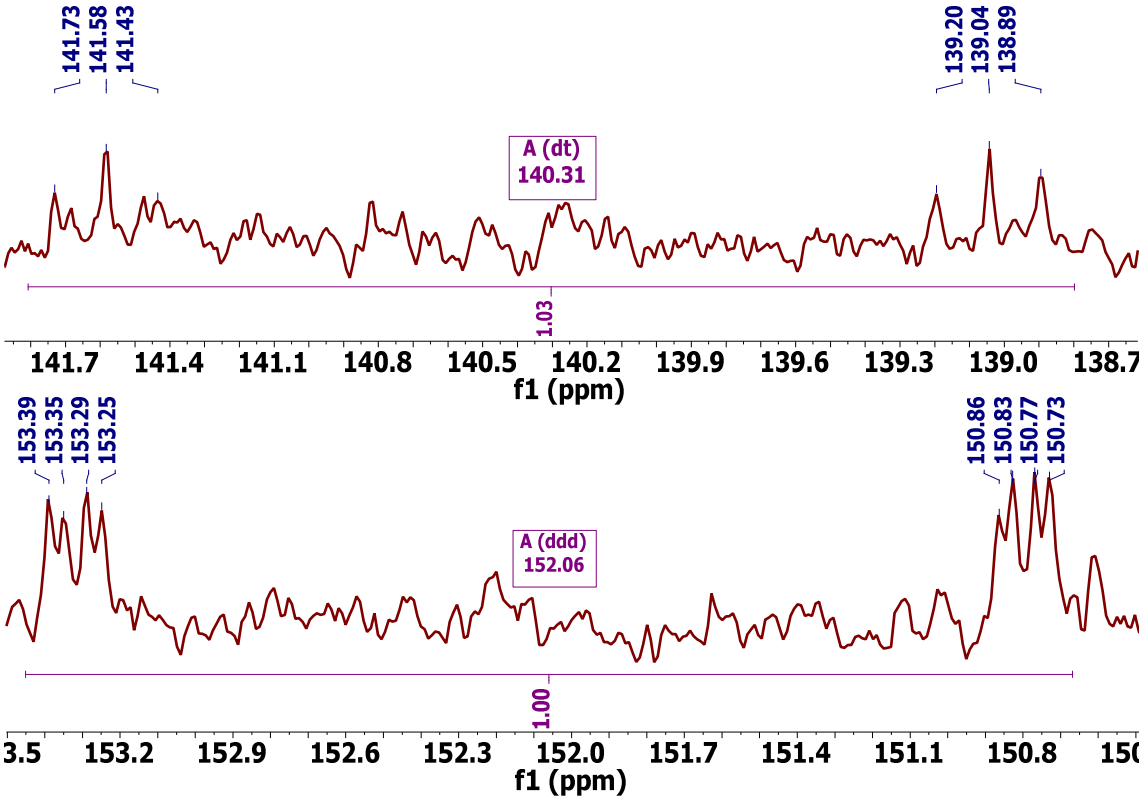

*Figure 11 The appearance of the ^{13}C NMR spectrum split by two inequivalent fluorine atoms in **27**. Spectra 1 - 152.06 (ddd, J = 253.2, 19.9, 3.9 Hz, bottom); Spectra 2 - 140.31 (dt, J = 255.3, 18.9 Hz, top).*

The presence of these splitting patterns is something which seldom is recognised in any published work where a perfluorinated aryl ring is present. Indeed the peaks are mostly reported as singlets in spite of the ^{13}C{^{1}H} spectra not being fluorine decoupled.

Carbon atoms which are adjacent to the two nitrogen atoms in the core of the bodipy are also subjected to splitting by ^{14}N atoms. Splitting by ^{14}N is typically difficult to see as the isotope ^{14}N has a spin 1 which often partially washes out both the signal and splitting to carbon due to quadrupole relaxation.[28]

The fluorine NMR spectra were certainly the most interesting out of all the NMR as fluorine interactions can be seen with each other NMR active nucleus in the series – with the exception of ^{14}N, though this was not fully explored.

The H-F splitting which is observed in the proton spectra can also be seen in the fluorine spectra. Due to the limitations seen in fluorine NMR spectra the

resolution of the spectra is often not good enough to determine splitting patterns or coupling constants.

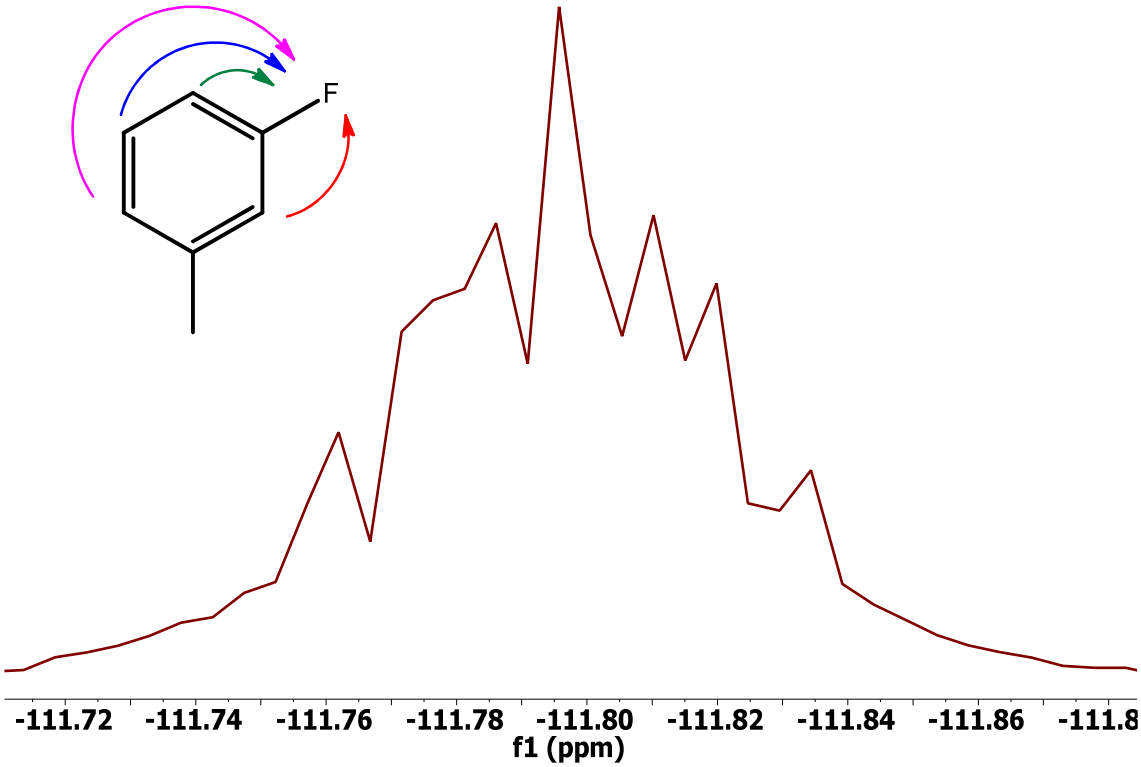

*Figure 12 ^{19}F NMR spectra of the aryl-F of **25**. Estimated coupling constants: red and green ca. 8.3 Hz; Blue ca. 5.9 Hz; Magenta – not determined.*

A lack of resolution was particularly prevalent in the compounds which were possessed less symmetry (**25** and **26**). The lack of resolution is due the coupling constant from the para-proton (magenta arrow in Figure 12) which is too small to cause further resolvable splitting of the peaks.

The fluorine spectra were modelled using MestreNova and the splitting patterns matched up with the observed data.

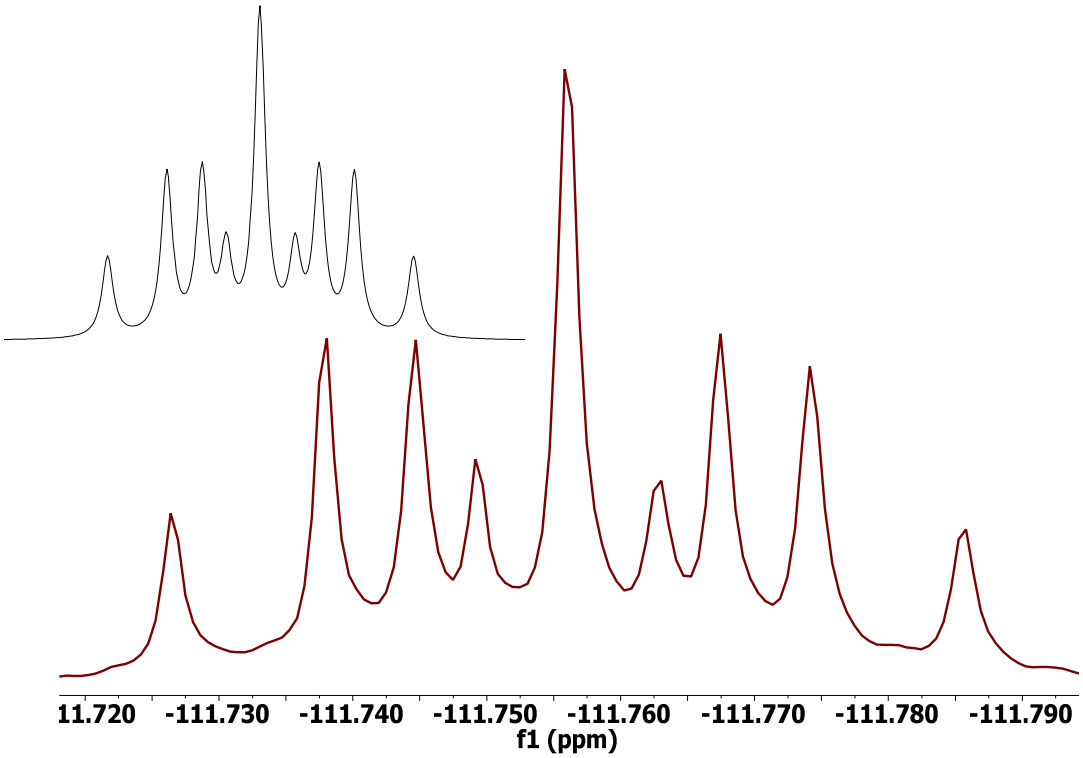

*Figure 13 ^{1}H-^{19}F NMR splitting observed for the aryl-F of **24**. Simulated splitting (inset) and the observed triplet of triplet splitting (bottom).*

A $^{1}H\{^{19}F\}$ NMR was performed for compound **26**, which had a particularly complex series of splitting patterns. The resulting spectrum demonstrated the expected splitting pattern observed for all ortho-substituted phenyl rings. This experiment confirmed that it is indeed the fluorine atoms which cause the complex ^{1}H splitting and not any other interactions through space or through bond.

It is possible to access the data which is hidden in the background noise of the ^{13}C spectra using ^{13}C-^{19}F correlation experiments.[29] As mentioned in the ^{13}C NMR section it is often very difficult to accurately measure carbon peaks in a perfluorinated system. The use of C-F correlations can shed light on exactly where the carbon peaks lie, if not totally reveal them, it can also reveal some of the splitting which occurs within the compound.

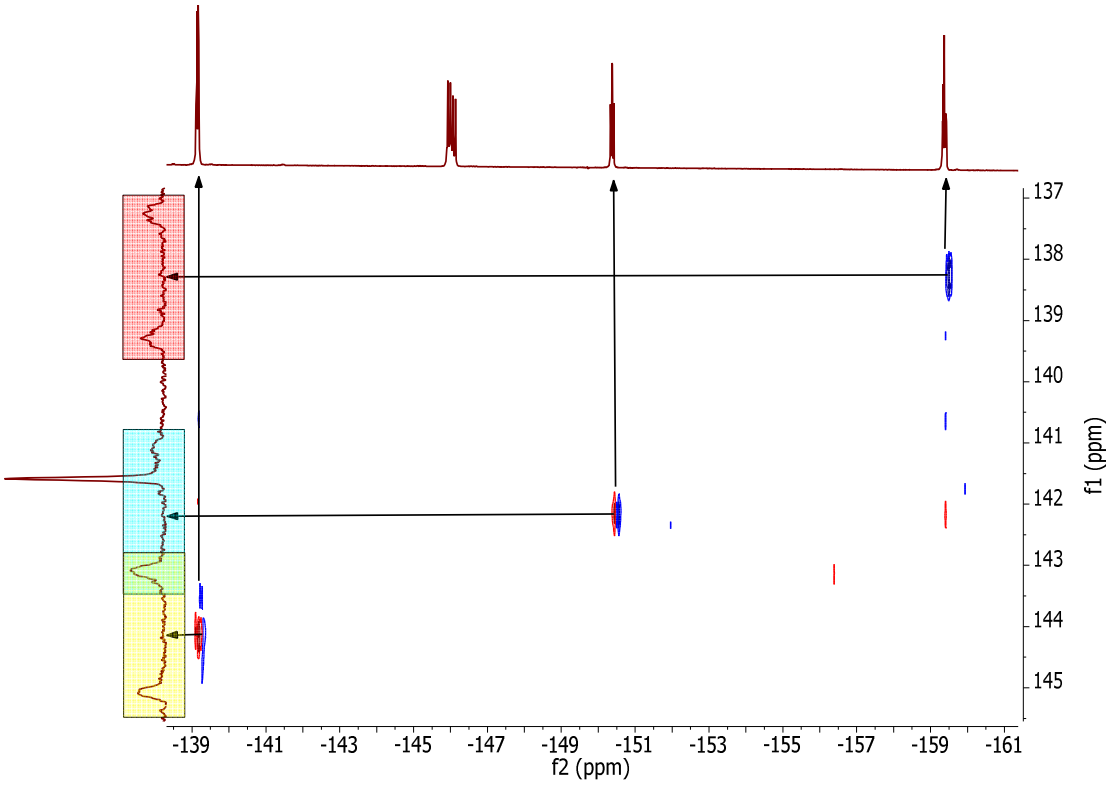

*Figure 14 ^{13}C-^{19}F NMR correlation of **23** with coloured definition of the correlating regions.*

It is clear to see the relationship between the ^{13}C and ^{19}F spectra in Figure 14. Each fluorine atom which is directly connected to a carbon splits the carbon signal to a doublet with coupling constant of ca. 250 Hz which is the expected value for direct C-F splitting.

There is an apparent overlap of two carbon peaks (yellow and cyan) which is revealed further when an integral of the relative peak heights is performed. When examined the peaks reveal relative intensities of 1 : 2 : 1, as anticipated for two doublets overlapping. This overlap is likely due to the increased broadness observed for the carbon peaks. The carbon peaks appear broad due to further splitting from the fluorine atoms present on the adjacent carbons, the coupling constants for which cannot be measured.

It is possible to use the ^{19}F NMR spectra to assign some carbon peaks using the F-F splitting patterns (Figure 15) in combination with the results of the C-F correlation experiments.

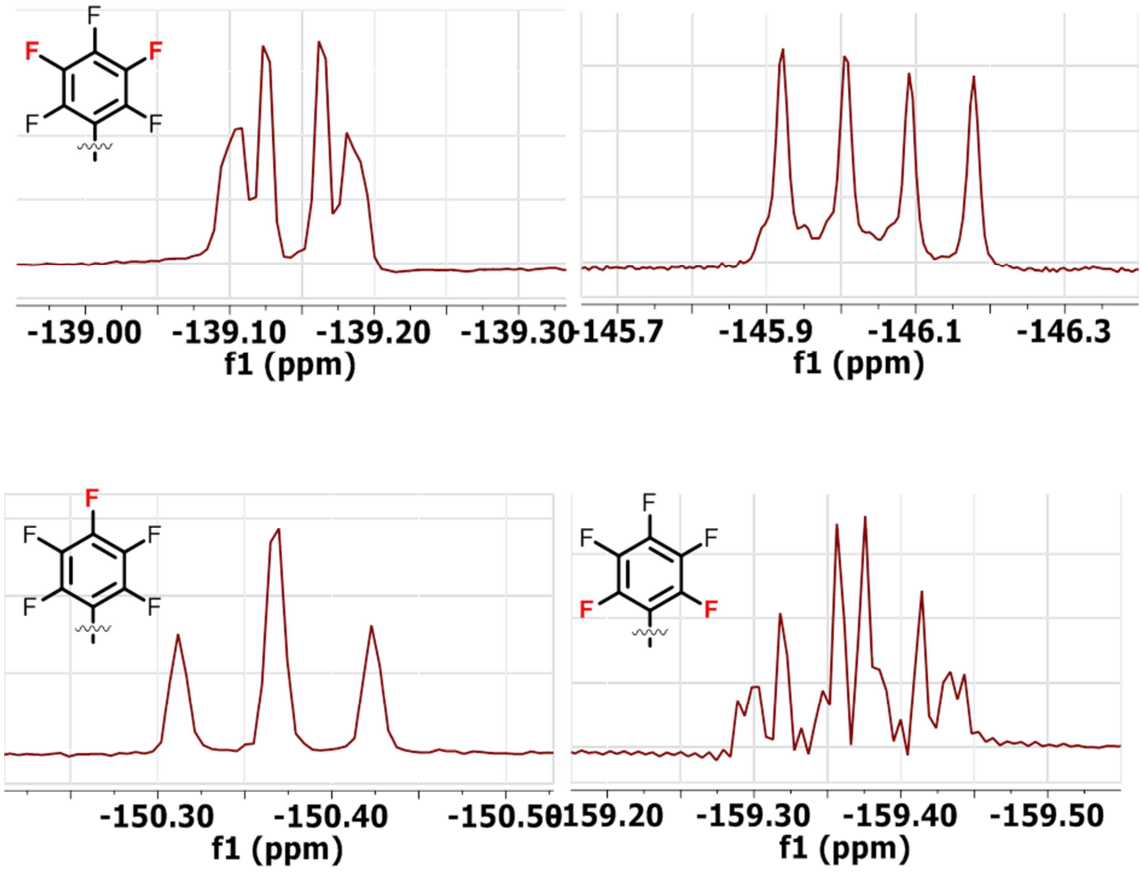

*Figure 15 Assignment and traces for ^{19}F of **26**, with all aryl-fluorine peaks identified (structures inset- with highlighted fluorine atoms denoting which fluorine(s) correspond to each set of peaks).*

Knowing which fluorine(s) are at what ppm allows the exact assignment of the carbon spectra: red = ortho-C, cyan = para-C, and yellow = meta-C (colours refer to Figure 14).

In bodipy systems it is standard to measure the ^{19}F NMR spectra in order to further verify the presence of a chelated BF_2 unit. Where the ^{11}B NMR confirms the presence of a boron atom, the ^{19}F NMR can confirm whether the boron has undergone any substitution reactions.

Boron has two isotopes which are NMR active ^{10}B and ^{11}B, the spins being 3 and 3/2 respectively. The relative abundance of ^{10}B is ca. 20 % with ^{11}B representing the remaining 80 %. It is not common to see F-splitting from ^{10}B in a ^{19}F NMR spectra, it is only seen for spectra with a high number of scans on an NMR machine with a larger field strength. The observed peaks typically consist of a quartet with intensity 2F if both fluorine atoms are identical. The ^{10}B trace is aligned slightly to the left of the ^{11}B peak to which it corresponds. The off-centre

alignment of the ^{10}B peak leads to the two left peaks of the ^{11}B quartet having a slightly increased intensity, due to isotopic splitting.[30]

As ^{11}B has a spin of 3/2 it will split two equivalent F atoms, such as those found in the BF_2 unit of a bodipy, into a quartet.

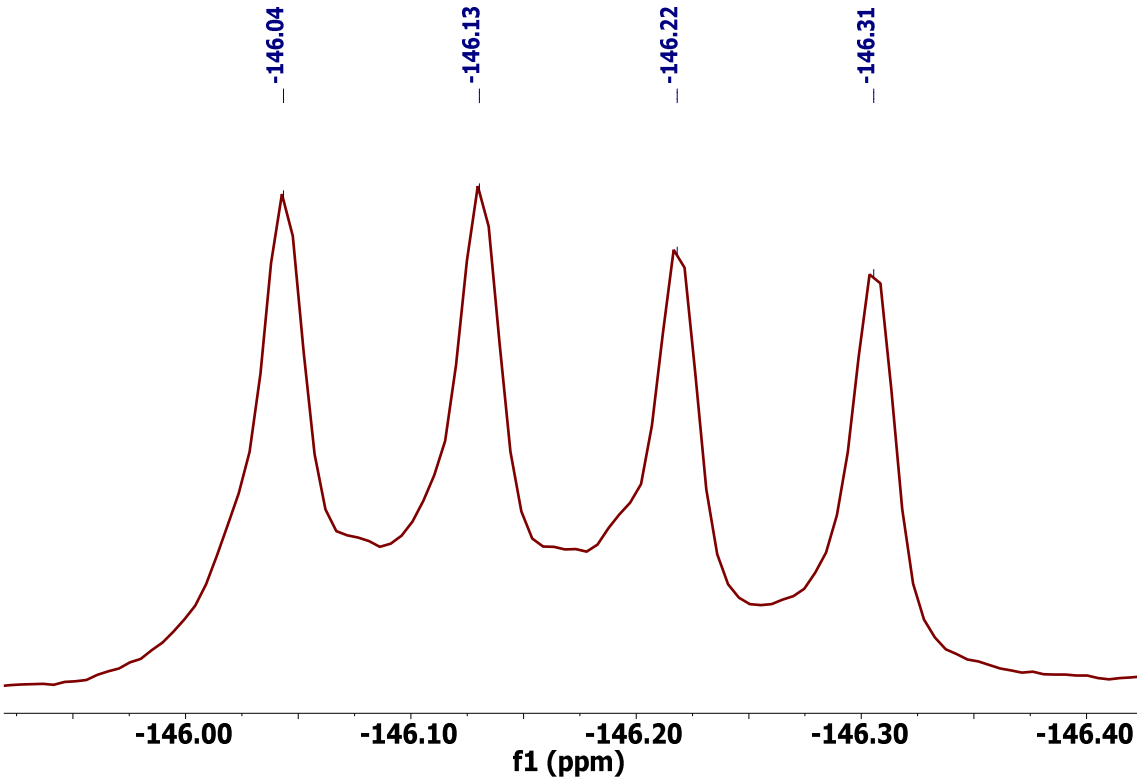

*Figure 16 The typical ^{19}F trace for a bodipy BF_2 unit - specifically that of bodipy **24**, which shows a quartet of intensity of 2F.*

Indeed a quartet pattern was observed for all of the compounds **22** - **28**, with the exception of **26** - where the observed peaks in this case comprised two distinct sets of peaks (Figure 17) each comprising 8 peaks.

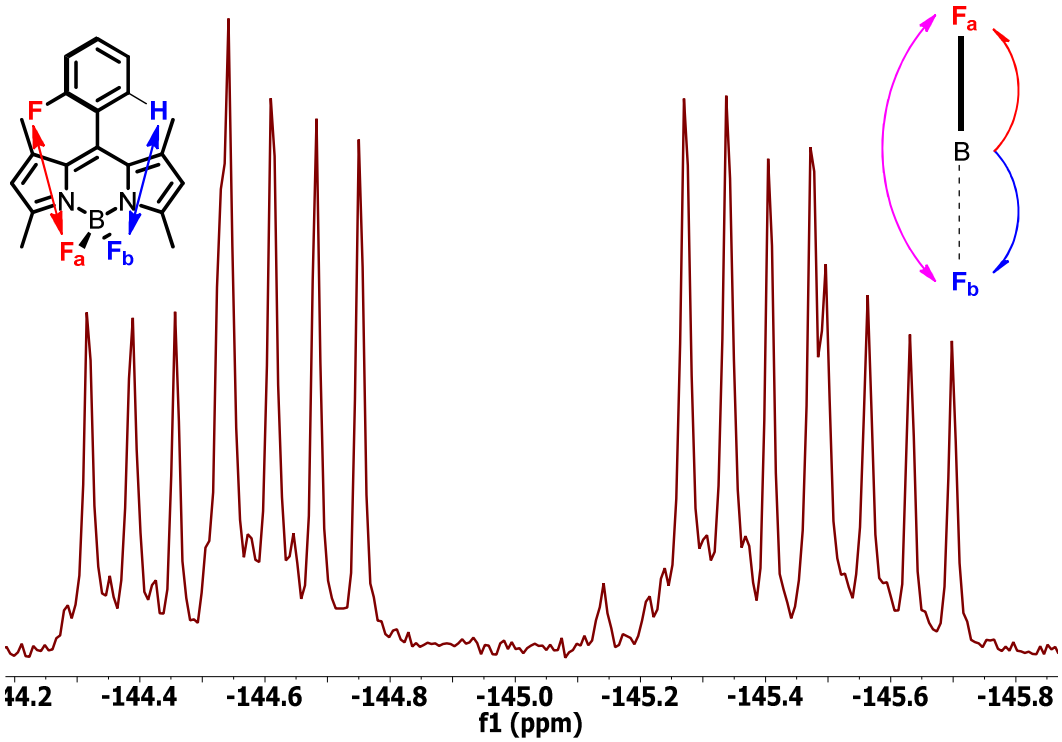

*Figure 17 ^{19}F spectra for the BF_2 unit of **26**, two sets of doublet of quartets. The structure of **26** with inequivalent fluorine atoms of the BF_2 unit (inset, left) and inter-fluorine splitting between the two BF_2 fluorine atoms (inset, right).*

The complicated splitting pattern is due to the two fluorine atoms on the BF_2 unit being inequivalent to each other. This inequivalence is bought about by the ortho-fluorine on the aryl moiety preventing the rotation of the phenyl ring around the C8-Ar bond. The lack of rotation means that there are effectively two faces of the bodipy, the first where the fluorine points up and the reverse where the ortho-proton resides. As the fluorine atoms of the BF_2 unit are arranged in a tetrahedral arrangement they are each exposed to difference faces of the bodipy thus making them inequivalent. F_a and F_b are both split by the boron, yet are now also split by each other.

The fluorine spectra of **25** and **26** were compared in order to ascertain if **25**, being unsymmetrical, would exhibit the same BF_2 splitting pattern. This splitting was not observed hence either an ortho-proton does not further hinder the rocking of the phenyl ring or alternatively that the meta-fluorine does not exert enough of an influence to BF_2 fluorines.

A variable temperature NMR was also performed on **26** in order to see if there was a barrier to rotation which could be overcome. **26** was dissolved in d_{10}-o-

xylene, as this was the highest boiling point NMR solvent available, thus giving the largest possible temperature range.

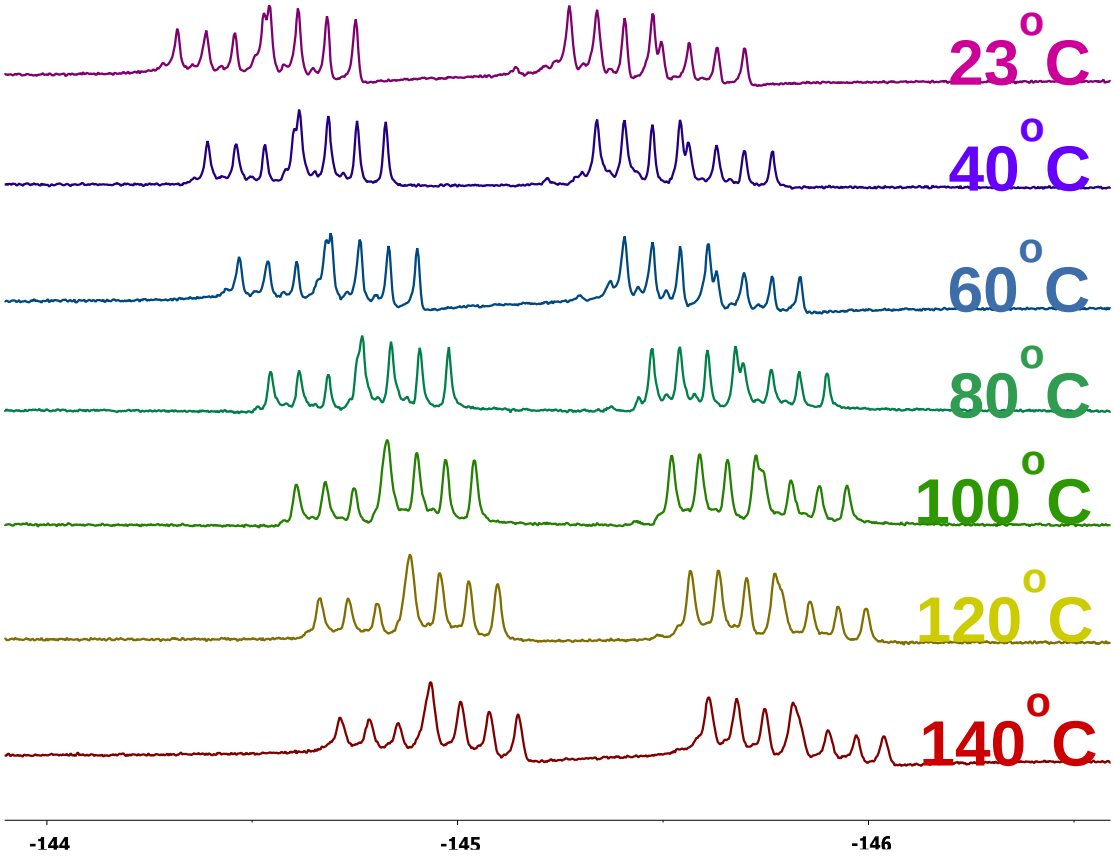

*Figure 18 A section of the ^{19}F VT-NMR trace of **26** in d_{10}-o-xylene, with temperatures ranging from 23 – 140 °C.*

The VT-NMR showed that there was no coalescence of the peaks and hence rotation around the C8-aryl bond of compound **26** is restricted. This restriction is caused by the steric bulk of the flanking 1,7-methyl groups and means that the rate of rotation of the aryl group must be < 1 s^{-1} at room temperature.

3.2.2.b X-Ray Crystallographic Structure Analysis

All compounds, with the exception of **22** and **24**, were also subjected to an X-Ray crystal structure determination. Compound **22** already exists in the literature, and crystals of **24** did not diffract. All torsion angles and crystal densities are summarised in Table 5.[31]

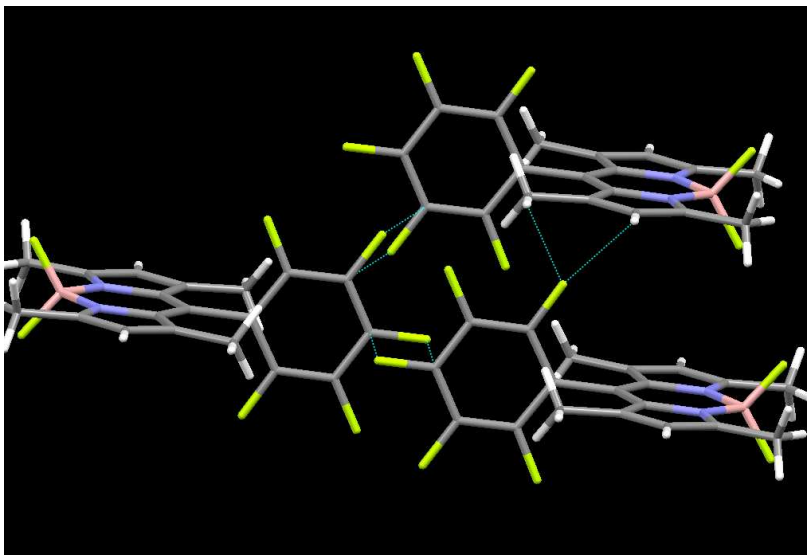

*Figure 19 Packing diagram for the crystal structure of **23**. Short contacts: H-F = 2.612 Å, C-F = 3.089 Å.*

The torsion angle between the bodipy core and the aryl moiety* is 0.34^{o} which is slightly lower than observed values for **22** (0.95^{o}).The torsion angle B-N-C_3-C_2 ('boron-planarity') was also analysed. The bodipy core of **23** is flat with the boron sitting perfectly in the plane of the molecule, 180.00^{o} vs 178.90^{o} for **22**.

Compound **23** showed a 'head-to-head' packing motif, where the perfluorinated rings of individual compounds line up parallel to each other. Short contact lengths were detected for both H-F and C-F interations. In spite of the short contact of 2.6 Å for H-F it is not likely that this is hydrogen bonding and is probably a weak interaction with values similar to that seen for van der Waals complexes.[32, 33]

The C-F bond is polarised due to the difference in electronegativity between carbon and fluorine (2.5 vs 4.0).[34, 35]The C-F interaction is therefore likely to be a similar weak force of attraction where the C-F bonds sit parallel to each other, with C-F' and C'-F each exerting a force.

Compounds **23** has the most ordered packing of the series of compounds **22**-**28**, showing a much higher crystal density that other molecules (see Table 5). The higher order is likely a result of the multiple weak forces of attraction seen between the fluorinated aryl groups at the head of the molecule.

* 'Aryl-twist'- refers to the difference in angle between the plane of the aryl-group and the bodipy core.

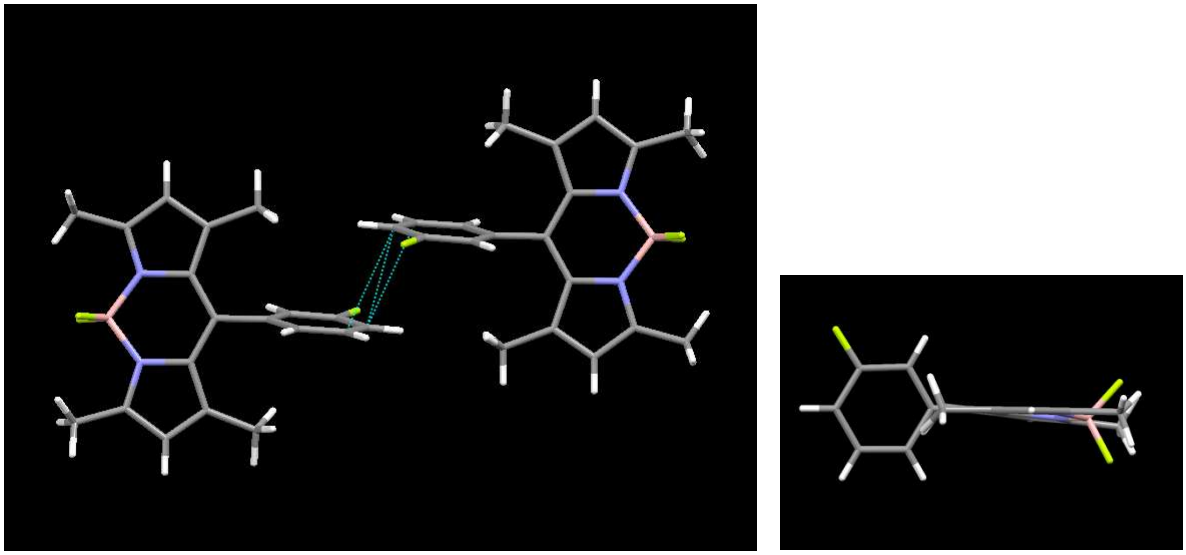

*Figure 20 Packing diagram for the crystal structure of **25**. Short contact: C-C 3.25 Å (left); side profile of **25** (right), showing the boron atom out of the plane of the bodipy core.*

The aryl-twist torsion angle for **25** is 3.41^{o} which is slightly different from **22** and **23** yet similar to all other compounds where both proton and fluorine atoms are present together on the phenyl ring. The increase in this angle is not thought to be due to the lack of symmetry throughout the molecule as **27** and **28** have similar values.

The boron-planarity torsion angle is the lowest of the series at 172.81^{o} which can be seen from the side profile of the compound, as the boron is clearly out of the plane of the compound, with the whole core adopting a more curved appearance.

Once again the crystal packing of **25** is 'head-to-head' however there are no C-F interactions observed. The shortest contact is a 3.25 Å C-C interaction. The overall packing has less order than that of **23** (density ca. 0.15 gcm^{-3} less).

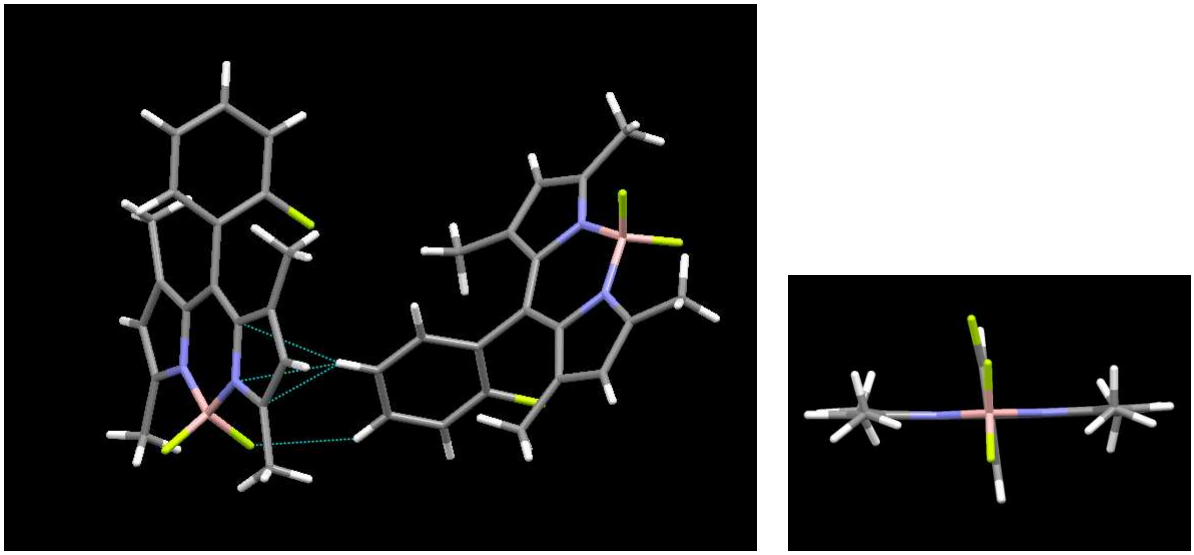

*Figure 21 Packing diagram for the crystal structure of **26**. Short contact: H-F = 2.581 Å, H-N = 2.661 Å (left); looking down the C8-aryl bond of **26** (right), which allows the aryl-twist angle to be better visualised.*

26 exhibits the largest change in the aryl-twist in the entire series (5.75^{o}). This angle is a surprising result as it would have been assumed that the larger fluorine atom would ensure an increased orthogonality between fluorophore and aryl group.

The boron-planarity is similar to that of **22** with a value of 177.99^{o} - virtually planar. Both the lack of planarity seen in the phenyl-fluorine and the boron planarity can be seen well in Figure 21.

26 demonstrates a 'pseudo-head-to-tail' packing arrangement which sees short contacts between multiple atoms, with no obvious reason to believe that these are weak forces of attraction. The crystal density for **26** is also the lowest of the series at 1.336 gcm^{-3}, which is understandable as there is little order in the crystal packing of the compound.

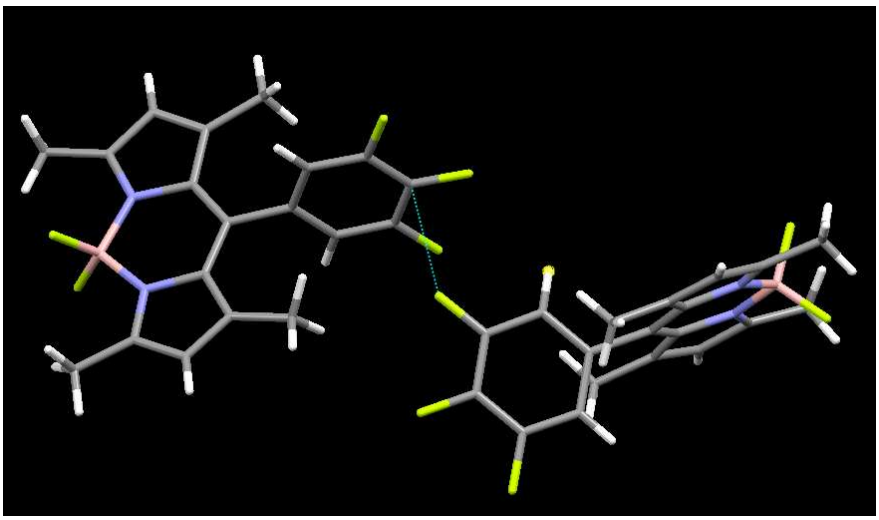

*Figure 22 Packing diagram for the crystal structure of **27**. Short contact: F-C = 3.006 Å*

Compound **27** shows a head-to-head arrangement in the packing diagram which differs from that of **23** as the aryl groups are not parallel to each other, though the high density of **27** (1.482 gcm^{-3}) suggests that the phenyl rings not being parallel does not have a large effect on the order of the packing.

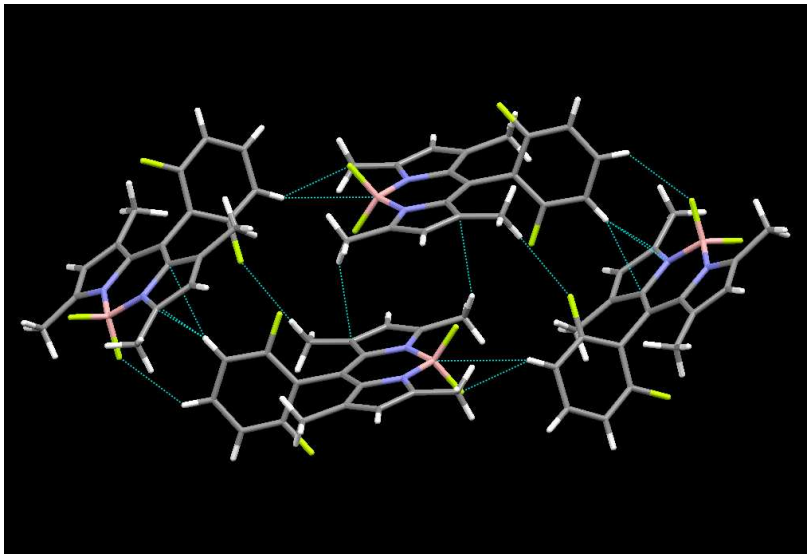

*Figure 23 Packing diagram for the crystal structure of **28**. Short contacts: smallest F-H = 2.434 Å, longest B-H = 3.137 Å. The compound appears in a cyclical head-tail-head-tail arrangement.*

Unlike **26** where the presence of an ortho-fluorine atom seems to increase the amount that the aryl-group twists out of planarity, **28** shows a more normal mode of behaviour with the increasing ortho-sterics causing further

orthogonality between core and aryl group. The boron of **28** is slightly out of plane sitting between the values of **27** and **25**.

The crystal packing is 'head-to-tail' and the lattice involves 4 separate molecules with various short contact points. The F-H short contact length (2.434 Å) is within the distance where hydrogen bonding can be observed (< 3 Å), again it is likely that there is simple a weak force of attraction.

	22	23	24	25	26	27	28
Torsion angle (°): B-N-C_3-C_2 (boron planarity)	178.90	180.00	179.68	172.81	177.99	176.33	174.45
Torsion angle (°): C_8-C_{Ar1}-C_{Ar2}-F/H (aryl twist)	0.95	0.34	0.05	3.41	5.75	3.36	2.90
Crystal Density (gcm^{-3})	1.357	1.561	1.349	1.408	1.336	1.482	1.411
Bond length ($C_{3,5}$—$Me_{3,5}$) Å	ND	1.396	1.498	1.494	1.480	1.484	1.487

Table 5 Assorted crystal structure data for the series of compounds detailing the boron-planarity and aryl twist torsion angles, the crystal packing density and the 3/5 methyl group bond length.

The bond length of the meso-aryl C-C bond was also measured to see if increasing the electron withdrawing capability of the aryl substituent affected this length. There were no significant shifts in bond length with increasing number of fluorine atoms. Indeed almost all bond lengths for all compounds were similar, with no significant changes. The exception being the length of the carbon-methyl bonds in the 3 and 5 positions of the bodipy core. Here the length of the bond in the perfluorinated compound (**23**) was much shorter than the rest of the series. An increased acidity has been observed previously upon the meso-substitution of a perfluoro group on the meso position.[3] An increasing acidity at the 3 and 5 methyl protons leads to more facile nucleophilic substitution reactions, such as the Knoevenagel reaction. In turn the increased acidity of the 3 and 5 positions would mean that meso-perfluoroaryl containing compounds would give enhanced yields when expanding the conjugation from these positions – owing to the more facile loss of the methyl protons at the 3 and 5 positions.

There are no obvious trends relating the substitution pattern of fluorine atoms to the crystal data. Though it appears that if there is m/p-fluorine substitution on

the aryl group there is a tendency of the bodipy molecules to align head-to-head which improves the packing densities.

3.2.2.c Infrared, Melting Point and Mass Spectral Analysis.

Each compound showed expected stretches: C-H (2950 cm^{-1}), C=C (1550 cm^{-1}), C=N 1510 cm^{-1}), and B-F (1190 cm^{-1}) without exception. The mass spectra of each compound either revealed the molecular ion peak $(M)^+$ or $(M+Na)^+$. Where $(M+Na)^+$ was seen it was also common to see $(2M+Na)^+$. Melting points for each compound fell in or around the ranges expected and bore likeness to similar literature compounds.

3.2.2.d Molecular Modelling

A computational study of the series **22**-**28** was performed in order to better understand the theoretical changes to the HOMO, LUMO and overall electron density with changing fluorine substitution. Initial calculations were performed using Gaussian 03, first running the ground-state energy minimised structures in the gas phase. These calculations were initially quite crude (using self-consistent field method), in order to reduce the run time of the calculations. After this the results were refined using DFT, and B3LYP with a 6-311G^{++} basis set.[36]

The results of these studies confirmed that for each compound the aryl ring sits orthogonal to the bodipy core. Ortogonality is also observed in the case of **22** where there is no fluorine substitution on the phenyl ring, suggesting that the presence of a proton might prevent rocking around the C8-aryl bond.

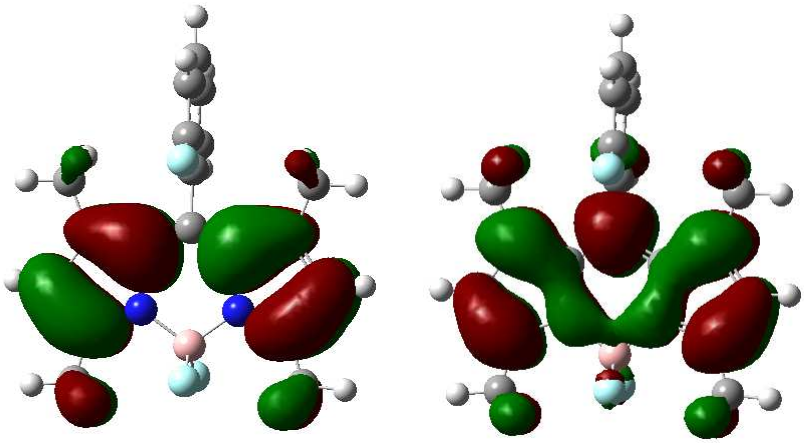

*Figure 24 HOMO (left) and LUMO (right) calculations of **26**, with red and green colours depicting the changing phases of each of the orbitals.*

The molecular geometries of the ground state structures all match those obtained from the crystal structures. The model shows that the orthogonality between aryl group and bodipy core is caused by the unfavourable steric interactions between the ortho substituent of the aryl group and the 1 and 7 methyl groups.

The electrostatic potential was calculated for the series (Figure 25). These calcuations showed an electron-withdrawing effect upon fluorination of the aryl ring, which is not surprising due to the electron affinity of fluorine atoms.

The simulation did not show that the perfluoro-aryl substituent on **23** caused any more electron withdrawing effects on the fluorophore than the other fluorine containing units. Though it does seem that the presence of ortho-fluorine(s) cause a high area of electron deficiency which is concentrated on and around the C8-aryl bond. This increase in electronegativity may have the effect of removing electron density at the meso position which in turn might affect the HOMO energy levels.

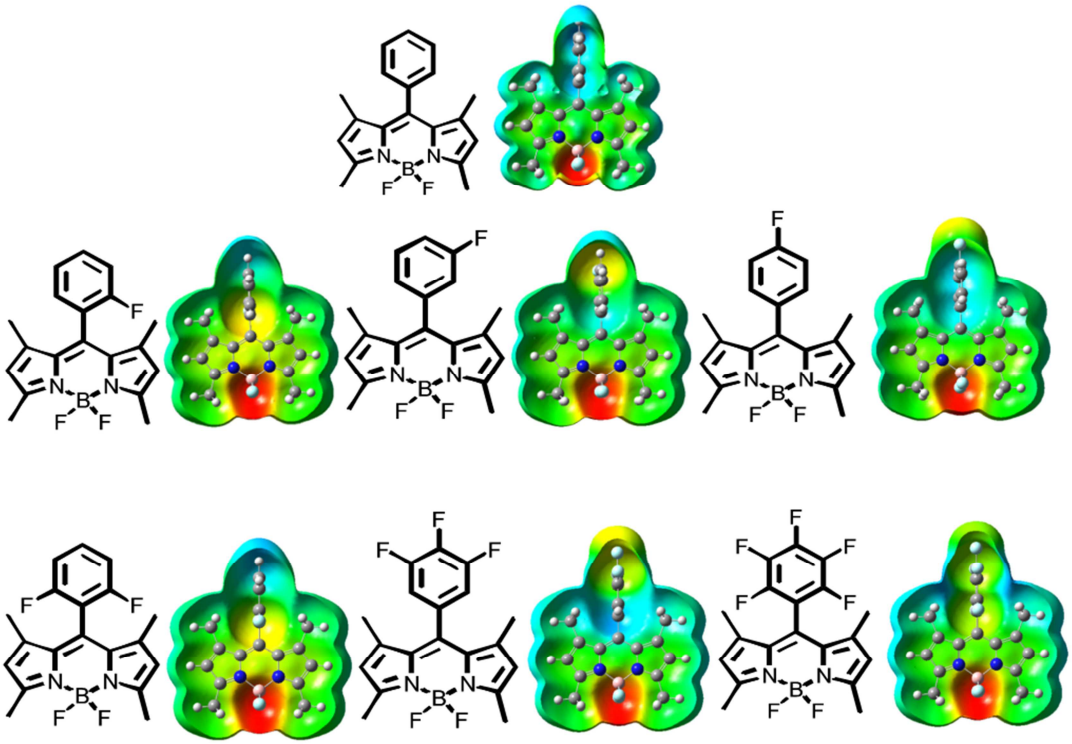

*Figure 25 Graphic representations of the electrostatic potential layed onto the isosurface of the molecular orbitals for the series **22**-**28**. A cyan colour is indicative of increased electron density, while the red-shifted colours (green through red) indicate areas of lower electron density.*

Both the HOMO and LUMO reside on the same regions across the series. The HOMO is mainly found over the dipyrromethene backbone of the fluorophore with little HOMO character found at the meso position of the bodipy, or indeed the boron centre. The LUMO spreads across much of the bodipy, with the phenyl moiety also involved. The results of these calculations are in accordance that have been published previously.[37] Table 6 contains the calculated values for the energy levels of both HOMO and LUMO for each compound as well as the difference in energy between these two orbitals.

Compound	E_{HOMO}[a]	E_{LUMO}[a]	ΔE (eV)[b]
22	-0.213	-0.103	2.99
25	-0.218	-0.108	2.99
24	-0.218	-0.108	2.99
27	-0.227	-0.118	2.97
26	-0.214	-0.106	2.94
28	-0.215	-0.108	2.91
23	-0.228	-0.123	2.86

*Table 6 Calculated energies for the HOMO and LUMO of **22**-**28** ordered by the HOMO-LUMO energy gap (Δ*E*). Calculations made using DFT and 6-311^{++} basis set as calculated for the energy minimised ground state structures. [a] energy displayed in Hartrees; [b] energy gap for HOMO-LUMO.*

Looking at the two extremes **22** and **23** it is clear to see that the introduction of 5 fluorine atoms lowers both the HOMO and LUMO energy levels. The series shows a dependence between the HOMO and LUMO energy levels and the quantity of fluorine atoms present on the ring, with increasing fluorine atoms lowering both energy levels.

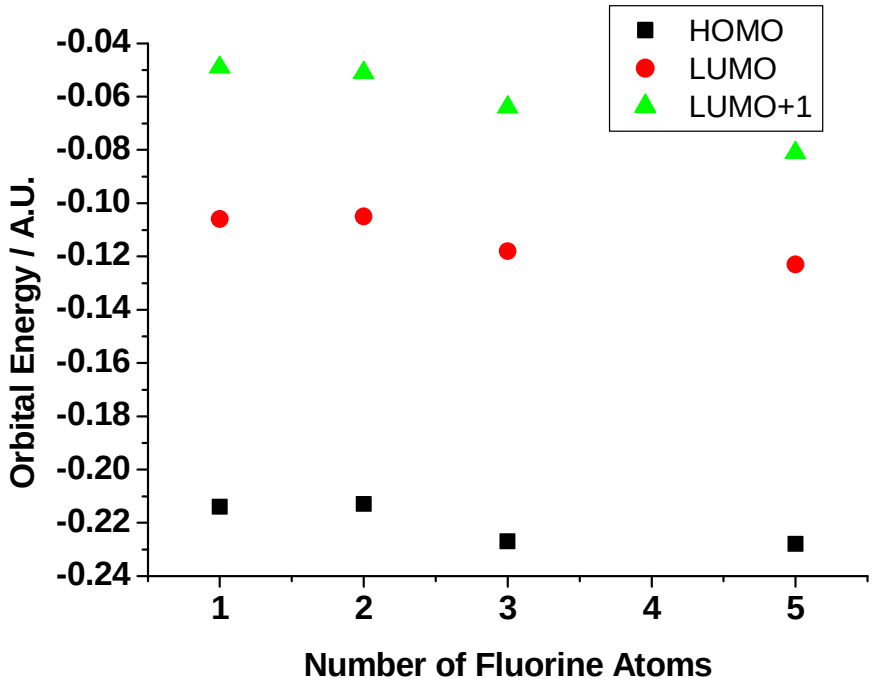

Figure 26 A graphical representation of the dependence of the calculated HOMO – LUMO levels and the number of fluorine atoms present on the aryl ring.

The exception to this rule seems to revolve around ortho-substitution, with both **26** and **28**. While **26** has one fluorine the HOMO-LUMO energy levels are slightly higher than those measured for **24** and **25**, both of which are mono-substituted. Mono-fluorination at the meta/para position though having an effect

on the HOMO/LUMO energy levels ultimately give large values for Δ*E* which are the same as those for **22** and not **26**.

While the HOMO and LUMO levels seem to rely heavily on the number of fluorine atoms present, values for Δ*E* do not follow the same trend. Δ*E* seems to rely on the pattern of F-substitution, where ortho-substitution causes the largest reduction to Δ*E*. Though the number of fluorine atoms present does seem to exert a mild effect on Δ*E* suggesting that the gap does rely on the cumulative effects of both the number and position of fluorine atoms.

Due to the relationship between Δ*E* and the colour of the compound it is possible to tentatively predict the order of the $\lambda_{abs\text{-}max}$ for the compounds. One would expect that order for the size of Δ*E* to be: **22** ~ **24** ~ **25** < **27** < **26** < **28** < **23**, and as discussed in the electrochemistry and photophysics sections this trend is remarkably accurate.

3.3 Electrochemistry

The redox potentials of the series were explored using cyclic voltammetry in identical conditions. At first the two compounds at the extremities of the series were explored in order to ascertain the extent of the differences in redox potentials (Figure 27).

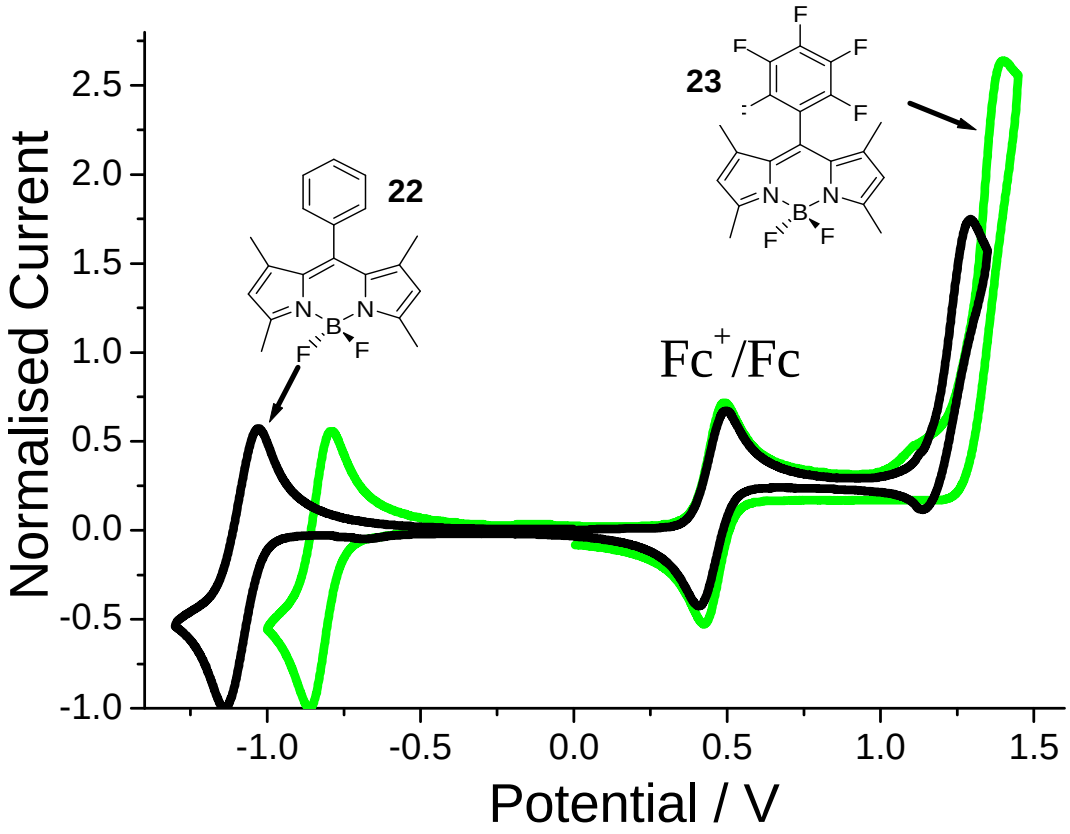

*Figure 27 Cyclic voltammetry of **22** and **23**, measured in CH_3CN vs. Ag/AgCl and an internal ferrocene reference.*

At negative potential redox peaks for both **22** and **23** showed a fully reversible $1e^-$ peaks. **23** ($E_{1/2}$ = -0.83 V) was easier to reduce than **22** ($E_{1/2}$ = -1.08 V) by some 250 mV. Hence the electron withdrawing effect, bought about by the perfluorination of the aryl ring, causes the bodipy accept an electron with more ease than if the meso substituent were a phenyl ring. This large anodic shift, from **22** to **23**, demonstrates that **23** has an increased capacity to stabilise a radical anion.

At positive potential both showed similar quasi-reversible waves at $E_{1/2}$ = +1.33 (**22**) and $E_{1/2}$ = +1.22 (**23**), which represent the oxidation of both compounds. There is a slight cathodic shift in the redox peak of **23** relative to **22** which can be accounted for by the effects of the perflourinated ring on the HOMO. The

removal of electron density towards the perfluorinated ring creates an enhanced dipole across **23**, with a more δ+ charge existing on the bodipy core. The removal of an electron from the core is therefore less favourable as the compound has a reduced capacity to stabilise a positive charge which would result from the removal of an electron. The results for the entire series are tabulated below (Table 7).

Compound	$E_{1/2\text{-}Ox}$ / V	$E_{1/2\text{-}Red}$ / V	ΔE / V [a]
22	1.22	-1.08	2.30
25	1.23	-1.04	2.27
24	1.24	-1.02	2.26
26	1.25	-0.99	2.24
28	1.30	-0.93	2.23
27	1.26	-0.96	2.22
23	1.33	-0.83	2.16

*Table 7 The electrode potentials of the series **22**-**28**. [a] Difference between redox potentials. Measured in CH_3CN vs. Ag/AgCl.*

The electrochemical results of the series appears to show a dual reliance of the redox potentials on both the number and positions of fluorine atoms. The mono substituted compounds all show a significant change from **22**, with ortho-substitution showing the most pronounced effect. Strangely the cumulative effect of addition of fluorine atoms was slightly less than anticipated, with Δ*E* for **28** differing by only 0.01 V from the monofluorinated **26**. This result differed from what was calculated in the DFT models, where the HOMO-LUMO gaps showed large discrepancy between mono and di ortho- substitution of fluorine atoms. By looking the DFT HOMO-LUMO gap trend we can also see a large difference between the calculated and observed values for **24**, **25** and **27**. It was anticipated that the presence of meta and para fluorine atoms would not have a significant effect on the HOMO-LUMO gap, with values not predicted to differ too much from those of **22**. The gap between **22** and **24/25** was 0.04 eV and 0.03 eV respectively, though these gaps were not as large as that between **22** and **26**.

From the electrochemical results it is clear to see a relationship between the number and position of fluorine atoms present on a meso phenyl group. Ortho substitution causes the largest shift in the reduction peaks while having a slight effect on the oxidation potential. The quantity of fluorine atoms causes a subtle

effect through the system with the cumulative effects of both meta and para fluorine atoms complementing the more pronounced ortho effect.

3.4 Photophysics

3.4.1 Absorption and Fluorescence

As with the electrochemistry initial absorption and fluorescence experiments were carried out on **22** and **23**. Both spectra can be seen combined below in Figure 28. The measurements revealed a large bathochromic shift in both the absorption (520 nm versus 503 nm) and emission (537 nm versus 515 nm) spectra of **23** relative to **22**.

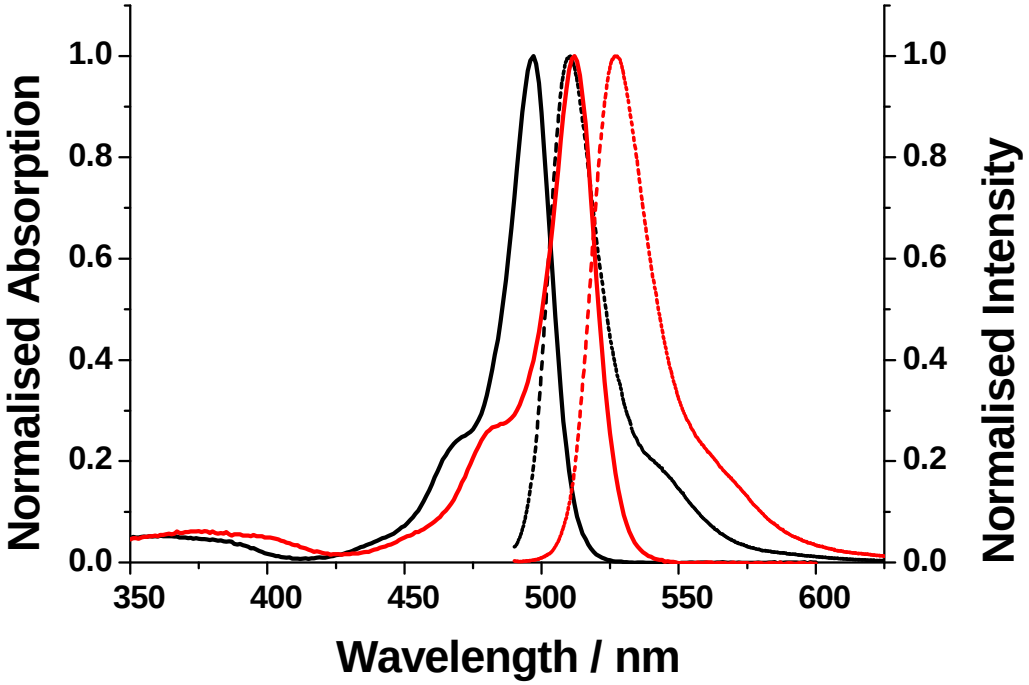

*Figure 28 Absorption and fluorescence emission spectra for **22** and **23**, measured in MeCN at ambient temperature. **22** – black, **23**– red, absorption – solid, emission – dashed.*

In the absorption measurements a sharp $S_0 – S_1$ band was observed for both **22** and **23**, along with a shallow-broad $S_0 – S_2$ band, which is typical for bodipy compounds. The $S_0 – S_2$ transition is similarly affected by the presence of fluorine atoms in the same way see for the $S_0 – S_1$ transition.

The quantum yields for both **22** and **23** were measured in toluene at ambient temperature and were in accordance with those reported in the literature with **22**

having a significantly lower quantum yield (Φ_F = 0.69) when compared with **23** (Φ_F = 1.00).

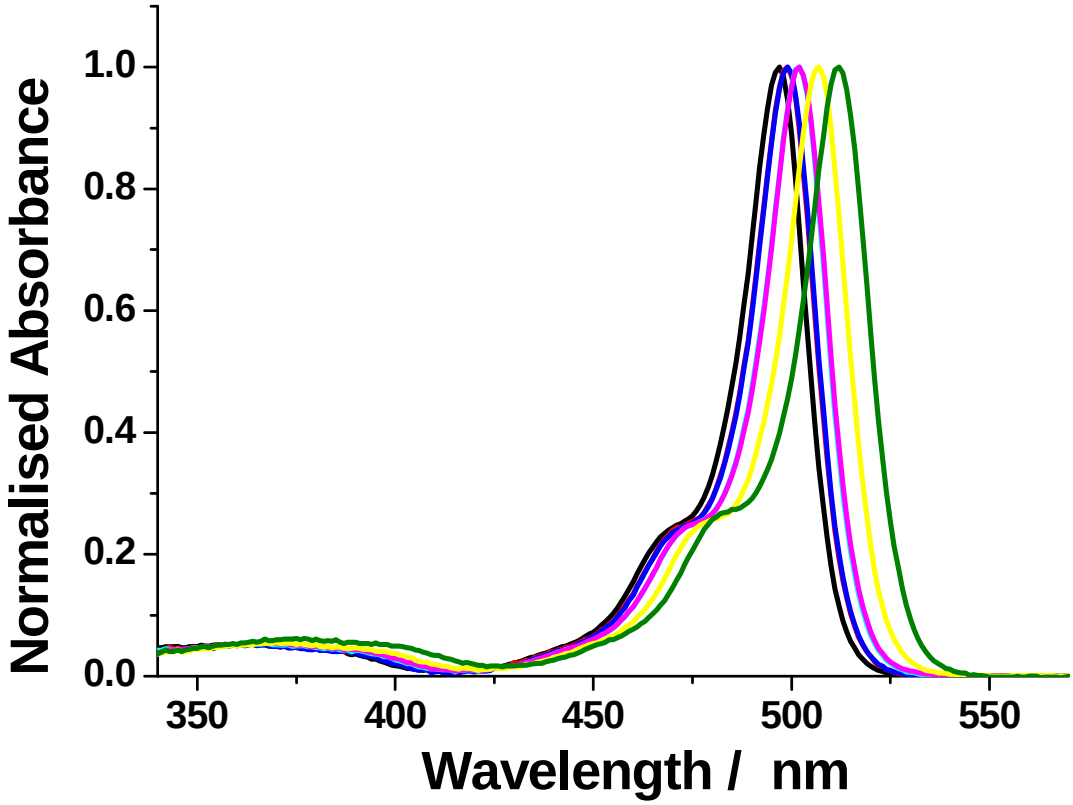

*Figure 29 Absorption spectra of **22**-**28**, measured in MeCN at ambient temperature. **22** – black, **23** – green, **24** – red (mostly obscured by **25**), **25** – blue, **26** – cyan (mostly obscured by **27**), **27** – magnolia, **28** – yellow.*

The absorption and emission spectra for all compounds was measured in MeCN at ambient temperatures which can be seen in Figure 29 and Figure 30. The absorption spectra show a red-shift, for the $S_0 – S_1$ transition, across the series. The shift relies on both the number of fluorine atoms present as well as the positioning. Once again the position of the fluorine atoms is the most important factor in determining the amount of red-shift observed, with compounds that have ortho fluorine-substitution causing the largest shift. The proportionality between the amount of red-shift observed and position of the fluorine atoms can be seen clearly when comparing **26** and **27**. Compound **26** has near identical spectra (in terms of absorption and emission shifts) in spite of having 2 less fluorine atoms substituted. Again the $S_0 – S_2$ transition shifted to a similar degree to that observed for the $S_0 – S_1$ transition, with an overall bathochromic shift observed that mirrored the trend seen for the $S_0 – S_1$ transitions.

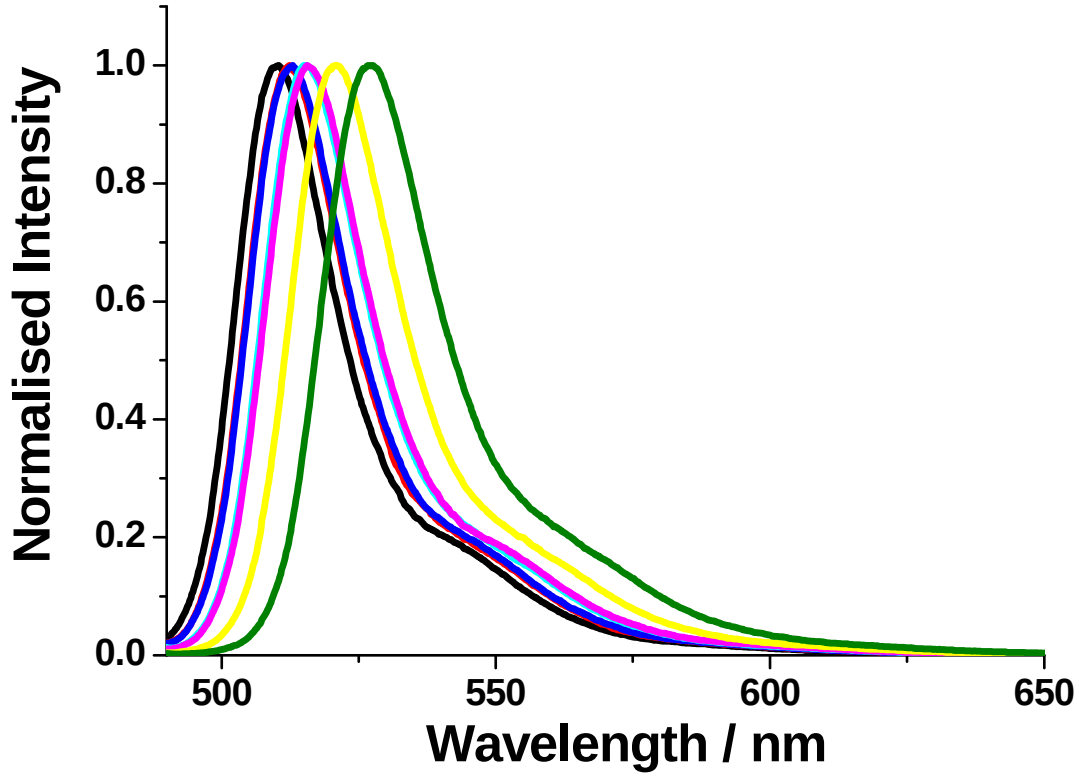

*Figure 30 Emission spectra of **22**-**28**, measured in MeCN at ambient temperature. **22** – black, **23** – green, **24** – red (mostly obscured by **25**), **25** – blue, **26** – cyan (mostly obscured by **27**), **27** – magnolia, **28** – yellow.*

The observed red shift over the series can be accounted for by the decrease in the HOMO-LUMO gap. This effect is concordant with both the DFT calculations and the electrochemical readings (ΔE).

The emission spectra for the series show the same pattern of bathochromic shifts as those observed in the absorption spectra. The emission profiles for the S_0 – S_1 transitions (λ_{Flu}) for all compounds were relatively good mirror images of the complementary absorption bands.

3.4.2 Molar Absorption Coefficients

All molar extinction values were large (between 76,000 cm^{-1} and 98,000 cm^{-1}) which is typical for the values of bodipy compounds. The values of the molar extinction coefficient seem to depend on the position of fluorine atoms, with ortho-substitution once again providing the largest change. Where ortho-fluorine atoms appear to decrease the extinction coefficient, meta- and para-substitution causes a ~25% increase.

Compound	MeCN		Toluene		
	λ_{Abs} / nm [b]	λ_{Flu} / nm [b]	λ_{Abs} / nm [b]	ε_{Max} / M^{-1} cm^{-1}	λ_{Flu} / nm [b]
22[a]	497	511	503	82,000	515
24	499	512	505	98,000	520
25	499	513	505	98,000	520
26	502	515	509	81,000	523
27	502	516	509	98,000	523
28	507	521	515	77,000	530
23	512	528	520	76,000	537

*Table 8 Electronic absorption and fluorescence parameters for the series **22-23** measured in MeCN and Toluene. [a] Taken from reference 38, [b] ± 2 nm.*[38]

Compound	Toluene				
	SS / cm^{-1} [c]	Φ_{Flu} [d]	τ_S / ns [e]	k_{Rad} / 10^8 s^{-1}	k_{NR} / 10^6 s^{-1}
22	464	0.71	3.9	1.82	76.40
24	571	0.88	3.5	2.50	35.70
25	571	0.87	3.5	2.54	35.70
26	526	0.98	4.9	2.00	4.10
27	526	0.91	3.6	2.50	27.80
28	549	0.99	5.1	1.94	2.00
23	609	1.0	5.7	1.75	<0.40

*Table 9 . Electronic absorption and fluorescence parameters for the series **22-23** measured in Toluene. [c] ± 25 cm^{-1}, [d] ± 10%, [e] ± 5%.*

3.4.3 Stokes Shift

The Stokes shift (SS) for all compounds was in accordance with analogous molecules found in the literature.[39] The values for the SS of the series seemingly increases with the presence of fluorine atoms on the meso-phenyl substituent, however the value shows no direct correlation to the position or number of fluorine atoms present. That said it is clear that the presence of 5 fluorine atoms vastly increases the SS.

3.4.4 Fluorescence Quantum Yield

There is a visible difference in fluorescence intensity across the series. The fluorescence quantum yield of the series demonstrates a direct correlation between the position of fluorine atoms and an increase in Φ_{Flu}. Once again ortho-substituted compounds (**23, 26** and **28**) have a vastly superior Φ_{Flu} when compared to those with no ortho-fluoro substitution (**22, 24, 25** and **27**). Hammett plots for fluorine substitution show little change in electron-

withdrawing capability based on the position of the fluorine. As a result the increase of Φ_{Flu} upon ortho substitution is likely due to steric effects.

There does appear to be a secondary electronic influence whereby the Φ_{Flu} increases upon the introduction of fluorine atoms. Here we see the quantum yield increase by 0.17 when comparing **22** (Φ_{Flu} = 0.71) to **24** (Φ_{Flu} = 0.88). This electronic effect can be accounted for in the Hammett plots of F-substituted phenyl groups. The introduction of electron-withdrawing substituents on the aryl moiety is known to cause an increase in the rigidity of the bodipy core thereby causing an increase in Φ_{Flu}, due to a diminished k_{NR}.[18, 40]

3.4.5 Lifetime Measurements

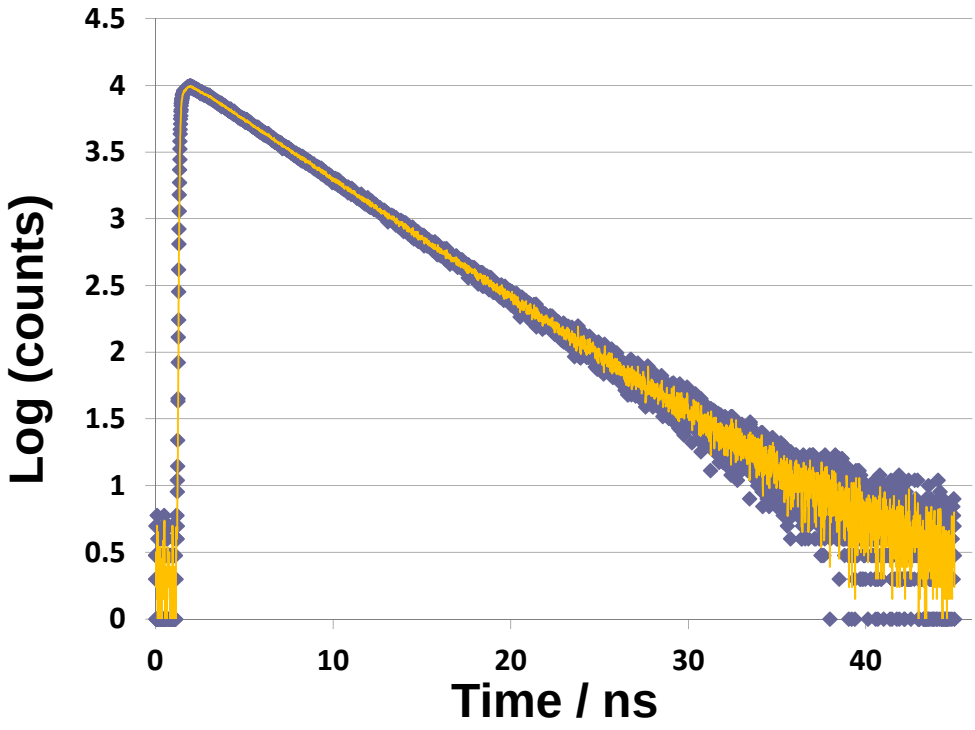

*Figure 31 Measurement of the fluorescence lifetime of **25** measured in toluene- diamond points represent the collected data, orange - line of fit.*

The lifetimes were measured by single-photon counting, and all measurements gave mono-exponential results. The lifetime measurements suggest that mono-substitution of fluorine atoms in the meta and para positions slightly decrease the lifetime relative to **22**. On the other hand ortho substitution increases the fluorescence lifetime substantially.

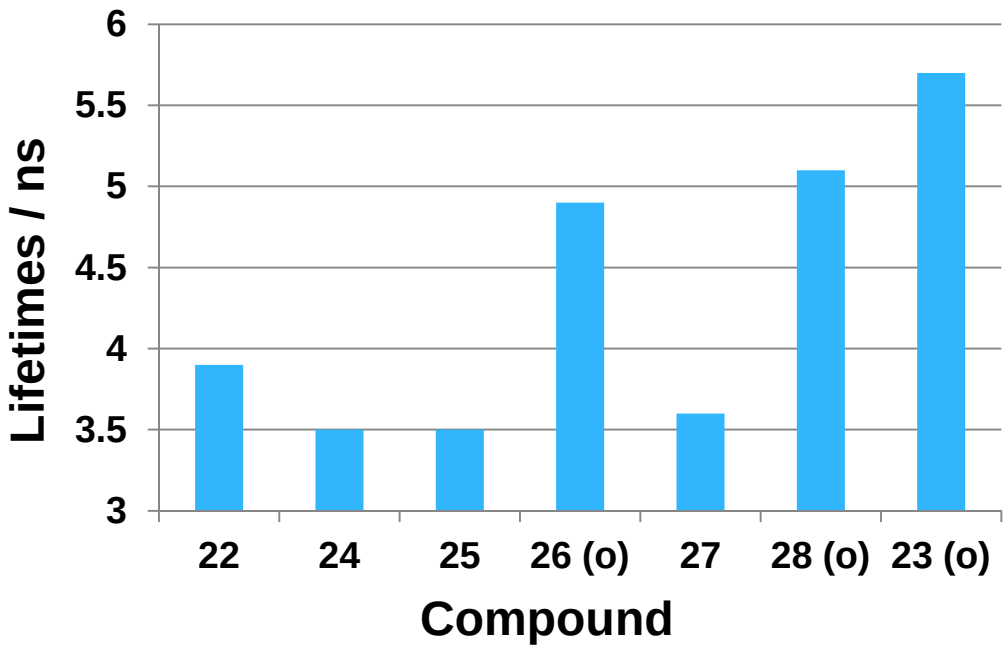

Figure 32 A graphic highlighting the increase in Φ_{Flu} upon ortho substitution of fluorine atoms on the meso phenyl group. (o) indicates the presence of one or more ortho fluorine.

All values for the radiative rate constant (k_{Rad}) did not differ greatly across the series. On the other hand the non-radiative rate constant (k_{NR}) displayed greatly decreased values when fluorine atoms were present in the ortho-positions. This value is in accordance with the values of Φ_{Flu} which follow a similar trend.

Changes in k_{NR} have been shown to depend on the degree that the dipyrrin core distorts upon excitation to the S_1 state. Distortion of the bodipy core creates a route to facilitate the deactivation of the bodipy excited state, where increasing distortion increases the rate of non-radiative decay.[41] In order to decrease k_{NR} the excited state structure must be made more rigid. In the case of ortho-containing aryl-bodipy compounds, the decreased k_{NR} can be linked to the steric bulk bought about by the fluorine atom drastically reducing the amount of 'rocking' which the aryl ring undergoes.

Fluorinated alkane chains have been seen to have an increased rigidity due to fluorine-fluorine repulsions and electrostatic charges.[40] It is conceivable that the afore mentioned repulsions and electrostatic charges might well increase the rigidity of the dipyrrin carbon network. This seems more likely considering the presence of fluorine atoms, regardless of the substitution pattern, causes a drop in k_{NR}. If the argument for increased rigidity lies solely with steric effects, and not electronics, then it would be expected that **24, 25** and **27** would have

similar k_{NR} values to that of **22**. The k_{NR} for **24, 25** and **27** do show a decrease when fluorine atoms are included, though not to the same scale seen for ortho-fluorine atoms and should be classed as secondary electronic effects.

In the case of toluyl-bodipy derivatives, the ortho-substituted analogues have been shown to have a largely increased quantum yield when compared with para-toluyl bodipy compounds.

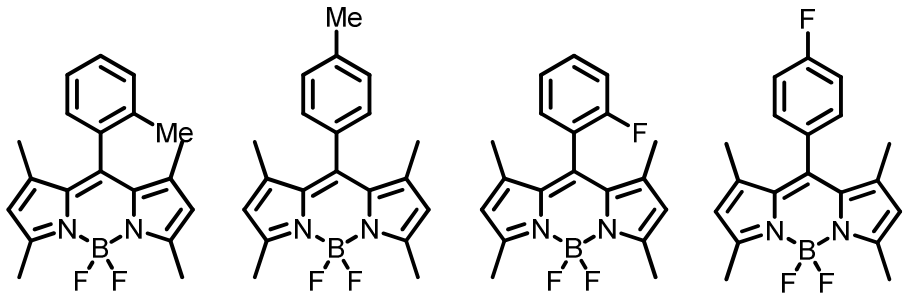

*Figure 33 A comparison between the quantum yields of ortho- and para-toluyl bodipy compounds (measured in DCM) versus the fluorine analogues (measured in toluene). Φ_{Flu} = 0.87 (o-Me), Φ_{Flu} = 0.60 (p-Me), compared with Φ_{Flu} = 0.98 (**26**), Φ_{Flu} = 0.88 (**24**).*[42, 43]

Though the quantum yields of toluyl and fluorophenyl bodipy compounds cannot be compared directly, the differences between the quantum yields between ortho- and para-substituted derivatives can be compared. There is a clear increase in quantum yield when a compound possesses a substituent, other than a proton, in the ortho position. The methyl substituent is relatively electron donating with regards to fluorine atoms and hence any electronic arguments would be disproven if similar levels of quantum yields were observed for the methyl analogues. Though the value of Φ_{Flu} for the ortho-methyl bodipy is much higher (Φ_{Flu} = 0.87) than that of the para-substituted bodipy (Φ_{Flu} = 0.60) - the final value is still some way off the Φ_{Flu} observed for **26** (Φ_{Flu} = 0.98). Hence, though the steric effect does seem to be very dominant, there also does appear to be an electronic effect on k_{NR}, resulting from the introduction of fluorine.

As mentioned previously the sterics do not allow for the full rotation of the phenyl group, even with protons present in both ortho positions. The phenyl ring simply rocks back and forth between two extreme points defined by an angle θ. Considering that the difference in Van der Waals volume between **22** and the mono and difluorine-substituted compounds (**26** and **28**) is 7% and 14% respectively, it is likely that θ is decreased for **26** and **28** with respect to **22**. The

increase in volume may in turn prevent the rocking motion which itself may be responsible for the non-radiative decay of the excited state observed in **22**. Alternatively a large θ might cause a higher extent of distortion in the singlet state of the dipyrrin backbone, hence a reduced θ might also minimise k_{NR}.

3.4.6 Pressure Dependant Fluorescent Studies

If k_{NR} was dependant on the distortion of the bodipy S_1 excited state structure it might be expected that changes in the pressure surrounding to cause changes in Φ_{Flu}. As such the fluorescence spectra for each of the compounds was recorded in methylcyclohexane (MeChx) with increasing pressure up to 550 MPa.

It should be noted that MeChx undergoes a phase change at around 280 MPa. A shift occurs due to the solvent switching from an axial conformation to the less voluminous equatorial conformation.[44]

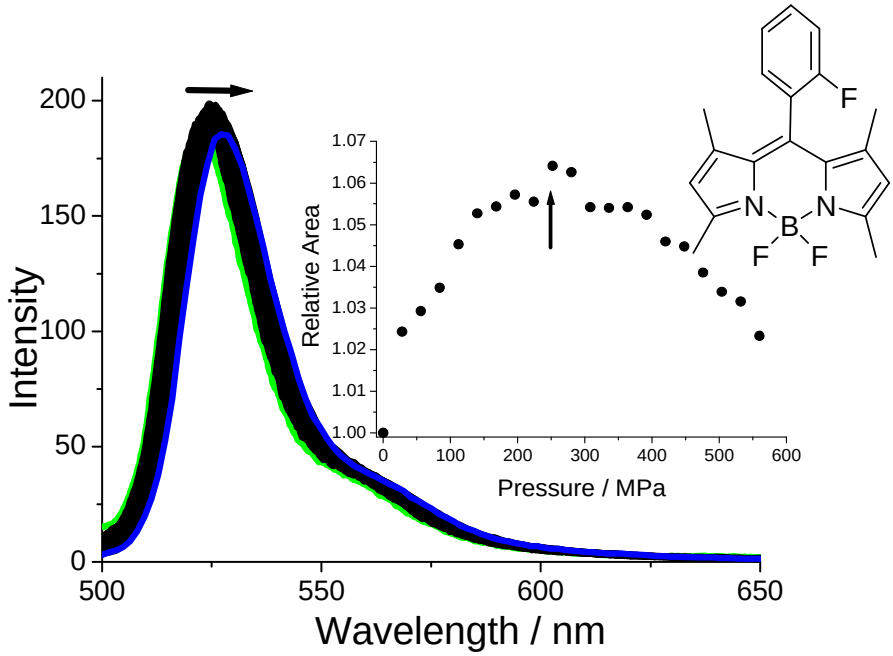

*Figure 34 Combined fluorescence spectra of **26** measured over different pressures, with the arrow denoting the overall red-shift as the pressure is increased. Inset – the relative area under the emission curve versus increasing pressure, where the arrow denoted the pressure at which MeChx undergoes its phase change. It should be noted that Φ_{Flu} for **26** in MeChx is 0.88 compared to the 0.98 found when measured in toluene. The initial increase in Φ_{Flu} is partly due to an increase in the optical density at the excitation wavelength.*

The increase in pressure upon **26** appears to cause an increase in Φ_{Flu} by approximately 6%. This increase is observed until the point at which the solvent undergoes its conformational shift, though it is not thought that the two are related. After 300 MPa the relative intensity begins to descend steadily. The trend whereby the intensity rises then falls is only seen for compound **26**. As the pressure is increased the emission wavelength also undergoes a bathochromic shift of 5 nm. The red-shift is caused by an increase in polarizability of the solvent.[45]

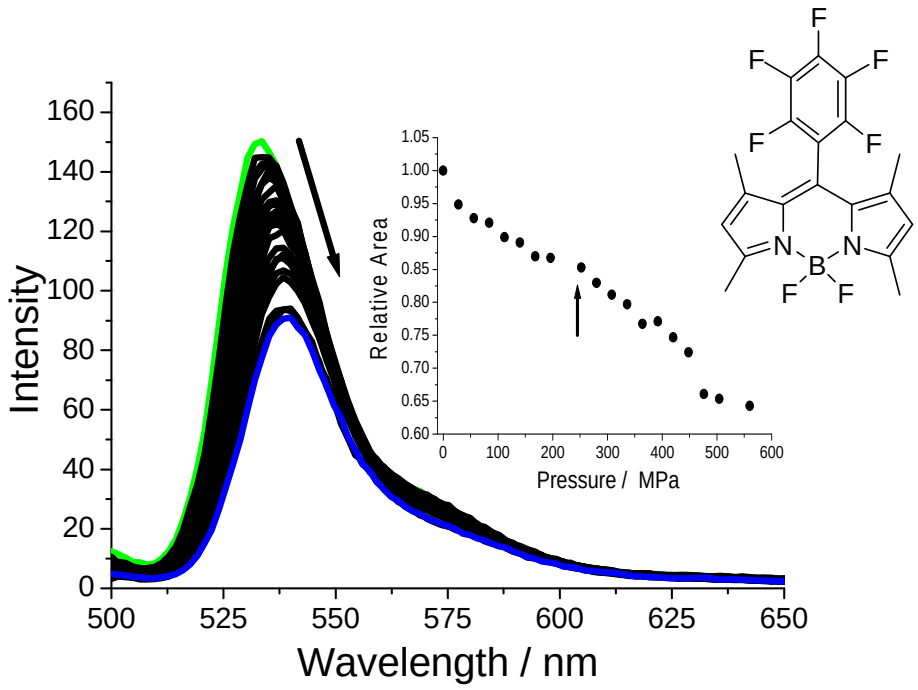

*Figure 35 Combined fluorescence spectra of **23** measured over different pressures, with the arrow denoting the overall red-shift as the pressure is increased. Inset – the relative area under the emission curve versus increasing pressure, where the arrow denoted the pressure at which MeChx undergoes its phase change.*

In comparison **23** acts very differently to **26**, as when the pressure is increased only a steady decline is observed. The total reduction in fluorescence is ca. 35%, which is significantly larger than the total decline observed in **26**. Once again there is an overall red-shift of around 5 nm. The behaviour of **28** is very similar to that of **23** whereby an increase in pressure is accompanied by a reduction of fluorescence intensity. This suggests that the presence of 2 ortho-fluorine atoms causes the decrease in fluorescence intensity by distorting the bodipy core.

In stark contrast when pressure is applied to the compounds which have no ortho-fluorine atoms the Φ_{Flu} increases over the entire pressure range. Whereas a small increase in the fluorescence yield can be attributed to an increase in the solute concentration, the >60% increase observed for compounds with two ortho protons can only be attributed to changes in the molecular geometry.[46]

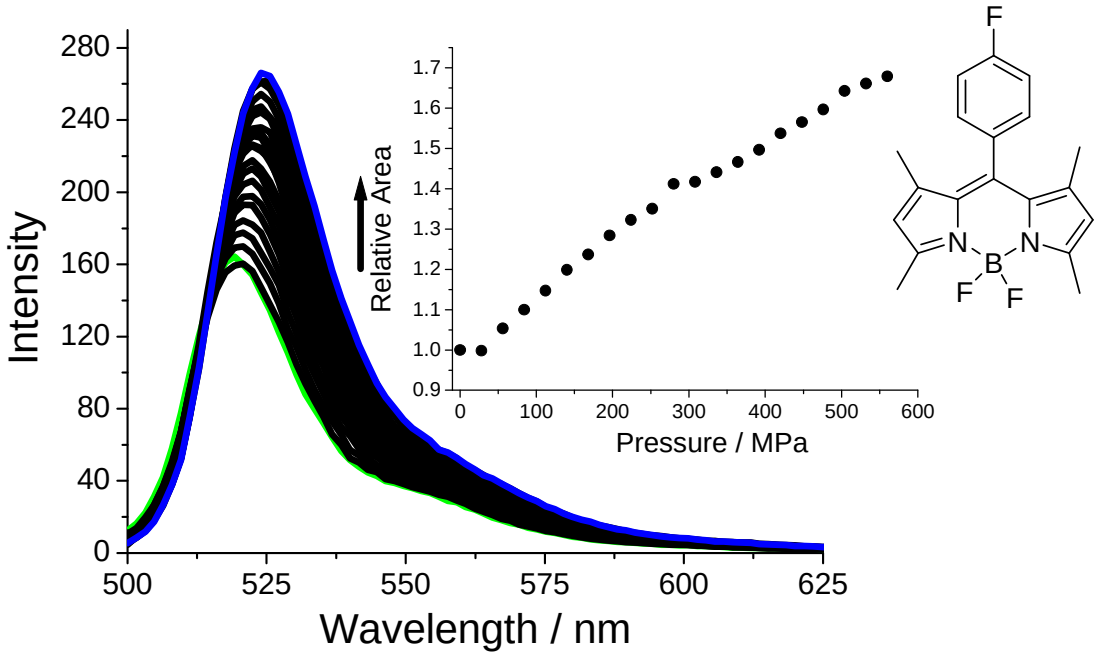

*Figure 36 Combined fluorescence spectra of **24** measured over different pressures, with the arrow denoting the overall red-shift as the pressure is increased. Inset – the relative area under the emission curve versus increasing pressure.*

Once the pressure had been released the emission spectra were recorded again to make sure that there were no irreversible processes occurring when the system was subjected to pressure. In all cases the original spectra was observed once the pressure was relieved.

3.4.6.a A Summary of the Pressure Dependant Study:

For both compounds **23** and **28** – where there exist two ortho-fluorine atoms – k_{NR} appears to be enhanced with increasing pressure. The increase in this decay pathway is likely due to the distortion of the dipyrrin backbone. The distortion is in turn caused by the larger fluorine atoms clashing with the 1,7-methyl groups as the molecule attempts to reduce its overall volume. The clash between fluorine and methyl group levers the bodipy core out of planarity thereby increasing k_{NR}.

For compounds with no ortho-fluorine atoms –k_{NR} does not increase. The lack of increase in k_{NR} might be because the difference in size between the fluorine and hydrogen atoms is enough to allow the F_n-aryl group to approach planarity without clashing too much with the methyl groups on the core. The observed increase in Φ_{Flu} is difficult to explain however, a pressure dependant measurement of the fluorescence lifetimes might shed some light on.

In the case where there is a single ortho-fluorine present the system seems to fall between the two extremes.

3.5 Exploring the Limits of the Fluorine Effect: Unsubstituted Bodipy Cores

Two further compounds were synthesised in order to test the effects of the perfluorination of phenyl rings on unsubstituted bodipy cores. It was though that while **29** could act as more efficient rotor[†] compared to 4,4'-difluoro-8-phenyl -4-bora-3a,4a-diaza-s-indacene (PhBod), **30** might act as an atom efficient version of compound **29**, while also being a useful comparative NMR tool for **26**.

The synthesis of **29** and **30** is discussed in the main synthesis section at the beginning of this chapter (Synthesis 3.1).

Once the crystals of the pure bodipy compound had been collected the samples were then subjected to a full characterisation including the following techniques: ^{1}H, ^{13}C, ^{11}B NMR spectroscopies, mass spectrometry, melting points and IR spectrometry. All of these results were similar to those discussed previously with compounds **22**-**28**.

3.5.1 ^{19}F NMR Spectral Analysis

The ^{19}F NMR spectrum for **29** was as expected for a bodipy compound and similar to those seen for compounds **22**-**25**, **27** and **28**- giving a quartet for the BF_2 unit equating to fluorine equivalence. The ^{19}F NMR spectrum for **30** however exhibited the same splitting pattern as the ^{19}F NMR spectrum of **26**. Inequivalent fluorine atoms were not anticipated, indeed **30** was expected to act as a molecular rotor and as a result the ^{19}F NMR spectrum was to be used as a direct comparison with that of **26**.

[†] In terms of fluorescence quantum yield.

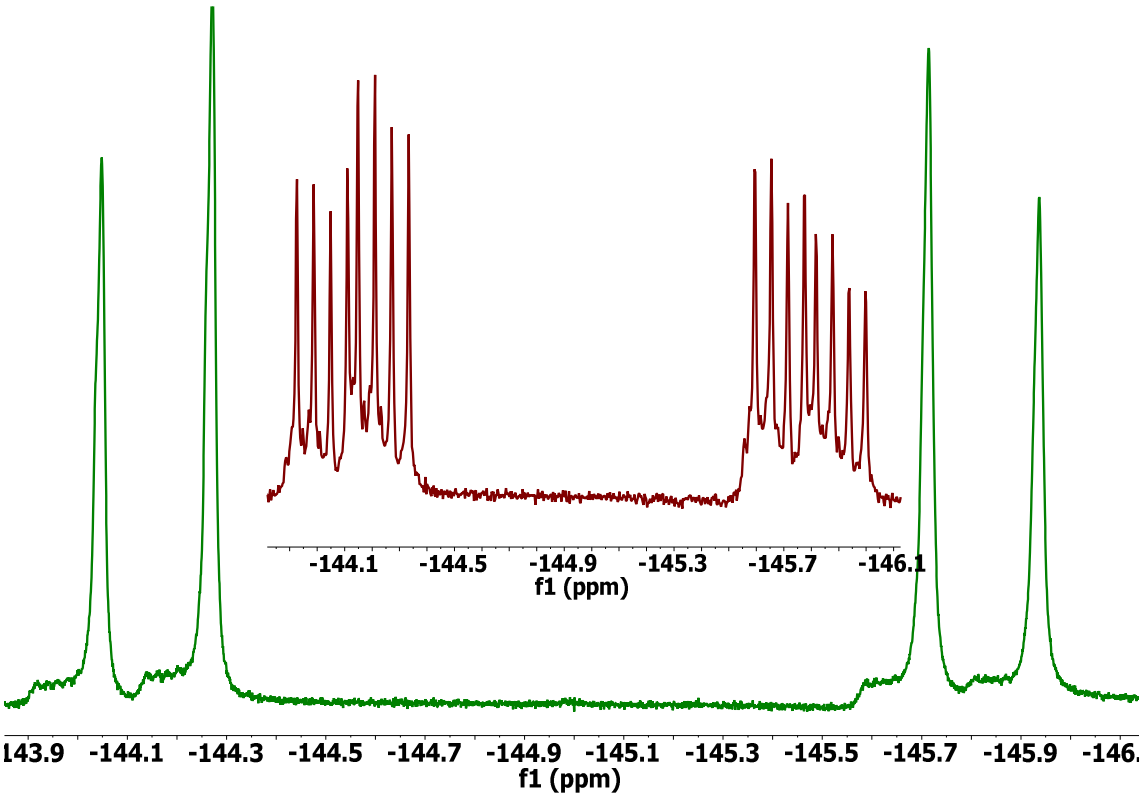

*Figure 37 $^{19}F\{^{11}B\}$ NMR spectrum of **30** with the ^{19}F NMR spectra inset (both spectra cover the same ppm region). Also apparent in the ^{11}B decoupled spectrum is evidence of the ^{10}B-^{19}F splitting at the base of each ^{11}B peak.*

The increase in steric bulk at the ortho position has once again prevented liberal movement around the meso-aryl bond. In this instance however the restriction has blocked a free rotation. A VT ^{19}F NMR was performed to see if the barrier to rotation could be overcome (Figure 38).

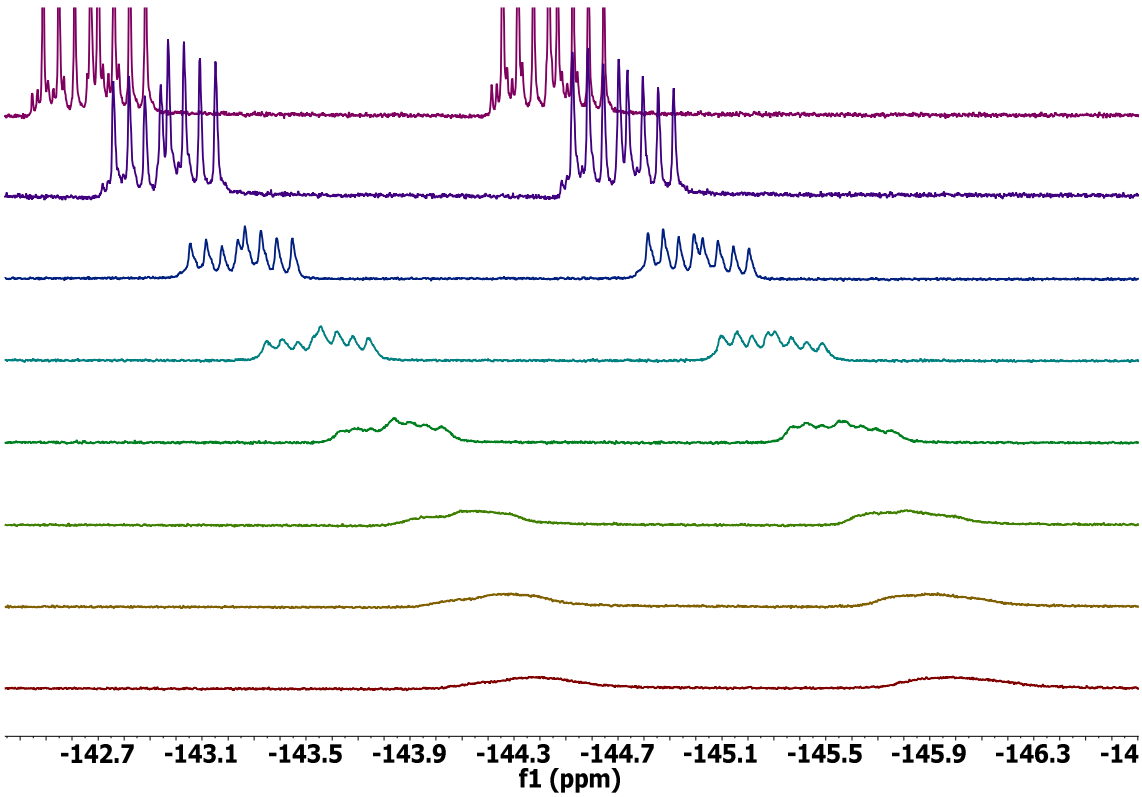

*Figure 38 ^{19}F VT-NMR spectra for **30** in d_{10}-o-xylene. Temperature increase (from top): 20, 40, 60, 80, 100, 120, 130, 140^{o}C.*

As seen in Figure 38, the effects of increasing the temperature to the solvent limits do not cause coalescence of the two sets of fluorine peaks. However unlike the VT NMR of **26** there is a dramatic loss of resolution for the peaks which indicates that the point of coalescence is not too far from 140^{o}C. Unfortunately the deuterated solvent with the highest boiling point, which is commercially available, is d_{10}-o-xylene. As a result of this limitation it is not possible to follow the progress of the coalescence any further using variable temperature ^{19}F-NMR.

3.5.2 Crystal Structure Analysis

Crystal structure analysis was performed on both compounds. There was no obvious patterns seen between the molecular make-up and the crystal packing arrangement.

Compound	29	30
Torsion angle (^{o}): B-N-C_3-C_2 (boron planarity)	173.14	174.78
Torsion angle (^{o}): C_8-C_{Ar1}-C_{Ar2}-F (aryl twist)	1.76	1.33
Crystal Density (g cm^{-3})	1.723	1.472

*Table 10 Selected crystal structure data for compounds **29** and **30**.*

For both compounds the boron sits slightly out of plane, whereas for compound **23** a complete planarity was observed (180^{o}). It appears the removal of the 3,5-methyl groups has removed steric bulk to allow for more flexibility in the bodipy core. As a result a slightly lower Φ_{Flu} is expected for both compounds.

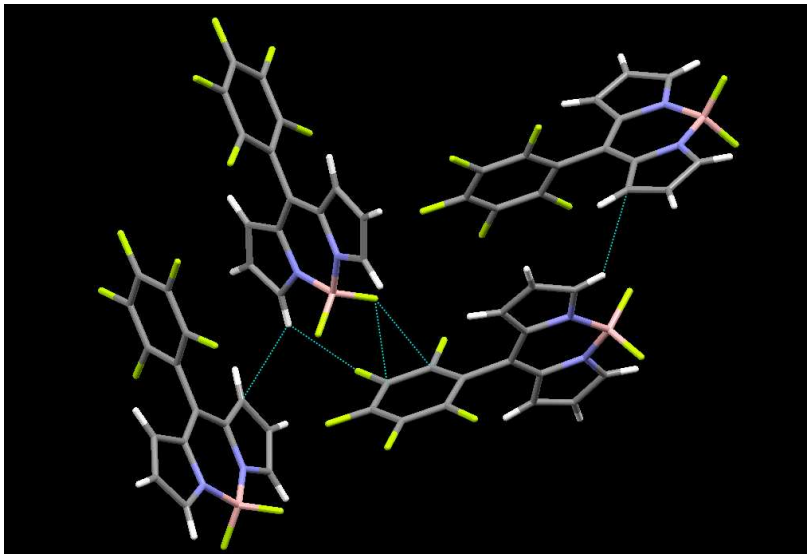

*Figure 39 Crystal packing of **29**.*

Surprisingly the aryl group, which should have more room to manoeuvre with the absence of the 1,7-methyl groups, adopt orthogonal aryl twist angles similar to those seen for **22**-**28**. Once again the presence of a perfluorinated ring in the system allows for more efficient packing, giving **29** a crystal density that is significantly larger than that of **30**.

3.5.3 Photophysical Analysis

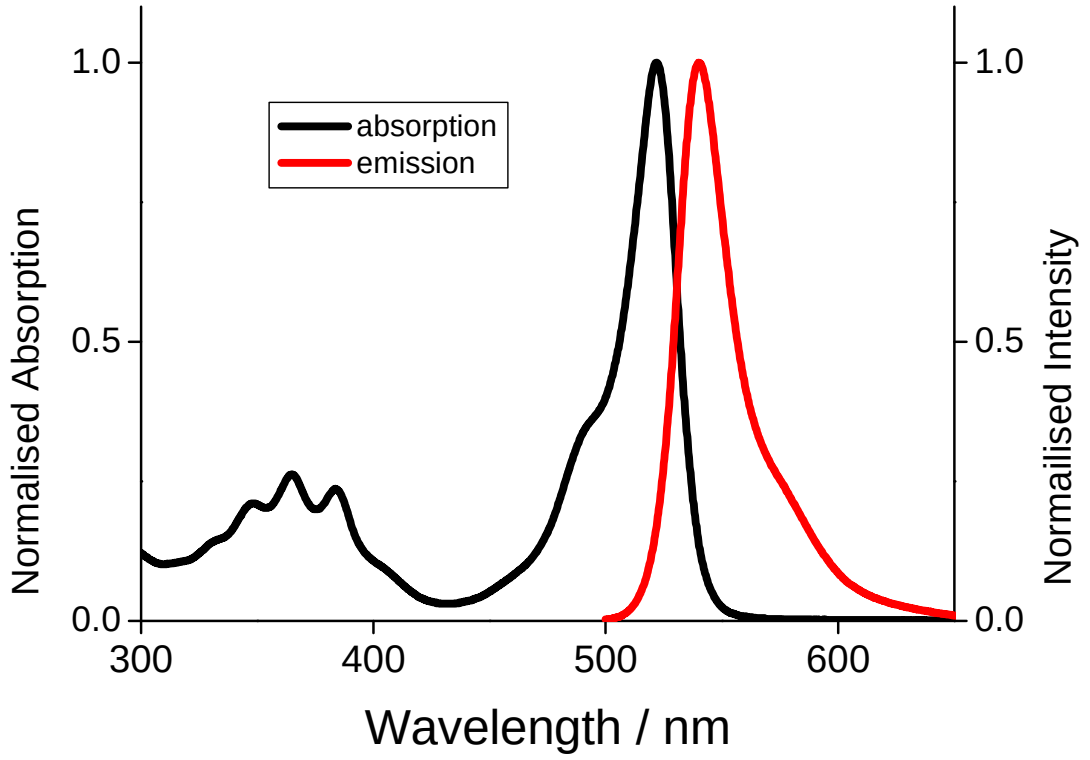

*Figure 40 Absorption and emission spectra for **29**, measured in MeCN.*

Basic photophysical measurements were performed for both compounds, the results of which can be found in Table 11. Good mirror imagery between the absorption and emission spectra was observed, there was also a better resolution of the S_0-S_2 absorption band than that seen for **22**-**28**. Indeed the increased structure observed for the S_0-S_2 absorption band is rarely seen for bodipy compounds.

The photochemistry of **29** and **30** cannot be compared with the previous series. That said the effects of the addition of fluorine are not expected to differ to a large degree from those which have already been discussed.

For the series **22**-**28** the introduction of one or more ortho-, or multiple fluorine atoms, resulted in a bathochromic shift of both λ_{Abs} and λ_{Flu}. **29**, **30** and **PhBod**, however do not behave in the same way as the previous series. The introduction of one ortho-fluorine is enough to red shift absorption and emission spectra by 23 nm, however there is no further shift with the addition of either a second ortho-fluorine, or the introduction of multiple fluorine atoms at the other sites, as was anticipated.

Compound	λ_{Abs} / nm [a]	λ_{Flu} / nm [a]	SS / cm^{-1} [b]	Φ_{Flu} [c]
29	522	540	639	0.76
30	522	541	673	0.64
PhBod[22]	497	518	815	0.044

*Table 11 Electronic absorption and fluorescent parameters for **29**, **30** and **PhBod**, measured in MeCN. [a] ± 2 nm, [b] ± 25 cm^{-1}, [c] ± 10%.*

In direct contrast to the results seen in the series **22**-**28**, the SS decreases with increasing electro withdrawing capacity on the aryl ring.

The measurements of the fluorescence quantum yield show an increase of a whole order of magnitude upon ortho-fluorination. This large increase suggest that the addition of fluorine has prevented the free rotation of the phenyl ring around the C8-aryl bond, a result confirmed by the ^{19}F NMR of **30**. There is a slight increase in Φ_{Flu} upon the introduction of a second ortho-fluorine, presumably due to the second fluorine further hindering rocking, as seen in the previous series.

In summary the addition of one ortho-fluorine atom is enough to both hinder rotation and to cause an identical red-shift to that seen with the total fluorination of the aryl moiety. Which in turn means that **30** is a more atom efficient fluorophore than **29**, giving similar quantum yields and SS without needing a fully substituted aryl ring. Furthermore the aldehyde required to synthesise **30** is more than 2 times cheaper than that of **29**, £1.40 g^{-1} versus £3.00 g^{-1} respectively. Since the various photonic properties of mono-orthofluorinated aryl bodipy compounds are either similar or identical to those of the perfluoroaryl bodipy compounds, it seems logical to suggest the use of the former unless absolutely necessary.

This subseries did not successfully provide an NMR result which could be used for direct comparison to that of **26**, due to the rotation surprisingly being prevented with the introduction of fluorine in the ortho position. However results from this series further back up the results seen from **22**-**28**, whereby steric effects bought about by fluorine indeed increase the Φ_{Flu}. Due to these steric implications **29** is not a good candidate to be used as a replacement for PhBod in sensing applications - such as aiding in the detection of changes in: viscosity, pressure and temperature.

3.6 Conclusion

The summary of all electrochemical and photophysical data reveals two factors which have an effect on the overall behaviour of the series. Firstly the presence of fluorine atoms: increase the fluorescence quantum yield, HOMO-LUMO gap, facilitate redox, cause a bathochromic shift of both absorption and emission spectra, and to a lesser extent decrease k_{NR}. The red-shift is likely due to electronic effects bought about by fluorine substitution.

Secondly that ortho-substitution of fluorine atoms enhances all of the afore mentioned effects, seen when the meta and para position are fluorinated as well as greatly decreasing k_{NR}. It is thought that these effects are bought about by a combination of electronic and steric effects.

The standout compound for the series appears to be **26** which exhibits unusual changes in the fluorescence lifetime when exposed to increasing pressure, high Φ_{Flu} in most solvents, and - according to the ^{19}F NMR - appears to be prochiral

3.7 Future Work

The continuation of this project can be found in the following chapter where the idea of axially chiral bodipy compounds is explored.

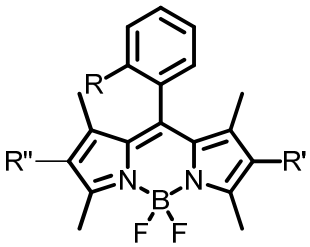

Figure 41 The general structure proposed for 1st generation axially chiral bodipy compounds.

Optically active fluorescent compounds have the potential to act as chiral imaging agents, which in theory should have independent photophysical properties in different chiral media depending of which enantiomer is present.

The legacy of this work should be the inclusion of ortho-fluorine atoms in 8-aryl bodipy systems, thereby introducing multiple advantages in respects to the photophysics of the compound.

3.8 References

1. K. Müller, C. Faeh and F. Diederich, *Science* 2007, **317**, 1881-1886.
2. B. K. Park, N. R. Kitteringham and P. M. O'Neill, *Annu. Rev. Pharmacol. Toxicol.* , 2001, **41**, 443 - 470.
3. O. Galangau, C. Dumas-Verdes, R. Méallet-Renault and G. Clavier, *Org. Biomed. Chem.*, 2010, **8**, 4546-4553.
4. S. Chai, S.-H. Wen and K.-L. Han, *Org. Elec.*, 2011, **12**.
5. W. Wu, Y. Liu and D. Zhu, *Chem. Soc. Rev.*, 2010, **39**, 1489–1502.
6. B. E. Smart, *J. Flu. Chem.*, 2001, **109**, 3-11.
7. A. Bondi, *J. Phys. Chem.*, 1964, **64**, 441-451.
8. D. E. Williams and D. J. Houpt, *Acta. Crystallogr. B*, 1986, **42**, 286-295.
9. G. A. Patani and E. J. LaVoie, *Chem. Rev.*, 1996, 3147-3176.
10. J. C. Biffinger, H. W. Kim and S. G. DiMagno, *Chem. Bio. Chem.*, 2004, **5**, 622-627.
11. J. D. Dunitz, *Chem. Bio. Chem.*, 2004, **5**, 614-621.
12. C. R. Patrick and G. S. Prosser, *Nature*, 1960, **187**, 1021.
13. G. Folkers, Hans-Joachim, B. Gisbert, S. Raimund and M. H. Kubinyi, *Protein-Binding Interactions*, Wiley-VCH, Weinheim, 2003.
14. H.-J. Böhm, D. Banner, S. Bendels, M. Kansy, B. Kuhn, K. Müller, U. Obst-Sander and M. Stahl, *Chem. Bio. Chem.*, 2004, **5**, 637-643.
15. C. R. Brundle, M. B. Robin and N. A. Kuebler, *J. Am. Chem. Soc.*, 1972, **94**, 1466–1475.
16. E. L. Spitler, J. M. Monson and M. M. Haley, *J. Org. Chem.*, 2008, **73**, 2211-2223.
17. M.-M. Shi, H.-Z. Chen, J.-Z. Sun, J. Ye and M. Wang, *Chem. Comm.*, 2003, 1710-1711.
18. F. Babudri, G. M. Farinola, F. Naso and R. Ragni, *Chem. Comm.*, 2007, 1003-1022.
19. H. J. Son, W. Wang, T. Xu, Y. Liang, Y. Wu, G. Li and L. Yu, *J. Am. Chem. Soc.*, 2011, **133**, 1885-1894.
20. F. C. Krebs and H. Spanggaard, *J. Org. Chem.*, 2002, **67**, 7185-7192.
21. A. C. Benniston, A. Harriman, V. L. Whittle, M. Zelzer, R. W. Harrington and W. Clegg, *Photochem. Photobiol. Sci.*, 2010, **9**, 1009-1017.
22. A. C. Benniston, S. Clift and A. Harriman, *J. Mol. Structure*, 2011, **985**, 346-354.
23. A. C. Benniston, G. Copley, H. Lemmetyinen and N. V. Tkachenko *Chem. Phys. Chem.*, 2010, **11**, 1685-1692.
24. A. Loudet and K. Burgess, *Chem. Rev.*, 2007, **107**, 4891-4932.
25. N. Watanabe, J. Morais and M. C. M. Alves, *J. Phys. Chem. B*, 2002, **106**, 11102-11107.

26. J. W. Emsley, J. Feeney and L. H. Sutcliffe, *High Resolution NMR Spectroscopy*, Pergamon Press, 1965.

27. J. D. Roberts and F. J. Weigert, *J. Am. Chem. Soc.*, 1971, **93**, 2361-2369.

28. F. J. Weigert and J. D. Roberts, *Inorg. Chem.*, 1973, **12**, 313-316.

29. R. A. Newmark and R. J. Webb, *J. Flu. Chem.*, 2005, **126**, 355-360.

30. B. Wrackmeyer and O. L. Tok, *Magn. Reson. Chem.*, 2002, **40**, 406-411.

31. M. Kollmannsberger, K. Rurack, U. Resch-Genger and J. Daub, *J. Phys. Chem.*, 1998, **102**, 10211-10220.

32. J. D. Dunitz and R. Taylor, *Chem. J. Eur.*, 1997, **3**, 89-98.

33. J. A. K. Howard, V. J. Hoy, D. O'Hagan and G. T. Smith, *Tetrahedron*, 1996, **52**, 12613-12622.

34. K. D. Sen and C. K. Jørgensen, *Electronegativity*, Springer-Verlag, New York, 1987.

35. D. M. Lemal, *J. Org. Chem.*, 2004, **69**, 1-11.

36. Gaussian Inc., Wallingford CT, Editon edn., 2004.

37. J. B. Prieto, F. L. Arbeloa, V. M. n. Martínez and I. L. Arbeloa, *Chem. Phys.*, 2004, **296**, 13-22.

38. W. Wu, H. Guo, W. Wu, S. Ji and J. Zhao, *J. Org. Chem.*, 2011, **76**, 7056-7064.

39. A. C. Benniston and G. Copley, *Phys. Chem. Chem. Phys.*, 2009, **11**, 4124-4131.

40. S. S. Jang, M. Blanco, W. A. G. III, G. Caldwell and R. B. Ross, *Macromolecules*, 2003, **36**, 5331-5341.

41. H. L. Kee, C. Kirmaier, L. Yu, P. Thamyongkit, W. J. Youngblood, M. E. Calder, L. Ramos, B. C. Noll, D. F. Bocian, W. R. Scheidt, R. R. Birge, J. S. Lindsey and D. Holten, *J. Phys. Chem. B*, 2005, **109**, 20433-20443.

42. H. Sunahara, Y. Urano, H. Kojima and T. Nagano, *J. Am. Chem. Soc.*, 2007, **129**, 5597-5604.

43. A. Cui, X. Peng, J. Fan, X. Chen, Y. Wu and B. Guo, *Photochem. Photobiol.*, 2007, **186**, 85-92.

44. V. I. Saranov and L. A. Gribov, *Appl. Spectorsc.*, 1984, **38**, 313-317.

45. *Bull. Soc. Chim. Belg.*, 1997, **106**, 565-572.

46. D. W. Brazier and G. R. Freeman, *Can. J. Chem.*, 1969, **47**, 893-899.

Chapter 4. A Novel Synthesis of Asymmetric Bodipy Compounds Leading to the First Examples of Axially Chiral Bodipy Molecules

4.1 Introduction

Interest in chiral fluorescence stems from the potential uses of such a system with applications in many fields of nanotechnology, pharmaceuticals, catalytic research, bio technology and food technology.[1-6]

Chiral fluorophores can be developed to detect differences in chiral environments within a wide range of dynamic systems. Conceptual work based on chiral fluorescent sensors does not have many differences to that of the designs of sensors in general. Provided that a different response can be elicited when the fluorophore is in the presence of different enantiomers then the principles of detection remain the same. This allows for the use of techniques such as PeT sensing to be used to allow chiral recognition.

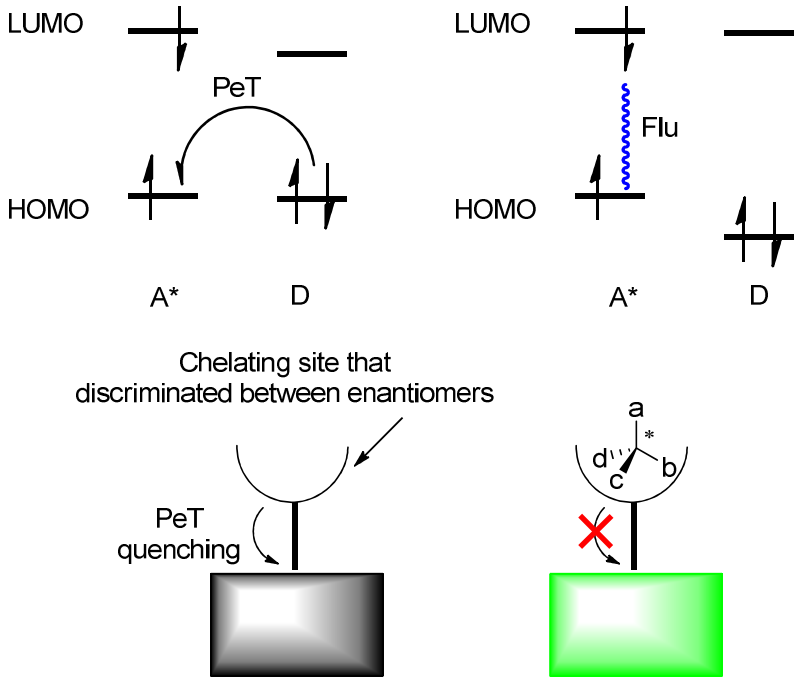

Figure 1 Using PeT to create a chiral sensor: energy level diagram depicting the relative energy levels required to achieve an 'on' / 'off' effect (top); and a depiction of a possible generic setup for such a system (bottom).

Photo-induced electron transfer (PeT – as discussed in the introduction) can potentially be used in order to achieve a chiral sensing effect. By taking a receptor which caused PeT quenching to an attached fluorophore, and was able to discriminate between enantiomers, one would expect to see a difference in

fluorescence intensities upon exposure to equal amounts of separate R and S enantiomers due to differences in the relative quantities of bound enantiomers.

Indeed enantiomeric sensors which contain bodipy groups are already a reality, Daub *et al*. attached two bodipy groups to a molecule of R-BINOL. The resulting enantiopure compound was shown to be able to chirally discriminate between the different enantiomers of 1-phenylethylamine. The system is a PeT sensor that could be turned 'on' and 'off' depending on whether the BINOL moiety underwent any interaction with the 1-phenylethylamine quencher.[7] The deprotonation of the OH, due to the presence of the basic 1-phenylethylamine, would lead to the PeT quenching of the singlet excited state thereby turning the fluorescence 'off'.

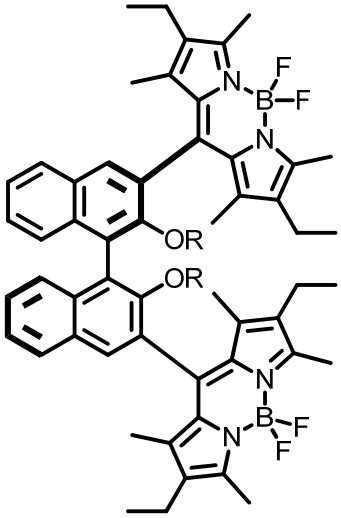

Figure 2 R-BINOL with two bodipy molecules attached creating a PeT sensor for basic conditions. Where R = H (λ_{abs} = 523 nm, λ_{em} = 542 nm, Φ_F = 0.61), CH_3 (λ_{abs} = 526 nm, λ_{em} = 542 nm, Φ_F = 0.80).

In this example however the chirality in the system stems from the BINOL section of the compound and not the fluorophore. Fluorophores which themselves possess chirality and as a result chiral sensing capabilities would certainly be more atom efficient and may even have an increased capacity as a sensor as well as potentially being easier to construct.

4.1.1 Chiral Lanthanide Complexes

An area of particularly intense research involves the use of chiral lanthanide complexes for use as enantioselective catalysts and chiroptical probes / sensors.[8, 9] Indeed the use of the circularly polarised luminescence (CPL) produced by these complexes makes them a useful tool when used as

biological probes or in imaging applications.[3, 8-12] Lanthanide complexes have a number of beneficial properties which lend themselves to the field of biological imaging such as having: a large Stokes shift, narrow fluorescence emission bands, large quantum yields of luminescence, and long lifetimes.[4]

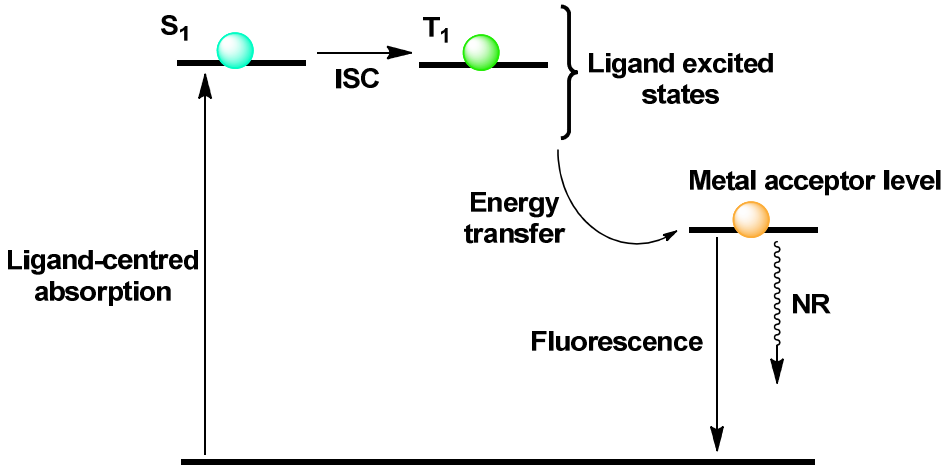

Figure 3 Diagram showing the general mechanism used for the sensitisation of lanthanide (III) complexes, whereby the ligand is first excited, causing energy transfer to the lanthanide ion. S_1 = excited singlet state, T_1 = excited triplet state, NR = non-radiative pathway, ISC = inter-system crossing.

Unfortunately due to the high kinetic lability of lanthanide metal ions, enantioselective control of the coordinations spheres is complicated, resulting in very few examples of enantiopure polynuclear lanthanide complexes. Mazzanti *et al.* were able to successfully synthesise and isolate enantiopure europium wheels, made via a diastereoselective self-assembly from diastereometric complexes of Λ- and Δ-$[Eu(R\text{-}Phbipox)_2]^+$.

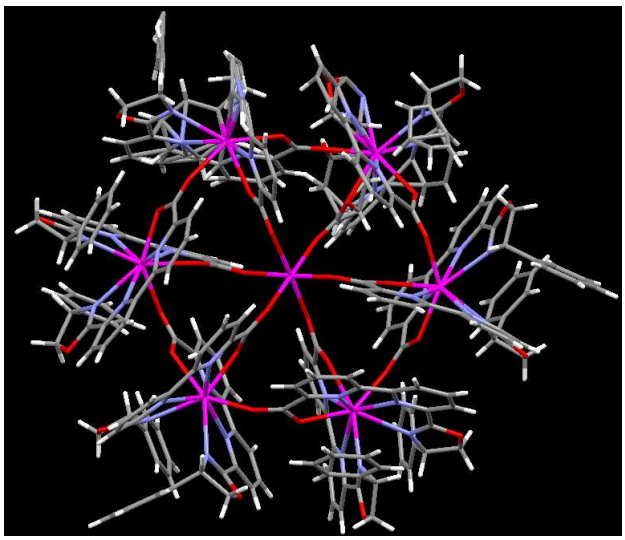

Figure 4 Eu_7L_{12} - [Eu⊂(ΛΔΛΔΛΔ-Eu_6)]; where L = R-Phbipox / S –Phbipox; one of the first and largest examples of self-assembling axially chiral lanthanide complexes.

This europium wheel is the largest example to date* of a luminescent Eu^{3+} wheel that also exhibits chirality. The molecules were found to have a relatively high quantum yield (Φ_F = 0.27) and also exhibited large CPL with an activity that varied depending on the nature of the assembly.[13]

4.1.2 Different Types of Chirality

There are various different ways that a molecule can exhibit chirality including: planar, helical, centred and axial. In all cases the mirror image of the chiral compound is non-superimposable.

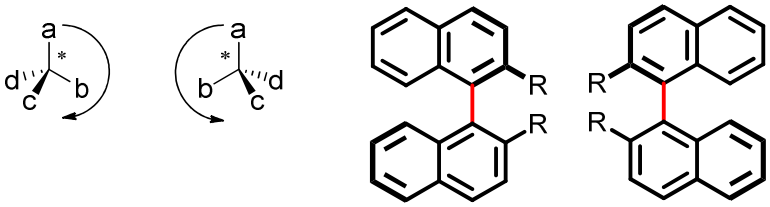

Figure 5 General examples of stereogenic and axial chirality, with the red highlighted bond representing the axis of chirality.

Centred chirality – Typically stereogenic chirality is the most commonly seen form and results from one atom which is chiral by virtue of the surrounding groups all being different.

Axial chirality – occurs when the compound does not possess a stereogenic centre but instead an axis of chirality. In most cases axial chirality is seen in

* As of August 2013

atropisomeric biaryl compounds such as BINOL and BINAP, where by the bond between the two biaryl groups is the axis of chirality.

Helical chirality – is an extension of axial chirality which sees the chirality stemming from the formation of helices. In this instance the axis of chirality is found running through the centre of the helix.

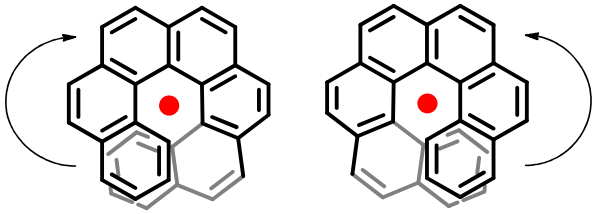

Figure 6 Helical chirality demonstrated with hexahelicene. With the red dot representing the axis of chirality as seen from above.

4.1.3 Examples of Chiral Bodipy Compounds

4.1.3.a Helical Bodipy Compounds

In 1999, while synthesising a highly red-shifted bodipy dye, Burgess *et al*. produced the first chiral bodipy. By performing two ring closing reactions using BBr_3, a chiral plane was created within the molecule. The resulting bodipy had unique chiral heptacyclic core which contained a distorted N_2BO_2 unit. Neither of the enantiomers were isolated and tested, though a chiral HPLC trace was run which confirmed the presence of both isomers.[14]

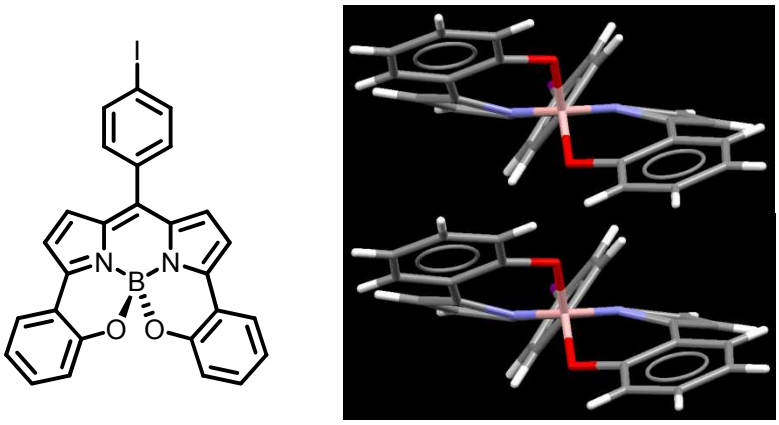

Figure 7 A constrained 3,5-bi-aryl bodipy (λ_{abs} = 630 nm, λ_{em} = 654 nm, left) with crystal structures of the two enantiomers (right).

Indeed the same chirality was also observed in 2008 when O'Shea *et al*. synthesised azabodipy systems which were similar to those produced by the Burgess group in 1999. Although once again the two individual enantiomers were not isolated.

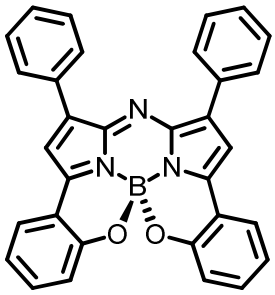

Figure 8 Chiral azabodipy systems are bought about with the same cyclisation reaction used by the Burgess group, which leads to a similar constrained N_2BO_2 chelated system.[15]

4.1.3.b Centred Chirality in Bodipy Compounds

Both Burgess' bodipy and O'Shea's azabodipy systems exhibited helical chirality. Bodipy compounds that demonstrated other forms of chirality had not been prepared until Nabeshima *et al*. to produce a compound that possessed a chiral centre at the boron of the bodipy core. Since the publication of this compound nearly all literature examples of chiral bodipy compound to date contain a stereocentre at the boron of the compound. This is most like due to the compound being relatively easy to prepare in high yields.[16]

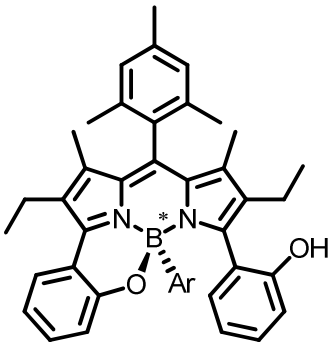

Figure 9 The first example of a chiral bodipy compound with the chirality stereogenic boron centre.

Up to this point all publications showing chiral bodipy compounds and the associated photophysics detailed the racemate, and not the individual enantiomers.[†] It wasn't until 2010 when Burgess *et al*. resolved a chiral bodipy using chiral HPLC. Once again this bodipy possessed a stereocentre at the boron of the bodipy core. This was achieved via the Grignard addition of a

[†] Though technically enantiopure bodipy containing compounds, such as the R-BINOL compound published by Daub, had been isolated the enantiomer stemmed from the appendages and not the chromaphore itself.16. C. Ikeda, T. Maruyama and T. Nabeshima, *Tetrahedron Letters*, 2009, **50**, 3349-3351, 17. A. Gossauer, F. Nydegger, T. Kiss, R. Sleziak and H. Stoeckli-Evans, *Journal of the American Chemical Society*, 2004, **126**, 1772-1780.

naphthyl group directly onto the boron, followed by a selective oxidation of the 3-methyl group of the bodipy.

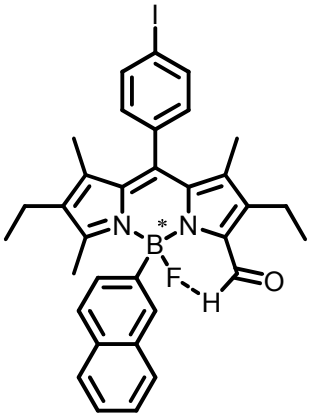

Figure 10 The first enantiomerically resolved chiral bodipy – the chirality is bought about by the presence of asymmetry at the bodipy core as well as the presence of two different molecules attached to the boron centre. The chirality has been shown to be stable to racemisation at room temperature. λ_{abs} = 534 nm, λ_{em} = 560 nm, Φ_F = 0.25.

Both enantiomers were found to have properties typically similar to that seen for equivalent bodipy compounds with sharp absorption and emission bands, high absorption coefficients and good quantum yields. Perfect mirror images were also observed for the CD spectra of the two enantiomers.

4.1.3.c Proposed Axially Chiral Bodipy Systems

Until now there have been no examples of axially chiral bodipy compounds, with current examples of chirality stemming from: a stereogenic boron, helical chirality or by virtue of the bodipy being attached to groups that already express axial chirality.

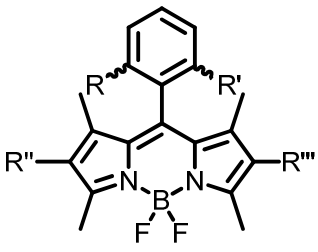

Figure 11 The generic make-up of axially chiral bodipy compounds, where R≠R'≠R''≠R'''. In this compound there exist two planes which are orthogonal to each other: the phenyl moiety and the bodipy core. Due to these two planes any molecule should be designed to create a large difference between the two sides of each plane so as to illicit an enhanced chiral sensitivity.

In this chapter a novel and facile series of pathways towards asymmetric bodipy compounds is detailed. Taking ideas from porphyrin chemistry, the extremely flexible routes provide a quick and simple way to produce diverse bodipy compounds. This work is also combined with that of the previous chapter, whereby the asymmetric bodipy core has an ortho-aryl containing group present in the meso position thereby turning the previously pro-chiral bodipy compounds into the first examples of axially chiral bodipys.

Chiral fluorescence in bodipy compounds is a subject that is in its infancy with development of the field only occurring in the last 5 years. As such there is major scope for work within the area focussing on both the synthesis of new types of chiral bodipy compound and also the refinement of the fluorescent properties of existing groups.

4.1.4 Strategic Synthetic Approach towards Axially Chiral Bodipy Systems

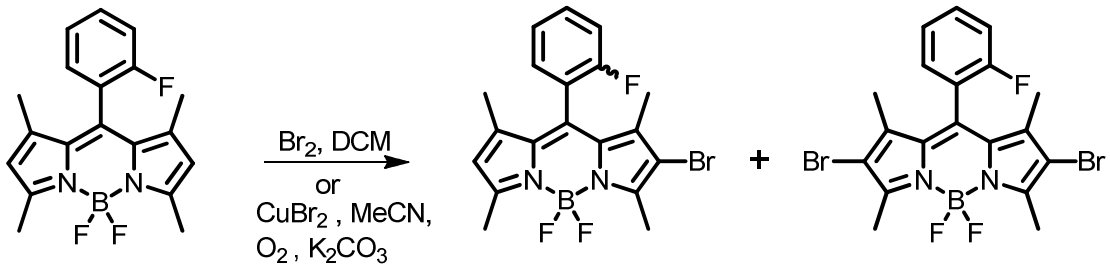

Scheme 1 The bromination of bodipy to form both mono and di-bromobodipy, several sets of conditions are available.[18-20]

A very quick route to axially chiral bodipy compounds is possible via the mono-bromination of the ortho-substituted pro-chiral precursor. There are two problems with the bromination of bodipy compounds, the first of which is that the synthesis is difficult to optimise. Typically the di-brominated product is the desired compound, as such most chemistry in this area is focussed on this aspect. The di-bromination can be achieved in high yields, often approaching unity, using bromine and DCM. For the selective mono-bromination of the bodipy core it is important for the reagents to be in an exact ratio. Deviations from this ratio will lead to an increased yield of the di-bromo compounds. With the optimised ratios it is possible to attain the mono-brominated compound in good to excellent yields (>50%), though there will always be a certain amount of the di-bromo bodipy present. Furthermore the purification of the mono and di-

substituted compounds is also awkward with the r.f. value for the two molecules typically being very similar.

The second problem with the brominated bodipy compounds is that they are not very emissive. The bromine atom causes a rapid conversion of the excited singlet state to the triplet state, via the heavy atom effect.[21] This sees the fluorescence quantum yield for these molecules drop significantly, often Φ_F = <0.05. Although these compounds might show chiral phosphorescence, the measurements of such a process are not practical. As such mono-bromobodipy was not considered to be a viable target for this study. That said the presence of a bromo group in the β-position would allow for the expansion of the system off this carbon using a coupling reaction, something that was taken advantage of during the project.

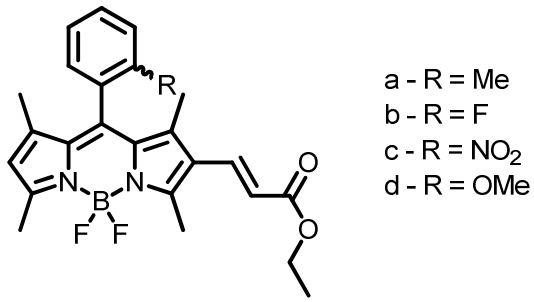

Figure 12 Axially chiral bodipy target compounds with extended conjugation off the β-position.

It was decided that the chromophore must be involved in an aspect of the chirality in order to increase the chances that the CD spectral results show the maximum possible difference between enantiomers.

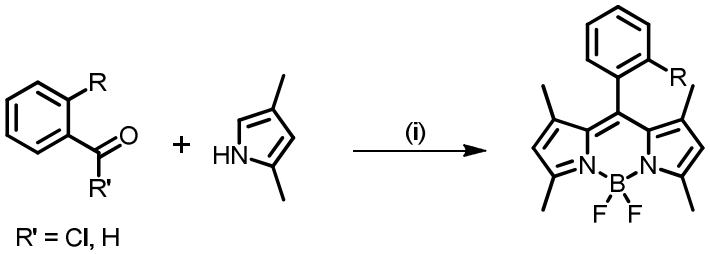

Figure 13 The initial synthesis of the prochiral bodipy complexes. (i) DCM, TFA; if R' = H; DDQ; $BF_3.OEt_2$, ^{i}PrNEt.

All of the bodipy compounds were produced using procedures modified from the standard literature preparations.[22] This typically involved the reaction of an acid chloride / aldehyde with a pyrrole to form the dipyrrin intermediate. A BF_2 unit

was then complexed into the intermediate dipyrrin to give the resulting bodipy. From this bodipy starting material it would be possible to mono-brominate at the β-position which would allow for further functionalisation at this position at a later stage.

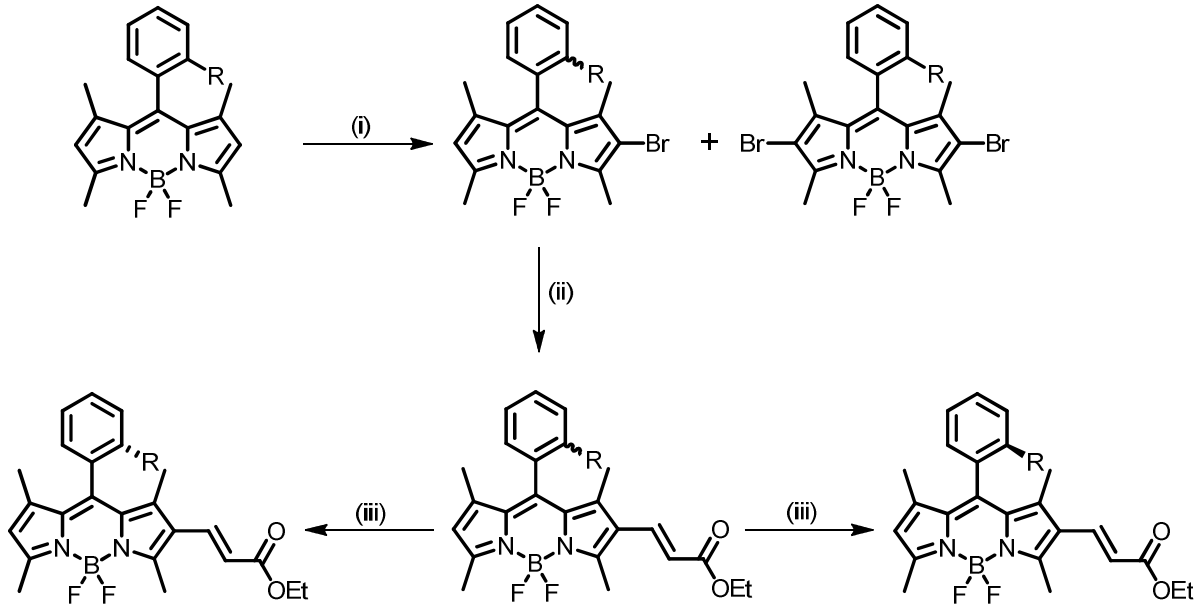

Scheme 2 A proposed route to the final set of compounds. (i) 1 eq. Br_2, DCM, 24 h; (ii) $Pd(OAc)_2$, PPh_3, Et_3N, DMF, Δ; (iii) The resolution was performed on a chiral HPLC column (Chiralcel OD-H Heptane/IPA 95/5). Yields where R = OMe: (i) 40% di-brominated, 45% mono-brominated; (ii) 65%[‡]

The problems which were discussed regarding the direct bromination of the core of bodipy compounds did apply to this synthesis, with yields affected greatly upon a slight deviation from the optimal ratio of reagents. Once optimised it was possible to attain a 45% yield of the mono-brominated product. While not at the same high yields seen for the subsequent bromination reactions, mentioned later in this chapter, these yields were more than acceptable providing ample starting material for the ensuing cross coupling reaction.

In spite of moderate yields for the final product the route proved successful and provided a relatively simple way to attain axially chiral bodipy compounds which contained expanded conjugation at the chromophores.

[‡] This particular synthetic route was successfully undertaken by Reinner Lerrick, and the chiral resolution was performed by Dr. Karen Haggarty.

A second, more elegant route was also examined alongside the afore mentioned synthesis. The inspiration for this synthesis arose from two pieces of published literature, the first of which was a paper on porphyrins by Smith *et al*. describing their rationalised syntheses.[23]

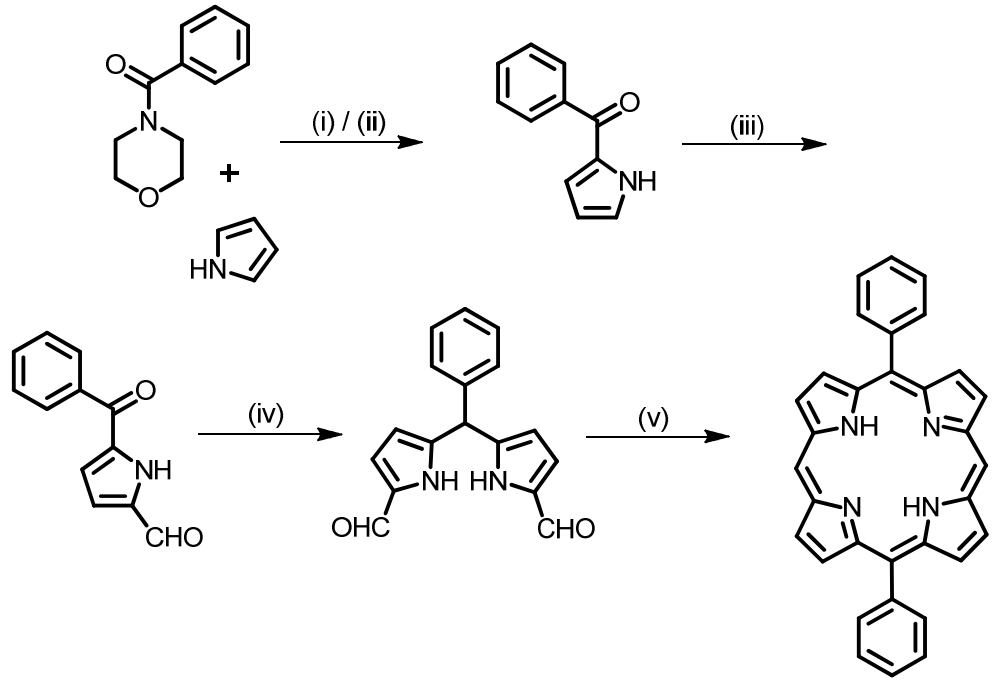

Scheme 3 A synthetic pathway to form a phenyl substituted porphyrin. (i) EtMgBr then PhCOCl; or (ii) $POCl_3$, N-benzoylmorpholine then Na_2CO_3; (iii) $POCl_3$, DMF then Na_2CO_3 (iv) 2-formylpyrrole, AcOH; (v) 2,2'-(phenylmethylene)bis(1H-pyrrole), PrOH, Δ.

The synthesis described above allows for complete control of the synthesis of the desired porphyrin at each step. Where traditional porphyrin syntheses involve a condensation of 4 equivalents of aldehyde with 4 equivalents of pyrrole, the Smith ‘rational’ synthesis contains several additional steps. The added steps in this synthesis do not significantly impact on the overall yield of the route when compared with that of the traditional synthesis.

In the Smith synthesis a Vilsmeier-Haack reagent is first formed by reacting N-benzoylmorpholine with phosphoryl chloride, after which point pyrrole is introduced forming a ketopyrrole. The yields for the Vilsmeier-Haack reaction are found to be 70 - 80% which is much greater when compared with the alternative approach (step ii) where 50 – 70% yields are observed for the reaction between a 2-pyrrolemagnesium bromide and the acid chloride. The ketopyrrole is the subject to a Vilsmeier formylation, followed by an intermolecular condensation afford the porphyrin in good overall yields ca. 20%.

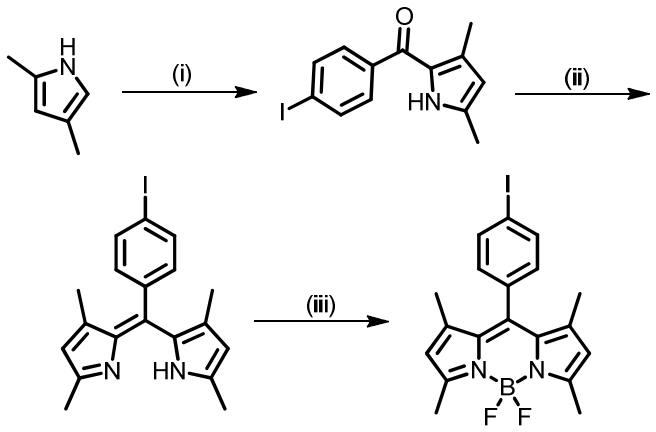

Scheme 4 Mély's synthesis of a bodipy. (i) IC_6H_4COCl, CH_3MgBr, ether; (ii) 2,4-dimethylpyrrole, $POCl_3$, DCM / pentane, 0^oC; (iii) $BF_3.OEt_2$, Et_3N, toluene.

The second paper, by Mély *et al*., demonstrated a similar approach to that of Smith yet this time using the synthesis to produce bodipy compounds. In spite of the increased number of synthetic steps and an increase in the complexity of the synthesis, the overall yield was ca. 30% which is in line with typical yields seen for standard bodipy preparations. Indeed it might have been easier if Mély had simply used the standard procedures as there appears to be no advantage gained from using this more complex route. That said the route did provide an opportunity for this particular project, specifically the second step of the Mély synthesis.[24, 25]

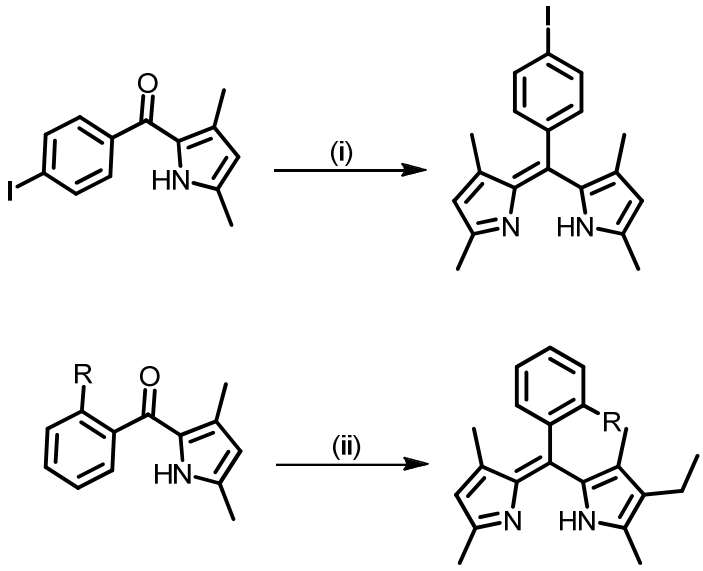

Scheme 5 A synthetic step from Mély et al. (top) where a dipyrrin is formed, and a modified version of the same step (bottom). (i) 2,4-dimethylpyrrole, $POCl_3$, DCM / pentane, 0^oC; (ii) The modified synthesis proposed: 2,4-dimethyl-3-ethylpyrrole, $POCl_3$, DCM / pentane, 0^oC.

By taking the Mély synthesis and introducing a different pyrrole at the second condensation step it would be possible to form unsymmetrical dipyrrin cores. The resulting flexibility of this approach would open out a plethora of asymmetric bodipy products. Furthermore if there was a group present in the ortho-position of the phenyl moiety of the resulting bodipy then that compound would be axially chiral.[§]

The structure of the second pyrrole to be introduced to the 2-aroylpyrrole can be varied, which has the potential of allowing the introduction of more complexity and functionality to the system with relative ease.

[§]NB THIS *Provided that the phenyl ring has two different groups in both ortho-positions then the phenyl ring cannot rotate. The size of these groups does not matter as the rotation is likely sterically hindered by the ortho protons anyway, as mentioned in chapter 3. If the dipyrrin core had no methyl substituents in the 1 and 7 positions then a group larger than a proton would need to be present, fortunately the next largest group, fluorine also prevents rotation around the meso-phenyl bond*.

4.2 Synthesis and Characterisation

4.2.1 Synthesis

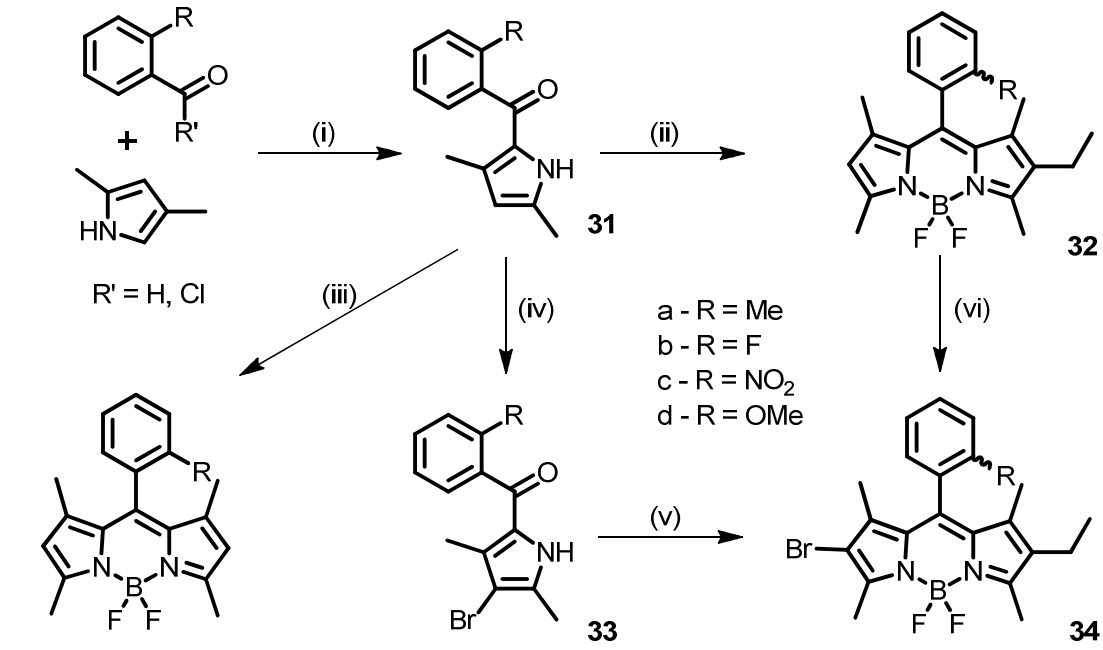

Scheme 6 The overall synthesis of the desired mono-bromobodipy. (i) EtMgBr, ether (ii) 2,4-dimethyl-3-ethylpyrrole, TFA, DCM; $BF_3.OEt_2$, $^iPr_2NEt$; (iii) if the prochiral symmetric system is required: 2,4-dimethylpyrrole, TFA, DCM; $BF_3.OEt_2$, $^iPr_2NEt$; (iv) Br_2, DCM; (v) 2,4-dimethyl-3-ethylpyrrole, TFA, DCM; $BF_3.OEt_2$, $^iPr_2NEt$; (vi) Br_2, DCM. All work on variants of 'd' where R = OMe, were performed by Reinner Lerrick and reaction conditions, if different, represent optimised conditions: (i) EtMgBr, THF; (iv) Br_2, DCM, H_2NEt.

The two synthetic approaches from Smith and Mély were combined to give the overall synthesis of axially chiral bodipy compounds. The formation of the 2-aroylpyrrole molecule was performed via the activation of the 3-position on the pyrrole using the Grignard reagent. It is also interesting to point out that while the Grignard activates the C2 position, equivalent lithium compounds will activate the nitrogen.[26, 27]

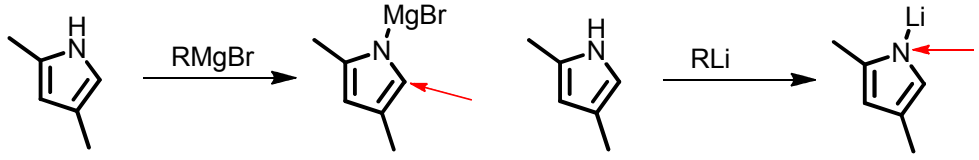

Scheme 7 The activation of the C2 position of the pyrrole by a Grignard (left), and the activation of the nitrogen by organolithium reagents (right).

The resulting pyrrolyl-Grignard was then reacted with an aryl acid chloride giving the aroylpyrrole. The yields varied depending on the ortho substituent,

with **31c** giving the worst yield of 16%. The yield for the other compounds **31a**,**b**,**d** was much better with typical yields higher than 60%.

The formation of the 2-aroylpyrrole was also attempted via the Vilsmeier-Haack preparation used in the Smith paper. The formation of the N-benzoylmorpholine intermediate was unsuccessful with the ortho-methyl substitent, hence further investigation was abandoned in favour of the more successful, but lower yielding, Grignard route.

Compound	Ortho-substituent			
	Me	F	NO_2	OMe
31	60	66	16	75[c]
32	26	-	18	85[c]
33	100	95	36	85[c]
34	47[a], 54[b]	54	13	-
35	46[d]	45[d]	-	35[d], 90[e]

*Table 1 Total percentage yields for the reactions. [a] formation of **34** via the pre-brominated **33**; [b] bromination of the bodipy core directly; [c] using modified conditions; [d] Ethyl acrylate, $Pd(OAc)_2$, PPh_3, Et_3N, DMF, Δ; [e] resulting from reactions on a 2-iodo substituted starting material.*

Upon isolation of the aroylpyrrole compounds work began on the reaction between these compounds and 2,4-dimethyl-3-ethylpyrrole to form the axially chiral bodipy **32**. While Mély used rather harsh conditions for the condensation of the second pyrrole, it was found that stirring the reaction in DCM at room temperature with a catalytic quantity of TFA gave the dipyrromethene intermediate. The dipyrromethene intermediate was not isolated, but instead treated with $BF_3.OEt_2$ and $^iPr_2NEt$ to give the chiral bodipy **32**. The overall yields for the bodipy were around the same for typical values seen for the classic one-pot procedure and to those published by Mély. Once again the ortho-nitro variant showed a marked drop in reaction yield relative to the compounds bearing different ortho-substituents.

Individual synthesis of **31** and **32** provided two possible routes towards the brominated bodipy. Either the ketopyrrole could be brominated and reacted to form the mono-brominated bodipy, or the bodipy itself could be brominated. The

flexibility of the bromination is also accompanied by the reaction itself being much less complicated. By brominating **31** a mono-β-bromine will exist in the resulting bodipy. This allows for the added benefit of being able to introduce a vast amount of flexibility to the system. For instance it would be possible to take **33** and introduce a pyrrole which is unsubstituted at the β-carbon. Allowing the expansion off the β-position followed by a second bromination, if that were desired, this would in turn give rise to systems which were potentially more complex.

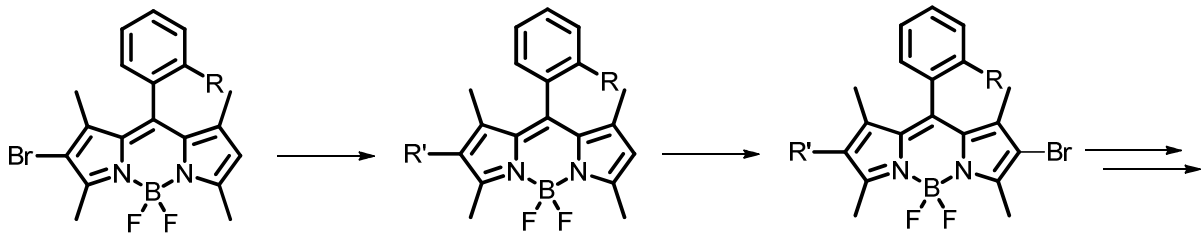

*Scheme 8 Flexibility of the selectivity of bodipy systems arising from **31**, allows one cross coupling reaction to be followed by a second bormination and subsequent cross coupling reaction. By doing this two individual components can be introduced with relative ease, and without a large loss of yield.*

A further benefit of the new synthetic route is that it is possible to introduce any pyrrole that is desired, in this case a pyrrole which is substituted at the β-carbon. Doing this effectively means that brominations of **32** will only affect one of the two β-positions, thereby avoiding the awkward conditions of the bromination reactions shown in Scheme 2.

The bromination of **32a** to form **34a** was performed using bromine in DCM, and resulted in a moderate yield of 53%. This particular route, though successful was abandoned in favour of the direct bromination of the aroylpyrrole precursor. This decision was solely based on the comparisons of the two overall reaction yields for **34a**, with direct bromination of the bodipy giving an overall yield of ca. 8% versus 28% for the route whereby the bodipy precursor was brominated.

Bromination of **31** to form **33** was also performed using Br_2 in DCM and progressed in high reaction yields, some of which approached unity. For the reactions involving **31a** and **31b** the recovered product was seen to be of adequate purity to continue to the next step without the need for further purification. Compound **31c** showed a large difference from the otherwise excellent yields for this reaction, again it is thought that the nitro group present

on the ring was the cause of the relatively low yield. Considering that reactions for the fluoro and methyl derivatives could progress without the need for further purification, along with the excellent yields, the bromination of the ketopyrrole was used preferentially used to introduce halide groups from this point on.

Brominated products of **33** were then reacted with a second equivalent of pyrrole in the presence of catalytic acid to form the equivalent bodipy compound **34**. The reaction yields for these reactions were substantially higher than those seen for the transition of **31** to **32** in spite of identical conditions being employed. That said the yield seen for the nitro containing bodipy was reduced significantly, as a result further reactions which involved the ortho-nitro group were abandoned in favour of the electron withdrawing fluorine.

The brominated bodipy **34** was then subject to a cross-coupling reaction aimed at increasing the conjugation which was linked to the bodipy core.

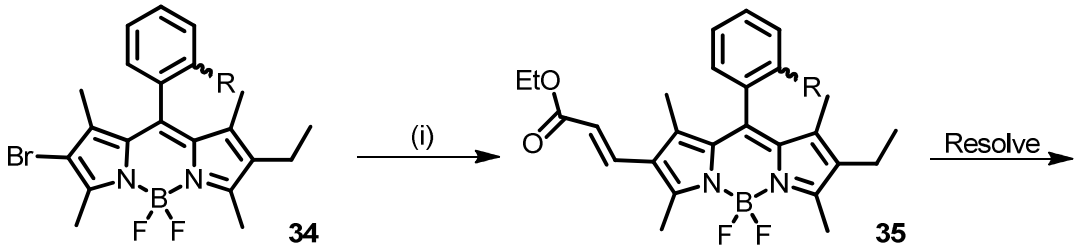

Scheme 9 Expansion of the bodipy chromaphore using a palladium cross coupling reaction. (i) Ethyl acrylate, $Pd(OAc)_2$, PPh_3, Et_3N, DMF, Δ; Or Ethyl acrylate, Pd_2DBA_3, $CsCO_3$, dioxane, $[HP(^tBu)_3].BF_4$.

The success of the cross coupling reaction relies on several factors the first of which is the strength of the bodipy-halide bond. The leaving group (halide) must have as weak a bond as is possible to the bodipy core in order to favour the reaction: I < Br < Cl < H; weaker bond from left to right. The ease of bond breakage does come at a cost, financially in this case, with the equivalent iodo-compounds by far the most expensive. As well as the expense, reactions forming the mono-iodo bodipy variants use harsh conditions that result in relatively poor yields - as such bromine was chosen as the leaving group.[28, 29]

The selection of the correct spectator ligand is also important as they allow for the manipulation of the rates of bond cleavage and dissociation of the final compound. Increasingly basic ligands will aid the rates of oxidative addition of the aryl halide onto the palladium species. In the case of this chapter

triphenylphosphine was selected, mainly because it is the common starting point for most un-tuned catalytic systems. That said the cross coupling was also attempted with several other spectator ligands though none of these gave yields which even approached those seen for triphenylphosphine.

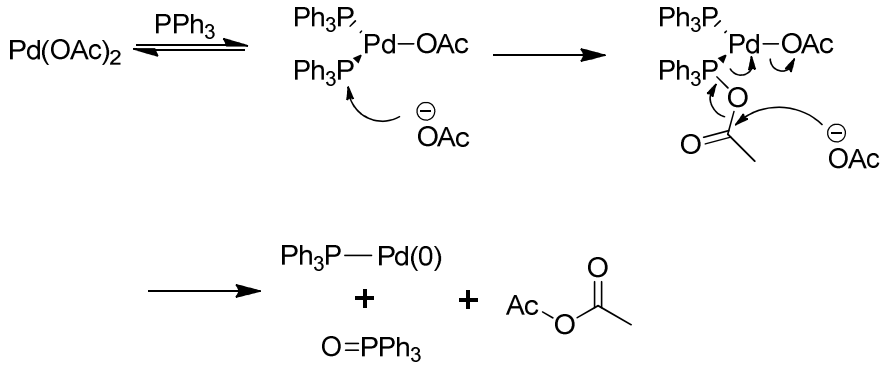

Scheme 10 Formation of the reactive palladium (0) species via reduction of $Pd(OAc)_2$ by PPh_3. This step is essential as it activates the palladium catalyst by reducing the metal from the Pd(II) species to Pd(0).

The catalyst is activated by the reduction of palladium (II) acetate by triphenylphosphine. Once the catalyst has been activated the bromo-bodipy undergoes the rate determining oxidative addition to the palladium.

At this point the ethyl acrylate coordinates to the metal centre from which point it undergoes a highly regioselective 1,2-insertion. It is important that the bodipy contains no protons β to the bromo group as β-elimination will compete with the alkene insertion.

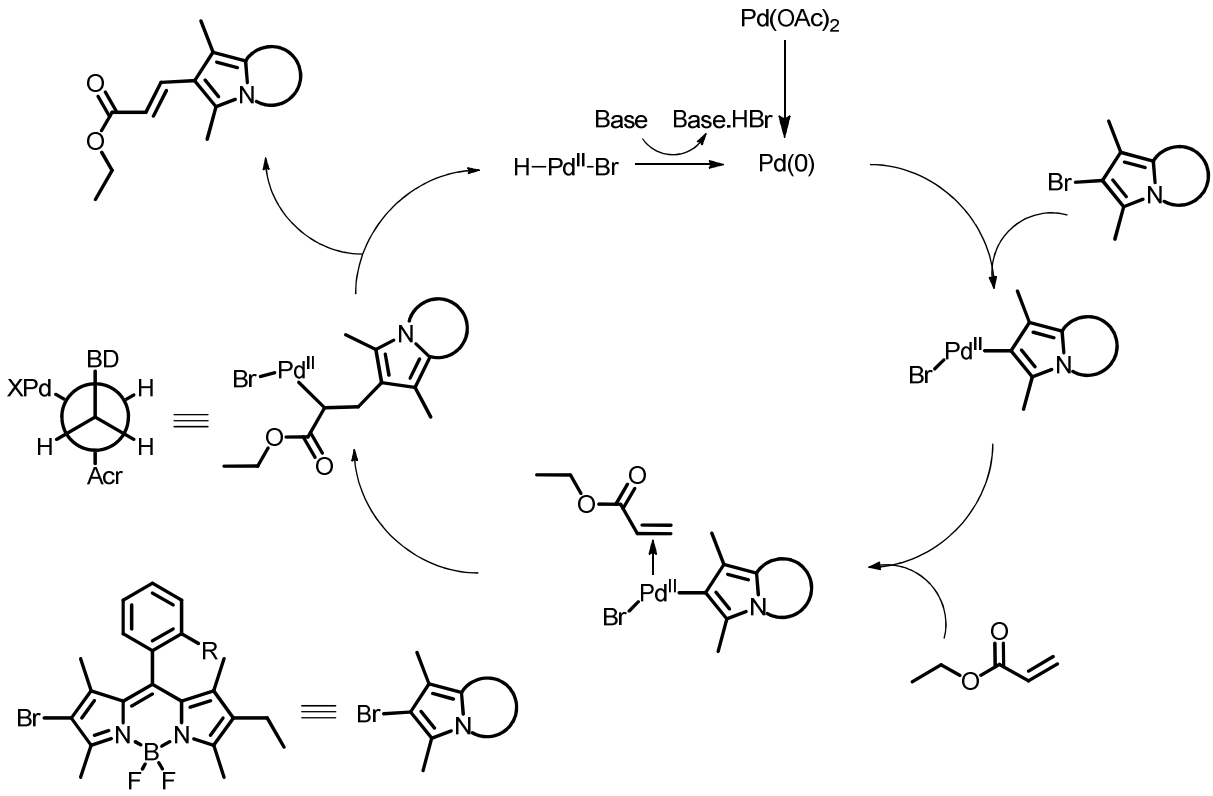

*Scheme 11 Mechanism for the Heck cross coupling reaction involved in forming **35**. BD = bodipy, acr = acrylate moiety.*

The syn addition of the alkene is then followed by a β–hydride elimination which results in the ejection of the product, **35**, from the metal complex and the production of a H-Pd^{II}-Br species. This species then undergoes a reductive elimination reaction with the base, which is present in excess, to regenerate the catalyst and produce $Et_3N.HBr$, thus completing the catalytic cycle.

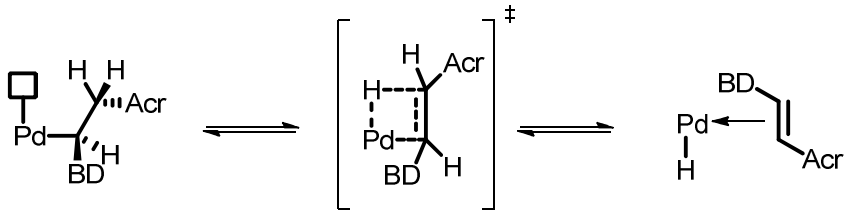

*Scheme 12 β-hydride elimination resulting in **35**. BD = bodipy, acr = acrylate moiety.*

Yields for the Heck cross coupling reactions were typically quite low (35 – 45%) with the lowest yield found for the OMe containing bodipy. Around 50% starting material was returned for reactions which formed **35a** and **35b**. These yields were obtained using the following conditions: Ethyl acrylate, $Pd(OAc)_2$, PPh_3, Et_3N, DMF, Δ. The size of the yield was found to vary greatly with the amount of time that the reaction was allowed to proceed. While the yield was seen to rise

with increasing time initially, yields eventually started to drop if the reaction was carried on over the 12 hour mark. It was thought that while the product is formed in these reaction conditions, the harsh temperatures which the compounds are subjected to eventually lead to the thermal decomposition of the product.

Attempts were made at optimising the reaction conditions with various combinations of palladium sources, phosphorus ligands, bases and solvents used. The only other combination of reagents which yielded measurable quantities of the desired product was: Ethyl acrylate, Pd_2DBA_3, $CsCO_3$, dioxane, $[HP(^tBu)_3].BF_4$, this particular combination gave poor yields typically ~2-5%.[30, 31]

Though there were several attempts to optimise the conditions used for the cross coupling step little progress was made to increase the reaction yields above those which were initially achieved. Ironically the 'un-optimised' conditions were indeed the optimum conditions. As such further work aimed at perfecting the catalytic step was curtailed, yet this remains a potential area for improvement in future work.

4.2.2 Characterisation.

Upon synthesis all compounds were firstly rigorously purified to remove any trace impurities which might show up in the photophysical analysis. The purification was two-fold. Firstly the crude material was passed through a standard silica column to remove the bulk of the impurities. Secondly the purified material was subjected to several crystallisations via slow-vapour diffusion – typically by dissolving the compounds in DCM and using petrol to form the crystals.

Once the crystals of the pure compounds had been collected the samples were then subjected to a full characterisation including the following techniques: ^1H, ^{13}C, ^{11}B (where needed), ^{19}F (where needed) NMR spectroscopies, mass spectrometry, melting points and infra-red spectrometry. All compounds that were characterised also underwent X-ray crystal structure analysis, though certain compounds did not diffract despite several attempts.

4.2.2.a ^{1}H NMR Spectral Analysis

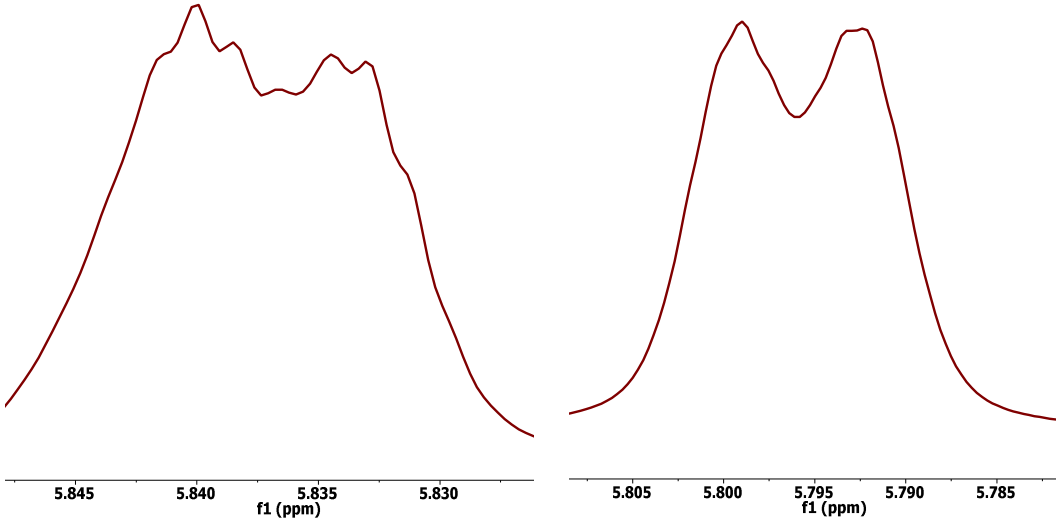

*Figure 14 **31b** 3-pyrrole proton (left), **31c** (right), showing splitting patterns which could not conclusively be accounted for.*

Proton NMR signals for compounds **31a-d** showed apparent splitting of the 3-proton of the pyrrole ring. The origin of the splitting of these protons is not entirely clear. The splitting patterns varied from compound to compound, however the common feature seen through each splitting was a significant broadening that may suggest an association with the NH proton of the pyrrole.

There is splitting of each amine proton, however the same splitting is not observed once the pyrrole has been brominated. The lack of splitting post-bromination seems to support the theory of an interaction between the C3 proton and the pyrrole N-H proton. That said there is no links between the coupling constants of either the 3-pyrrole proton and pyrrole amine, or any other proton in the NMR spectrum. This causes the source of the splitting at the 3-pyrrole proton to be particularly ambiguous.

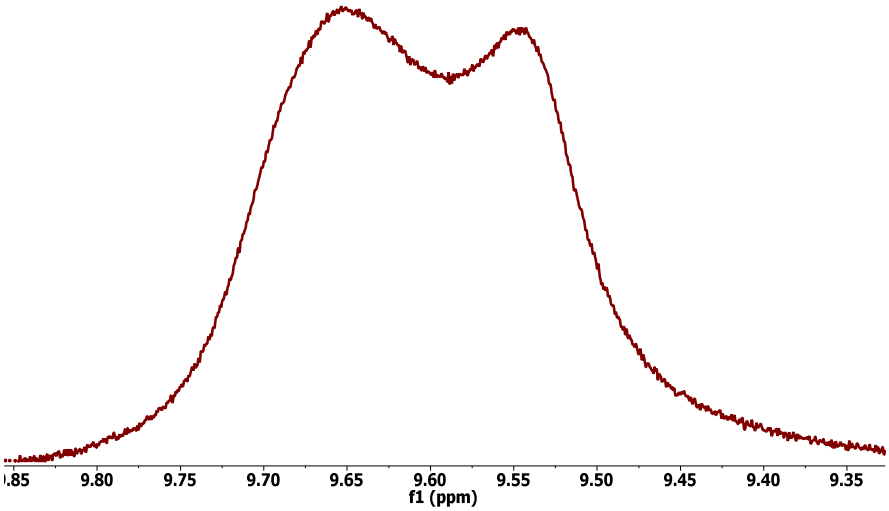

*Figure 15 The broad NH peak of the pyrrole proton of **31b**. As with each of compounds **31a-d** the expected singlet appeared to be split.*

As with the ^{1}H and ^{13}C NMR spectra discussed in chapter 4 samples of each compound which included an ortho-fluorine atom caused significant additional splitting of signals of atoms up to 4 bonds away from the fluorine atom.

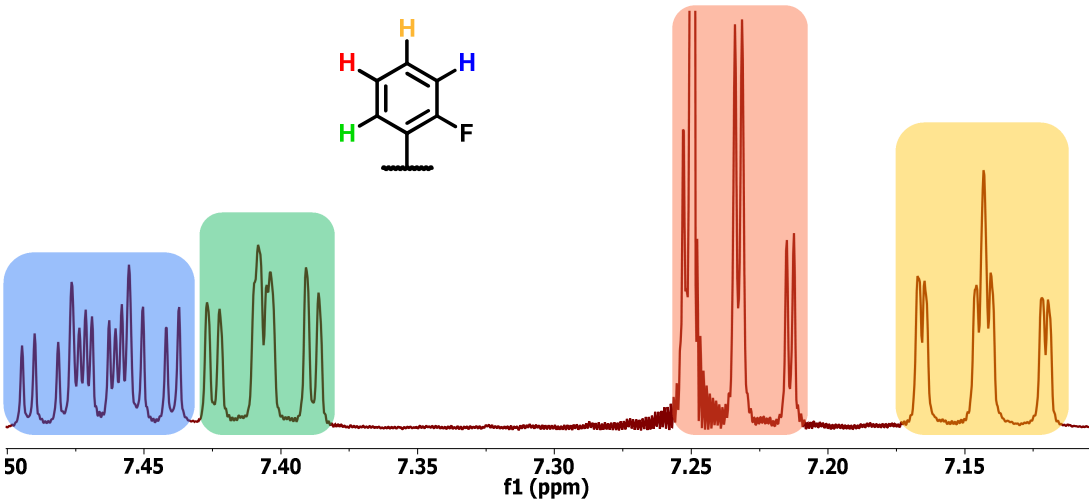

*Figure 16 Aromatic region of figure **33b** showing complex splitting, exacerbated by the presence of an ortho-fluorine atom.*

Figure 16 shows the aromatic region of **33b**, the splitting patterns of these four protons do not vary throughout each compound which includes an ortho-fluorine - though the shifts at which they are found do vary. The meta proton next to the fluorine shows the expected dddd splitting, while each other proton shows an apparent td splitting. There also is evidence of much finer coupling to the ortho and para protons, evidenced by the slight broadening of their peaks.

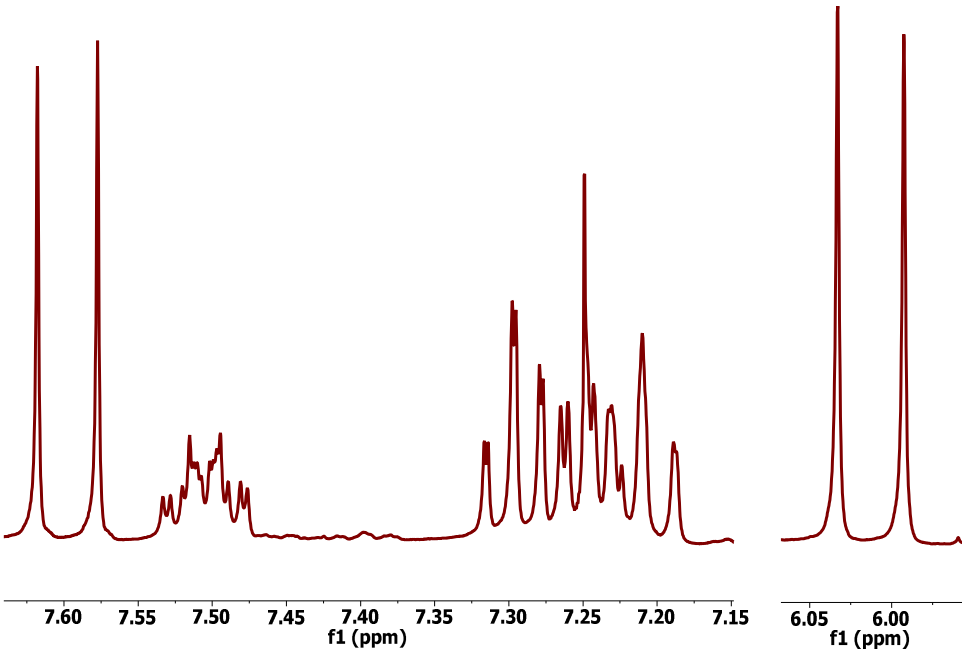

*Figure 17 Aromatic region of the ^{1}H NMR spectrum of **35b**, while more complex due to the presence of a fluorine atom on the aryl moiety, some of the aryl protons have shifted closer together merging their peaks. Also present are the two doublets which represent the newly introduced E-alkene- which demonstrated coupling constants which were in accordance with literature values.*

The final Heck coupled bodipy compounds gave coupling constants (16.2 Hz) for the newly attached alkene group which pointed towards alkene having an E-conformation, as expected with Heck coupling reactions.

4.2.2.b ^{19}F NMR Spectral Analysis

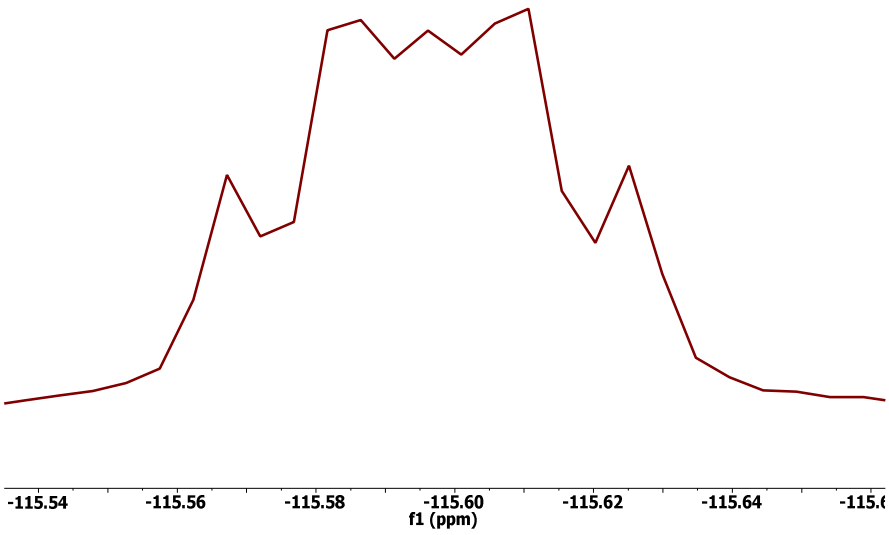

*Figure 18 **33b** ^{19}F NMR trace of the ortho-fluorine, here it is possible to see some of the splitting caused by the neighbouring protons on the aryl ring.*

^{19}F NMR spectra for each compound with an ortho fluorine atom showed the fluorine molecule along with the corresponding splitting to the neighbouring protons, seen in the ^{1}H NMR.

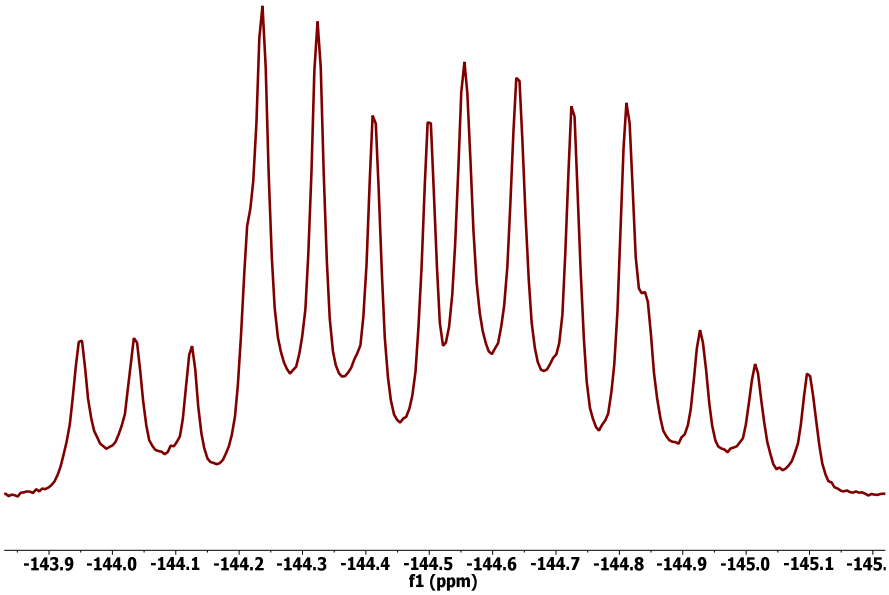

*Figure 19 ^{19}F NMR trace of the inequivalent fluorine atoms of the bodipy BF_2 unit for **35b**. Similar splitting patterns and coupling constants were observed for **35b** as were seen in the equivalent bodipy compounds of the previous chapter.*

All chiral bodipy compounds displayed the expected inequivalence of the BF_2 fluorine atoms, thereby confirming the presence of axial chirality. The values for the coupling constants for BF_2 fluorine inequivalence were in accordance with the literature precident.[32] A significant change in the coupling constant could be observed depending on which group occupied the ortho position of the meso-aryl moiety. For compound **35a** (Figure 20) there is an obvious difference in appearance of the ^{19}F traces of the BF_2 unit when compared with **35b** (Figure 19). This particular change is thought to depend on the nature of the groups which exist at the ortho position. While methyl substituents have a far less pronounced effect upon the BF_2 fluorine atoms through space, an ortho-fluorine is totally different in nature. The difference in the nature of these two ortho-groups means that the two BF_2 fluorine atoms will exhibit differing coupling constants in **35a** and **35b** thereby changing the complexion of the ^{19}F NMR spectra.

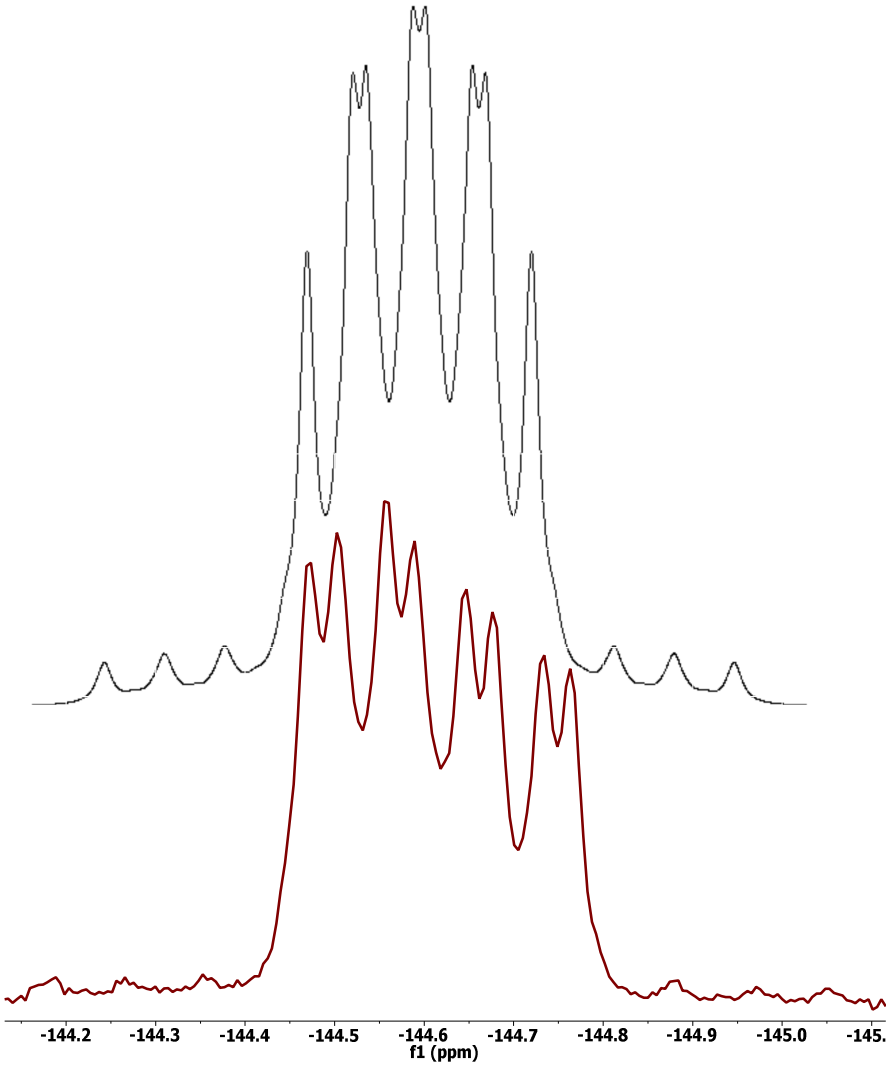

*Figure 20 ^{19}F NMR trace of the inequivalent fluorine atoms of the bodipy BF_2 unit for **35a** (maroon), simulated ^{19}F spectra (black). There is a noticeable difference between the splitting of **35a** and **35b (**Figure 19**)**, with the fluorine of **35b** eliciting a more pronounced effect upon the inequivalence of BF_2 fluorine atoms.*

Each compound also underwent the following analysis: ^{11}B NMR, infrared spectrometry, melting point analysis, and mass spectrometry. For all of these techniques there was nothing remarkable observed with any of the compounds.

4.2.2.c X-Ray Crystallographic Analysis

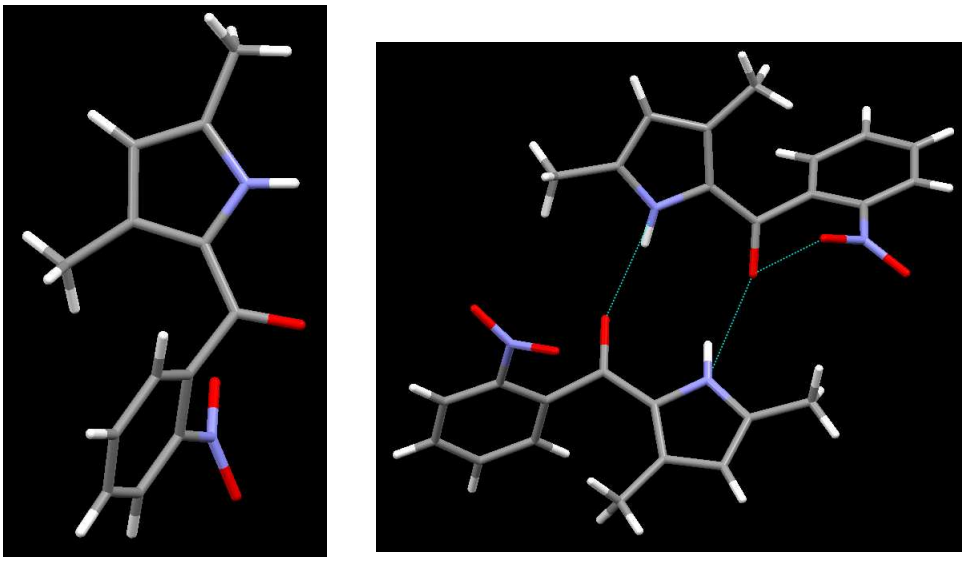

*Figure 21 X-Ray crystal structure for **31c** (left), and the associated packing diagram (right).*

Compounds **31b**-**d** (pure crystals of **31a** were unobtainable) all demonstrated similar hydrogen bonding networks, with interactions observed between the ketone of the benzoyl moiety and the pyrrole proton. The lengths of the hydrogen bonds (Table 2) were found to be between 2.808 and 2.822 Å, which are well in the range of accepted literature values.[33]

Compound	O – HN	NO – O	Br – ON
31b	2.821	-	-
31c	2.814	3.000	-
33a	2.822	-	-
33b	2.808	-	-
33c	2.814	2.935	3.142

Table 2 A summary of the intermolecular interactions in the crystal structure, with measurements given in Å.

Crystals of **31c** was found to contain apparent additional interactions between the aromatic nitro groups and the ketone functionality. The nitro group has been recognised as a weak acceptor of hydrogen bonds with a combination of the directionality of the lone pairs at the nitro oxygen and the electronic properties of the ketone and nitro groups leading to an interaction.[34, 35]

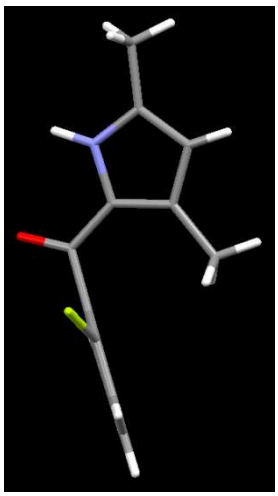

Figure 22 ***31b*** *- an ortho fluorine which appears to be ca. 20^{o} out of plane with the attached benzoyl moiety.*

The crystal structure diagram of **31b** showed some distortion associated with the fluorine atom located on the benzoyl section of the compound. The crystal structure diagram appeared to show a fluorine atom which was around 20^{o} out of the plane of phenyl moiety to which it was attached. The packing diagrams showed no signs of any intermolecular-sterics that might be distorting the bond between the fluorine and the phenyl ring, nor was the fluorine involved in any intra or intermolecular interactions.

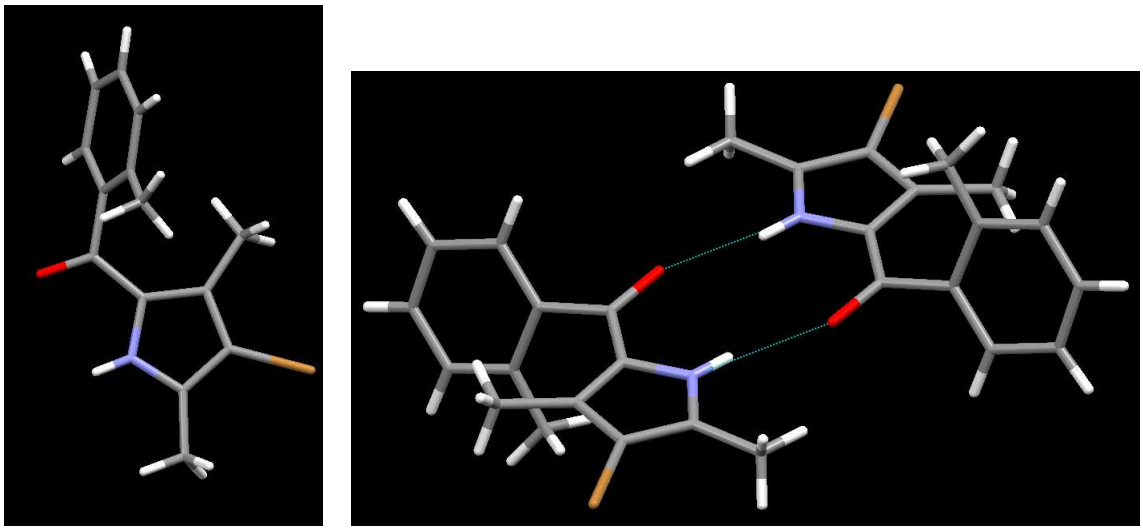

Figure 23 ***33a*** *(left) and the corresponding crystal packing diagram for* ***33a*** *with hydrogen bonding interactions shown (right).*

Brominated variants of **31** were seen to have similar bonding motifs to their unbrominated counterparts. Hydrogen bonds existed in the same positions with the similar lengths observed (Table 2).

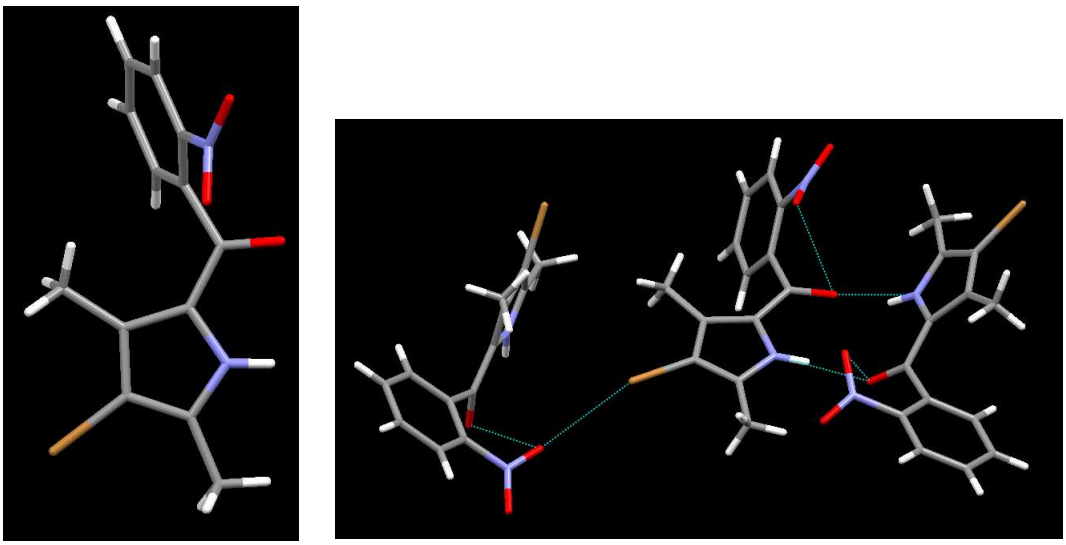

*Figure 24 **33c** (left) and the associated crystal packing diagram which includes both hydrogen bonding and halogen bonding interactions.*

Once again there were extra interactions observed for the nitro variant **33c**, the first of which was the same as the weak interaction discussed for **31c**. The second, through-space interaction, came in the form of a halogen bond between bromine and the oxygen atoms of a nitro group. Both the bond length (3.142Å) and the bond angles θ1 and θ2 (161^{o} and 155^{o} –Figure 15 Chapter 2) are consistent with previous literature values.[33]

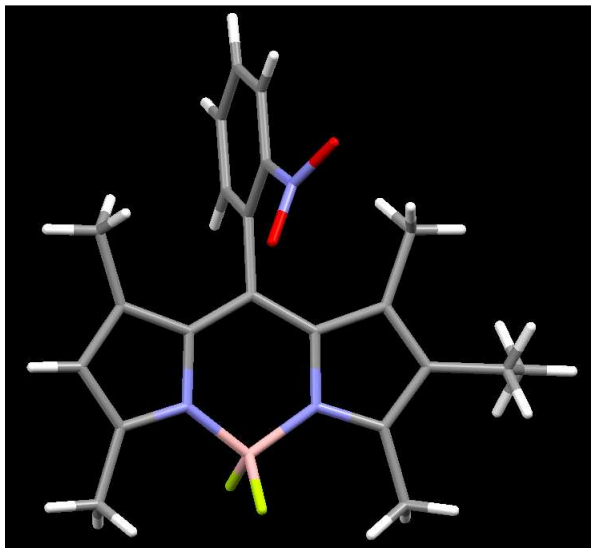

*Figure 25 The above figure of **32c** represents the first example of an axially chiral bodipy to undergo a structural determination using X-Ray crystal data.*

The crystallisation of the bodipy variants was successful in most cases, with all crystal structures also showing the presence of both R and S enantiomers in the crystal packing diagram.

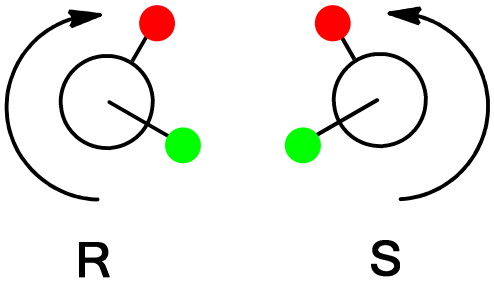

Figure 26 The determination of R and S enantiomers when dealing with axial chirality.

In all cases the bond lengths and bond angles did not vary for either of the two enantiomers, with each enantiomer displaying almost perfect mirror symmetry. In order to ascertain which enantiomer was which the packing diagrams had to be analysed. Axially chiral bodipy compounds, like BINAP and BINOL, contains no stereogenic centre and hence R and S cannot be identified using the standard procedures for compounds with a chiral centre.

To identify R and S the compound should first be viewed down the meso-aryl bond. Next two ‘markers’ should be identified within the molecule, each existing at either end of the meso-aryl bond. In the case of **32c** the two markers can be the pyrrole ethyl group and the aryl nitro group. Finally, and whilst viewing along the meso-aryl bond, the longest distance from the group in the foreground to that in the background is measured (Figure 26). If the pathway is clockwise then the enantiomer is R and counter-clockwise S.

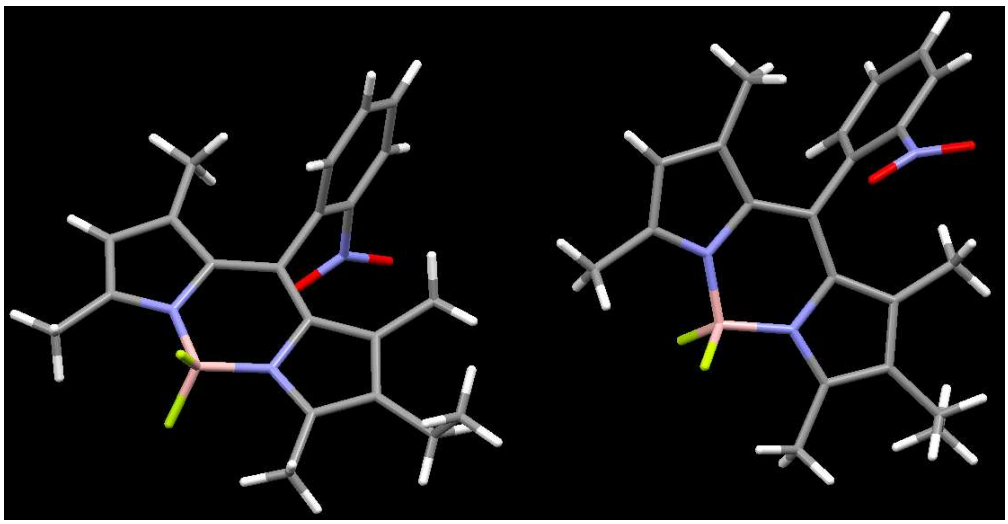

*Figure 27 Both R (right) and S (left) enantiomers of **32c**, taken from the crystal packing diagram. NB – the unit cell of **32c** consisted of 4 molecules, 2 of which have been removed in order to aid the clarity of the above figure.*

The crystal structure for **32c** showed a BF_2 unit which was out of the plane of the dipyrromethene core as well as the whole core curving slightly. The meso aryl group has also been forced downwards so that the aryl-meso bond falls some 12^o out of plane with the core. Both of these deformations of the core are likely due to the bulk of the nitro group, the sterics of which force the aryl group downwards and this resulted in the warping of the dipyrromethene core.

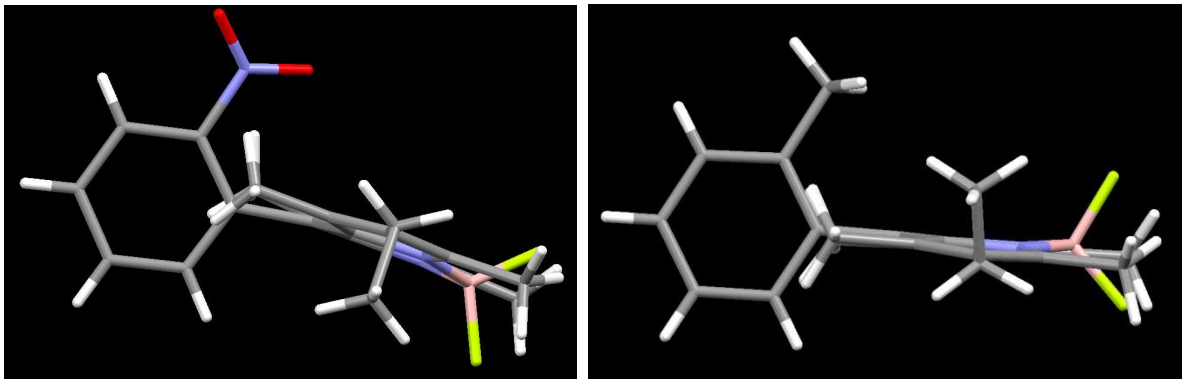

*Figure 28 A comparison of two bodipy compounds [**33a** (right) and **33c** (left)] from a side-on view. For **33a** there is a visible bendng of the bodipy core due to the steric bulk of the nitro group. In comparison the methyl variant, **33c**, displays a bodipy core which is much more flat.*

A comparison of **33c** with **33a** shows the extent that the size of the ortho group affects the planarity of the core of the bodipy, with an ortho-methyl group giving rise to a relatively flat core.

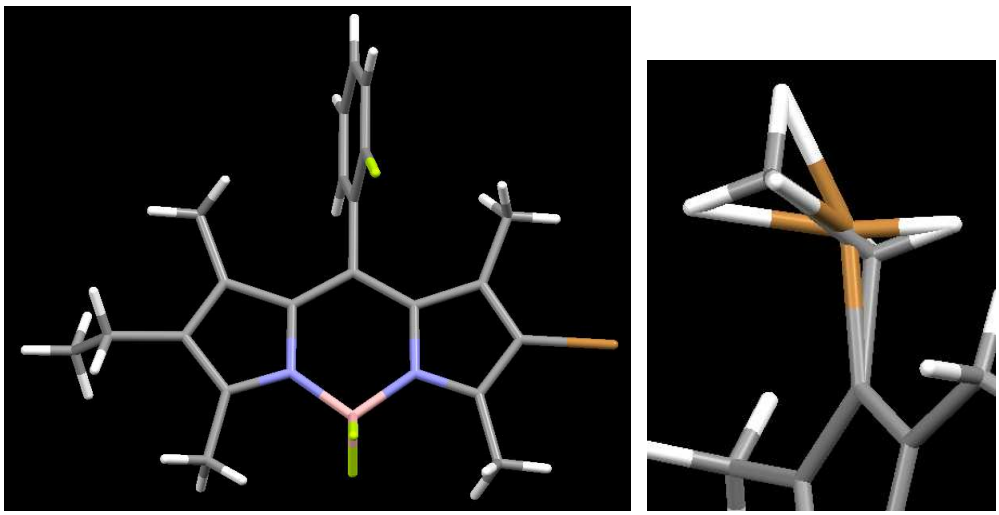

*Figure 29 The brominated bodipy, **34b** (left) the disorder seen in the crystal structure (right).*

All of the bromine containing bodipy compounds each exhibited some degree of distortion which centred around the two β-positions of the bodipy core. This was likely due to the presence of both R and S enantiomers, both of which contained a large bromine atom.

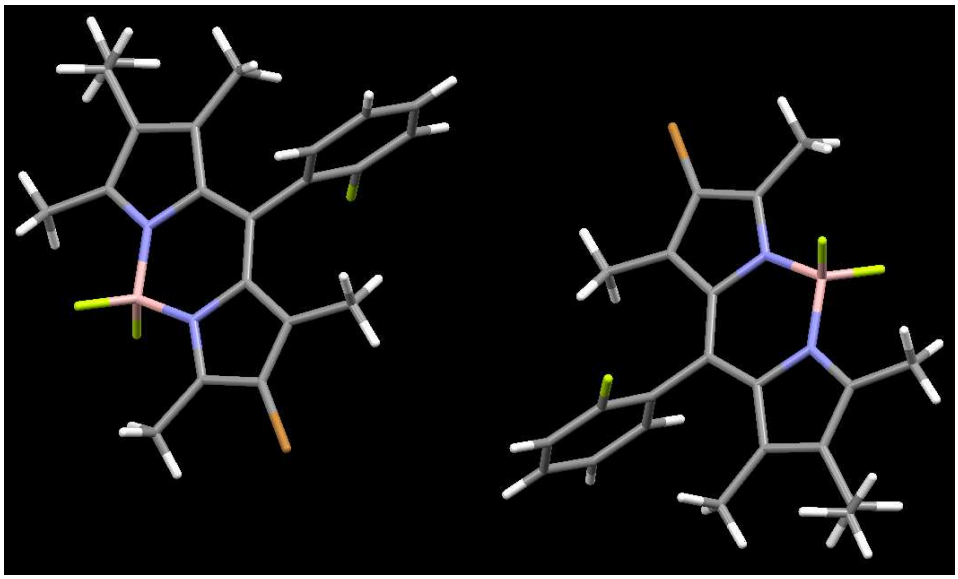

*Figure 30 Both R (right) and S (left) enantiomers of **34b**, taken from the crystal packing diagram. NB – the unit cell of **34b** consisted of 4 molecules, 2 of which have been removed in order to aid the clarity of the above figure.*

All of the ortho-fluorine containing compounds showed remarkable rigidity along the backbone of the compound. This observation is in direct contrast to molecules where the ortho-position contained groups which had more steric bulk such as a nitro group. In these cases the dipyrrin core was significantly distorted. For each ortho-fluorine bodipy the core was almost totally planar, the

aryl group was not sterically forced out of plane and the aryl group was at a 90^{o} angle with regards to the bodipy core.

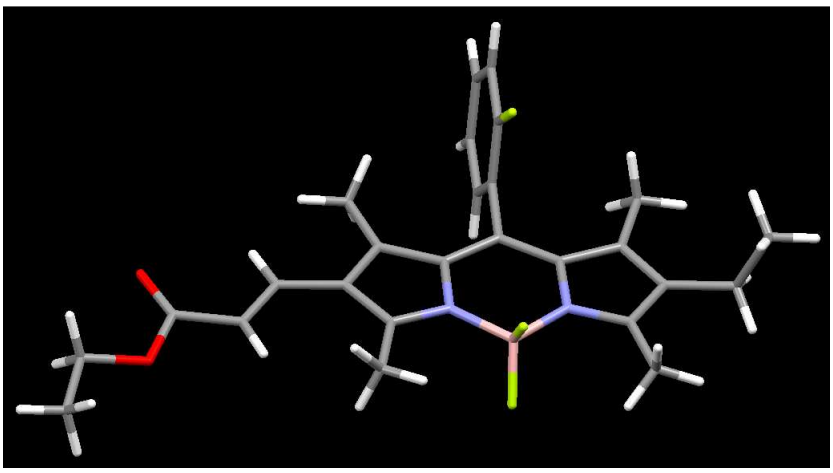

*Figure 31 Compound **35b**, the Heck coupled bodipy showing clearly the E-alkene conformation attached to the bodipy core.*

Crystal structures of the Heck coupled bodipy products further confirmed the presence of the E-alkene, the isomer which should result from the palladium catalysed coupling reaction. The newly attached alkene section was found to exist in the same plane as the core of the bodipy. This was surprising as it was expected to take up an orthogonal position either due to steric effects or simply to minimise the energy of the structure.

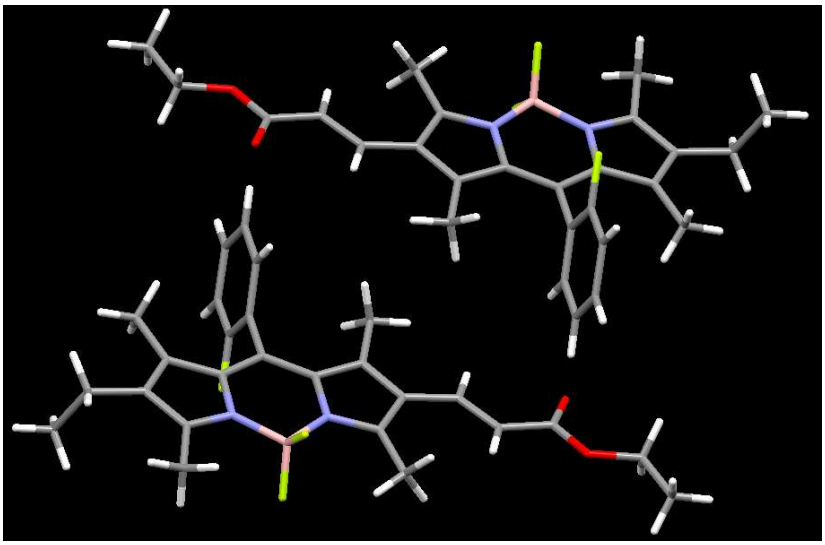

*Figure 32 Both R (bottom, left) and S (top, right) enantiomers of **35b**, taken from the crystal packing diagram. NB – the unit cell of **35b** consisted of 4 molecules, 2 of which have been removed in order to aid the clarity of the above figure.*

4.3 Photophysics

Compound	λ_{Abs} / nm [a,b]	λ_{Em} / nm [a,b]	SS / cm^{-1} [c]	ε_{Max} / M^{-1} cm^{-1} [b]	Φ_{Flu} [d,e,f]
32a	515	525	370	81600	0.85
32c	525	ND	ND	57600	ND
34a	526	540	493	98900	0.15
34b	532	545	448	63200	0.14
34d	528	541	455	64900	0.19
35a	526	537	389	95600	0.23
35b	544	562	589	78200	0.59
35d	539	556	567	81800	0.23

Table 3 The photophysical data for all compounds which produced luminescence when excited[**]. [a] ± 2 nm, [b] measured in $CHCl_3$, [c] ± 25 cm^{-1}, [d] Rhodamine B was used as a standard (Φ_{Flu} = 0.7 in MeOH), [e] ± 10%, [f] all values measured in MeOH.

4.3.1 Absorption

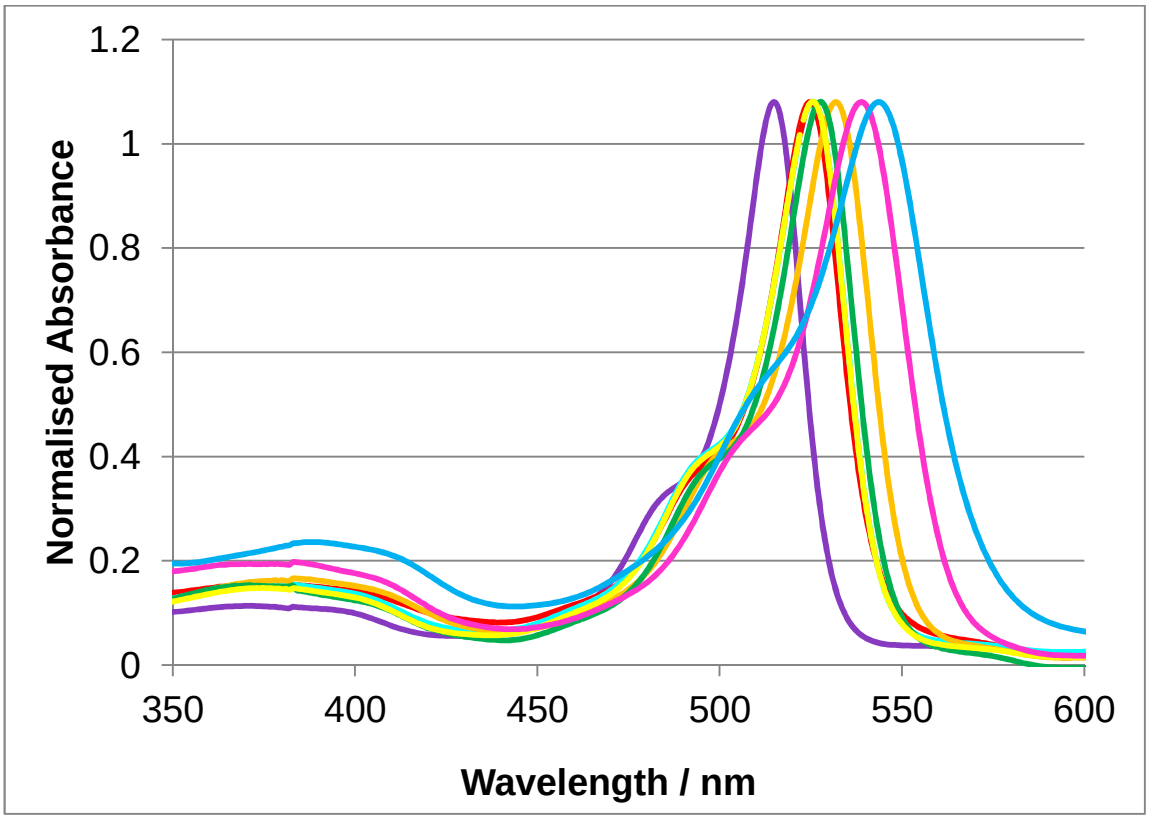

*Figure 33 Absorption spectra for all bodipy compounds in the series **32** – **35** measured in DCM at ambient conditions. **32a** - Purple, **32c** – Red (mostly obscured by **35a**), **34a** - Cyan, **34b** - Orange, **34d** - Green, **35a** - Yellow, **35b** - Magnolia, and **35d** - Blue.*

[**] Compound **34c** was not measured as the synthetic pathway towards **35c** had been abandoned.

Absorption spectra were measured in $CHCl_3$ at ambient temperature and all resembled a typical bodipy absorption spectra. For each compound there was a distinct S_0-S_2 absorption band with an absorbance maxima at around 370 nm. Ground state to singlet excited state transitions were all sharp and contained a shoulder peak.

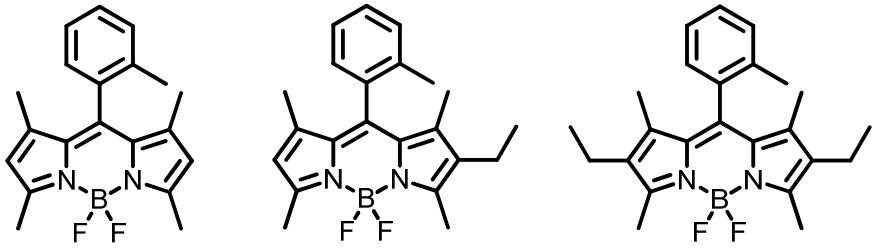

*Figure 34 A comparison of bodipy compounds similar to **32a** (middle), found in the literature, reveals that λ_{Abs} for **32a** holds more in common with that of the more highly substituted bodipy (right).*

Compounds **32a** absorbed at the highest energy wavelength, 515 nm, which was expected due to the relative lack of complexity shown by the core of the compound. The absorbance value of **32a** is much more red-shifted when compared with the equivalent 1,3,5,7-tetramethyl bodipy variant, for which the absorption maximum is found at 503 nm. Indeed it was expected that the photophysical profile of **32a** should resemble a hybrid of the tetramethyl bodipy (Figure 34, left) and the 1,3,5,7-tetramethyl-2,4-diethyl (Figure 34, right) analogues. Both the absorption and emission maxima for **32a** demonstrated a much closer relationship to the analogous diethyl substituted bodipy core (λ_{Abs} – 517 nm).[36, 37]

When compared with **32a**, λ_{Abs} for **32c** was found to be red-shifted by around 10 nm. This bathochromic shift is thought to be due to the electronic effects bought about by the ortho-nitro group. This observation has parallels to the previous chapter wherein the inclusion of electron-withdrawing groups at the ortho position precipitated a bathochromic shift.

Brominated **34a** shows an absorption maximum at 526 nm which represents a significant red-shifted relative to that of **32a**. A further red shift is observed when comparing **34a** to **34b** again presumably due to the electron-withdrawing effect of the ortho-substituent.

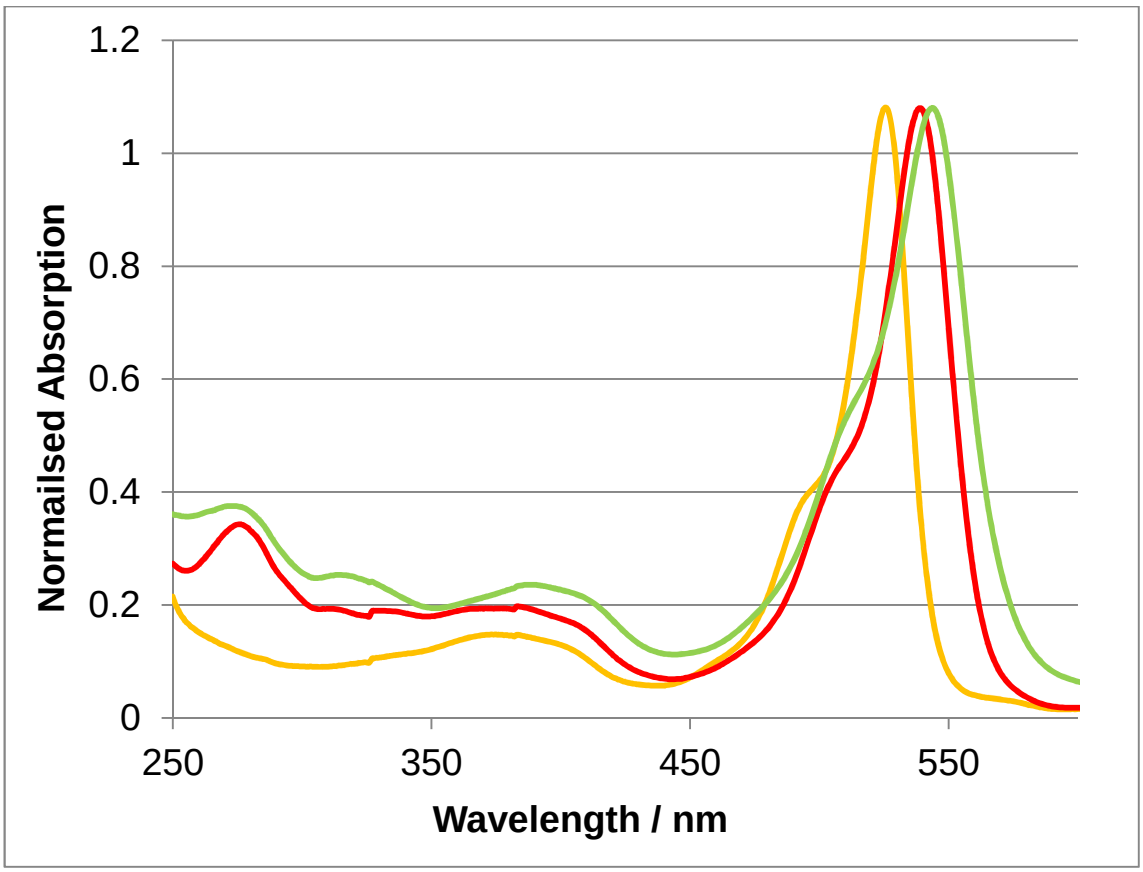

*Figure 35 An expanded absorption spectrum for the acrylate containing bodipy compounds **35a**, **35b** and **35d**.*

Absorption values for the acrylate containing bodipy products mostly demonstrated the desired red-shifted absorption spectra, with the notable exception of **35a** where the absorption maximum was found at 526 nm – representing no change from the brominated precursor. This result came as a surprise compared with the results for the methoxy variant **35d** (where there is a bathochroic shift of around 11 nm) as there is little or no change in the absorption maximum despite the inclusion of an acrylate group thereby extending the conjugation significantly.

There is also evidence of the acrylate group in the absorption spectra of **35b** and **35d**, with a peak observable at around 270 nm, which is typical of this group.[38]

4.3.1.a Molar absorption coefficient

Values for the molar absorption coefficient for all compounds are similar to comparable literature examples.[39] Throughout the series the methyl containing compounds are shown to have a considerably larger molar absorption

coefficient than the other equivalent compounds. With a value nearing 100,000 M^{-1} cm^{-1}, for the brominated compound **34a**, compounds **34b** and **34d** are only about 60% of the value.

While there are larger increases in the molar absorption coefficient for both **35b** and **35d**, relative to their brominated counterparts, the same could not be said about **35a** which varied little from **34a**.

4.3.2 Emission

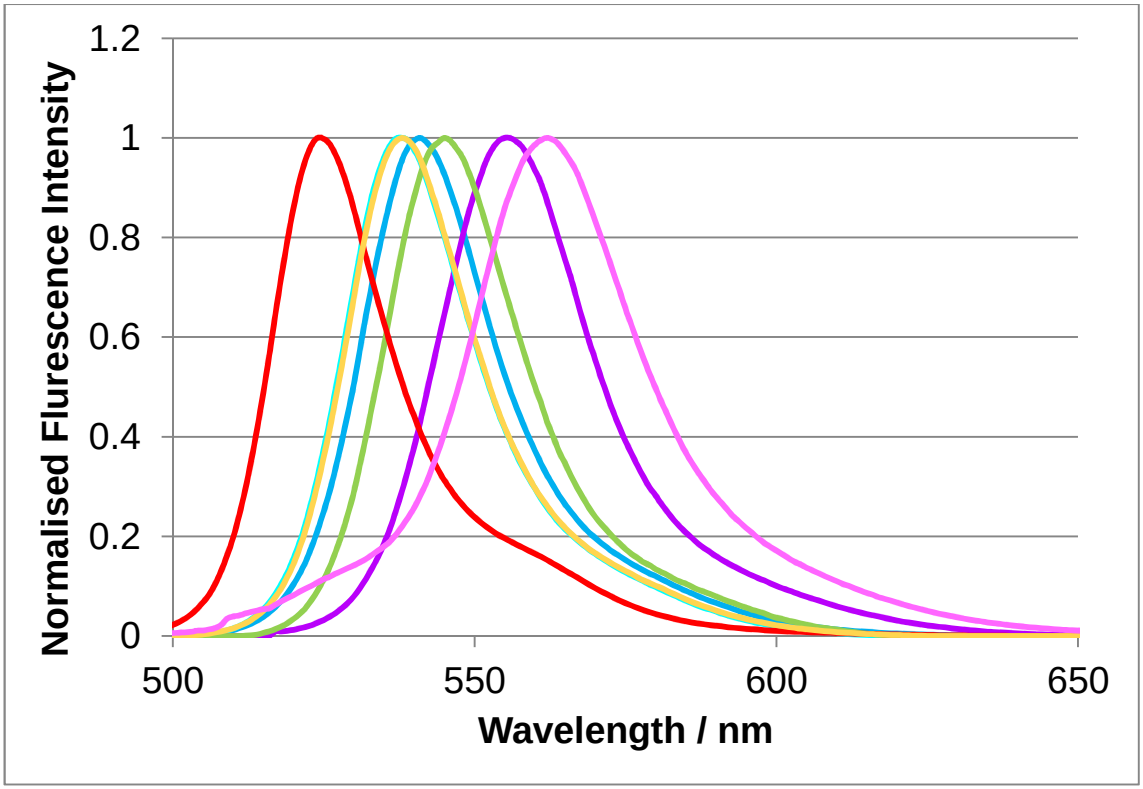

*Figure 36 Emission spectra for **32** – **35**; measured in DCM at ambient temperature. **32a** - Red, **34a** - Orange, **34b** - Green, **34d** - Blue, **35a** - Cyan, **35b** - Magnolia, and **35d** - Purple.*

Emission maxima for all compounds fell in a similar range to one another, between 10 and 17 nm from the absorption peak. All emission peaks were good mirror images for their equivalent absorption peak – if a little broader. The emission maximum for **35a** was hypsochromically shifted 3nm from the value of **34a** a similar observation to the absorbance value for **35a**. In stark contrast to the emission maxima for **35a** – **35b** and **35d** show the expected bathochromic shift (both around 16 nm) with **35b** giving the most extreme value of 562 nm.

4.3.2.a Stokes Shift

Stokes shifts were calculated for all compounds with all values seen to be in a acceptable range relative to the literature precedents.

There is a large transition of Stokes shift from **32a** to **34a** resulting from the bromination of the original compound. However the Heck-coupled product **35a** revealed a retraction in the SS back to the value seen for **32a**.

Compound **34a** has a the largest Stokes shift out of all of the brominated intermediates (493 cm^{-1} versus ca. 450 cm^{-1} for the other two compounds). Upon introducing the acrylate group the SS for **35a** plummets relative to its methoxy and fluorine counterparts (389 cm^{-1} vs 567 cm^{-1} for **35d**)

4.3.3 Fluorescence Quantum yield

Product **32a** gave a high quantum yield (Φ_{Flu} = 0.85) which can largely be attributed to the cessation of the rocking of the phenyl group as described in the previous chapter. This fluorescence is diminished greatly upon the inclusion of a bromine atom at the β-position at the core of the bodipy (compound **34a**).

As noted in the introduction of this chapter a drop in Φ_{Flu} upon the introduction of heavy atoms is not a surprise and falls into line with similar compounds.[40]

More efficient emission is not restored when the bromine atom is replaced with the acrylate group. **35a** shows a meagre increase in Φ_{Flu} rising from 0.19 to 0.23. However this is not the case for all permutations of **35** with **35b** showing a large increase in quantum yield growing from 0.14 to an impressive 0.59 upon the introduction of the acrylate moiety. Drawing largely on conclusions from the previous chapter: ortho-fluoro substituted phenyl bodipy compounds have a relatively large Φ_{Flu} – observations that might explain the difference in quantum yield when compared with the methyl and methoxy variants.

The likely reason for the low quantum yield of **35a** and **35d** is the flexibility of the acrylate group, which will flail at will likely bending the bodipy core and increasing the k_{NR}. A solution to the moderate amount of emission attained from the final systems would be to use a group that had less flexibility than that of the acrylate group. A possible alternative would be to use Sonogashira cross

coupling to introduce an aryl alkyne to the bodipy core thereby removing a large portion of the flexibility from the extended conjugation.[41]

4.3.4 Polarimetry- α_D^{20}

Compound	α_D^{20} (°)
35a[i]	+ 12.98
35a[ii]	- 12.98
35b[i]	- 32.50
35b[ii]	+ 32.50

*Table 4 Polarimetry results for compound **35a** and **35b**, both of which demonstrate the rotation of light. λ - 589 nm (Sodium Lamp); l - 0.5 dm; solvent - $CHCl_3$. [i] refers to the first compound collected from the chiral HPLC purification while [ii] refers to the second peak to be collected.*

The polarimetry results for compounds **35a** and **35b** both showed a complementary rotational value for the two enantiomers of the compounds. The degree of rotation increased by around 20° upon changing the ortho substituent from methyl to fluorine.

4.4 Conclusion

To conclude, the goal of producing the first example of an axially chiral bodipy fluorophore was a complete success. With the synthesis of more basic chiral bodipy compounds possible in similar yields to those seen for standard literature preparations of bodipy. These chiral systems are extremely flexible at both the bodipy core as well as the meso-aryl position. The chiral bodipy molcules which were brominated could successfully undergo Heck cross coupling reactions, though the optimisation of this process should be something of a priority if more complicated variants are considered.

Unfortunately the enantiomers of compound **35** failed to show a large enough difference in their CD spectra to make polarised fluorescence testing worthwhile. The lack of optical activity in this case is thought to be due to be due to the size of one or both of the ortho substituent or ethyl acrylate group. It is thought that by increasing the size of these substituents enhanced CD spectra should be observed.

As well as the creation of axially chiral systems a completely new approach towards the synthesis of asymmetric bodipy cores was also demonstrated. The

synthesis is robust and flexible and does not impact upon the total yield[††] for the synthesis of the final bodipy product.

4.4.1 Future work

Work in the field of axially chiral bodipy compounds is in its infancy and there are several possible directions that could be explored. These include: the synthesis of second generation axially chiral bodipy compounds, exploration of possible axial chirality being derived from the β-positions of the bodipy core, new routes towards diasteroemeric porphyrin compounds, the creation of functional chiral probes, or more generally the generation of new routes to resolve the enanitomeric bodipy compounds.

4.4.1.a Further Development of Axially Chiral Bodipy Dyes

There are two aspects of axially chiral bodipy dyes that should be addressed following the work outlined in this chapter: firstly efforts should be made to increase the overall quantum yields for the system, and secondly the chirality of the final compound should be enhanced.

The low quantum yields seen for the acrylate containing products (Φ_{Flu} ~ 0.20) was lower than originally expected. As a result it might be prudent to swap the acrylate group for a different group with less flexibility. The use of Sonogashira coupling reactions in order to introduce a less flexible aryl-alkyne moiety - as suggested in 4.3.3.

Secondly further investigations should be undertaken with the aim of enhancing the chiral response of the final two enantiomers with respects to both chiral media (which is as yet untouched) and CD / CPL measurements.

4.4.1.b Making Use of the Asymmetric Bodipy Core to Create Functional Systems

In the synthesis described in this chapter has seen a bromine containing pyrrole introduced to a bodipy followed by a cross coupling reaction to attach further functionality. This particular route satisfies aims of synthesising an axially chiral bodipy. Yet there is potential to expand upon the method in order to create more complex bodipy systems by introducing further functionality at the

[††] (NB – In most cases with the exception of compounds containing a nitro group)

opposite end of the bodipy core to where the initial expansion of conjugation occurred.

By introducing bromine to the a free β-position on the bodipy core of **35** it would be possible for the system to undergo a second cross coupling reaction thereby allowing a complex asymmetric bodipy core to be constructed.

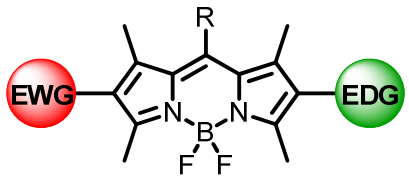

Figure 37 The ability to introduce two different groups to a bodipy core, thereby creating an asymmetric bodioy core, could lead to the possibility of new functional bodipy compounds. Above is a possible solvatochromic probe, where EWG and EDG = electron withdrawing group and electron donating group respectively.

Asymmetric bodipy cores could see the creation of new forms of solvatochromic probes, though the synthesis of such probes would rely on being able to separately introduce electron withdrawing and donating groups. Indeed if the meso group were to contain an ortho-substituted phenyl moiety this could open up a new niche for bodipy chemistry – that of chiral solvatochromics.[42]

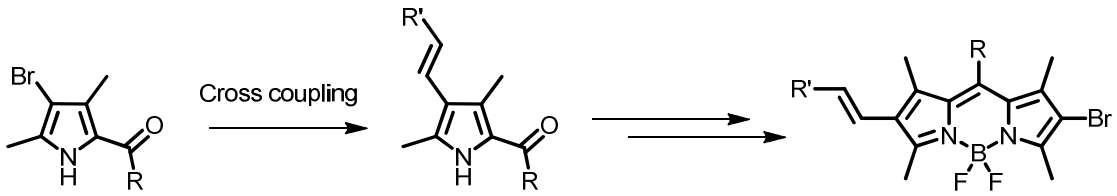

Scheme 13 Pre-functionalisation of the brominated pyrrole allowing for the formation of a 3-bromo bodipy which may be further functionalised to give a di-substituted bodipy core.

One further aspect of asymmetric bodipy core construction that could be further investigated is the pre-functionalization of one or both of the pyrroles that are to be introduced. By subjecting the pyrrole to a cross-coupling reaction prior to synthesising the bodipy it would facilitate the creation of complex unsymmetrical bodipy cores in higher yields. In turn it would then also be possible to introduce a second bromine to the intermediate bodipy, much in the same way as that described in this chapter. Then this brominated bodipy could be further expanded allowing for complexity at both pyrrole groups on the bodipy core.

4.4.1.c Resolving both R and S Isomers Without using Chiral Chromatography

One major problem with chiral organic compounds is the resolution of large quantities of the two enanitomers. Where standard chiral HPLC will successfully purify on the 10 mg scale (depending on column size), the technique is slow, expensive, and does not purify much at a time.

A more old-fashioned approach towards chiral resolution is to somehow create diastereomers of the enantiomers. The diastereomers can be purified via standard column chromatography, hence on a scale approaching the tens of grams. In order to create diastereomers from the axially chiral bodipy systems it is possible to introduce a second chiral group onto the boron centre (Scheme 14).[24] Indeed it might also be possible to chelate a pre-functionalised boron centre, thereby avoiding a loss in overall yield.[43]

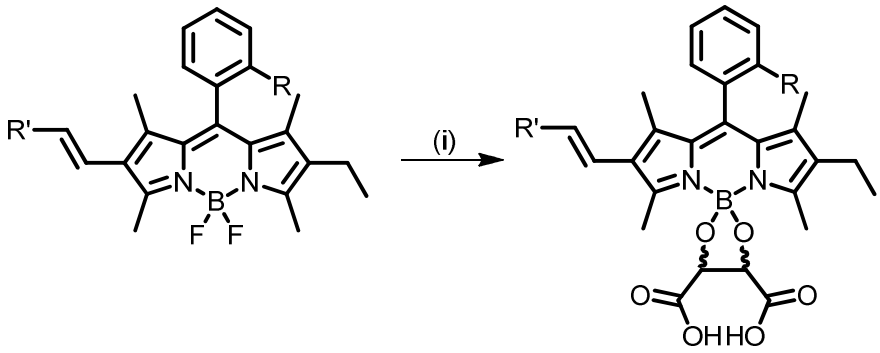

Scheme 14 The complexation of a bodipy boron with a tartaric acid to form a diastereomeric complex. (i) $AlCl_3$, DCM; tartatic acid.

Once the chiral chelating group has been attached to the boron centre should then be possible to resolve the two diastereomers. The problematic step following the resolution would be the removal of the boron chelated chiral ligand. There is currently no literature precedent for the cleavage of B-OR bonds within bodipy systems. This is likely due to interest in bodipy compounds revolving around the insertion of boron-chelating groups in place of fluorine, and not the other way around. Though there are few literature examples of B-O bond cleavage there are some suggestions that methyllithium / trimethylaluminium might work, though this would result in the methylation of the boron centre.[44]

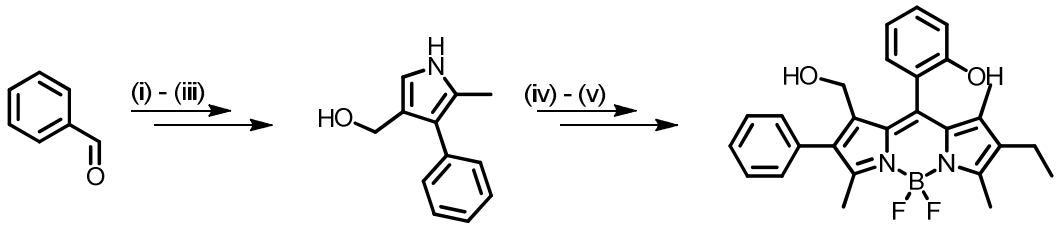

Scheme 15 Using aromatic aldehydes to form pyrroles which themselves can be made into a bodipy compound capable of chelation to metal ions. (i) $EtNO_2$, $AcONH_4$, Δ; (ii) ^tBuOH, DBU, THF, ethyl cyanoacetate, Δ; (iii) $NaBH_4$, MeOH; (iv) 2,4-dimethyl-3-ethylpyrrole, TFA, DCM; $BF_3.OEt_2$, $^iPr_2NEt$; (v) BBr_3.

Another possible route is to synthesise a bodipy-ligand which might interact with a labile metal such as zinc(II). The synthesis outlined in Scheme 15 would provide just such a molecule. The benefit of having a zinc ion bound ligand is that it is relative simple to remove from complexes meaning that, upon resolution of separate diastereomers, the individual enantiomers can also be isolated.[‡‡]

4.4.1.d Exploring the Concept of Axial Chirality using the β-Position of the Bodipy Core

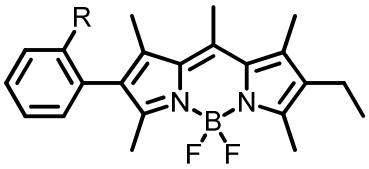

Figure 38 Expansion off the 3 position with a ortho-substituted aryl group; where R is of a bulk that allows for restricted rotation around the C2-aryl bond on the bodipy core.

Theoretically axial chirality can also be derived via the substitution off the β-position of the bodipy core. Provided a phenyl group with an ortho substituent large enough to restrict rotation were in place then axial chirality could easily be arrived at. Indeed attaining axial chirality this is perhaps more simple than the route outlined in this chapter as the only requirement is large enough sterics at the ortho-position of the 3-phenyl group.

[‡‡] The system outlined in Scheme 15 may also act as an on / off chiral zinc sensor

4.4.1.e Creating Diastereomeric Porphyrin Compounds Based on the Synthesis of Axially Chiral Bodipy Molecules

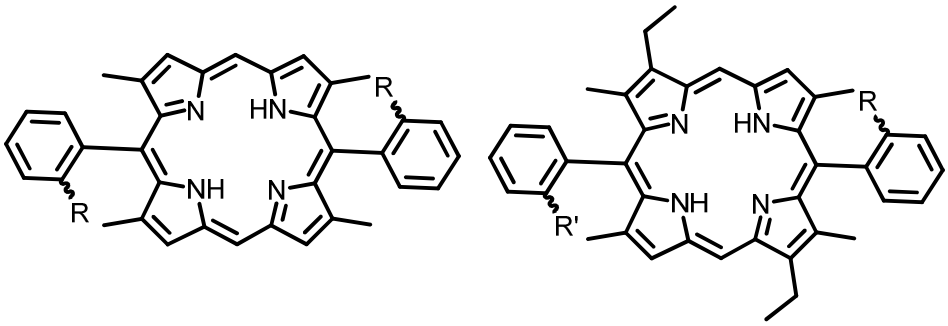

Figure 39 Porphyrin compounds containing two ortho-substituted aryl groups creating rotamers (left, where R ≠ H), diastereomerics (right, where R,R' ≠ H) and chiral compounds (right, where R ≠ H).

By combining the synthetic approach towards asymmetric bodipy compounds with porphyrin syntheses it would also allow for the creation of rotameric, chiral and diastereomeric porphyrin compounds. There are not many literature examples of extrinsic rotameric, diastereotopic or axially chiral within porphyrin compounds. For instance most examples of axially chirality in porphyrin systems derive from bis-porphyrin structures where two different porphyrin compounds are covalently bound.[45, 46]

4.5 References

1. R. Marchelli, A. Dossena and G. Palla, *Trends in Food Science & Technology*, 1996, **7**, 113-119.
2. S. Stinson, *Chem. Eng. News*, 1998, **76**, 83-103.
3. H. Tsukube and S. Shinoda, *Chem. Rev.*, 2002, **102**, 2389-2404.
4. J.-C. G. Bunzli and C. Piguet, *Chem. Soc. Rev.*, 2005, **34**, 1048-1077.
5. F. Miao, J. Zhou, D. Tian and H. Li, *Org. Lett.*, 2012, **14**, 3572-3575.
6. J. Jiao, X. Liu, X. Mao, J. Li, Y. Cheng and C. Zhu, *New J. Chem.*, 2013, **37**, 317-322.
7. G. Beer, K. Rurack and J. Daub, *Chem. Commun.*, 2001, 1138-1139.
8. C. P. Montgomery, B. S. Murray, E. J. New, R. Pal and D. Parker, *Acc. Chem. Res.*, 2009, **42**, 925-937.
9. O. P. Lam, C. Anthon and K. Meyer, *Dalton Trans.*, 2009, 9677-9691.
10. M. Seitz, E. G. Moore, A. J. Ingram, G. Muller and K. N. Raymond, *J. Am. Chem. Soc.*, 2007, **129**, 15468-15470.
11. J. W. Walton, L. D. Bari, D. Parker, G. Pescitelli, H. Puschmann and D. S. Yufit, *Chem. Commun.*, 2011, **47**, 12289-12291.
12. J. I. Bruce, R. S. Dickins, L. J. Govenlock, T. Gunnlaugsson, S. Lopinski, M. P. Lowe, D. Parker, R. D. Peacock, J. J. B. Perry, S. Aime and M. Botta, *J. Am. Chem. Soc.*, 2000, **122**, 9674-9684.
13. G. Bozoklu, C. Gateau, D. Imbert, J. Pécaut, K. Robeyns, Y. Filinchuk, F. Memon, G. Muller and M. Mazzanti, *J. Am. Chem. Soc.*, 2012, **134**, 8372-8375.
14. H. Kim, A. Burghart, M. B. Welch, J. Reibenspies and K. Burgess, *Chem. Commun.*, 1999, 1889-1890.
15. A. Loudet, R. Bandichhor, K. Burgess, A. Palma, S. O. McDonnell, M. J. Hall and D. F. O'Shea, *Org. Lett.*, 2008, **10**, 4771-4774.
16. C. Ikeda, T. Maruyama and T. Nabeshima, *Tet. Lett.*, 2009, **50**, 3349-3351.
17. A. Gossauer, F. Nydegger, T. Kiss, R. Sleziak and H. Stoeckli-Evans, *J. Am. Chem. Soc.*, 2004, **126**, 1772-1780.
18. M. Shah, K. Thangaraj, M.-L. Soong, L. T. Wolford, J. H. Boyer, I. R. Politzer and T. G. Pavlopoulos, *Heteroat. Chem.*, 1990, **1**, 389-399.

19. G. Duvanel, N. Banerji and E. Vauthey, *J. Phys. Chem. A*, 2007, **111**, 5361-5369.
20. J.-H. Ye, G. Wang, C. Huang, Z. Hu, W. Zhang and Y. Zhang, *Synthesis*, 2012, **44**, 104-110.
21. R. H. Hofeldt, R. Sahai and S. H. Lin, *J. Chem. Phys.*, 1970, **53**, 4512-4518.
22. A. Loudet and K. Burgess, *Chem. Rev.*, 2007, **107**, 4891-4932.
23. S. Ma and X. Lu, *J. Org. Chem.*, 1993, **5**, 1245-1251.
24. C. Tahtaoui, C. Thomas, F. Rohmer, P. Klotz, G. Duportail, Y. Mély, D. Bonnet and M. Hibert, *J. Org. Chem.*, 2006, **72**, 269-272.
25. B. Brizet, A. Eggenspiller, C. P. Gros, J.-M. Barbe, C. Goze, F. Denat and P. D. Harvey, *J. Org. Chem.*, 2012, **77**, 3646-3650.
26. N.-C. Wang, K.-E. Teo and H. J. Anderson, *Can. J. Chem.*, 1977, **55**, 4112-4116.
27. J. T. Kuethe and D. L. Comins, *J. Org. Chem.*, 2004, **69**, 2863-2866.
28. T. Yogo, Y. Urano, Y. Ishitsuka, F. Maniwa and T. Nagano, *J. Am.Chem. Soc.*, 2005, **127**, 12162-12163.
29. G. C. Fu, *Acc. Chem. Res.*, 2008, **41**, 1555-1564.
30. M. R. Netherton and G. C. Fu, *Org. Lett.*, 2001, **3**, 4295-4298.
31. A. F. Littke and G. C. Fu, *J. Am. Chem. Soc.,* 2001, **123**, 6989-7000.
32. M. A. H. Alamiry, A. C. Benniston, J. Hagon, T. P. L. Winstanley, H. Lemmetyinenb and N. V. Tkachenkob, *RSC Adv.*, 2012, **2**, 4944-4950.
33. P. Auffinger, F. A. Hays, E. Westhof and P. S. Ho, *Proceedings of the National Academy of Sciences of the United States of America*, 2004, **101**, 16789-16794.
34. B. Szczesna and Z. Urbanczyk-Lipkowska, *New J. Chem.*, 2002, **26**, 243-249.
35. *Chem. Des. Autom. News*, 1993, **8**.
36. H. Sunahara, Y. Urano, H. Kojima and T. Nagano, *J. Am. Chem. Soc.*, 2007, **129**, 5597-5604.
37. A. Cui, X. Peng, J. Fan, X. Chen, Y. Wu and B. Guo, *Photochem. Photobiol.*, 2007, **186**, 85-92.
38. D. H. Williams and I. Flemming, *Spectrosc. Methods Org. Chem.*, 5 edn., McGraw-Hill Co., London.
39. A. Loudet and K. Burgess, *Chem. Rev.*, 2007, **107**, 4891-4932.

40. J. Wang , Y. Hou, W. Lei, Q. Zhou, C. Li, B. Zhang and X. Wang, *Chem. Phys. Chem.*, 2012, **13**, 2739-2747.
41. T. Rohand, W. Qin, N. Boens and W. Dehaen, *Eur. J. Org. Chem.*, 2006, **2006**, 4658-4663.
42. P. Milosevic and S. Hecht, *Org. Lett.*, 2005, **7**, 5023-5026.
43. H. L. Kee, C. Kirmaier, L. Yu, P. Thamyongkit, W. J. Youngblood, M. E. Calder, L. Ramos, B. C. Noll, D. F. Bocian, W. R. Scheidt, R. R. Birge, J. S. Lindsey and D. Holten, *J. Phys. Chem. B*, 2005, **109**, 20433-20443.
44. A. Maderna, H. Pritzkow and W. Siebert, *Angew. Chem. Int. Ed. in English*, 1996, **35**, 1501-1503.
45. G. Bringmann, D. C. G. Götz, T. A. M. Gulder, T. H. Gehrke, T. Bruhn, T. Kupfer, K. Radacki, H. Braunschweig, A. Heckmann and C. Lambert, *J. Am. Chem. Soc.*, 2008, **130**, 17812-17825.
46. G. Bringmann, S. Rüdenauer, D. C. G. Götz, T. A. M. Gulder and M. Reichert, *Org. Lett.*, 2006, **8**, 4743-4746.

Chapter 5 Experimental Procedures

5.1. Instrumental

5.1.1. Nuclear Magnetic Resonance Spectroscopy

^{1}H, ^{13}C, ^{11}B and ^{19}F NMR spectra were recorded with either a Bruker AVANCE 300MHz, JEOL ECS-400 MHz or a JEOL Lambda 500MHz spectrometer. Chemical shifts for ^{1}H and ^{13}C NMR spectra are referenced relative to the residual protiated solvent. The ^{11}B NMR chemical shift is referenced to $BF_3.Et_2O$ (δ = 0ppm) and the ^{19}F NMR chemical shift is given relative to $CFCl_3$ (δ = 0 ppm). Simulated ^{19}F NMR spectra were created using the program NUMARIT.*

5.1.2. Melting Point

The melting points of solid compounds were taken using a Stuart melting point apparatus (SMP3, AC input 110 V). Samples were ground using a pestle and mortar until a fine powder was formed. This powder was then places into capillary tubes and a ranging melting point was performed, followed by a second more accurate reading. The limit of the melting point apparatus was at around 250 ^{o}C, a point which several samples passed - denoted as >250 ^{o}C.

5.1.3. Mass Spectrometry

Mass spectral analysis was largely performed with a UNICAM 701 Series Emission Spectrometer. Samples were dissolved in methanol and made up to an appropriate concentration via volumetric dilution with further quantities of methanol. The sample was directly injected onto the column, which was heated to 80 ^{o}C and the MS run thereafter.

5.1.4. Absorption spectra

Absorption spectra were recorded on a Hitachi U3310 UV/Visible dual-beam spectrophotometer. A baseline was recorded prior to making the measurement using spectroscopic grade solvent in a cuvette of 1 cm pathlength placed in each beam. Spectra were recorded with a solvent cuvette in the reference beam.

* A.R. Quirt, J.S. Martin and K.M. Worvill, NUMARIT, EPSRC

5.1.5. Emission spectra

Emission spectra were recorded in quartz cuvettes using a Hitachi F4500 spectrofluorimeter. Solutions used were optically dilute, with an absorbance at the excitation wavelength of <0.1 nm, and were purged with nitrogen. Spectra were corrected by reference to a standard lamp.

5.1.6. Fluorescence lifetimes

The fluorescence lifetime measurements were carried out using time-correlated single-photon-counting instrument (PicoHarp- 300, PicoQuant GmbH). The samples were excited at 483 nm by a pulsed diode laser (LDH-P-C-485, PicoQuant GmbH). The emission was detected by a microchannel plate photomultiplier tube (R3809U-50, Hamamatsu) coupled with a monochromator. The time resolution of the system was 80 ps (FWHM). This work was performed by Professors Helge Lemmetyinen and Nikolai V. Tkachenko.

5.1.7. Pressure Dependant Emission Spectra

High pressure studies were carried out using a custom built rig supplied by Stansted Fluid Power Ltd and used in conjunction with a high-pressure sample holder equipped with optically transparent windows. Fluorescence measurements were made using a low-power laser diode (l_{max} = 406 nm) to excite the sample, and collecting emission with a focussing lens connected to a fibre optic cable that was fed to a red-sensitive photomultiplier tube by way of a high-radiance monochromator and amplifier. Scattered excitation light was minimized with optical filters. In a typical run, the sample, dissolved in MChx, was pressurized up to ca. 550 MPa. Spectra were measured at regular intervals as the pressure exerted on the sample was released in a controlled manner. Fluorescence background spectra were recorded using solvent only and the final emission spectrum corrected as needed. Several runs were recorded for each sample. In other runs, the spectra were recorded as the pressure was increased progressively. In all cases, the temperature was maintained at 22 ^{o}C.

5.1.8. Infrared Spectrometry

A Varian 800 FT-IR spectrometer system produces spectra between 4000 cm^{-1} and 400 cm^{-1} from solid, liquid or oil samples using a Pike Technologies diamond crystal plate ATR unit.

5.1.9. Cyclic Voltammetry

Cyclic voltammetry experiments were performed using a fully automated HCH Instruments Electrochemical Analyzer and with a three-electrode set-up consisting of a glassy carbon working electrode, a platinum wire counter electrode and a silver wire reference electrode. Ferrocene was used as an internal standard. All studies were performed in deoxygenated solvent containing tetra-*N*-butyl ammonium tetrafluoroborate (TBATFB) (0.2 M) as background electrolyte. The solute concentrations were typically 0.5 mM. Solvents were distilled immediately before making the measurement and were purged thoroughly with dried N_2.

5.1.10. Crystal Structure Determination

X-Ray crystal structure analysis was performed and solved solely by the crystallography department using an Agilent dual-source single-crystal diffractometer with a CCD detector. The resulting crystal structure data was analysed using Mercury 3.0 (Build RC5).

5.2. Chemicals Used

Chemical Name	Supplier	Purity
2,3,4,5,6-pentafluorobenzaldehyde	Sigma-Aldrich	98%
2,3-dichloro-5,6-dicyano-*p*-benzoquinone	Sigma-Aldrich	98%
2,4-dimethyl-3-ethylpyrrole	Sigma-Aldrich	97%
2,4-dimethylpyrrole	Sigma-Aldrich	97%
2,4-ditertbutylphenol	Sigma-Aldrich	99%
2,6-difluorobenzaldehyde	Sigma-Aldrich	98%
2-bromophenol	Sigma-Aldrich	99%
2-ethylphenol	Sigma-Aldrich	99%
2-fluorobenzaldehyde	Sigma-Aldrich	98%
2-iodophenol	Sigma-Aldrich	99%
2-isopropylphenol	Sigma-Aldrich	99%
2-napthol	Sigma-Aldrich	99%
2-phenylphenol	Sigma-Aldrich	99%
2-sec-butylphenol	Sigma-Aldrich	99%
2-tertbutyl-4-methylphenol	Sigma-Aldrich	99%
2-tertbutylphenol	Sigma-Aldrich	99%
3,4,5-trifluorobenzoyl chloride	Sigma-Aldrich	97%
3-fluorobenzaldehyde	Sigma-Aldrich	98%
4-bromophenol	Sigma-Aldrich	99%
4-fluorobenzaldehyde	Sigma-Aldrich	98%
4-hydroxybenzaldehyde	Sigma-Aldrich	98%
4-tertbutyl-2-methylphenol	Sigma-Aldrich	99%
4-tertbutylphenol	Sigma-Aldrich	99%
acetic acid	Sigma-Aldrich	>99%
ammonium chloride	Sigma-Aldrich	99.998%
aniline	Sigma-Aldrich	99%
benzaldehyde	Sigma-Aldrich	>99.5%
benzoyl chloride	Sigma-Aldrich	99%
boron trifluoride diethyl etherate	Sigma-Aldrich	Purified by redistillation
bromine	Sigma-Aldrich	99.995%
butyllithium solution 2.5M in hexanes	Sigma-Aldrich	-
chloroform-d_3	Sigma-Aldrich	99.96 atom %
diethyl-2,5-dihydroxyterephthalate	Sigma-Aldrich	99%
dimethyl sulfoxide-d_6	Cambridge Isotope Laboratories	D, 99.9%
ethyl acrylate	Sigma-Aldrich	>99.5%
ethyl Magnesium Bromide 3.0M in diethylether	Sigma-Aldrich	-
hydrochloric acid	Sigma-Aldrich	37%
magnesium sulphate	Sigma-Aldrich	99%
m-cresol	Sigma-Aldrich	99%
methanol-d_4	Cambridge Isotope Laboratories	D, 99.8%

N,N-diisopropylethylamine	Sigma-Aldrich	Purified by redistillation
nitric Acid	Sigma-Aldrich	70%
o-fluorobenzoylchloride	Sigma-Aldrich	99%
o-nitrobenzoylchloride	Fluka	>97%
o-toluoylchloride	Sigma-Aldrich	99%
palladium acetate	Sigma-Aldrich	>99.9%
phenol	Sigma-Aldrich	>99%
potassium carbonate	Sigma-Aldrich	99.99%
potassium hydroxide	Sigma-Aldrich	>85%
pyridine	Sigma-Aldrich	99.8%
pyrrole	Sigma-Aldrich	98%
sodium bicarbonate	Sigma-Aldrich	>99.7%
sodium borohydride	Sigma-Aldrich	99.99%
sodium carbonate	Sigma-Aldrich	99.995%
sodium hydroxide	Sigma-Aldrich	pellets, 99.998%
sodium sulphate	Sigma-Aldrich	>99.0%
sulfuric acid	Sigma-Aldrich	99.999%
tert-butyllithium solution 1.7M in pentane	Sigma-Aldrich	-
tetrahydrofuran-d_8	Cambridge Isotope Laboratories	D, 99.95%
Tetrakis(triphenylphosphine)	Sigma-Aldrich	99%
triethylamine	Sigma-Aldrich	>99.0%
trifluoroacetic acid	Sigma-Aldrich	99%
triphenylphosphine	Sigma-Aldrich	99%
zinc powder	Fluka	>99.99%

Table 1 A list of all chemicals used during the subsequent procedures, including details of the supplier and purity

5.3. Solvents Used

All solvents used in preparative work are listed in *Table 2*, along with the method of purification.

Solvent	Purification Method
acetone	Distilled from 4Å molecular sieves under nitrogen
dichloroethane	Distilled from calcium hydride under nitrogen
dichloromethane	Distilled from calcium hydride under nitrogen
diethyl ether	Distilled from sodium/benzophenone under nitrogen
ethanol	Used as received from Sigma-Aldrich (anhydrous, sure seal)
ethyl acetate	Used as received from Riedel-de-Haën
hexane	Used as received from Riedel-de-Haën
methanol	Used as received from Sigma-Aldrich (anhydrous, sure seal)
N,N-Dimethylformamide	Used as received from Sigma-Aldrich (anhydrous, sure seal)
petroleum ether	Used as received from Riedel-de-Haën
tetrahydrofuran	Distilled from sodium/benzophenone under nitrogen
toluene	Distilled from sodium under nitrogen

Table 2 Solvents used in preparative work and their respective preparation methods.

5.3.1. Synthetic protocol

The experimental protocols for all compounds synthesized during this research programme now follow. All synthetic experiments were carried out in an inert atmosphere of N_2 unless otherwise stated. When the target compound was known in the literature, ^{1}H NMR spectra and melting points were recorded and compared. When unknown compounds were synthesized, ^{1}H NMR and ^{13}C

NMR spectra, mass spectra, and melting points were recorded. Where appropriate and possible, this was supported with IR spectra, ^{11}B NMR and ^{19}F NMR spectra and X-ray crystallography.

5.4. Synthetic Procedures

5.4.1. Chapter 2

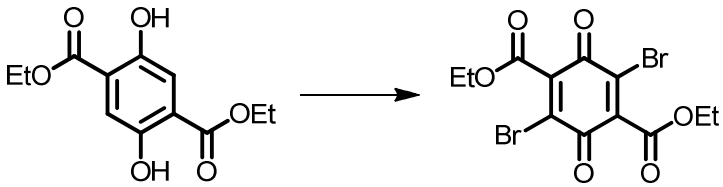

1 **2**

Diethyl-2,5-dihydroxyterephthalate (**1**) (25.0 g, 0.1 mol) was placed on a petri dish which in turn was placed in a vacuum desiccator along with a sample vial containing liquid bromine (10 mL). The desiccator was closed, evacuated and the material left under a bromine atmosphere for 4 days. The reaction progress was monitored via ^{1}H NMR spectroscopy daily until there was no sign of starting material. Once complete the product was recrystallised from ethanol and HNO_3 (5 mL). The HNO_3 was used to oxidise any material that had formed the dibromohydroquinone **2a**. The product, **2**, was a yellow needle-like crystalline material produced in excellent yield (39.8 g, 99%, 0.1 mol).

^{1}H NMR ($CDCl_3$, 300 MHz): δ = 4.47 (q, *J* = 7.2 Hz, 4H), 1.41 (t, *J* = 7.2 Hz, 6H)

^{13}C{H} NMR (75 MHz, $CDCl_3$): δ = 173.6, 161.3, 140.9, 133.5, 63.5, 14.1.

MP = 226 ^{o}C

IR – 2991, 1731, 1677, 1284 cm^{-1}

MS – calc. for $C_{12}H_{10}Br_2O_6$ = 410 found. 410 (M+)

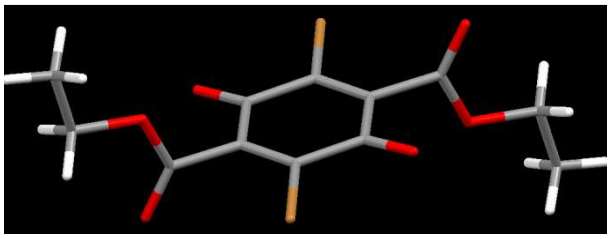

2a: ^{1}H NMR (CDCl3, 300 MHz): δ 9.0 (s, 2H), 4.51 (td, *J* = 7.2, 1.9 Hz, 4H), 1.47 (td, *J* = 7.1, 2.0 Hz, 6H)

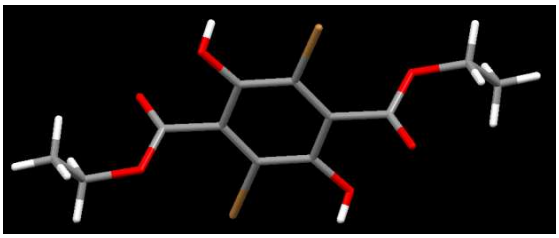

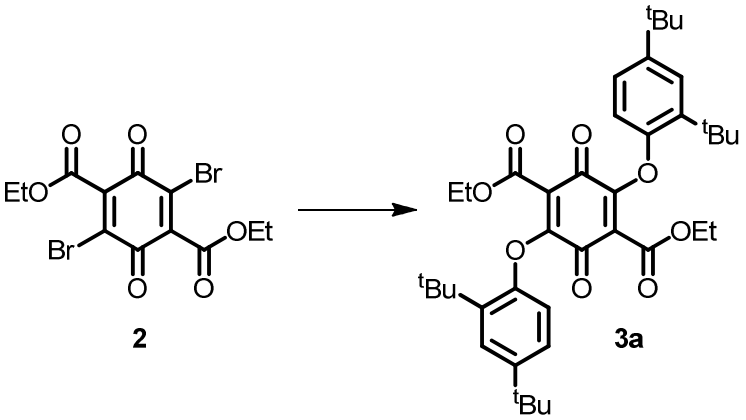

Compound **2** (1.5 g, 3.7 mmol), 2,4-ditertbutylphenol (1.5 g, 7.2 mmol), pyridine (1.5 mL, 18.5 mmol) and acetone (15 mL) was charged to a 100 mL round bottomed flask and refluxed for 10 minutes. The clear/ yellow suspension quickly turned dark red/ brown upon addition of pyridine and application of heat. The reaction mixture was diluted with water (100 mL) causing a precipitate to form*. The precipitate was filtered off and washed with water, air dried and dissolved in DCM (100 mL). The organic mixture was dried over $MgSO_4$, which was filtered and the cake washed with excess DCM. The combined organic solvents were removed under reduced pressure to give a dark red solid, **3a** (1.6 g, 2.4 mmol, 66 %).

* On occasion an oil would form in place of the expected solid. In this case the compound was purified via column chromatography (silica gel, DCM : Petrol, 1:1).

^{1}H NMR ($CDCl_3$, 300 MHz): δ = 7.31 (d, *J* = 2.5 Hz, 2H), 7.05 (dd, *J* = 8.4, 2.5 Hz, 2H), 6.63 (d, *J* = 8.4 Hz, 2H), 3.89 (q, *J* = 7.1 Hz, 4H), 1.33 (s, 18H), 1.22 (s, 18H), 1.07 (t, *J* = 7.1 Hz, 6H).

^{13}C{H} NMR (75 MHz, $CDCl_3$): δ = 178.1, 161.3, 151.7, 151.1, 147.6, 138.4, 124.7, 123.7, 117.7, 115.4, 62.4, 35.1, 34.7, 31.5, 30.1, 13.9.

MP = >250^{o}C

MS – calc. for $C_{40}H_{52}O_8$ = 660.8 found. 661 (M+)

IR – 2963, 1731, 1674, 1175 cm^{-1}.

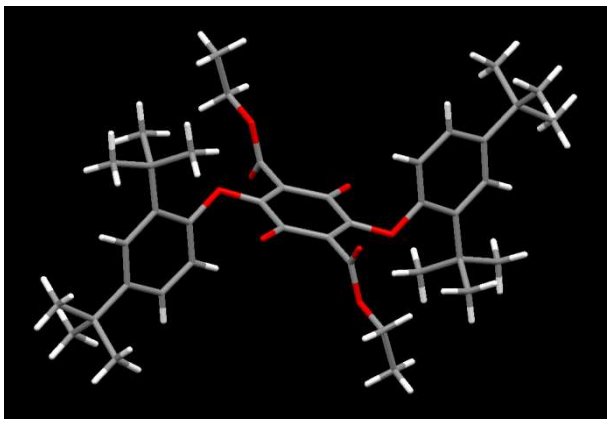

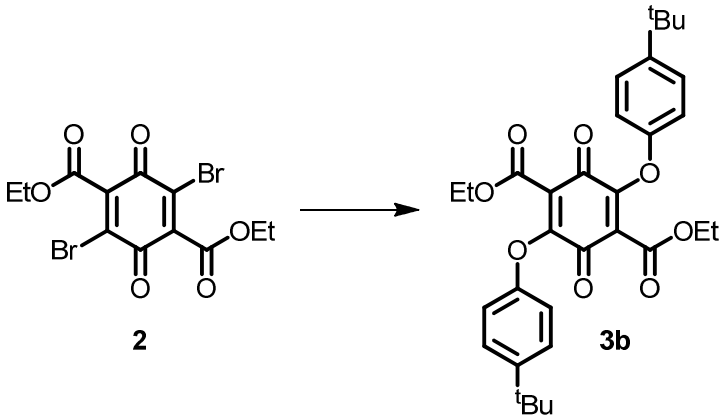

2 **3b**

Compound **2** (2 g, 4.9 mmol), 4-tertbutylphenol (1.5 g, 18.0 mmol), pyridine (2 mL, 24.6 mmol) and acetone (15 mL) was charged to a 100 mL round bottomed flask and refluxed for 10 minutes. The clear/ yellow suspension quickly turned dark red/ brown upon addition of pyridine and application of heat. The reaction mixture was diluted with water (100 mL) causing a precipitate to form*. The precipitate was filtered off and washed with water, air dried and dissolved in DCM (100 mL). The organic mixture was dried over $MgSO_4$, which was filtered and the cake washed with excess DCM. The combined organic solvents were removed under reduced pressure to give a dark red solid this solid was purified via a recrystallization from ethanol leaving pure **3b** (2.6 g, 4.8 mmol, 99 %).

* On occasion an oil would form in place of the expected solid. In this case the compound was purified via column chromatography (silica gel, DCM : Petrol, 1:1).

^{1}H NMR ($CDCl_3$, 300 MHz): δ = 7.28 – 7.17 (m, 4H), 7.00 – 6.78 (m, 4H), 4.11 (q, *J* = 7.1 Hz, 4H), 1.24 (s, 18H), 1.00 (t, *J* = 7.1 Hz, 6H).

MP = >250^{o}C

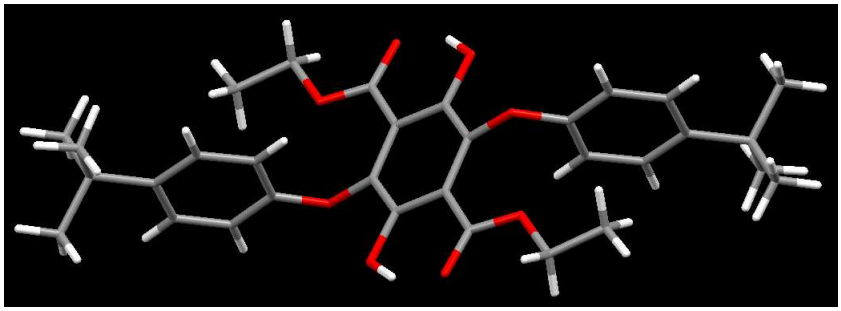

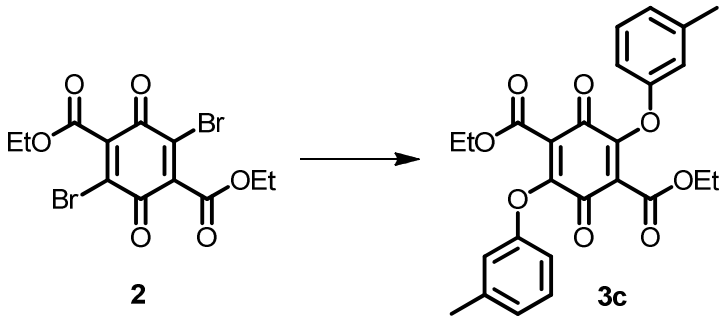

Compound **2** (1.5 g, 3.7 mmol), m-cresol (1.5 g, 13.9 mmol), pyridine (1.5 mL, 18.5 mmol) and acetone (15 mL) was charged to a 100 mL round bottomed flask and refluxed for 10 minutes. The clear/ yellow suspension quickly turned dark red/ brown upon addition of pyridine and application of heat. The reaction mixture was diluted with water (100 mL) causing a precipitate to form*. The precipitate was filtered off and washed with water, air dried and dissolved in DCM (100 mL). The organic mixture was dried over $MgSO_4$, which was filtered and the cake washed with excess DCM. The combined organic solvents were removed under reduced pressure to give a dark red solid, **3c** (1.3 g, 2.4 mmol, 67 %).

* On occasion an oil would form in place of the expected solid. In this case the compound was purified via column chromatography (silica gel, DCM : Petrol, 1:1).

^{1}H NMR ($CDCl_3$, 300 MHz): δ = 7.15 (t, *J* = 7.5 Hz, 2H), 6.92 (ddd, *J* = 7.5, 1.6, 0.8 Hz, 2H), 6.84 – 6.76 (m, 4H), 3.92 (q, *J* = 7.1 Hz, 4H), 2.28 (s, 6H), 1.10 (t, *J* = 7.1 Hz, 6H).

^{13}C{H} NMR (75 MHz, $CDCl_3$): δ = 178.4, 161.0, 151.5, 147.8, 140.1, 129.4, 126.3, 122.7, 119.5, 115.9, 62.5, 21.4, 13.9.

MP = 162^{o}C

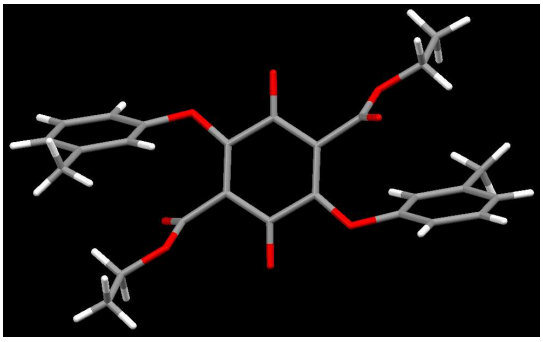

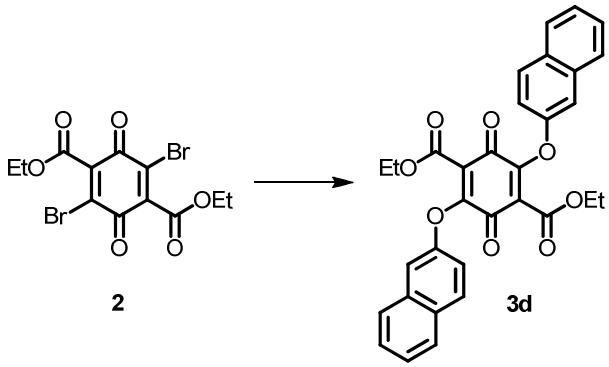

Compound **2** (1.5 g, 3.7 mmol), 2-napthol (3.0 g, 20.0 mmol), pyridine (1.5 mL, 18.5 mmol) and acetone (15 mL) was charged to a 100 mL round bottomed flask and refluxed for 10 minutes. The clear/ yellow suspension quickly turned dark red/ brown upon addition of pyridine and application of heat. The reaction mixture was diluted with water (100 mL) causing a precipitate to form. The precipitate was filtered off and washed with water, air dried and dissolved in DCM (100 mL). The organic mixture was dried over $MgSO_4$, which was filtered and the cake washed with excess DCM. The compound was purified via column chromatography (silica gel, DCM : Petrol, 1:1) often more than one column was required. The combined organic solvents were removed under reduced pressure to give a dark red solid, **3d** (1.5 g, 2.8 mmol, 75 %).

^{1}H NMR ($CDCl_3$, 300 MHz): δ = 7.78 (d, *J* = 8.9 Hz, 2H), 7.71 (dd, *J* = 8.0, 1.4 Hz, 2H), 7.78 –7.74 (m, 2H), 7.48 – 7.34 (m, 6H), 7.24 (dd, *J* = 8.9, 2.5 Hz, 2H), 3.76 (q, *J* = 7.1 Hz, 4H), 0.97 (t, *J* = 7.1 Hz, 6H).

^{13}C{H} NMR (75 MHz, $CDCl_3$): δ = 160.9, 152.9, 151.7, 133.6, 131.1, 130.1, 127.9, 127.6, 127.1, 125.9, 123.1, 119.1, 115.2, 62.5, 13.7.[†]

MP = 180^{o}C

MS – calc. for $C_{32}H_{24}O_8$ = 536.5 found. 537 (M+)

IR – 2987, 1717, 1670, 1191 cm^{-1}

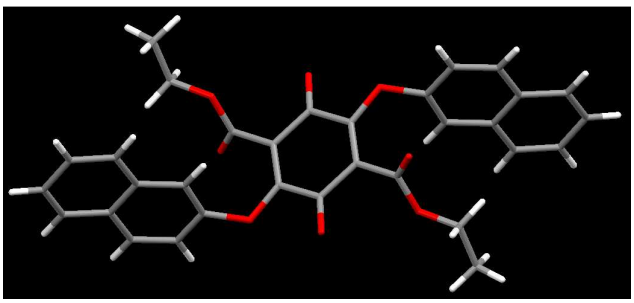

[†] 1 Carbon peak missing, like found in the aromatic region obscured by another peak.

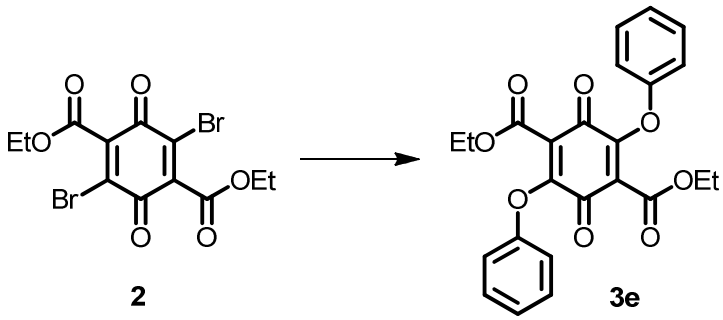

2 **3e**

Compound **2** (0.25 g, 0.6 mmol), phenol (0.25 g, 2.7 mmol), pyridine (0.25 mL, 3.1 mmol) and acetone (15 mL) was charged to a 100 mL round bottomed flask and refluxed for 10 minutes. The clear/ yellow suspension quickly turned dark red/ brown upon addition of pyridine and application of heat. The reaction mixture was diluted with water (100 mL) causing a precipitate to form. The precipitate was filtered off and washed with water, air dried and dissolved in DCM (100 mL). The organic mixture was dried over $MgSO_4$, which was filtered and the cake washed with excess DCM. The combined organic solvents were removed under reduced pressure to give a dark red solid this solid was purified via a recrystallization from ethanol leaving pure **3e** (0.25 g, 0.6 mmol, 95 %).

^{1}H NMR ($CDCl_3$, 300 MHz): δ = 7.32 – 7.23 (m, 4H), 7.16 – 7.08 (m, 2H), 7.08 – 6.95 (m, 4H), 3.92 (q, *J* = 7.2 Hz, 4H), 1.10 (t, *J* = 7.2 Hz, 6H).

^{13}C{H} NMR (75 MHz, $CDCl_3$): δ = 178.3, 160.9, 155.1, 151.5, 129.8, 125.5, 122.9, 118.9, 62.5, 13.9.

MP = 171^{o}C

IR – 2980, 1731, 1672, 1185 cm^{-1}

MS – calc. for $C_{24}H_{20}O_8$ = 436.4 found. 437 (M+)

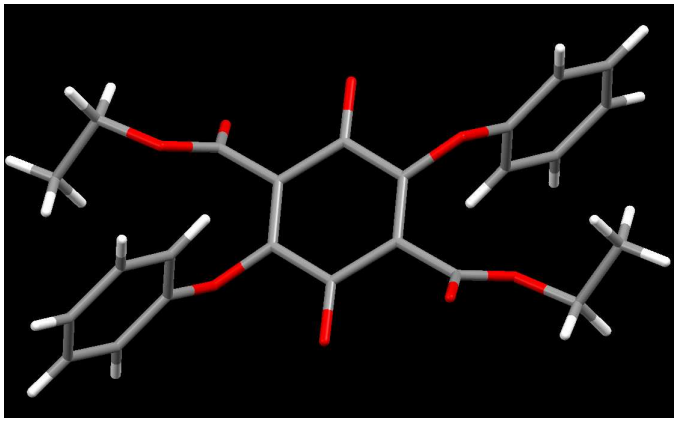

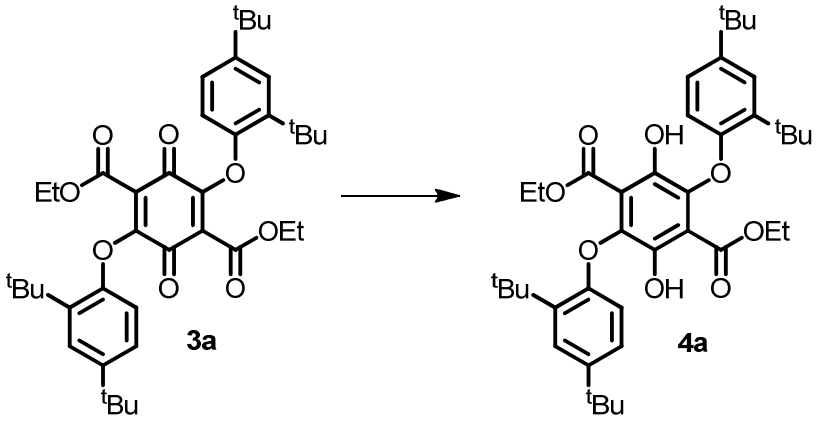

3a (2.0 g, 3.0 mmol), zinc powder (0.5 g, excess) and acetic acid (75 mL) was charged to a 100 mL round bottomed flask and the reaction mixture was placed in a sonicator for 60 minutes. The red/brown suspension quickly turned to a clear yellow solution with a zinc precipitate. Product was extracted using DCM (100 mL) and water (3 x 150 mL). The organic phase was dried over $MgSO_4$, which was filtered and the cake washed with DCM (as required). The solvent was removed under reduced pressure giving a yellow solid (2.0 g, 3.0 mmol, 100 %).

^{1}H NMR ($CDCl_3$, 75 MHz): δ = 10.57 (s, 1H) 10.55 (s, 1H) 7.53 (t, *J* = 2.2 Hz, 2H) 6.95 (dq, *J* = 5.9, 2.9, 2.4 Hz, 2H) 6.57 (d, *J* = 8.4 Hz, 1H) 6.35 (d, *J* = 8.5 Hz, 1H) 3.90 – 3.75 (m, 2H) 3.74 – 3.63 (m, 2H) 1.72 (s, 9H) 1.72 (s, 9H) 1.26 (s, 9H) 1.25 (s, 9H) 0.80 (t, *J* = 7.1 Hz, 3H).

Isomer A (population = 1.0, approx)

^{1}H NMR (d_8-toluene, 296 K, 500.16 MHz): δ = 0.553 (t, $^3J_{HH}$ = 7.10 Hz, 3H), 1.282 (s, 3H), 1.745 (s, 3H), 3.704 (dq, $^2J_{HH}$ = 10.95 Hz, $^3J_{HH}$ = 7.10 Hz, 1H), 3.850 (dq, $^2J_{HH}$ = 10.95 Hz, $^3J_{HH}$ = 7.10 Hz, 1H), 6.384 (d, $^3J_{HH}$ = 8.48 Hz, 1H), 6.980 (dd, $^3J_{HH}$ = 8.48 Hz, $^4J_{HH}$ = 2.43 Hz, 1H), 7.565 (d, $^4J_{HH}$ = 2.43 Hz, 1H), 10.582 (s, 1H)

Isomer B (population = 0.8, approx)

^{1}H NMR (d_8-toluene, 296 K, 500.16 MHz): δ = 0.555 (t, $^3J_{HH}$ = 7.10 Hz, 3H), 1.275 (s, 3H), 1.741 (s, 3H), 3.719 (dq, $^2J_{HH}$ = 10.76 Hz, $^3J_{HH}$ = 7.10 Hz, 1H), 3.842 (dq, $^2J_{HH}$ = 10.76 Hz, $^3J_{HH}$ = 7.10 Hz, 1H), 6.600 (d, $^3J_{HH}$ = 8.46 Hz, 1H), 6.995 (dd, $^3J_{HH}$ = 8.46 Hz, $^4J_{HH}$ = 2.47 Hz, 1H), 7.570 (d, $^4J_{HH}$ = 2.47 Hz, 1H), 10.563 (s, 1H)

$^{13}C\{H\}$ NMR (*d*8-toluene, 296 K, 125.765 MHz): δ = 168.9, 155.4, 147.3, 143.5, 138.7, 136.0, 123.8, 123.3, 115.0, 112.6, 61.9, 35.2, 34.1, 31.4, 30.2, 12.9.

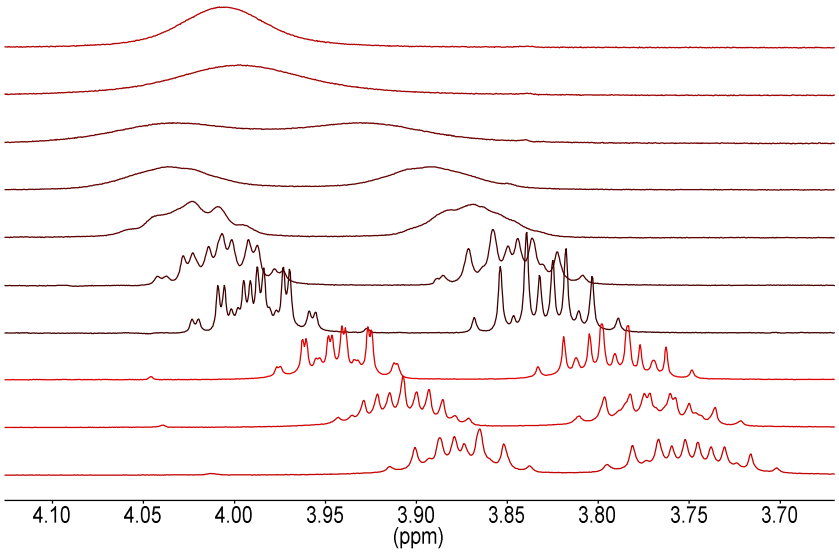

VT ^{1}H NMR detailing the methylene proton region, measured in d_{10}-xylene, where the temperature increase from the bottom up.

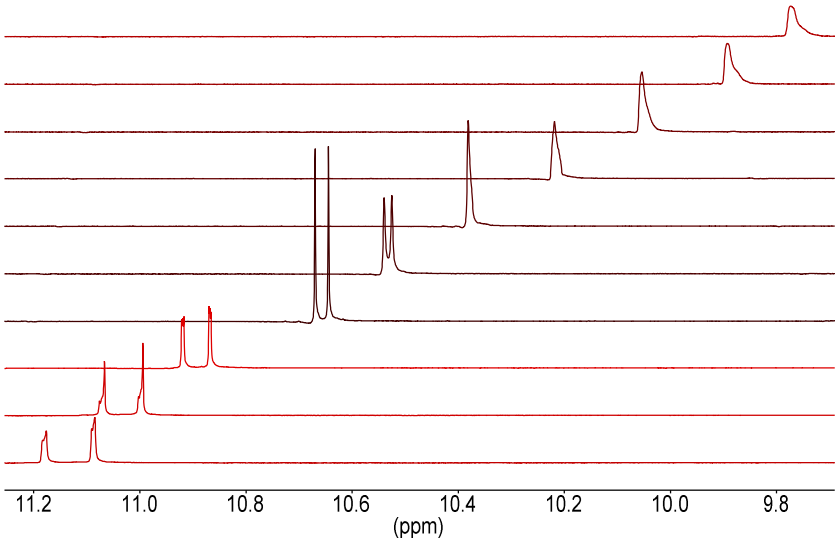

VT ^{1}H NMR detailing the hydroxyl proton region, measured in d_{10}-xylene, where the temperature increase from the bottom up.

MP = 166^{o}C

MS – calc. for $C_{40}H_{54}O_8$ = 662.9 found. 663 [M+]

IR – 2979, 1667, 1193 cm^{-1}.

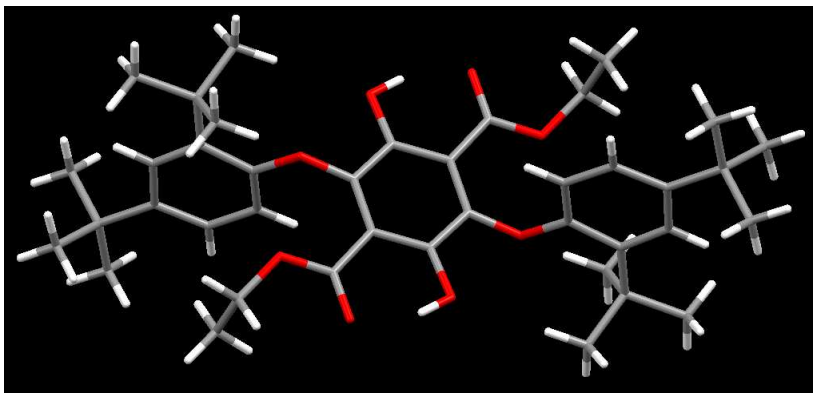

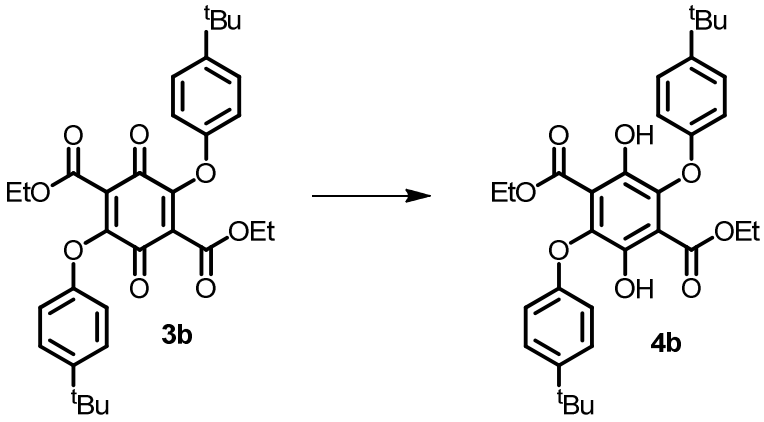

3b (2.6 g, 4.7 mmol), zinc powder (0.5 g, excess) and acetic acid (50 mL) was charged to a 100 mL round bottomed flask and the reaction mixture was placed in a sonicator for 60 minutes. The red/brown suspension quickly turned to a clear yellow solution with a zinc precipitate. Product was extracted using DCM (100 mL) and water (3 x 150 mL). The organic phase was dried over $MgSO_4$, which was filtered and the cake washed with DCM (as required). The solvent was removed under reduced pressure giving a yellow solid (2.6 g, 4.7 mmol, 100 %).

^{1}H NMR ($CDCl_3$, 300 MHz): δ = 10.21 (s, 2H), 7.27 (d, *J* = 8.8 Hz, 4H), 6.75 (d, *J* = 8.8 Hz, 4H), 4.20 (q, *J* = 7.1 Hz, 4H), 1.27 (s, 18H), 0.96 (t, *J* = 7.1 Hz, 6H).

^{13}C{H} NMR (75 MHz, $CDCl_3$): δ = 168.5, 156.1, 147.2, 144.7, 138.7, 126.3, 114.8, 113.9, 62.6, 34.2, 31.6, 13.4.

MP = 175^{o}C

IR – 2961, 1165, 1194 cm^{-1}.

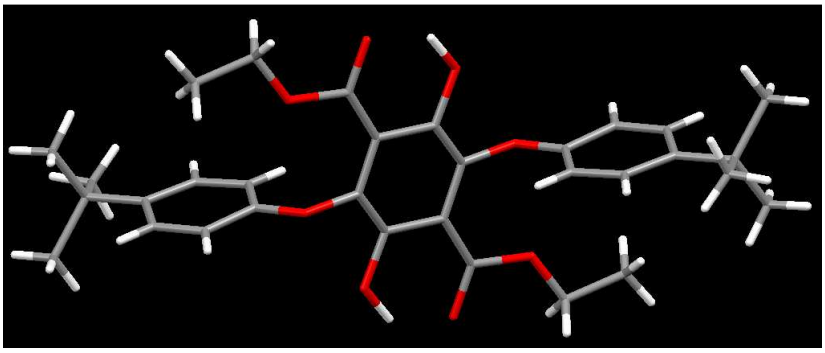

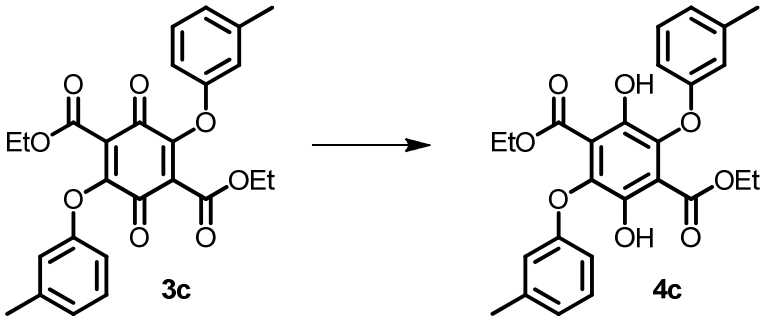

3c (1.00 g, 1.9 mmol), zinc powder (0.5 g, excess) and acetic acid (50 mL) was charged to a 100 mL round bottomed flask and the reaction mixture was placed in a sonicator for 60 minutes. The red/brown suspension quickly turned to a clear yellow solution with a zinc precipitate. Product was extracted using DCM (100 mL) and water (3 x 150 mL). The organic phase was dried over $MgSO_4$, which was filtered and the cake washed with DCM (as required). The solvent was removed under reduced pressure giving a yellow solid (1.00 g, 1.9 mmol, 100 %).

^{1}H NMR ($CDCl_3$, 300 MHz): δ = 10.24 (s, 2H), 7.09 (t, *J* = 7.8 Hz, 2H), 6.76 (d, *J* = 7.8 Hz, 2H), 6.62 (s, 2H), 6.57 (dd, *J* = 7.8, 2.2 Hz, 2H), 4.16 (q, *J* = 7.1 Hz, 4H), 2.26 (s, 6H), 0.95 (t, *J* = 7.1 Hz, 6H).

^{13}C{H} NMR (75 MHz, $CDCl_3$): δ = 168.6, 158.3, 147.2, 139.7, 138.7, 129.2, 122.9, 115.4, 114.8, 111.6, 62.5, 13.4.

MP = 156 ^{o}C

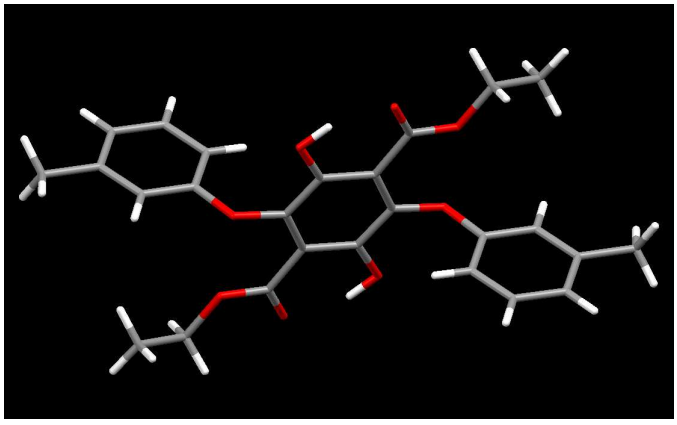

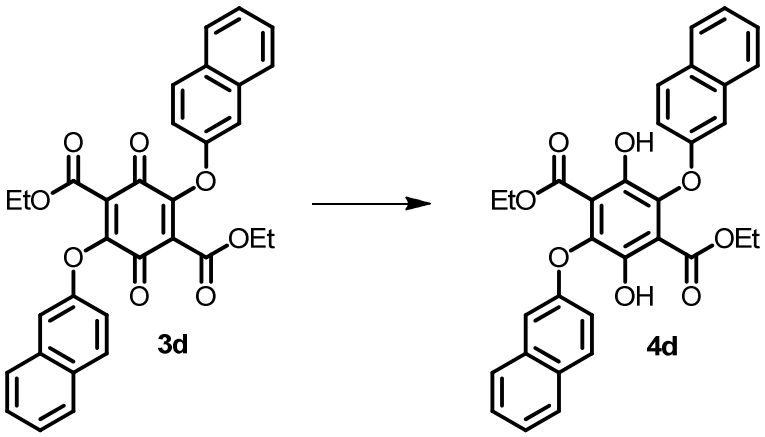

3d (1.00 g, 1.9 mmol), zinc powder (0.5 g, excess) and acetic acid (75 mL) was charged to a 100 mL round bottomed flask and the reaction mixture was placed in a sonicator for 60 minutes. The red/brown suspension quickly turned to a clear yellow solution with a zinc precipitate. Product was extracted using DCM (100 mL) and water (3 x 150 mL). The organic phase was dried over $MgSO_4$, which was filtered and the cake washed with DCM (as required). The solvent was removed under reduced pressure giving a yellow solid (0.98 g, 1.8 mmol, 95 %).

^{1}H NMR ($CDCl_3$, 300 MHz): δ = 10.39 (s, 2H), 7.76 (t, *J* = 9.3 Hz, 4H), 7.61 (d, *J* = 8.1 Hz, 2H), 7.43 – 7.33 (m, 2H), 7.33 – 7.22 (m, 4H), 6.95 (d, *J* = 2.6 Hz, 2H), 4.13 (q, *J* = 7.1 Hz, 4H), 0.89 (t, *J* = 7.1 Hz, 6H).

^{13}C{H} NMR (75 MHz, $CDCl_3$): δ = 168.6, 156.3, 147.4, 138.9, 134.3, 129.8, 129.7, 127.8, 127.0, 126.6, 124.2, 117.5, 114.8, 108.7, 62.7, 13.6.

MP = 156 ^{o}C

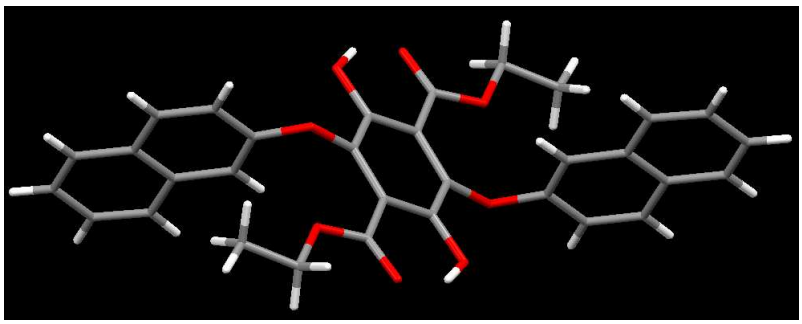

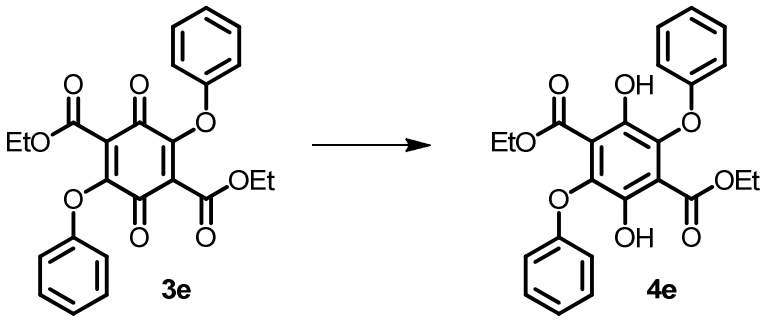

3e (0.25 g, 0.6 mmol), zinc powder (0.25 g, excess) and acetic acid (75 mL) was charged to a 100 mL round bottomed flask and the reaction mixture was placed in a sonicator for 60 minutes. The red/brown suspension quickly turned to a clear yellow solution with a zinc precipitate. Product was extracted using DCM (100 mL) and water (3 x 150 mL). The organic phase was dried over $MgSO_4$, which was filtered and the cake washed with DCM (as required). The solvent was removed under reduced pressure giving a yellow solid (0.25 g, 0.6 mmol, 100 %).

^{1}H NMR ($CDCl_3$, 300 MHz): δ = 10.25 (s, 2H), 7.22 (dt, *J* = 7.2, 1.4 Hz, 4H), 6.94 (t, *J* = 7.2 Hz, 2H), 6.79 (d, *J* = 7.6 Hz, 4H), 4.14 (q, *J* = 7.1 Hz, 4H), 0.92 (t, *J* = 7.1 Hz, 6H)

^{13}C{H} NMR (75 MHz, $CDCl_3$): δ = 177.6, 168.5, 158.3, 147.2, 138.6, 129.5, 122.0, 114.7, 62.7, 13.5.

MP = 176 ^{o}C

IR = 3077, 2980, 1658, 1206 cm^{-1}.

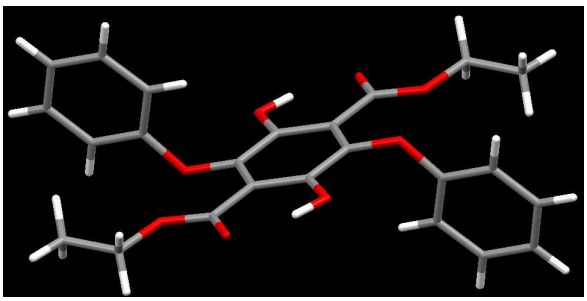

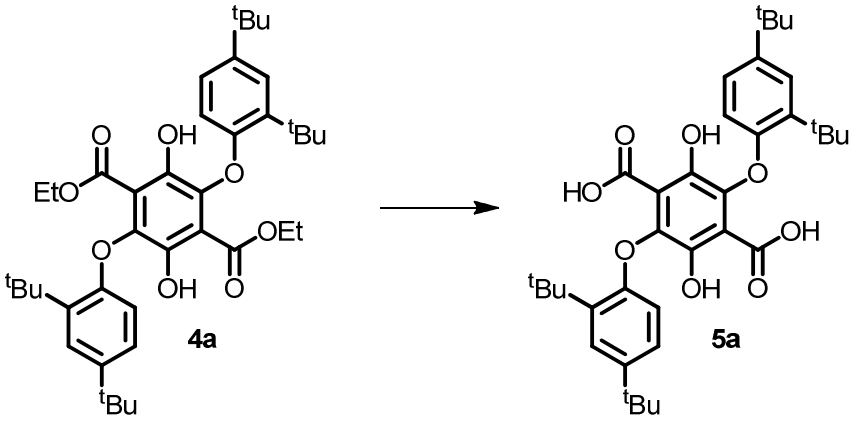

4a (2.0 g, 3.0 mmol), ethanol (0.5 mL) and 10% KOH (50 mL) was charged to a 100 mL round bottomed flask and the reaction mixture was heated at reflux for 24 hours. The yellow suspension changed colour to a dark red solution upon heating. The reaction mixture was removed from the heat source and allowed to cool to RT. Once at RT HCl was added to the reaction mixture until the pH was acidic. Once acidic the product crashed out of solution as a yellow solid. The product was filtered off and washed with water and air dried. The solid was recrystallized from acetic acid to give yellow needle-like crystals (0.5 g, 0.77 mmol, 25 %).

^{1}H NMR ($CDCl_3$, 300 MHz): δ = 11.17 (s, 2H), 7.49 (m, 2H), 7.15 (dd, *J* = 8.5, 2.4 Hz, 1H), 7.10 (dd, *J* = 8.5, 2.4 Hz, 1H), 6.55 (d, *J* = 8.2 Hz, 1H), 6.53 (d, *J* = 8.2 Hz, 1H), 1.56 (s, 9H), 1.55 (s, 9H), 1.35 (s, 9H), 1.33 (s, 9H).‡

^{13}C{H} NMR (75 MHz, $CDCl_3$): δ = 189.8, 168.8, 153.0, 147.1, 145.9, 138.6, 137.2, 125.1, 124.1, 114.0, 35.2, 34.6, 31.5, 30.5.

MP = >250 ^{o}C

MS – calc. for $C_{36}H_{46}O_8$ = 606.8 found. 605 $(M-H)^-$

IR – 2962, 1652, 1191 cm^{-1}.

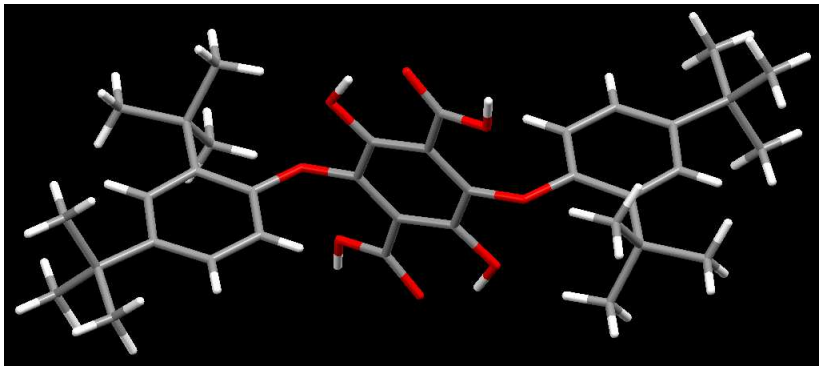

‡ Carboxylic acid protons were not evident.

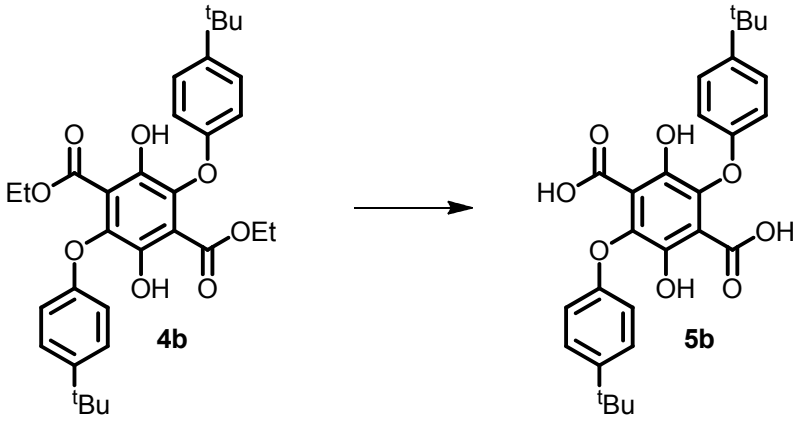

4b (2.6 g, 4.7 mmol), ethanol (0.5 mL) and 10% KOH (50 mL) was charged to a 100 mL round bottomed flask and the reaction mixture was heated at reflux for 24 hours. The yellow suspension changed colour to a dark red solution upon heating. The reaction mixture was removed from the heat source and allowed to cool to RT. Once at RT HCl was added to the reaction mixture until the pH was acidic. Once acidic the product crashed out of solution as a yellow solid. The product was filtered off and washed with water and air dried. The solid was recrystallized from acetic acid to give yellow needle-like crystals (1.40 g, 2.8 mmol, 60 %).

^{1}H NMR ($CDCl_3$, 300 MHz): δ = 9.82 (brs, 2H), 7.26 (dd, *J* = 8.7, 2.0 Hz, 4H), 6.71 (dd, *J* = 8.7, 2.0 Hz, 4H), 2.46 (s, 2H), 1.21 (s, 18H)

^{13}C{H} NMR (75 MHz, $CDCl_3$): δ = 167.4, 156.3, 144.4, 142.7, 137.4, 126.5, 120.1, 115.1, 34.4, 31.9.

MP = >250 ^{o}C

MS – calc. for $C_{28}H_{30}O_8$ = 494.5 found. 493 $(M-H)^-$

IR – 2969, 2538, 1690, 1190 cm^{-1}.

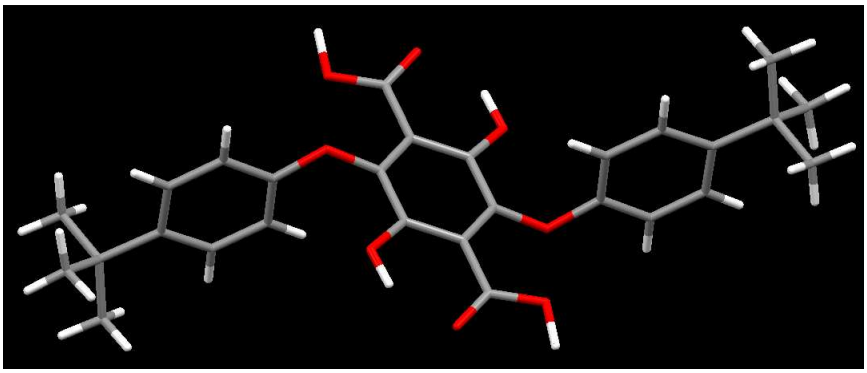

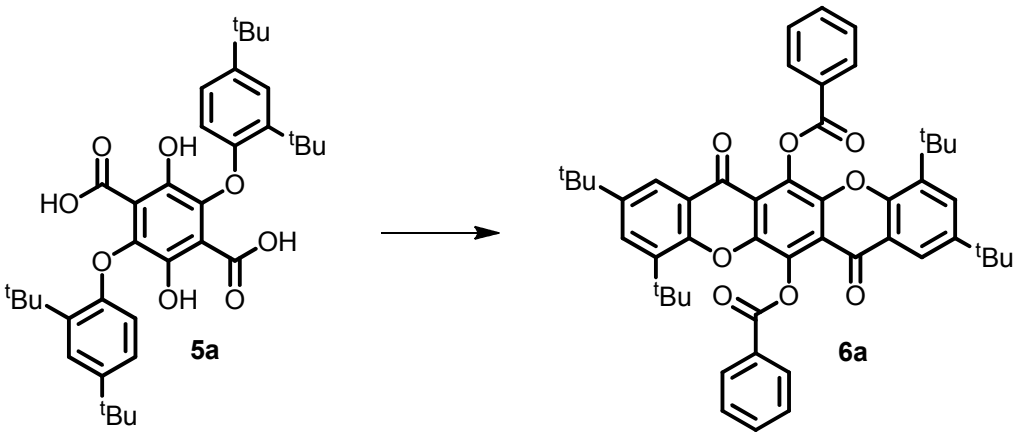

5a (1.54 g, 2.5 mmol), benzoyl chloride (10 mL) and H_2SO_4 (1 drop) were charged to a 100 mL round bottomed flask and the reaction mixture was heated at reflux for 1 hour. The yellow solution changed colour to brown upon heating. The reaction mixture was removed from the heat source and allowed to cool to RT. Once at RT, water (50 mL) was added and the reaction heated at reflux for 30 minutes. After this time the reaction was allowed to cool to RT. Once cool a yellow/ brown precipitate formed. This was filtered off and washed with water, ethanol and ether. The yellow solid was crystallised via slow vapour diffusion (chloroform/ petrol ether) to give yellow needle-like crystals (1.59 g, 1.8 mmol, 72 %).

^{1}H NMR (CDCl3, 300 MHz): δ = 8.40 (d, *J* = 7.5 Hz, 4H), 8.10 – 8.07 (m, 2H), 7.74 – 7.69 (m, 4H), 7.60 (t, *J* = 7.5 Hz, 4H), 1.34 - 1.33 (m, 18H), 1.31 – 1.30 (m, 18H)

^{13}C{H} NMR (75 MHz, CDCl3): δ = 176.1, 165.0, 164.6, 152.5, 146.9, 143.7, 138.3, 135.9, 134.0, 133.9, 130.9, 129.2, 129.1, 128.8, 128.8, 121.7, 120.9, 118.8, 35.2, 35.0, 31.4, 29.7.[§]

MP = >250 ^{o}C

MS – calc. for $C_{50}H_{50}O_8$ = 778.9 found. 779 (M^+)

IR – 2961, 1739, 1228 cm^{-1}.

[§] There exists some minor inequivalence between each of the two sets of tertiary-butyl groups on the xanthene core.

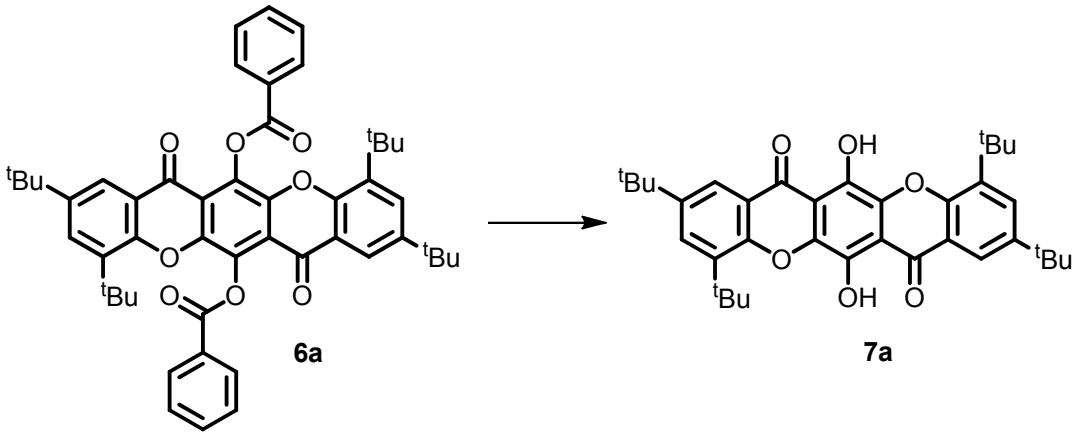

6a (1.50 g, 1.8 mmol) and aniline (15 mL) were charged to a 100 mL round bottomed flask and the reaction mixture was heated at reflux for 2 hours. The yellow/ orange solution changed colour to a dark red solution upon heating. The reaction mixture was removed from the heat source and allowed to cool to RT. Once at RT, ethanol (50 mL) was added and the reaction heated at reflux for a further hour. After this time the reaction was allowed to cool to RT. Once at RT, water was added to the mixture forming a red precipitate. The precipitate was filtered off and washed with water and air dried. The solid was dissolved in DCM and dried over $MgSO_4$. The slurry was filtered and the solvent removed under reduced pressure. The red solid was recrystallized from ethanol to give red crystals (0.98 g, 1.7 mmol, 95 %).

^{1}H NMR ($CDCl_3$, 300 MHz): δ = 12.35 (s, 2H), 8.16 (d, *J* = 2.4 Hz, 2H), 7.85 (d, *J* = 2.3 Hz, 2H), 1.64 (s, 18H), 1.40 (s, 18H)

^{13}C{H} NMR (75 MHz, $CDCl_3$): δ = 183.6, 153.8, 146.7, 140.2, 139.2, 136.8, 131.8, 129.4, 119.9, 119.7, 118.6, 115.2, 112.0, 35.7, 35.1, 31.4, 29.9.[**]

MP = >250 ^oC

MS – calc. for $C_{36}H_{42}O_6$ = 570.7 found. 571 (M^+)

IR – 2956, 1652, 1475 cm^{-1}.

[**] There exists some minor inequivalence between each of the two sets of tertiary-butyl groups on the xanthene core.

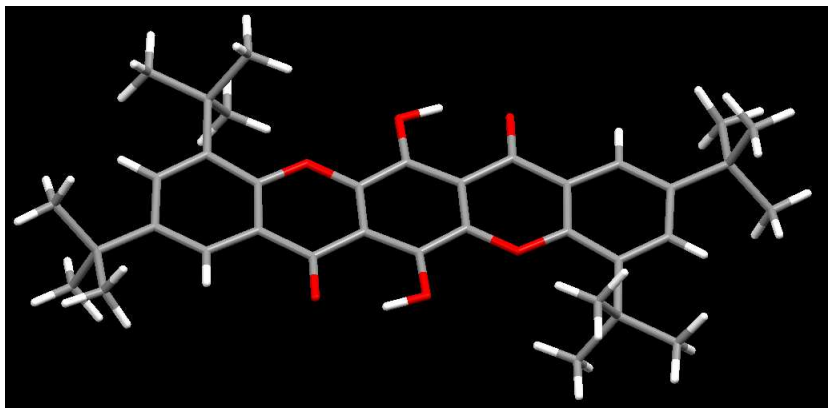

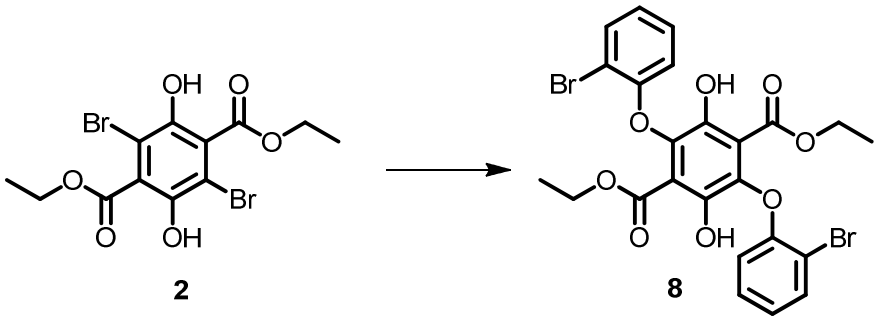

Compound **2** (0.5 g, 1.2 mmol), 2-bromophenol (0.4 g, 2.7 mmol, 2.1 eq), pyridine (0.5 mL, excess) and acetone (15 mL) was charged to a 100 mL round bottomed flask and refluxed for 10 minutes. The clear/ yellow suspension quickly turned dark red/ brown upon addition of pyridine and application of heat. The reaction mixture was diluted with water (100 mL) causing a dark brown precipitate to form. The precipitate was filtered off and washed with water, air dried and dissolved in DCM (100 mL). The organic mixture was dried over $MgSO_4$, which was filtered and the cake washed with excess DCM. The combined organic solvents were removed under reduced pressure to give a dark red solid this solid was purified via a recrystallization from ethanol.

The red solid was then combined with zinc powder (0.25 g, excess) and acetic acid (25 mL) in a 100 mL round bottomed flask and the reaction mixture was placed in a sonicator for 60 minutes. The red/brown suspension quickly turned to a clear yellow solution with a zinc precipitate. Water (100 mL) was added to the reaction mixture causing the product to precipitate out of solution. The resulting slurry was filtered, washed with water (3 x 100 mL) and the clear, colourless mother liquors discarded. The solid filtrate was then washed with DCM (150 mL) so as to dissolve the solid product, after which point the remaining zinc was filtered off. The mother liquors were dried over $MgSO_4$ and the slurry filtered and washed with DCM (50 mL). The solvent was removed under reduced pressure giving a bright yellow solid **8** (0.5 g, 0.9 mmol, 75 %).

^{1}H NMR (400 MHz, $CDCl_3$) δ = 10.50 (s, 2H), 7.62 (dd, *J* = 7.9, 1.6 Hz, 2H), 7.16 (ddd, *J* = 8.3, 7.4, 1.6 Hz, 2H), 6.90 (ddd, *J* = 7.9, 7.4, 1.4 Hz, 2H), 6.49 (dd, *J* = 8.3, 1.4 Hz, 2H), 4.24 (q, *J* = 7.1 Hz, 4H), 1.01 (t, *J* = 7.1 Hz, 6H).

^{13}C{H} NMR (100 MHz, $CDCl_3$) δ = 168.35, 154.58, 147.23, 138.49, 133.68, 128.31, 123.13, 114.46, 113.57, 110.80, 62.97, 13.39.

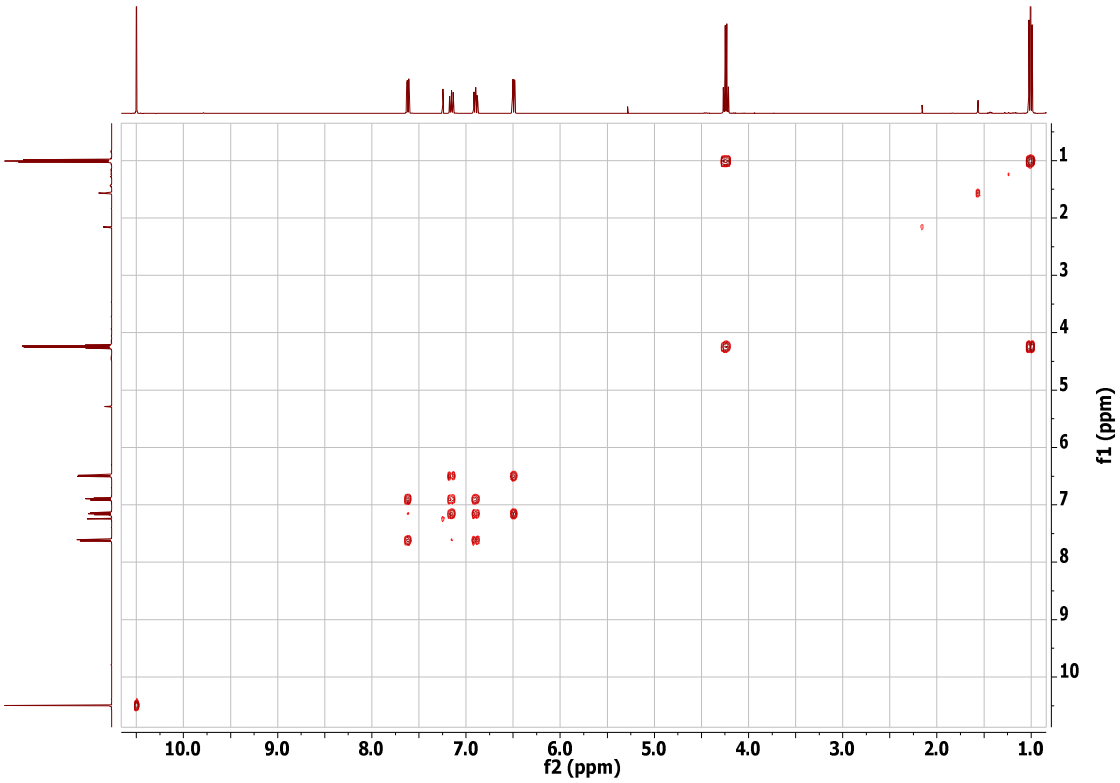

COSY

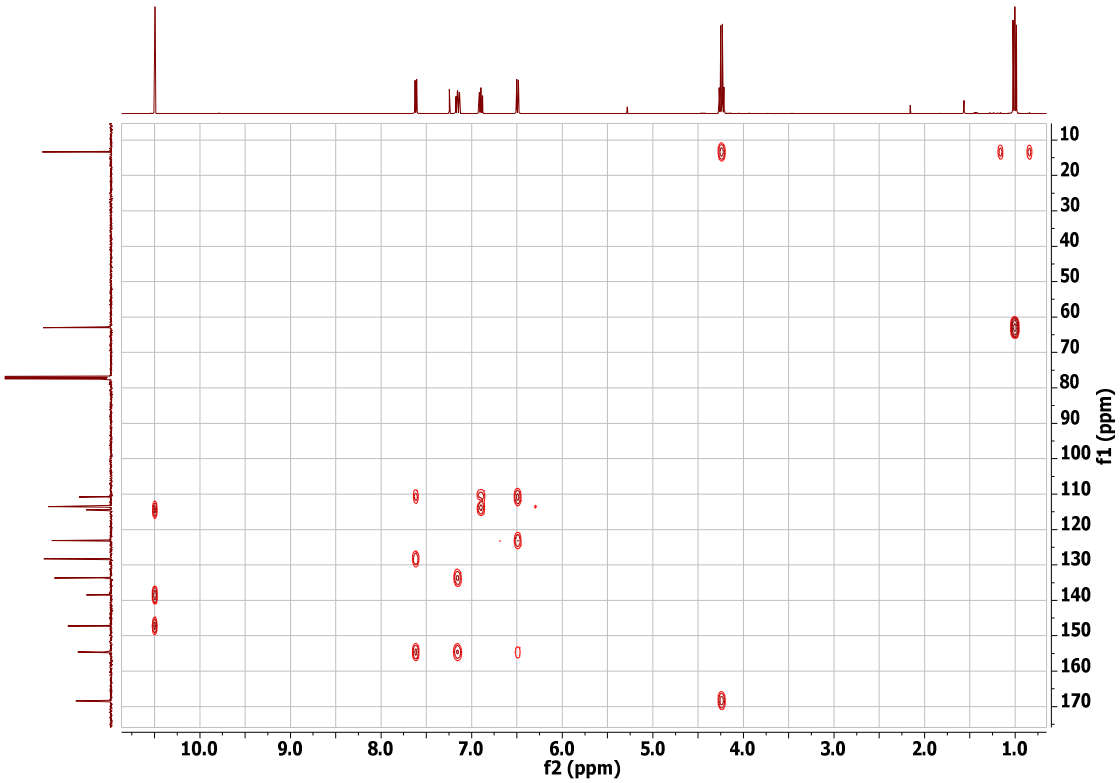

HMBC

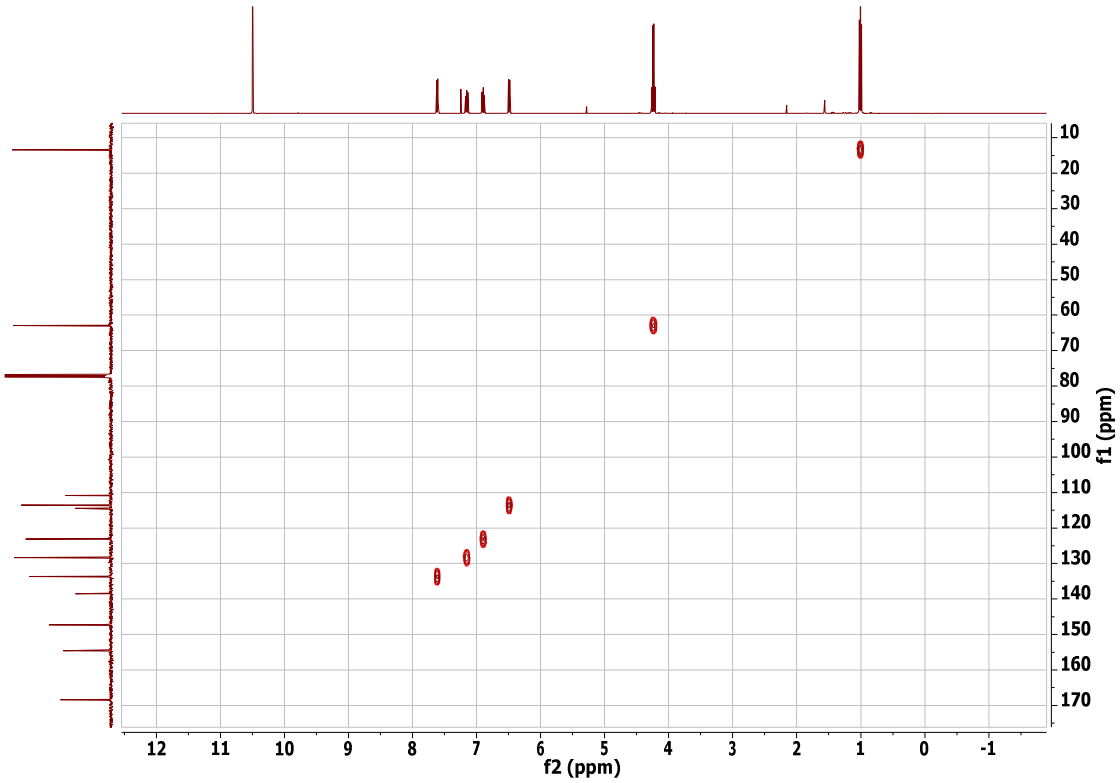

HMQC

MS = calc. for $C_{24}H_{20}O_8Br_2$ = 595 found. 596 $(M+H)^+$

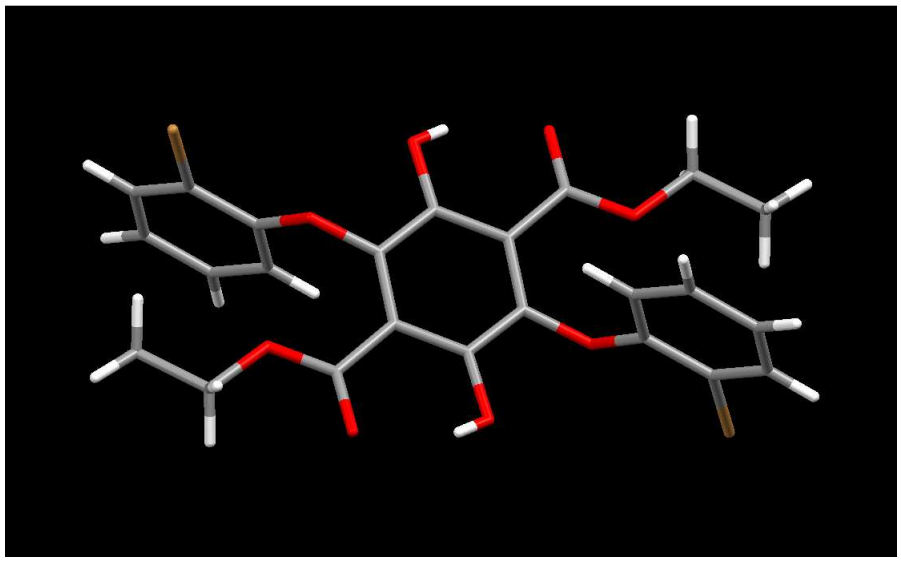

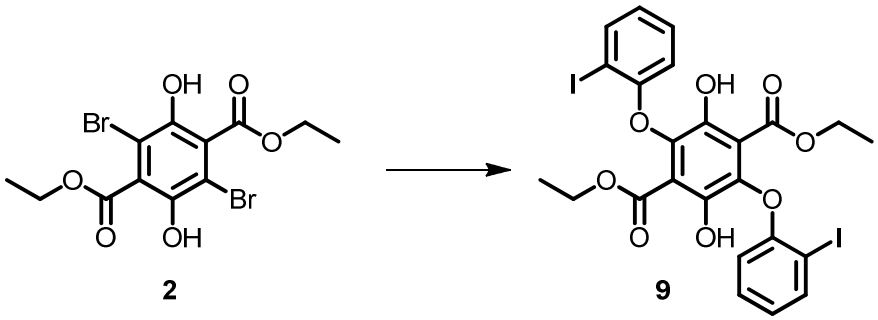

2 **9**

Compound **2** (0.5 g, 1.2 mmol), 2-iodophenol (0.6 g, 2.6 mmol, 2.1 eq), pyridine (0.5 mL, excess) and acetone (15 mL) was charged to a 100 mL round bottomed flask and refluxed for 10 minutes. The clear/ yellow suspension quickly turned dark red/ brown upon addition of pyridine and application of heat. The reaction mixture was diluted with water (100 mL) causing a dark brown precipitate to form. The precipitate was filtered off and washed with water, air dried and dissolved in DCM (100 mL). The organic mixture was dried over $MgSO_4$, which was filtered and the cake washed with excess DCM. The combined organic solvents were removed under reduced pressure to give a dark red solid this solid was purified via a recrystallization from ethanol.

The red solid was then combined with zinc powder (0.25 g, excess) and acetic acid (25 mL) in a 100 mL round bottomed flask and the reaction mixture was placed in a sonicator for 60 minutes. The red/brown suspension quickly turned to a clear yellow solution with a zinc precipitate. Water (100 mL) was added to the reaction mixture causing the product to precipitate out of solution. The resulting slurry was filtered, washed with water (3 x 100 mL) and the clear, colourless mother liquors discarded. The solid filtrate was then washed with DCM (150 mL) so as to dissolve the solid product, after which point the remaining zinc was filtered off. The mother liquors were dried over $MgSO_4$ and the slurry filtered and washed with DCM (50 mL). The solvent was removed under reduced pressure giving a bright yellow solid **9** (0.7 g, 1.0 mmol, 79 %).

^{1}H NMR (400 MHz, $CDCl_3$) δ = 10.46 (d, *J* = 0.7 Hz, 2H), 7.84 (ddd, *J* = 7.8, 1.6, 0.7 Hz, 2H), 7.24 – 7.09 (m, 2H), 6.77 (tdd, *J* = 7.8, 1.6, 0.9 Hz, 2H), 6.43 (dt, *J* = 8.2, 0.9 Hz, 2H), 4.24 (qd, *J* = 7.1, 0.7 Hz, 4H), 1.00 (td, *J* = 7.1, 0.7 Hz, 6H).

^{13}C{H} NMR (100 MHz, $CDCl_3$) δ = 168.35, 156.94, 147.15, 139.74, 138.67, 129.32, 123.71, 114.51, 112.65, 84.45, 62.94, 13.54.

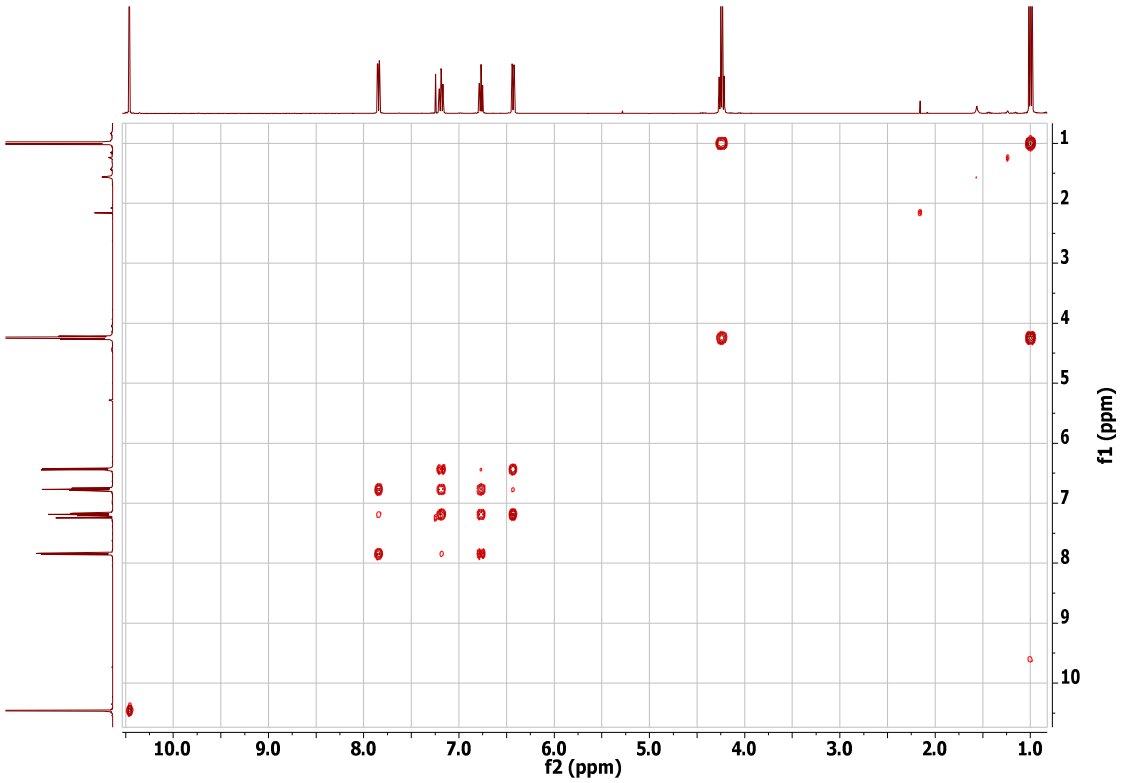

COSY

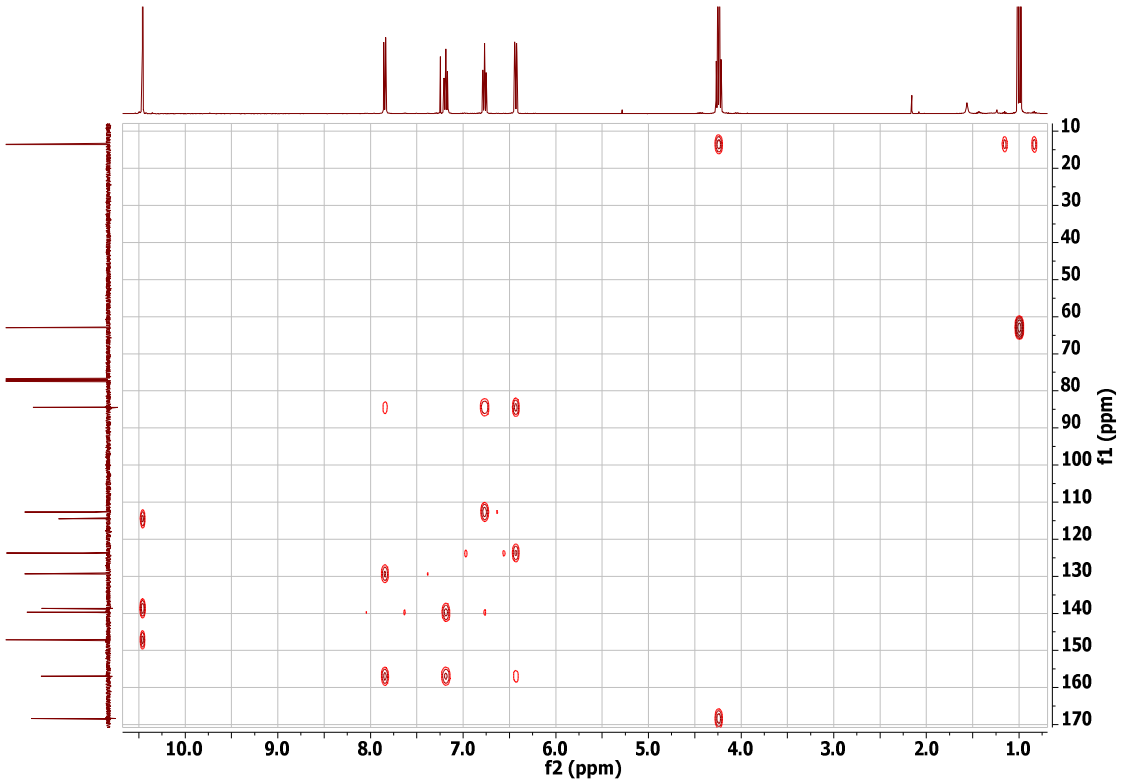

HMBC

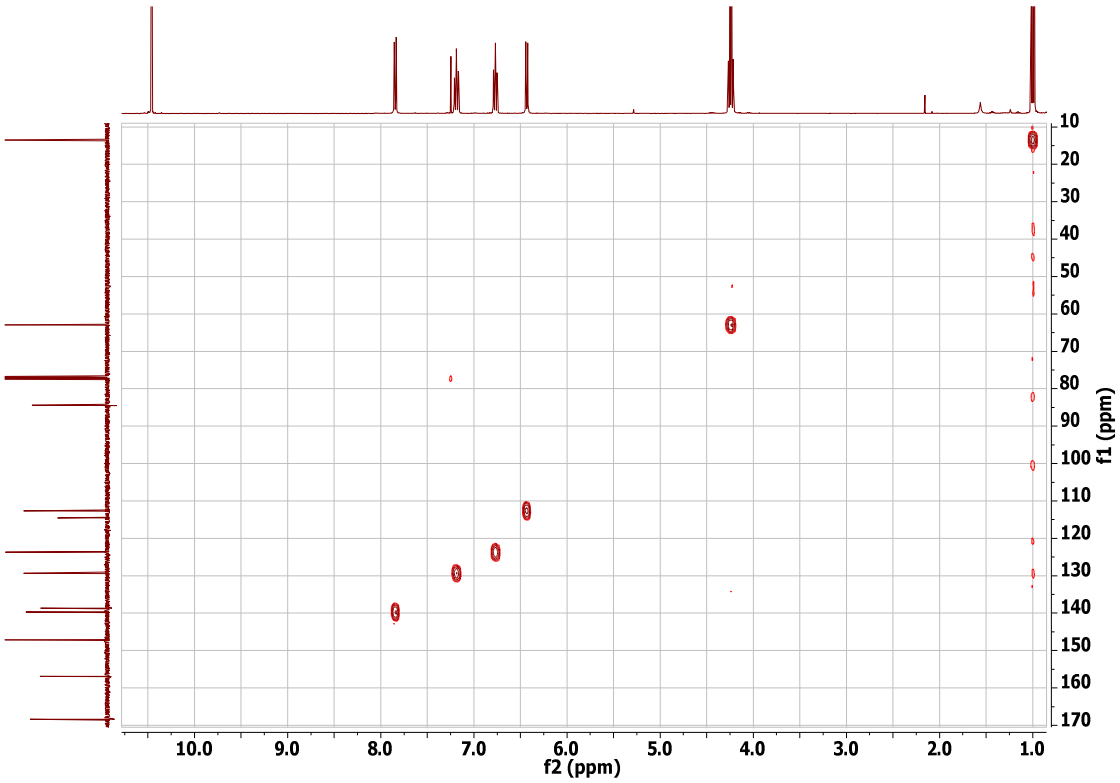

HMQC

MS = calc. for $C_{24}H_{20}O_8I_2$ = 689 found. 690 $(M+H)^+$

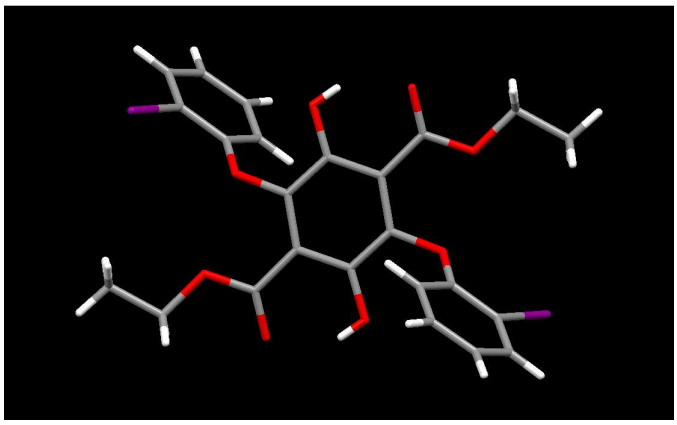

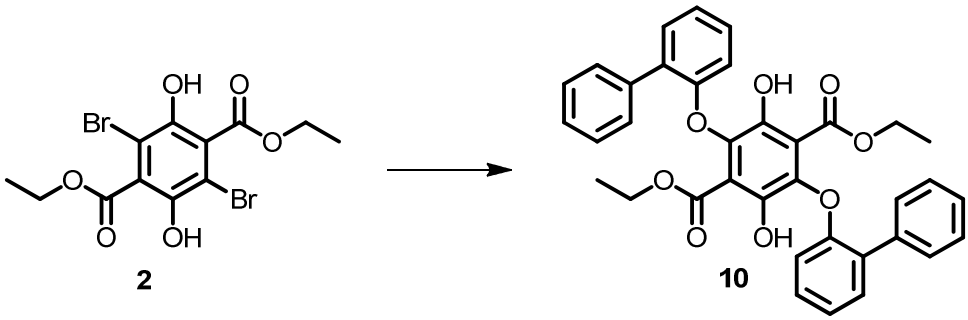

Compound **2** (0.5 g, 1.2 mmol), 2-phenylphenol (0.4 g, 2.6 mmol, 2.1 eq), pyridine (0.5 mL, excess) and acetone (15 mL) was charged to a 100 mL round bottomed flask and refluxed for 10 minutes. The clear/ yellow suspension quickly turned dark red/ brown upon addition of pyridine and application of heat. The reaction mixture was diluted with water (100 mL) causing a dark brown precipitate to form. The precipitate was filtered off and washed with water, air dried and dissolved in DCM (100 mL). The organic mixture was dried over $MgSO_4$, which was filtered and the cake washed with excess DCM. The combined organic solvents were removed under reduced pressure to give a dark red solid this solid was purified via a recrystallization from ethanol.

The red solid was then combined with zinc powder (0.25 g, excess) and acetic acid (25 mL) in a 100 mL round bottomed flask and the reaction mixture was placed in a sonicator for 60 minutes. The red/brown suspension quickly turned to a clear yellow solution with a zinc precipitate. Water (100 mL) was added to the reaction mixture causing the product to precipitate out of solution. The resulting slurry was filtered, washed with water (3 x 100 mL) and the clear, colourless mother liquors discarded. The solid filtrate was then washed with DCM (150 mL) so as to dissolve the solid product, after which point the remaining zinc was filtered off. The mother liquors were dried over $MgSO_4$ and the slurry filtered and washed with DCM (50 mL). The solvent was removed under reduced pressure giving a bright yellow solid **10** (0.42 g, 1.0 mmol, 54 %).

^{1}H NMR (300 MHz, $CDCl_3$) δ = 10.31 (s, 2H), 7.74 – 7.65 (m, 4H), 7.43 – 7.33 (m, 4H), 7.31 – 7.23 (m, 4H), 7.12 (ddd, *J* = 8.2, 7.4, 1.8 Hz, 2H), 7.02 (td, *J* = 7.4, 1.2 Hz, 2H), 6.50 (dd, *J* = 8.2, 1.2 Hz, 2H), 4.08 (q, *J* = 7.1 Hz, 4H), 0.79 (t, *J* = 7.1 Hz, 6H).

$^{13}C\{H\}$ NMR (125 MHz, $CDCl_3$) δ = 168.61, 155.14, 147.10, 138.58, 138.25, 131.19, 129.89, 129.70, 128.26, 128.18, 127.16, 122.17, 114.91, 112.87, 62.55, 13.25.

MS = calc. for $C_{36}H_{30}O_8$ = 590 found. 591 $(M+H)^+$

MP – DNM

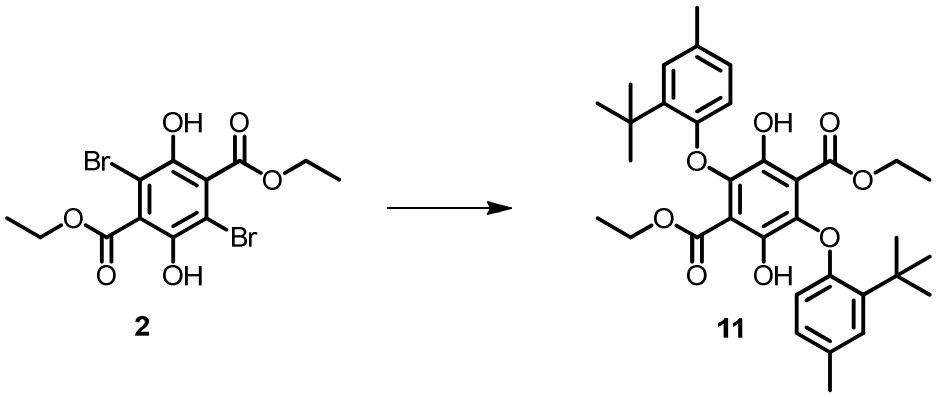

Compound **2** (0.5 g, 1.2 mmol), 2-tertbutyl-4-methylphenol (0.4 g, 2.6 mmol, 2.1 eq), pyridine (0.5 mL, excess) and acetone (15 mL) was charged to a 100 mL round bottomed flask and refluxed for 10 minutes. The clear/ yellow suspension quickly turned dark red/ brown upon addition of pyridine and application of heat. The reaction mixture was diluted with water (100 mL) causing a dark brown precipitate to form. The precipitate was filtered off and washed with water, air dried and dissolved in DCM (100 mL). The organic mixture was dried over $MgSO_4$, which was filtered and the cake washed with excess DCM. The combined organic solvents were removed under reduced pressure to give a dark red solid this solid was purified via a recrystallization from ethanol.

The red solid was then combined with zinc powder (0.25 g, excess) and acetic acid (25 mL) in a 100 mL round bottomed flask and the reaction mixture was placed in a sonicator for 60 minutes. The red/brown suspension quickly turned to a clear yellow solution with a zinc precipitate. Water (100 mL) was added to the reaction mixture causing the product to precipitate out of solution. The resulting slurry was filtered, washed with water (3 x 100 mL) and the clear, colourless mother liquors discarded. The solid filtrate was then washed with DCM (150 mL) so as to dissolve the solid product, after which point the remaining zinc was filtered off. The mother liquors were dried over $MgSO_4$ and the slurry filtered and washed with DCM (50 mL). The solvent was removed under reduced pressure giving a bright yellow solid **11** (0.6 g, 1.0 mmol, 84 %).

^{1}H NMR (500 MHz, $CDCl_3$) δ = 10.04 (s, 1H), 9.97 (s, 1H), 7.18 (dd, *J* = 4.1, 2.1 Hz, 2H), 6.87 (ddd, *J* = 8.2, 2.0, 0.9 Hz, 1H), 6.82 (ddd, *J* = 8.5, 2.1, 1.0 Hz, 1H), 6.43 (d, *J* = 8.1 Hz, 1H), 6.37 (d, *J* = 8.2 Hz, 1H), 4.26 (dqd, *J* = 10.5, 7.1, 4.6 Hz, 2H), 4.18 (dq, *J* = 10.8, 7.1 Hz, 2H), 2.31 (s, 3H), 2.29 (s, 3H), 1.53 (s, 9H), 1.51 (s, 9H), 0.99 – 0.94 (m, 6H).

$^{13}C\{H\}$ NMR (101 MHz, $CDCl_3$) δ = 168.79, 168.75, 154.94, 146.45, 146.37, 138.32, 138.26, 136.55, 136.48, 130.62, 130.59, 127.99, 127.95, 127.06, 126.99, 115.60, 115.47, 113.06, 113.02, 62.44, 62.42, 34.92, 30.04, 21.06, 21.02, 13.60.††

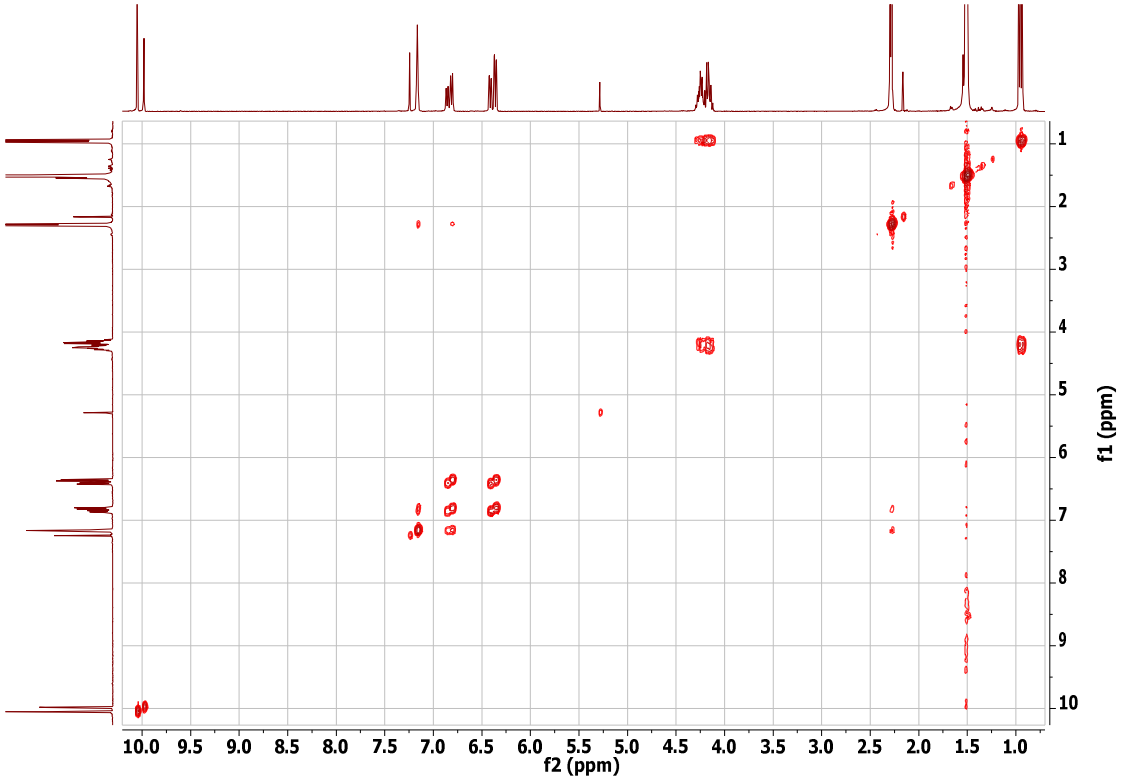

COSY

†† Evidence of the two isomers resulting in two peaks per carbon environment, though there is some overlap with certain signals.

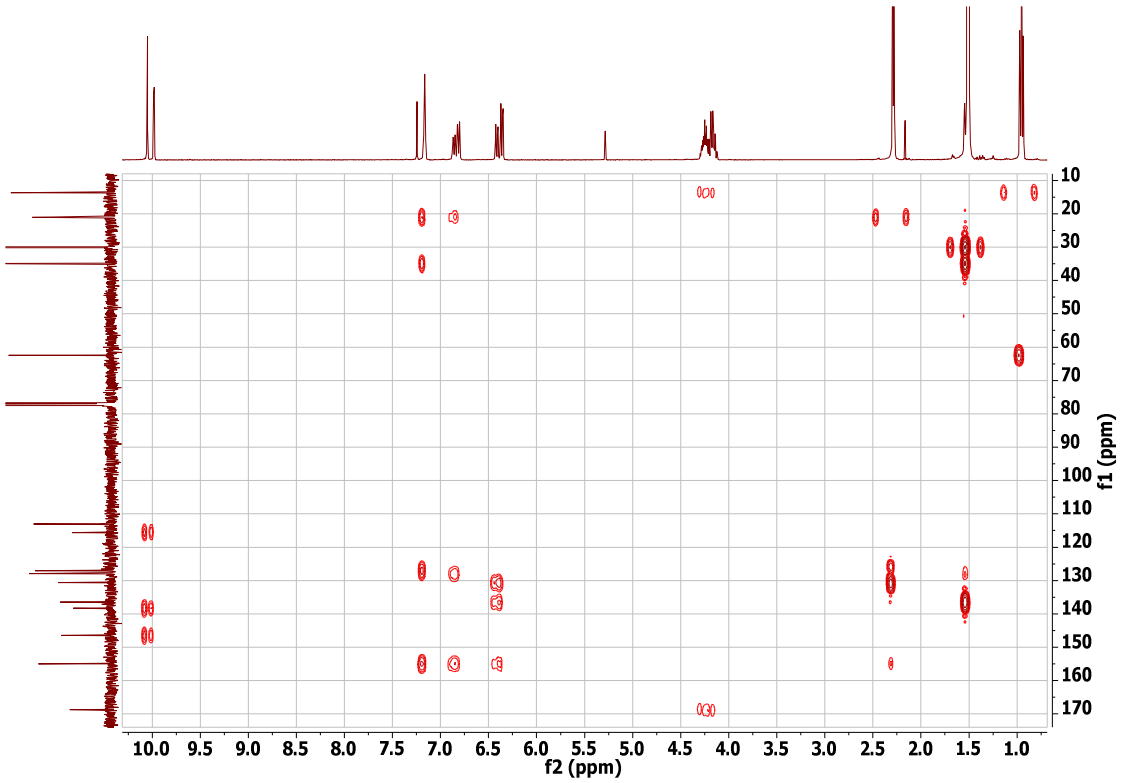

HMBC

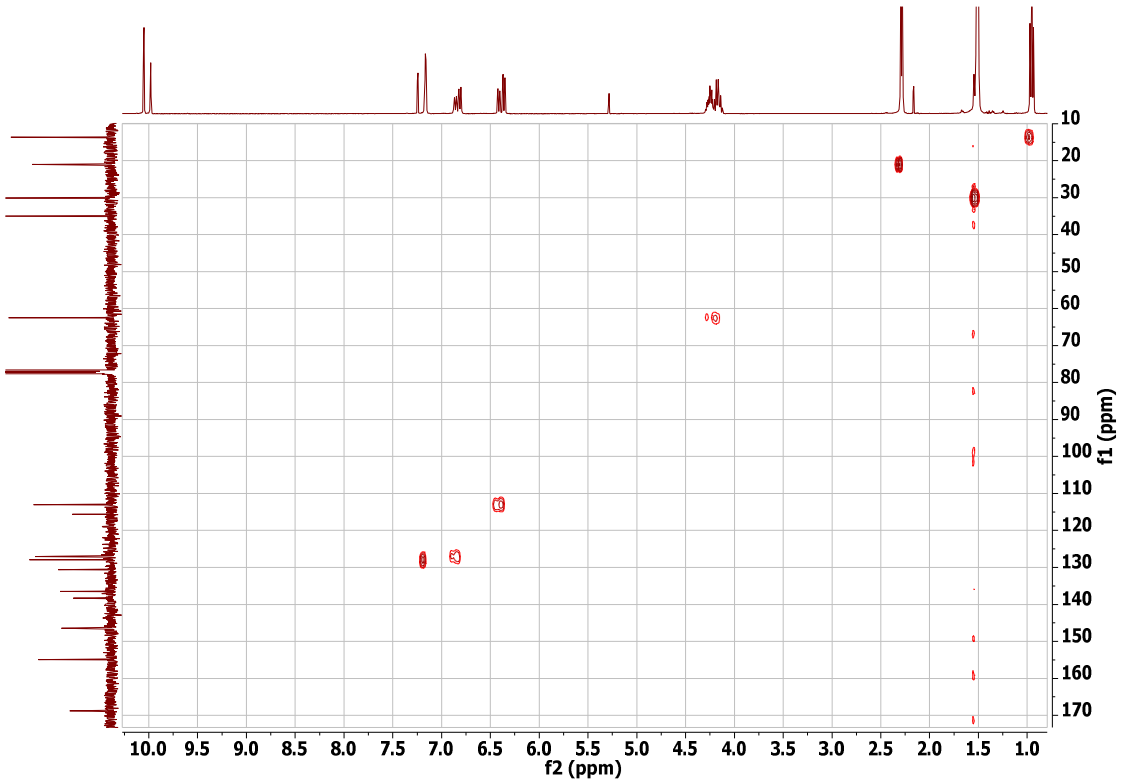

HMQC

MS = calc. for $C_{34}H_{42}O_8$ = 578 found. 579 $(M+H)^+$

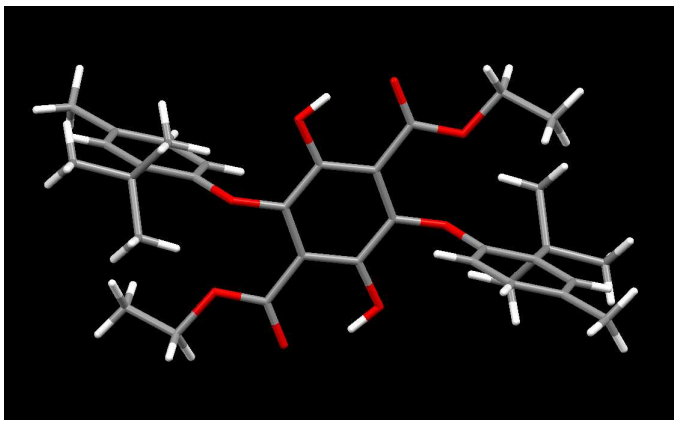

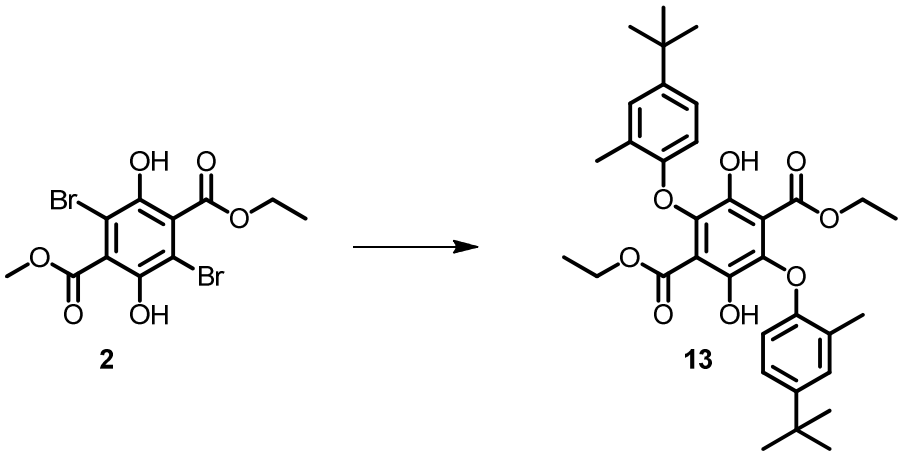

Compound **2** (0.5 g, 1.2 mmol), 4-tertbutyl-2-methylphenol (0.4 g, 2.6 mmol, 2.1 eq), pyridine (0.5 mL, excess) and acetone (15 mL) was charged to a 100 mL round bottomed flask and refluxed for 10 minutes. The clear/ yellow suspension quickly turned dark red/ brown upon addition of pyridine and application of heat. The reaction mixture was diluted with water (100 mL) causing a dark brown precipitate to form. The precipitate was filtered off and washed with water, air dried and dissolved in DCM (100 mL). The organic mixture was dried over $MgSO_4$, which was filtered and the cake washed with excess DCM. The combined organic solvents were removed under reduced pressure to give a dark red solid this solid was purified via a recrystallization from ethanol.

The red solid was then combined with zinc powder (0.25 g, excess) and acetic acid (25 mL) in a 100 mL round bottomed flask and the reaction mixture was placed in a sonicator for 60 minutes. The red/brown suspension quickly turned to a clear yellow solution with a zinc precipitate. Water (100 mL) was added to the reaction mixture causing the product to precipitate out of solution. The resulting slurry was filtered, washed with water (3 x 100 mL) and the clear, colourless mother liquors discarded. The solid filtrate was then washed with DCM (150 mL) so as to dissolve the solid product, after which point the remaining zinc was filtered off. The mother liquors were dried over $MgSO_4$ and the slurry filtered and washed with DCM (50 mL). The solvent was removed under reduced pressure giving a bright yellow solid **13** (0.7 g, 1.1 mmol, 90 %).

^{1}H NMR (400 MHz, $CDCl_3$) δ = 10.16 (s, 2H), 7.22 (dd, *J* = 2.5, 0.9 Hz, 2H), 7.01 (ddd, *J* = 8.5, 2.5, 0.9 Hz, 2H), 6.31 (d, *J* = 8.5 Hz, 2H), 4.20 (q, *J* = 7.1 Hz, 4H), 2.43 (s, 6H), 1.27 (s, 18H), 0.94 (t, *J* = 7.1 Hz, 6H).

$^{13}C\{H\}$ NMR (101 MHz, $CDCl_3$) δ = 168.56, 154.36, 147.03, 144.35, 138.90, 128.26, 125.01, 123.20, 114.84, 111.03, 62.48, 34.12, 31.64, 16.65, 13.27.

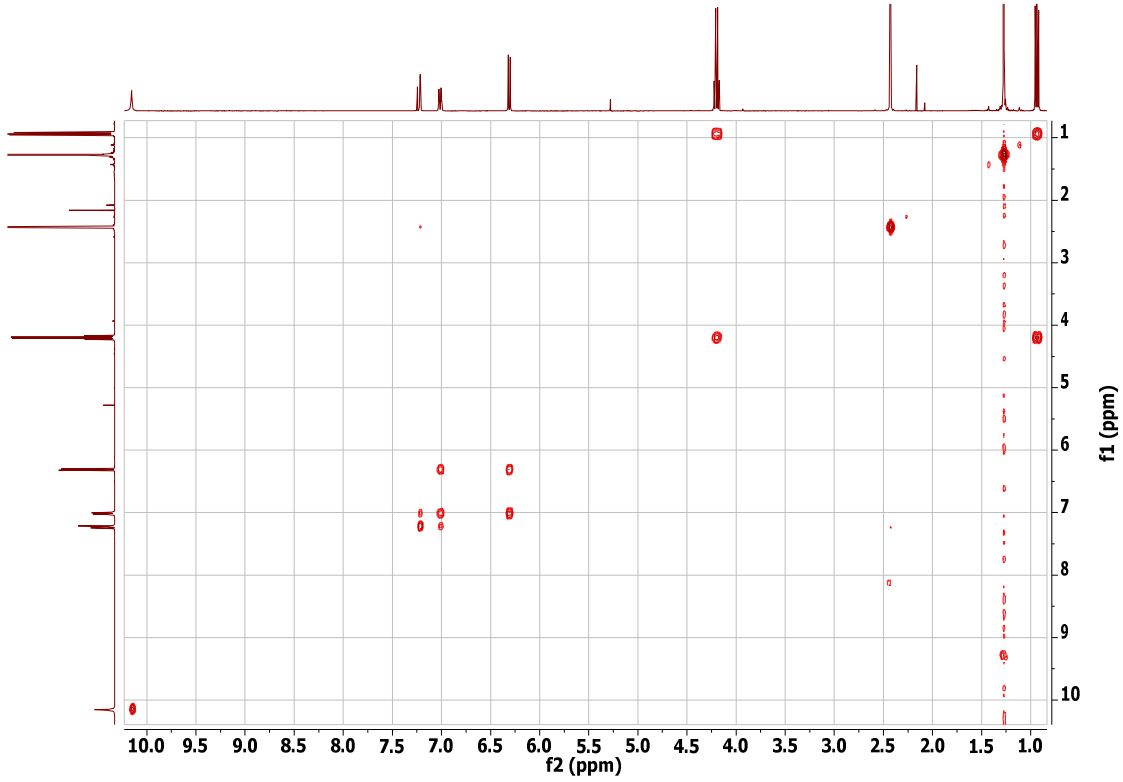

COSY

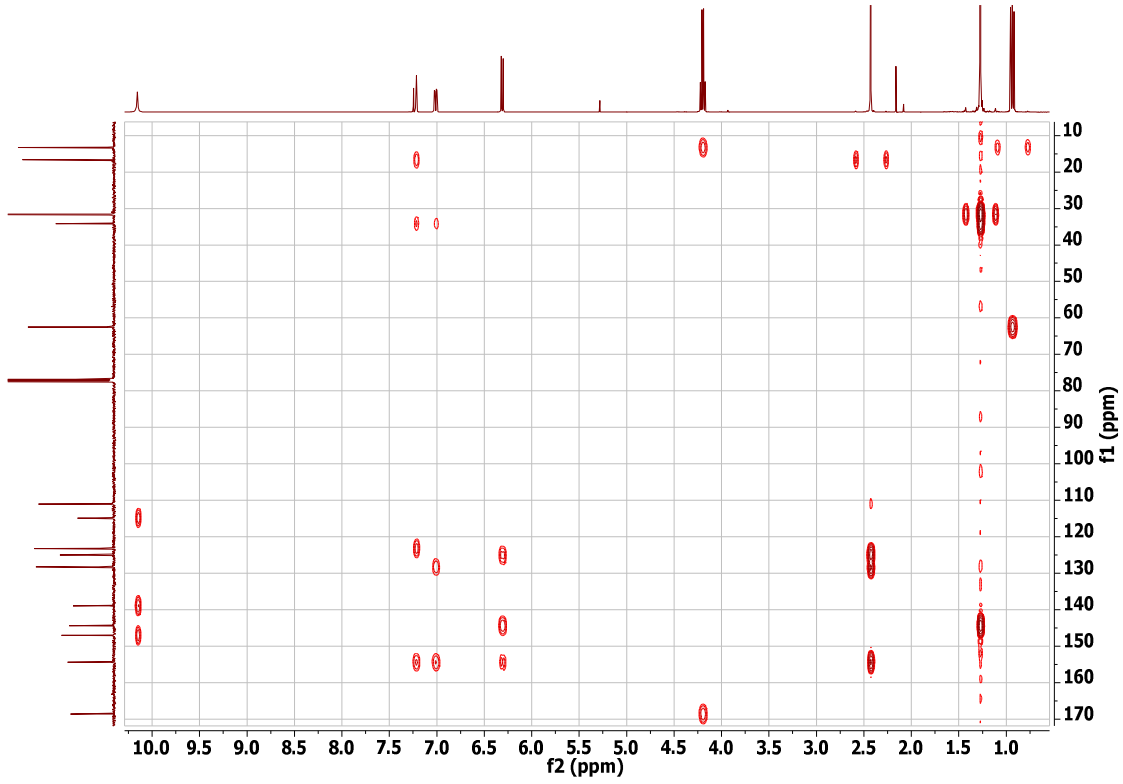

HMBC

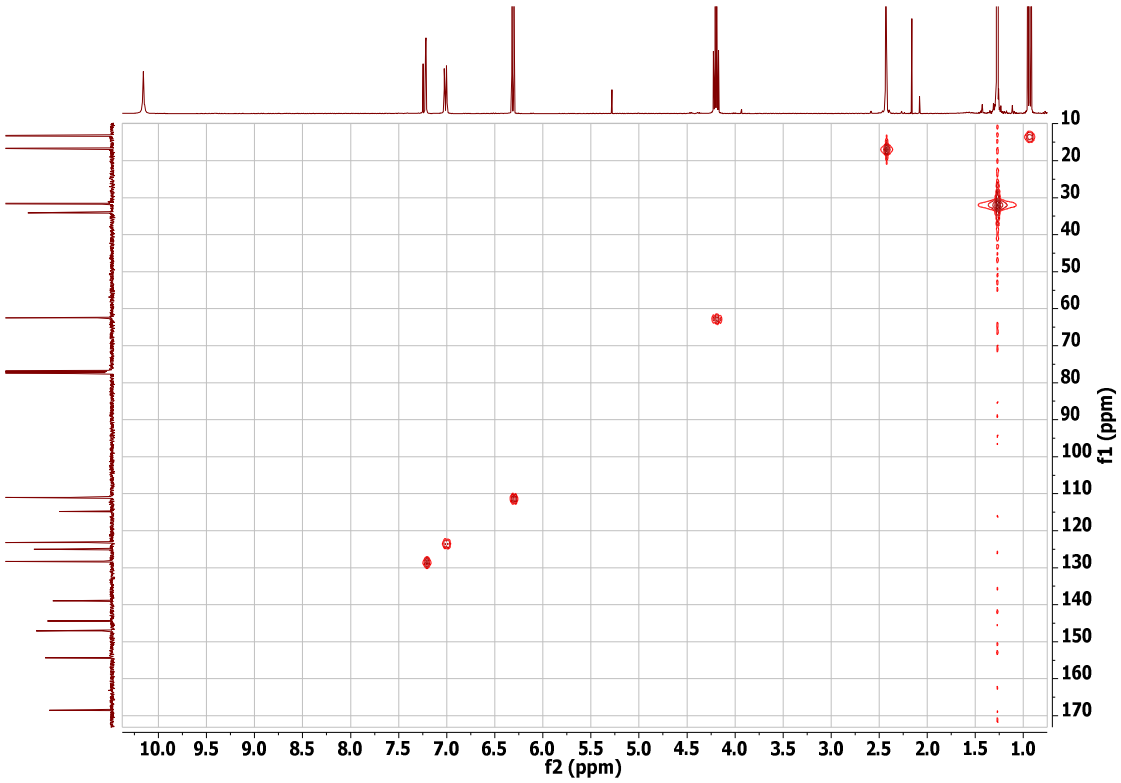

HMQC

MS = calc. for $C_{34}H_{42}O_8$ = 578 found. 579 $(M+H)^+$

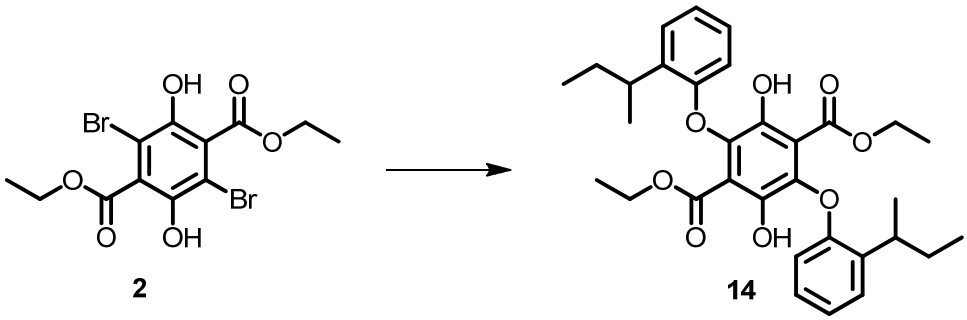

Compound **2** (0.5 g, 1.2 mmol), 2-sec-butylphenol (0.4 mL, 2.6 mmol, 2.1 eq), pyridine (0.5 mL, excess) and acetone (15 mL) was charged to a 100 mL round bottomed flask and refluxed for 10 minutes. The clear/ yellow suspension quickly turned dark red/ brown upon addition of pyridine and application of heat. The reaction mixture was diluted with water (100 mL) causing a dark brown precipitate to form. The precipitate was filtered off and washed with water, air dried and dissolved in DCM (100 mL). The organic mixture was dried over $MgSO_4$, which was filtered and the cake washed with excess DCM. The combined organic solvents were removed under reduced pressure to give a dark red solid this solid was purified via a recrystallization from ethanol.

The red solid was then combined with zinc powder (0.25 g, excess) and acetic acid (25 mL) in a 100 mL round bottomed flask and the reaction mixture was placed in a sonicator for 60 minutes. The red/brown suspension quickly turned to a clear yellow solution with a zinc precipitate. Water (100 mL) was added to the reaction mixture causing the product to precipitate out of solution. The resulting slurry was filtered, washed with water (3 x 100 mL) and the clear, colourless mother liquors discarded. The solid filtrate was then washed with DCM (150 mL) so as to dissolve the solid product, after which point the remaining zinc was filtered off. The mother liquors were dried over $MgSO_4$ and the slurry filtered and washed with DCM (50 mL). The solvent was removed under reduced pressure giving a bright yellow solid **14** (0.4 g, 0.7 mmol, 55 %).

^{1}H NMR (500 MHz, $CDCl_3$) δ = 10.08 (s, 2H), 7.28 – 7.24 (m, 2H), 7.05 – 7.00 (m, 2H), 6.98 (td, *J* = 7.5, 1.5 Hz, 2H), 6.47 – 6.42 (m, 2H), 4.21 (qd, *J* = 7.2, 2.1 Hz, 4H), 3.32 (h, *J* = 7.0 Hz, 2H), 1.83 (dq, *J* = 14.4, 7.0 Hz, 2H), 1.74 – 1.58 (m, 2H), 1.34 (s, 6H), 1.32 (s, 6H), 0.95 (td, *J* = 7.1, 0.8 Hz, 6H).

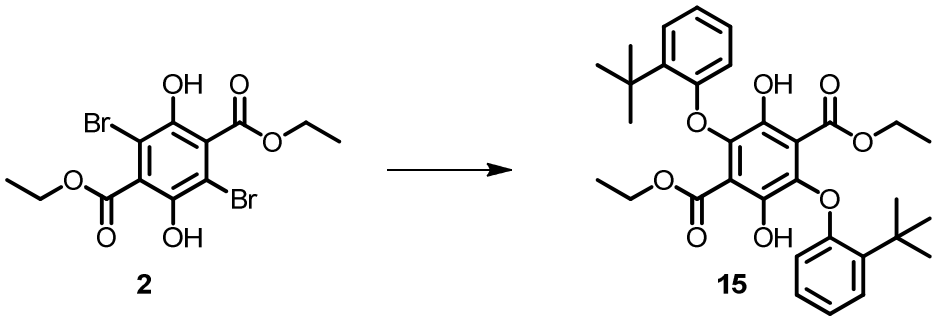

Compound **2** (0.5 g, 1.2 mmol), 2-tertbutylphenol (0.4 mL, 2.6 mmol, 2.1 eq), pyridine (0.5 mL, excess) and acetone (15 mL) was charged to a 100 mL round bottomed flask and refluxed for 10 minutes. The clear/ yellow suspension quickly turned dark red/ brown upon addition of pyridine and application of heat. The reaction mixture was diluted with water (100 mL) causing a dark brown precipitate to form. The precipitate was filtered off and washed with water, air dried and dissolved in DCM (100 mL). The organic mixture was dried over $MgSO_4$, which was filtered and the cake washed with excess DCM. The combined organic solvents were removed under reduced pressure to give a dark red solid this solid was purified via a recrystallization from ethanol.

The red solid was then combined with zinc powder (0.25 g, excess) and acetic acid (25 mL) in a 100 mL round bottomed flask and the reaction mixture was placed in a sonicator for 60 minutes. The red/brown suspension quickly turned to a clear yellow solution with a zinc precipitate. Water (100 mL) was added to the reaction mixture causing the product to precipitate out of solution. The resulting slurry was filtered, washed with water (3 x 100 mL) and the clear, colourless mother liquors discarded. The solid filtrate was then washed with DCM (150 mL) so as to dissolve the solid product, after which point the remaining zinc was filtered off. The mother liquors were dried over $MgSO_4$ and the slurry filtered and washed with DCM (50 mL). The solvent was removed under reduced pressure giving a bright yellow solid **15** (0.4 g, 0.7 mmol, 59 %).

^{1}H NMR (500 MHz, $CDCl_3$) δ = 10.09 (s, 1H), 10.04 (s, 1H), 7.39 (ddd, *J* = 7.8, 4.0, 1.7 Hz, 2H), 7.11 – 7.06 (m, 1H), 7.03 (ddd, *J* = 8.2, 7.2, 1.7 Hz, 2H), 6.96 (qd, *J* = 7.4, 1.3 Hz, 2H), 6.54 (dd, *J* = 8.1, 1.3 Hz, 1H), 6.49 (dd, *J* = 8.1, 1.3 Hz, 2H), 4.27 (dqd, *J* = 11.0, 7.1, 4.9 Hz, 2H), 4.14 (dqd, *J* = 10.8, 7.1, 1.1 Hz, 2H), 1.54 (s, 9H), 1.53 (s, 9H), 0.91 (td, *J* = 7.1, 1.3 Hz, 6H).

^{1}H NMR ($OCH_2\mathbf{CH_3}$ decoupled, 500 MHz, $CDCl_3$) δ = 10.09 (s, 1H), 10.04 (s, 1H), 7.39 (ddd, *J* = 7.8, 4.0, 1.7 Hz, 2H), 7.08 (td, *J* = 7.5, 1.6 Hz, 1H), 7.04 (ddd, *J* = 8.2, 7.2, 1.7 Hz, 2H), 6.96 (qd, *J* = 7.4, 1.3 Hz, 2H), 6.54 (dd, *J* = 8.1, 1.3 Hz, 1H), 6.49 (dd, *J* = 8.1, 1.3 Hz, 2H), 4.28 (dd, *J* = 11.0, 5.0 Hz, 2H), 4.20 – 4.09 (m, 2H), 1.55 (s, 9H), 1.54 (s, 9H), 0.91 (s, 6H).

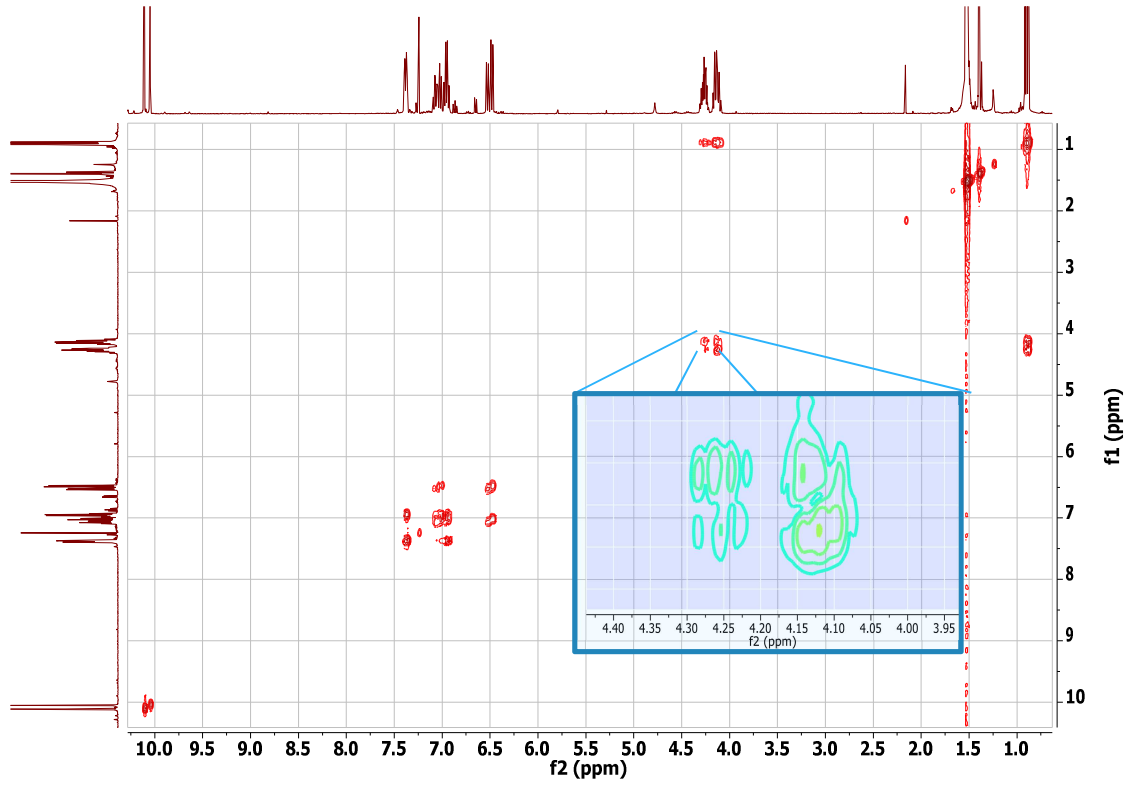

COSY

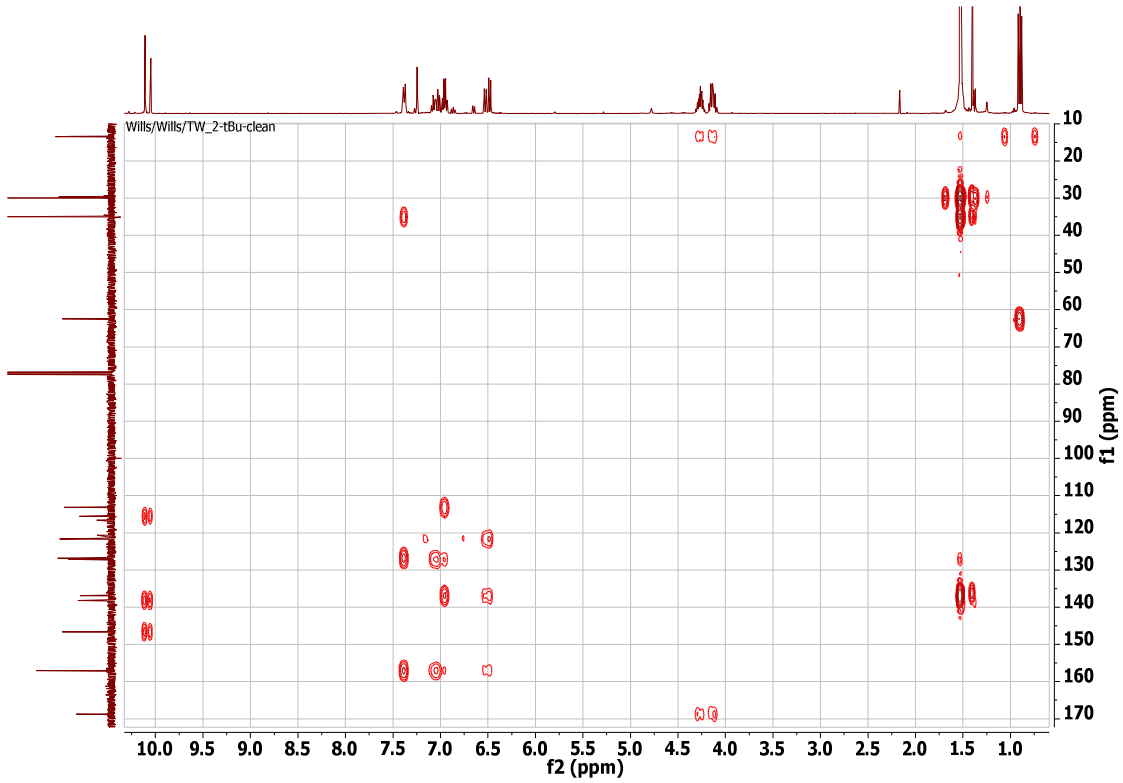

HMBC

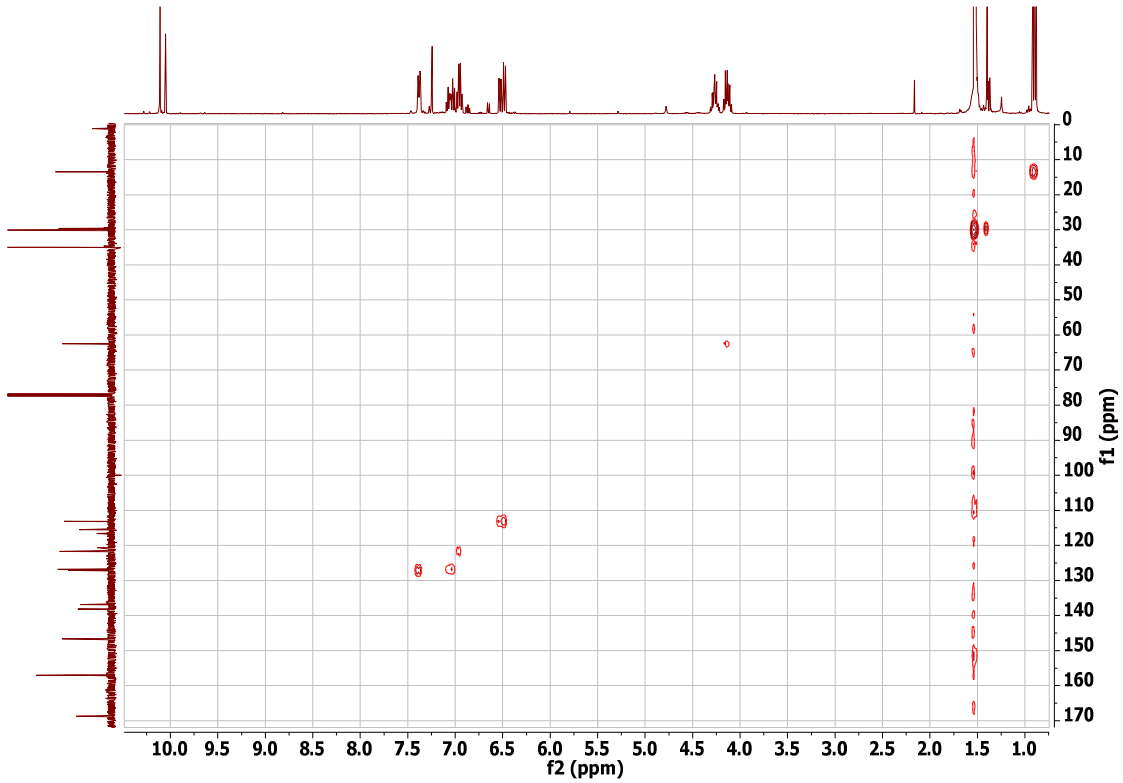

HMQC

MS = calc. for $C_{32}H_{38}O_8$ = 550 found. 551 $(M+H)^+$

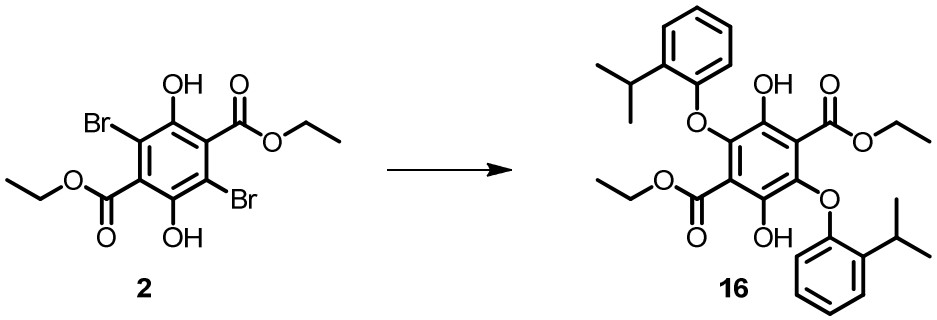

Compound **2** (0.5 g, 1.2 mmol), 2-isopropylphenol (0.3 g, 2.6 mmol, 2.1 eq), pyridine (0.5 mL, excess) and acetone (15 mL) was charged to a 100 mL round bottomed flask and refluxed for 10 minutes. The clear/ yellow suspension quickly turned dark red/ brown upon addition of pyridine and application of heat. The reaction mixture was diluted with water (100 mL) causing a dark brown precipitate to form. The precipitate was filtered off and washed with water, air dried and dissolved in DCM (100 mL). The organic mixture was dried over $MgSO_4$, which was filtered and the cake washed with excess DCM. The combined organic solvents were removed under reduced pressure to give a dark red solid this solid was purified via a recrystallization from ethanol.

The red solid was then combined with zinc powder (0.25 g, excess) and acetic acid (25 mL) in a 100 mL round bottomed flask and the reaction mixture was placed in a sonicator for 60 minutes. The red/brown suspension quickly turned to a clear yellow solution with a zinc precipitate. Water (100 mL) was added to the reaction mixture causing the product to precipitate out of solution. The resulting slurry was filtered, washed with water (3 x 100 mL) and the clear, colourless mother liquors discarded. The solid filtrate was then washed with DCM (150 mL) so as to dissolve the solid product, after which point the remaining zinc was filtered off. The mother liquors were dried over $MgSO_4$ and the slurry filtered and washed with DCM (50 mL). The solvent was removed under reduced pressure giving a bright yellow solid **16** (0.4 g, 0.6 mmol, 52 %).

^{1}H NMR (400 MHz, $CDCl_3$) δ = 10.19 (d, *J* = 1.0 Hz, 2H), 7.30 (ddd, *J* = 7.3, 2.0, 1.0 Hz, 2H), 7.02 (dddd, *J* = 8.4, 7.9, 2.0, 1.0 Hz, 2H), 6.97 (tt, *J* = 7.3, 1.2 Hz, 2H), 6.42 (dt, *J* = 7.9, 1.2 Hz, 2H), 4.19 (qd, *J* = 7.1, 1.0 Hz, 4H), 3.54 (hept, *J* = 7.1 Hz, 2H), 1.35 (dd, *J* = 7.1, 1.0 Hz, 12H), 0.92 (td, *J* = 7.1, 1.0 Hz, 6H).

^{13}C{H} NMR (101 MHz, $CDCl_3$) δ = 168.70, 155.62, 146.95, 138.68, 136.02, 126.33, 121.93, 115.07, 111.95, 62.48, 27.23, 22.60, 13.39.

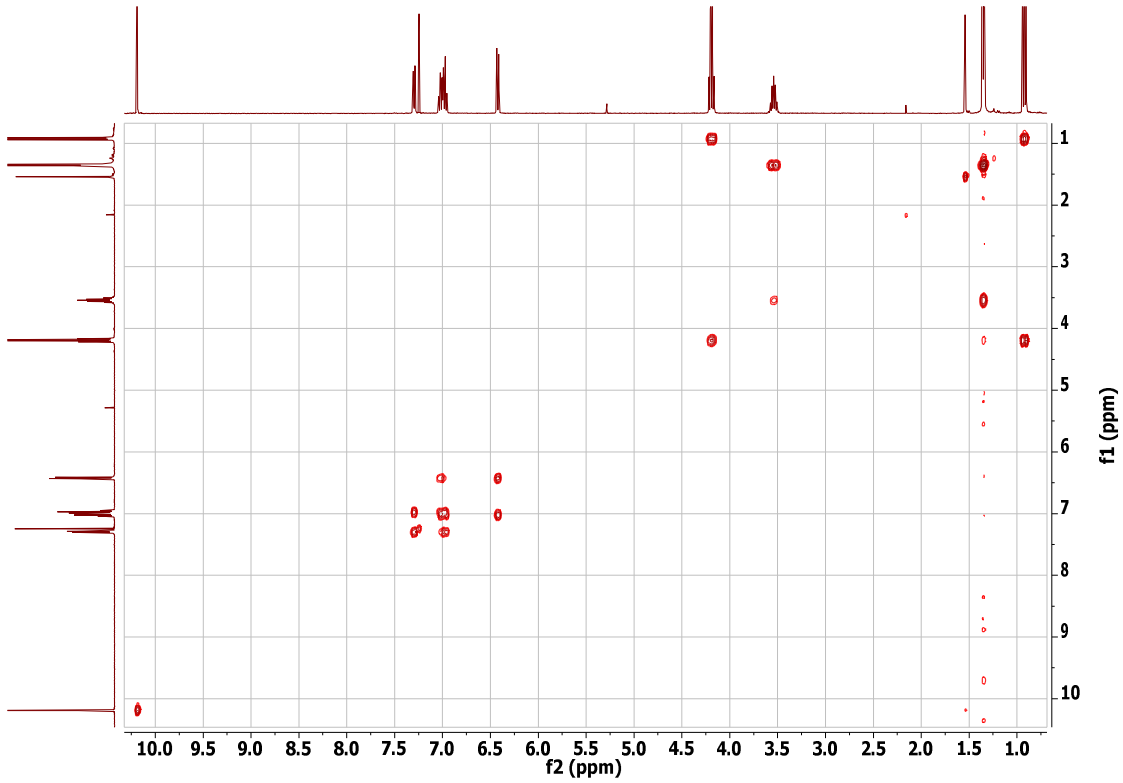

COSY

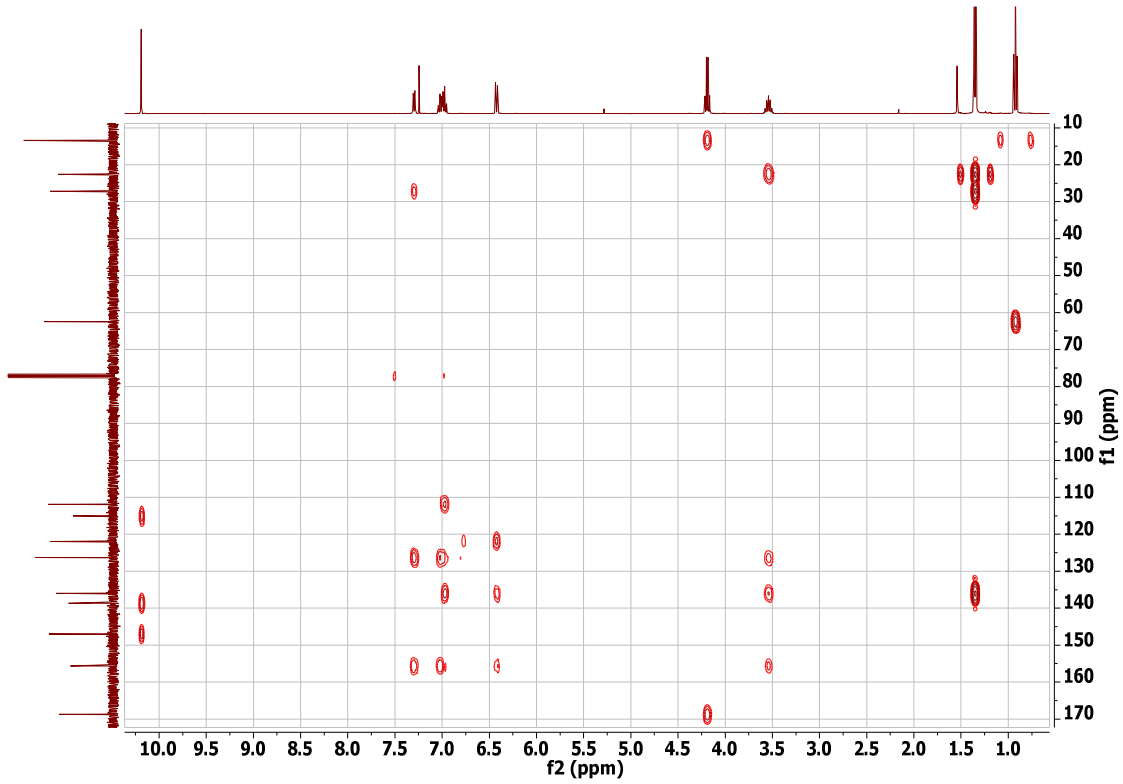

HMBC

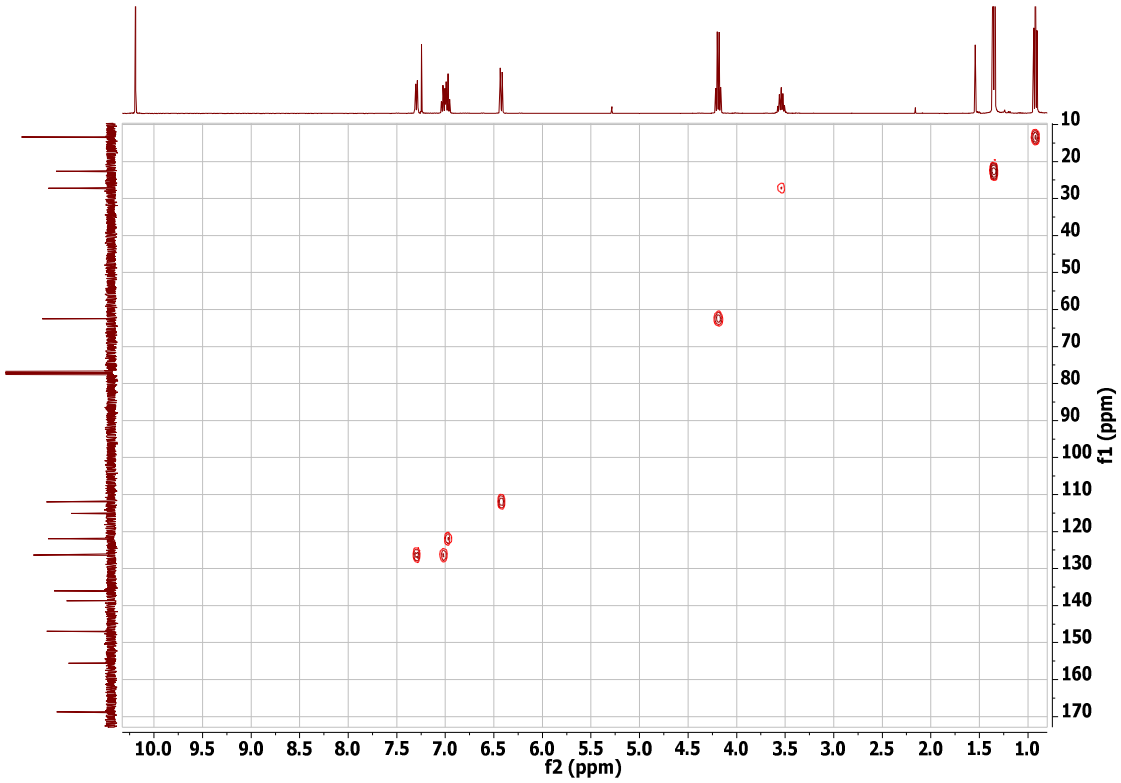

HMQC

MS = calc. for $C_{30}H_{34}O_8$ = 522 found. 523 $(M+H)^+$

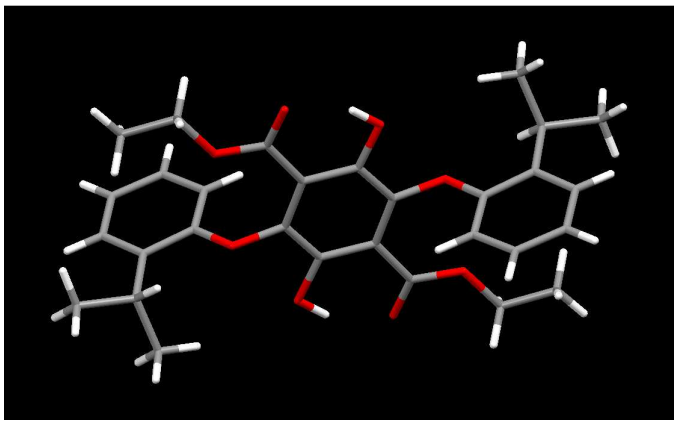

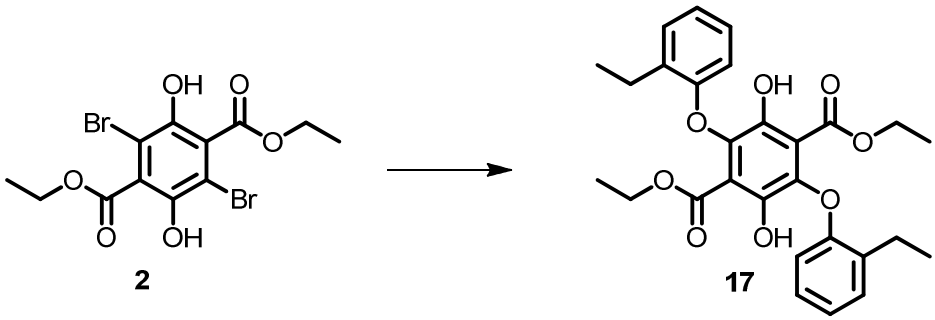

Compound **2** (0.25 g, 0.6 mmol), 2-ethylphenol (0.14 mL, 1.2 mmol), pyridine (0.25 mL, 3.1 mmol) and acetone (15 mL) was charged to a 100 mL round bottomed flask and refluxed for 10 minutes. The clear/ yellow suspension quickly turned dark red/ brown upon addition of pyridine and application of heat. The reaction mixture was diluted with water (100 mL) causing a precipitate to form. The precipitate was filtered off and washed with water, air dried and dissolved in DCM (100 mL). The organic mixture was dried over $MgSO_4$, which was filtered and the cake washed with excess DCM. The combined organic solvents were removed under reduced pressure to give a dark red solid this solid was purified via a recrystallization from ethanol.

The red solid was then combined with zinc powder (0.25 g, excess) and acetic acid (25 mL) in a 100 mL round bottomed flask and the reaction mixture was placed in a sonicator for 60 minutes. The red/brown suspension quickly turned to a clear yellow solution with a zinc precipitate. Water (100 mL) was added to the reaction mixture causing the product to precipitate out of solution. The resulting slurry was filtered, washed with water (3 x 100 mL) and the clear, colourless mother liquors discarded. The solid filtrate was then washed with DCM (150 mL) so as to dissolve the solid product, after which point the remaining zinc was filtered off. The mother liquors were dried over $MgSO_4$ and the slurry filtered and washed with DCM (50 mL). The solvent was removed under reduced pressure giving a bright yellow solid **17** (0.5 g, 1.0 mmol, 85 %).

^{1}H NMR (400 MHz, $CDCl_3$) δ = 9.84 (s, 2H), 7.22 (dd, *J* = 7.4, 1.7 Hz, 2H), 7.02 (td, *J* = 8.1, 1.7 Hz, 2H), 6.93 (td, *J* = 7.4, 1.1 Hz, 2H), 6.42 (dd, *J* = 8.1, 1.1 Hz, 2H), 4.18 (q, *J* = 7.1 Hz, 4H), 2.85 (q, *J* = 7.5 Hz, 4H), 1.33 (t, *J* = 7.5 Hz, 6H), 0.92 (t, *J* = 7.1 Hz, 6H).

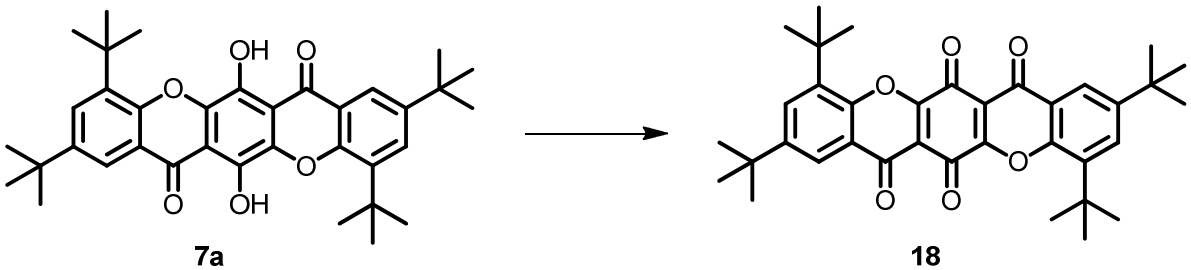

7a **18**

Compound **7a** (0.5 g, 0.9 mmol) was mixed with ethanol (10 mL) and the mixture stirred until homogeneous. Once a solution was formed HNO_3 (1 mL, excess) was added dropwise, causing a change in colour from dark red to orange. The reaction mixture was stirred at room temperature for 12 hours after which time it appeared as a clear yellow solution. The reaction mixture was combined with DCM (50 mL) then subjected to a basic aqueous work up with saturated Na_2CO_3 (3 x 30 mL). The organic layer was collected and dried over $MgSO_4$ and the solvent removed to give **18** (0.5 g, 0.9 mmol, 100%).

^{1}H NMR (300 MHz, $CDCl_3$) δ = 8.11 (d, *J* = 2.5 Hz, 2H), 7.78 (d, *J* = 2.5 Hz, 2H), 1.53 (s, 18H), 1.34 (s, 18H).

^{13}C NMR (126 MHz, $CDCl_3$) δ = 175.25, 174.07, 155.47, 151.69, 150.38, 140.85, 130.85, 126.30, 120.70, 114.59, 35.69, 35.39, 31.35, 30.28.

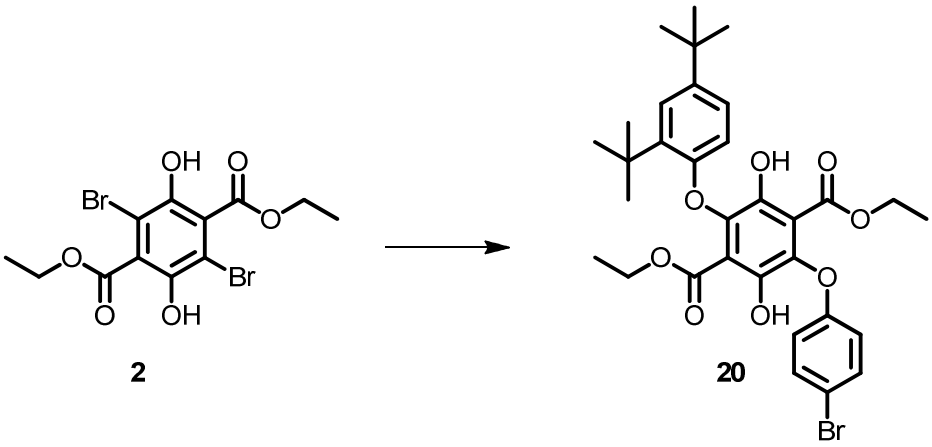

Compound **2** (1.0 g, 2.4 mmol), 2,4-ditertbutylphenol (0.5 g, 2.5 mmol, 1.1 eq), 4-bromophenol (0.4 mL, 2.4 mmol, 1.0 eq) pyridine (0.5 mL, excess) and acetone (15 mL) was charged to a 100 mL round bottomed flask and refluxed for 10 minutes. The clear/ yellow suspension quickly turned dark red/ brown upon addition of pyridine and application of heat. The reaction mixture was diluted with water (100 mL) causing a dark brown precipitate to form. The precipitate was filtered off and washed with water, air dried and dissolved in DCM (100 mL). The organic mixture was dried over $MgSO_4$, which was filtered and the cake washed with excess DCM. The combined organic solvents were removed under reduced pressure to give a dark red solid this solid was purified via column chromatography (DCM : Petrol [1:1] – gradient). The like fractions were combined and the solvent removed to give the desired product as a dark red solid **19** (0.6 g, 0.91 mmol, 38%) and the bis-(4-bromophenol) substituted product – also a dark red solid (0.5 g, 0.93 mmol, 39 %). There was no sign of the bis-(2,4-ditertbutylphenol) substituted product.

The isolated product, **19**, was then combined with zinc powder (0.25 g, excess) and acetic acid (25 mL) in a 100 mL round bottomed flask and the reaction mixture was placed in a sonicator for 60 minutes. The red/brown suspension quickly turned to a clear yellow solution with a zinc precipitate. Water (100 mL) was added to the reaction mixture causing the product to precipitate out of solution. The resulting slurry was filtered, washed with water (3 x 100 mL) and the clear, colourless mother liquors discarded. The solid filtrate was then washed with DCM (150 mL) so as to dissolve the solid product, after which point the remaining zinc was filtered off. The mother liquors were dried over $MgSO_4$ and the slurry filtered and washed with DCM (50 mL). The solvent was

removed under reduced pressure giving a bright yellow solid **20** (0.6 g, 0.9 mmol, 100 %).

^{1}H NMR (300 MHz, $CDCl_3$) δ = 10.29 (s, 1H), 10.14 (d, *J* = 0.5 Hz, 1H), 7.40 – 7.37 (m, 1H), 7.02 (d, *J* = 2.4 Hz, 1H), 7.00 (d, *J* = 2.4 Hz, 1H), 6.77 (d, *J* = 0.5 Hz, 1H), 6.75 (d, *J* = 0.5 Hz, 1H), 6.34 (s, 1H), 6.32 (s, 1H), 4.30 (dq, *J* = 10.9, 7.1 Hz, 1H), 4.21 (q, *J* = 7.1 Hz, 2H), 4.12 (dq, *J* = 10.9, 7.1 Hz, 1H), 1.52 (s, 9H), 1.28 (s, 9H), 1.13 – 0.98 (m, 3H), 0.85 (t, *J* = 7.1 Hz, 3H).

^{13}C{H} NMR (101 MHz, $CDCl_3$) δ = 168.73, 168.35, 157.51, 154.70, 147.25, 146.60, 143.98, 139.32, 137.43, 135.74, 132.36, 124.23, 123.26, 116.56, 115.47, 114.75, 114.58, 114.15, 113.02, 112.12, 62.65, 62.59, 35.19, 34.42, 31.69, 30.06, 13.69, 13.20.

MS = calc. for $C_{32}H_{37}O_8Br$ = 628 found. 629 $(M+H)^+$

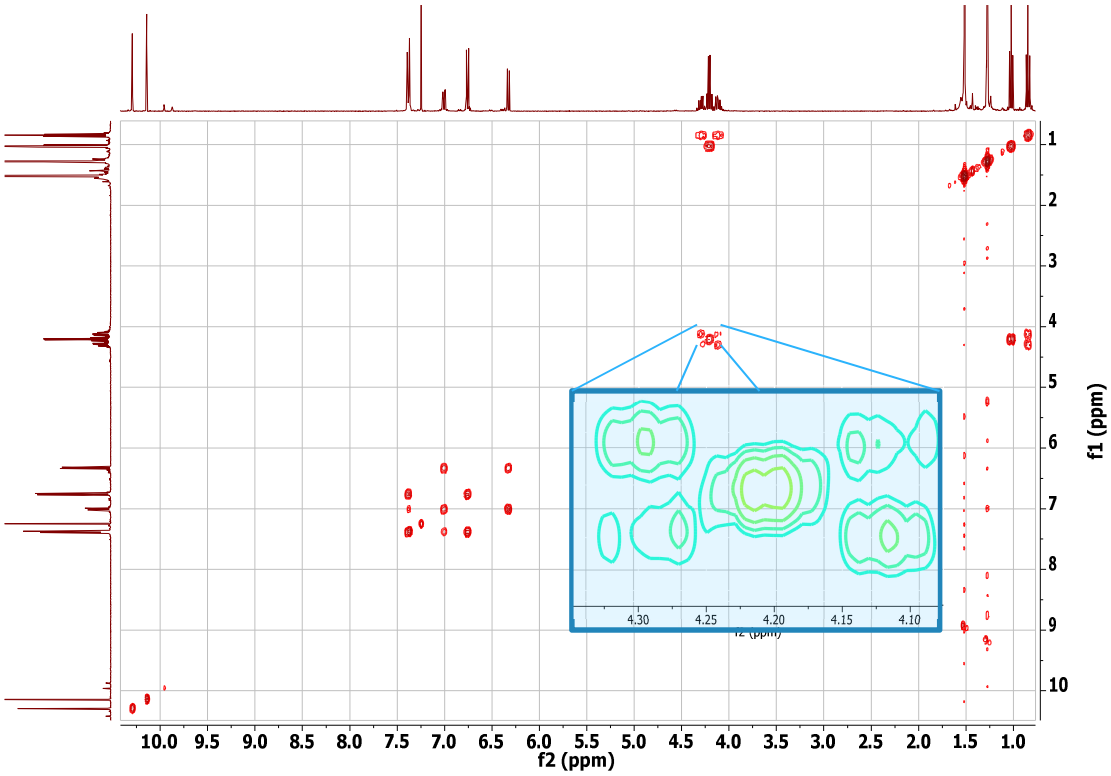

COSY

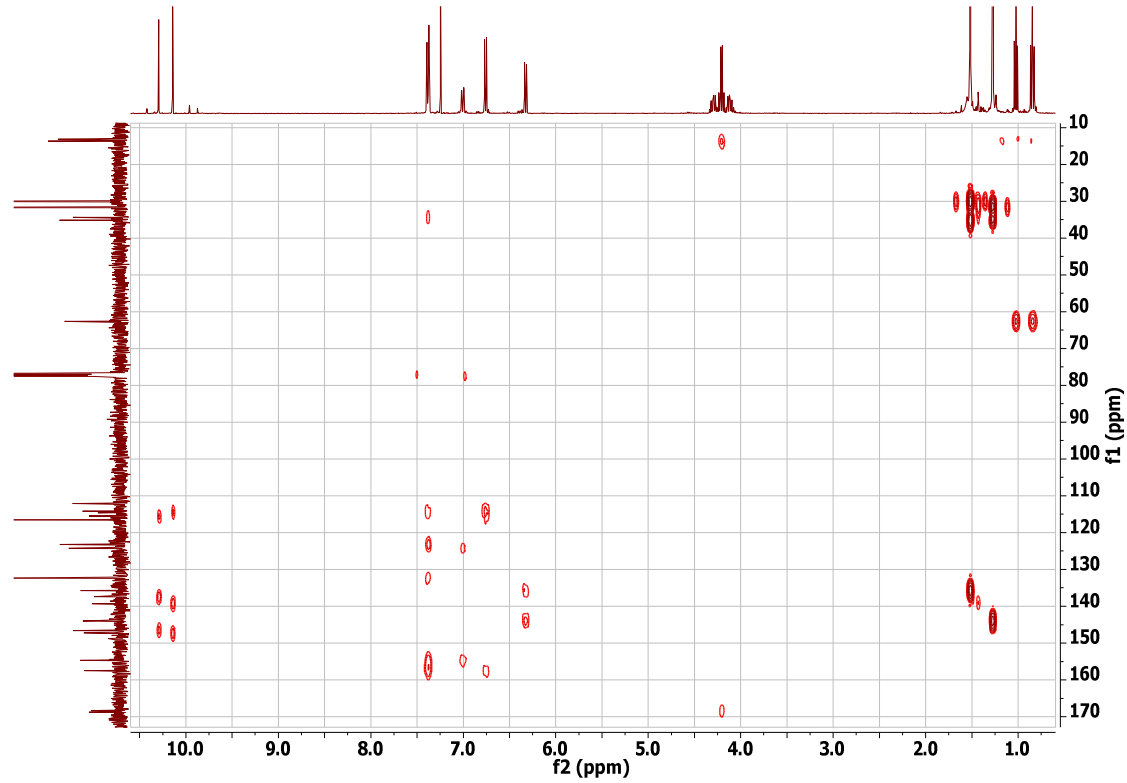
10
20
30
40
50
60
70
80
90
100
110
120
130
140
150
160
170
f1 (ppm)
10.0
9.0
8.0
7.0
6.0
5.0
4.0
3.0
2.0
1.0
f2 (ppm)

HMBC

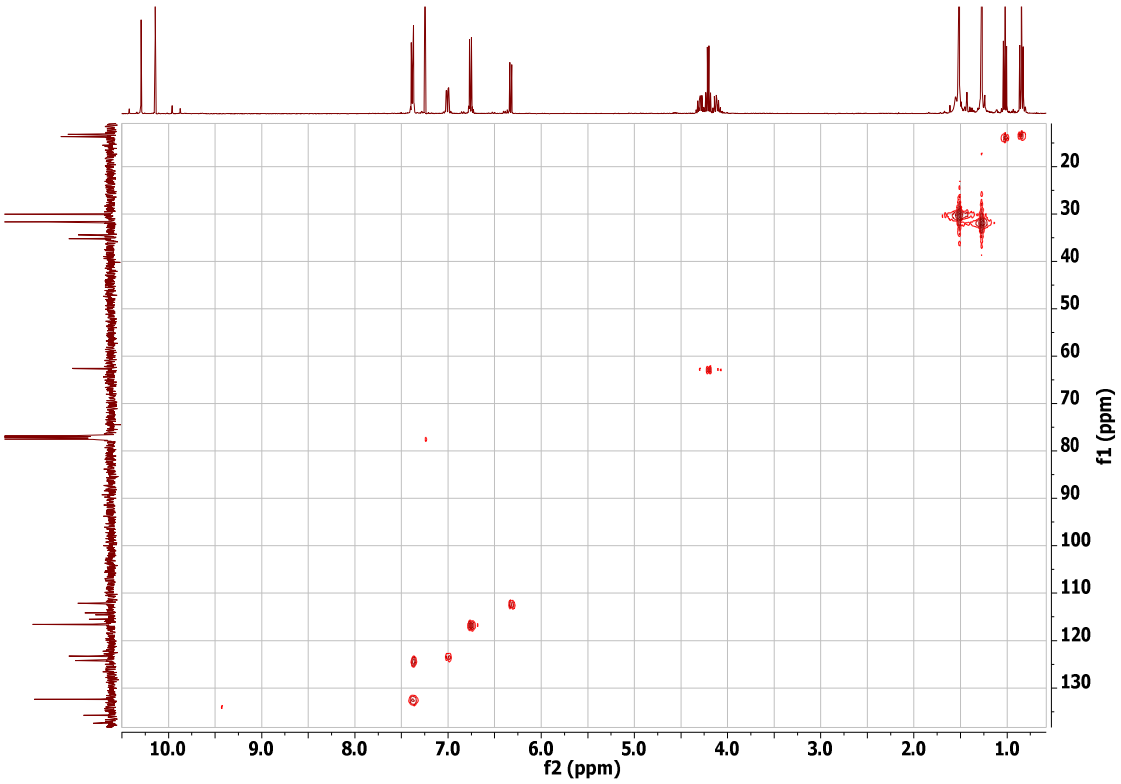
20
30
40
50
60
70
80
90
100
110
120
130
f1 (ppm)
10.0
9.0
8.0
7.0
6.0
5.0
4.0
3.0
2.0
1.0
f2 (ppm)

HMQC

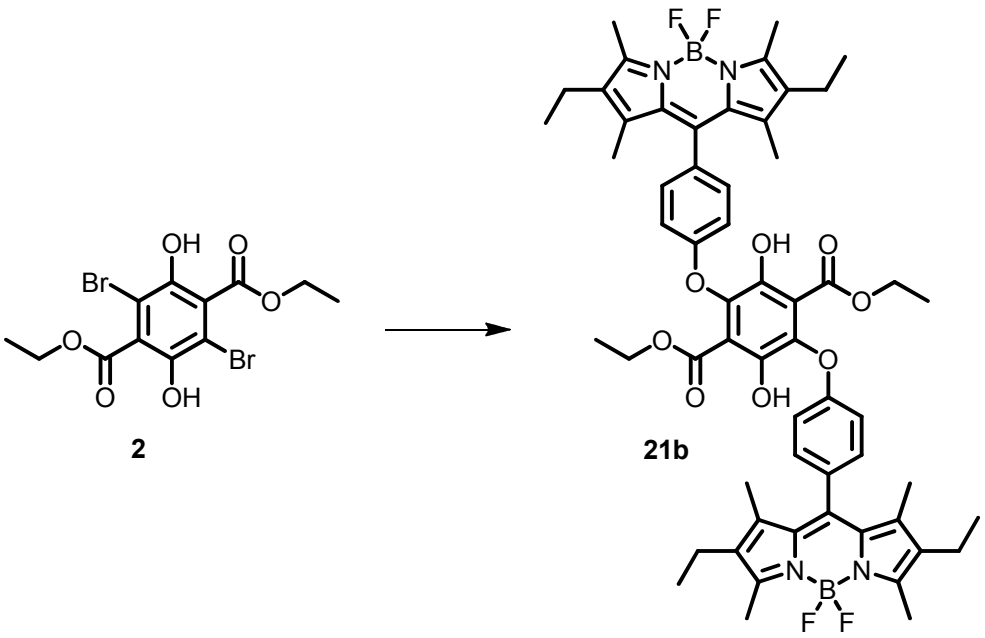

Compound **2** (0.12 g, 0.3 mmol), 2,6-Diethyl-4,4-difluoro-1,3,5,7-tetramethyl-8-[4-(hydroxy)phenyl]-4-bora-3a,4a-diaza-s-indacene (0.3g, 0.7 mmol, 2.4 eq), pyridine (0.5 mL, excess) and acetone (15 mL) was charged to a 100 mL round bottomed flask and refluxed for 10 minutes. The clear/ yellow suspension quickly turned dark red/ brown upon addition of pyridine and application of heat. The reaction mixture was diluted with water (100 mL) causing a dark brown precipitate to form. The precipitate was filtered off and washed with water, air dried and dissolved in DCM (100 mL). The organic mixture was dried over $MgSO_4$, which was filtered and the cake washed with excess DCM. The combined organic solvents were removed under reduced pressure to give a dark red solid this solid was purified via a recrystallization from ethanol.

The red solid, **21a**, was then combined with zinc powder (0.25 g, excess) and acetic acid (25 mL) in a 100 mL round bottomed flask and the reaction mixture was placed in a sonicator for 60 minutes. The red/brown suspension quickly orange-fluorescent solution with a zinc precipitate. Water (100 mL) was added to the reaction mixture causing the product to precipitate out of solution. The resulting slurry was filtered, washed with water (3 x 100 mL) and the clear, colourless mother liquors discarded. The solid filtrate was then washed with DCM (150 mL) so as to dissolve the solid product, after which point the remaining zinc was filtered off. The mother liquors were dried over $MgSO_4$ and the slurry filtered and washed with DCM (50 mL). The solvent was removed and

the product purified via column chromatography (DCM – 100%) giving **21b** a red / orange solid (0.3 g, 0.3 mmol, 99 %).

^{1}H NMR (400 MHz, $CDCl_3$) δ = 10.41 (d, *J* = 1.7 Hz, 2H), 7.25 – 7.10 (m, 4H), 6.98 (dd, *J* = 8.5, 2.0 Hz, 4H), 4.28 (qd, *J* = 6.9, 1.9 Hz, 4H), 2.51 (s, 12H), 2.37 – 2.19 (m, 6H), 1.35 (s, 12H), 1.26 – 1.16 (m, 8H), 1.07 – 0.87 (m, 12H).

^{13}C{H} NMR (101 MHz, $CDCl_3$) δ = 168.75, 158.59, 153.81, 147.27, 139.83, 138.68, 138.30, 132.85, 131.15, 129.60, 129.38, 115.52, 114.56, 62.83, 17.17, 14.72, 13.93, 12.58, 11.91.

^{11}B NMR (128 MHz, $CDCl_3$) δ = -0.15 (t, *J* = 33.7 Hz).

^{19}F NMR (376 MHz, $CDCl_3$) δ = -145.52 – -145.86 (m).

MS = calc. for $C_{58}H_{64}O_8B_2N_2F_4$ = 1041 found. 1041 (M^+)

5.4.2. Chapter 3

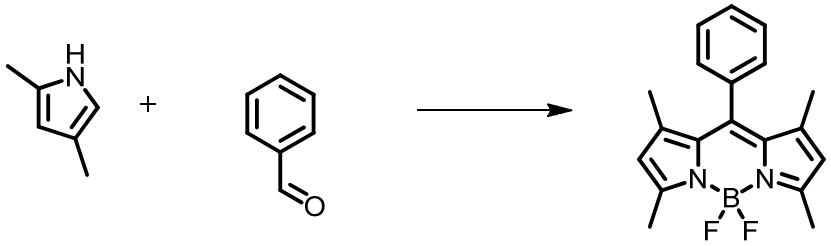

22

A 500 mL round bottomed flask was charged with DCM (250 mL), and purged with N_2 for 1 h. To the flask were added benzaldehyde (0.6 mL, 5.1 mmol), 2,4-dimethylpyrrole (1.1 mL, 10.7 mmol), TFA (3 drops), and the reaction mixture was stirred at room temperature until all the aldehyde was consumed. Upon completion of the reaction DDQ (1.2 g, 5.1 mmol) was added, and the reaction mixture was stirred at room temperature for 12 h. After this time, N,N-diisopropylethylamine (5.0 mL, 29.1 mmol) and $BF_3.Et_2O$ (5.0 mL, 40.8 mmol) were added and the reaction mixture was monitored by tlc until reaction appears complete. The organic solvent mixture was extracted with water (3 x 100 mL) and brine (200 mL). The aqueous layer was backwashed with DCM (100 mL), and the organic portions were combined and dried over $MgSO_4$. After filtration the solvent was removed under reduced pressure. The crude product was purified via column chromatography (silica gel, DCM: petrol gradient elution) to give a red solid, **22**, yield: 190 mg, 0.45 mmol, 9%.

^{1}H NMR (400 MHz, DMSO-d_6) δ = 7.51 (dd, J = 5.1, 1.9 Hz, 2H), 7.33 – 7.29 (m, 2H), 6.21 – 6.05 (m, 1H), 3.30 (s, 2H), 2.41 (s, 6H), 1.28 (s, 6H).

^{13}C{H} NMR (100 MHz, DMSO-D_6) δ = 155.38, 143.25, 142.46, 134.52, 131.21, 129.80, 129.69, 128.23, 121.90, 14.74, 14.45.

^{11}B{H} NMR ($CDCl_3$, 75 MHz): δ = -0.18 (t, J = 33.0 Hz)

^{19}F NMR ($CDCl_3$, 75 MHz): δ = -146.18 (q , J =33.0 Hz, 2F)

MP = 237 ^{o}C

Values measured agree with those seen in the literature.

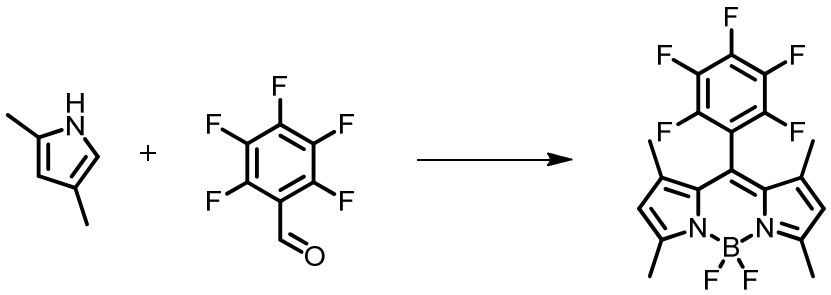

23

A 500 mL round bottomed flask was charged with DCM (250 mL), and purged with N_2 for 1 h. To the flask were added 2,3,4,5,6-pentafluorobenzaldehyde (0.6 mL, 5.1 mmol), 2,4-dimethylpyrrole (1.1 mL, 10.7 mmol), TFA (3 drops), and the reaction mixture was stirred at room temperature until all the aldehyde was consumed. Upon completion of the reaction DDQ (1.2 g, 5.1 mmol) was added, and the reaction mixture was stirred at room temperature for 12 h. After this time, N,N-diisopropylethylamine (5.0 mL, 29.1 mmol) and $BF_3.Et_2O$ (5.0 mL, 40.8 mmol) were added and the reaction mixture was monitored by tlc until reaction appears complete. The organic solvent mixture was extracted with water (3 x 100 mL) and brine (200 mL). The aqueous layer was backwashed with DCM (100 mL), and the organic portions were combined and dried over $MgSO_4$. After filtration the solvent was removed under reduced pressure. The crude product was purified via column chromatography (silica gel, DCM: petrol gradient elution) to give a red solid, **23**, yield: 190 mg, 0.45 mmol, 9%.

^{1}H NMR ($CDCl_3$, 400 MHz): δ = 6.05 (s, 2H), 2.56 (s, 6H), 1.60 (s, 6H).

^{13}C{H} NMR ($CDCl_3$, 100 MHz): δ = 157.86, 145.09, 143.09, 143.08 141.59, 139.34, 137.25, 131.07, 122.82, 122.33, 109.60, 14.85, 13.65.

^{11}B{^{1}H} NMR ($CDCl_3$, 125 MHz): δ = 20.29 (t, J = 33.2 Hz).

^{19}F NMR ($CDCl_3$, 400 MHz): δ = -139.14 (2F), -146.10 (2F), -150.37 (1F), -159.56 (2F).

^{13}C – ^{19}F HSQC NMR spectrum

IR - 2923 (C–H), 1540, 1496 (C=C, C=N), 1160 cm^{-1} (B–F).

MP = 237 ^{o}C.

MS - calc. for $C_{19}H_{14}F_7N_2B$ = 414.1 found. 414.1 (M^+)

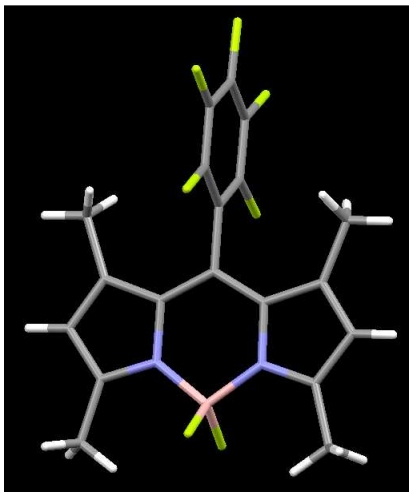

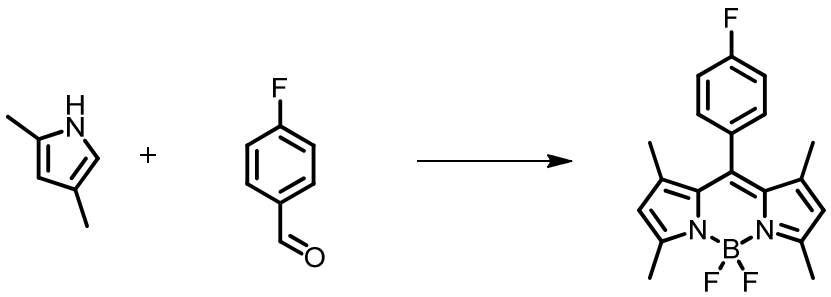

24

A 500 mL round bottomed flask was charged with DCM (250 mL), and purged with N_2 for 1 h. To the flask were added 4-fluorobenzaldehyde (0.9 mL, 8.1 mmol), 2,4-dimethylpyrrole (1.8 mL, 17.0 mmol), TFA (3 drops), and the reaction mixture was stirred at room temperature until all the aldehyde was consumed. Upon completion of the reaction DDQ (2.0 g, 8.9 mmol) was added, and the reaction mixture was stirred at room temperature for 12 h. After this time, N,N-diisopropylethylamine (8.1 mL, 48.3 mmol) and $BF_3.Et_2O$ (8.1 mL, 64.4 mmol) were added and the reaction mixture was monitored by tlc until reaction appears complete. The organic solvent mixture was extracted with water (3 x 100 mL) and brine (200 mL). The aqueous layer was backwashed with DCM (100 mL), and the organic portions were combined and dried over $MgSO_4$. After filtration the solvent was removed under reduced pressure. The crude product was purified via column chromatography (silica gel, DCM: petrol gradient elution) to give a red solid, **24**, yield: 275 mg, 0.8 mmol, 10%.

^{1}H NMR ($CDCl_3$, 296K, 500. MHz): δ = 7.26 (m, $^3J_{HH}$ = 8.3 Hz, $^4J_{HH}$ = 2.2 Hz, 2H). 7.19 (m, $^3J_{HF}$ = 8.6 Hz, $^3J_{HH}$ = 8.3 Hz, $^4J_{HH}$ = 2.2 Hz, 2H), 5.98 (s, 2H), 2.55 (s, 6H), 1.40 (s, 6H),

^{13}C{H} NMR ($CDCl_3$, 296K, 125. MHz): δ = 14.60, 14.67 (t, $^4J_{CF}$ = 2.3 Hz), 116.47 (d, $^2J_{CF}$ = 21.6 Hz), 121.48 (m), 130.04 (d, $^3J_{CF}$ = 8.1 Hz), 131.00 (d, $^4J_{CF}$ = 3.5 Hz), 131.61 (br s), 140.54, 143.05, 155.87, 163.25 (d, $^1J_{CF}$ = 248 Hz).

^{11}B{^{1}H} NMR ($CDCl_3$, 296K, 160 MHz): δ = 0.20 (t, $^1J_{BF}$ = 32.6 Hz).

^{19}F NMR ($CDCl_3$, 296K, 500 MHz): δ = -146.13 (q, $^1J_{FB}$ = 32.6 Hz, 2F), -111.76 (m, $^3J_{FH}$ = 8.4 Hz, $^4J_{FH}$ = 5.3 Hz, 1F).

MP = 156–158 ^{o}C.

MS - calc. for $C_{19}H_{18}BF_3N_2$ = 342, found. 365 (M + Na^+), 707 (2 M + Na^+).

IR = 2926 (C–H), 1547, 1508 (C=C, C=N), 1186 cm^{-1} (B–F).

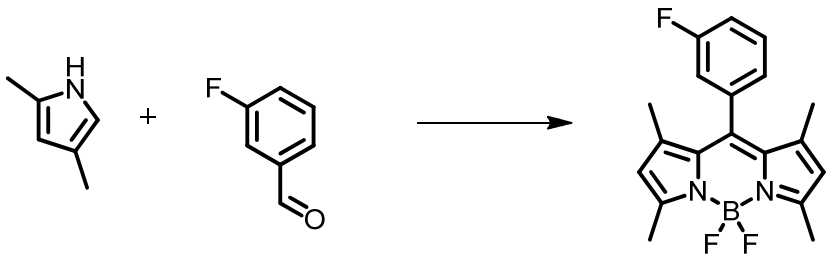

25

A 500 mL round bottomed flask was charged with DCM (250 mL), and purged with N_2 for 1 h. To the flask were added 3-fluorobenzaldehyde (0.9 mL, 8.1 mmol), 2,4-dimethyl pyrrole (1.8 mL, 17.0 mmol), TFA (3 drops), and the reaction mixture was stirred at room temperature until all the aldehyde was consumed. Upon completion of the reaction DDQ (2.0 g, 8.9 mmol) was added, and the reaction mixture was stirred at room temperature for 12 h. After this time, N,N-diisopropylethylamine (8.1 mL, 48.3 mmol) and $BF_3.Et_2O$ (8.1 mL, 64.4 mmol) were added and the reaction mixture was monitored by tlc until reaction appears complete. The organic solvent mixture was extracted with water (3 x 100 mL) and brine (200 mL). The aqueous layer was backwashed with DCM (100 mL), and the organic portions were combined and dried over $MgSO_4$. After filtration the solvent was removed under reduced pressure. The crude product was purified via column chromatography (silica gel, DCM: petrol gradient elution) to give a red solid, **25**, yield: 305 mg, 0.9 mmol, 11%.

^{1}H NMR ($CDCl_3$, 400 MHz): δ = 7.46 (td, J = 8.0, 5.8 Hz, 1H), 7.17 (tdd, J = 8.9, 2.8, 1.1 Hz, 1H), 7.08 (dt, J = 7.6, 1.5 Hz, 1H), 7.02 (ddd, J = 8.9, 2.6, 1.5 Hz, 1H), 5.93 (s, 2H), 2.49 (s, 6H), 1.35 (s, 6H).

^{13}C{H} NMR ($CDCl_3$, 100 MHz): δ = 164.35, 162.37, 156.05, 143.01, 139.71, 137.14, 131.04, 124.11, 121.55, 116.02, 115.57, 14.69, 14.44.

^{11}B{^{1}H} NMR ($CDCl_3$, 128 MHz): δ = -0.22 (t, *J* = 33.2 Hz).

^{19}F NMR ($CDCl_3$, 400 MHz): δ = -111.38 (1F), -146.17 (2F).

MP = 170–172 ^{o}C.

MS calc. for $C_{19}H_{18}BF_3N_2$ = 342, found. 365 ($M + Na^+$), 707 ($2M + Na^+$).

IR = 2929 (C–H), 1540, 1505 (C=C, C=N), 1185 cm^{-1} (B–F).

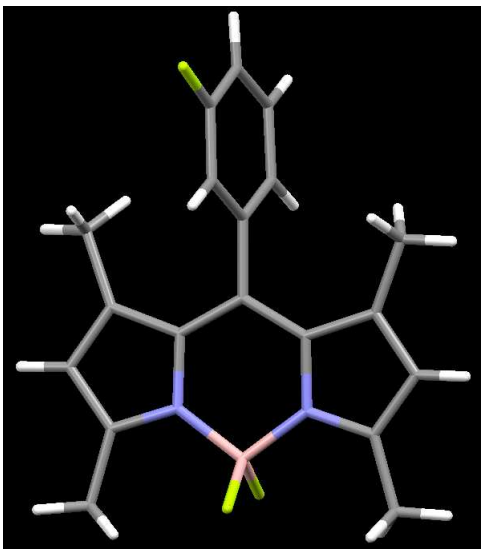

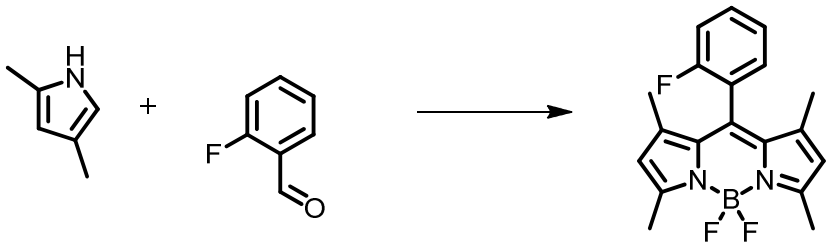

26

A 500 mL round bottomed flask was charged with DCM (250 mL), and purged with N_2 for 1 h. To the flask were added 2-fluorobenzaldehyde (0.9 mL, 8.1 mmol), 2,4-dimethylpyrrole (1.8 mL, 17.0 mmol), TFA (3 drops), and the reaction mixture was stirred at room temperature until all the aldehyde was consumed. Upon completion of the reaction DDQ (2.0 g, 8.9 mmol) was added, and the reaction mixture was stirred at room temperature for 12 h. After this time, N,N-diisopropylethylamine (8.1 mL, 48.3 mmol) and $BF_3.Et_2O$ (8.1 mL, 64.4 mmol) were added and the reaction mixture was monitored by tlc until reaction appears complete. The organic solvent mixture was extracted with water (3 x 100 mL) and brine (200 mL). The aqueous layer was backwashed with DCM (100 mL), and the organic portions were combined and dried over $MgSO_4$. After filtration the solvent was removed under reduced pressure. The crude product was purified via column chromatography (silica gel, DCM: petrol gradient elution) to give a red solid, **26**, yield: 394 mg, 1.2 mmol, 15%.

^{1}H NMR ($CDCl_3$, 400 MHz): δ = 7.46–7.37 (m, 1H), 7.21 (dd, J = 6.1, 1.7 Hz, 2H), 7.13 (t, J = 8.9 Hz, 1H), 5.93 (s, 2H), 2.49 (s, 6H), 1.39 (s, 6H).

^{13}C{H} NMR ($CDCl_3$, 100 MHz): δ = 189.76, 160.42, 157.96, 142.74, 134.63, 131.43, 130.47, 125.12, 122.79, 122.62, 116.53, 14.70, 13.86.

^{11}B{^{1}H} NMR ($CDCl_3$, 125 MHz): δ = -0.19 (t, J = 32.9 Hz)

^{19}F NMR ($CDCl_3$, 75 MHz): δ = -114.36 (1F), -146.16 (2F).

MP = 175–176 ^{o}C.

MS calc. for $C_{19}H_{18}BF_3N_2$ = 342, found. 365 ($M + Na^+$), 707 ($2M + Na^+$).

IR = 2979 (C–H) 1545, 1509 (C=C, C=N), 1187 cm^{-1} (B–F).

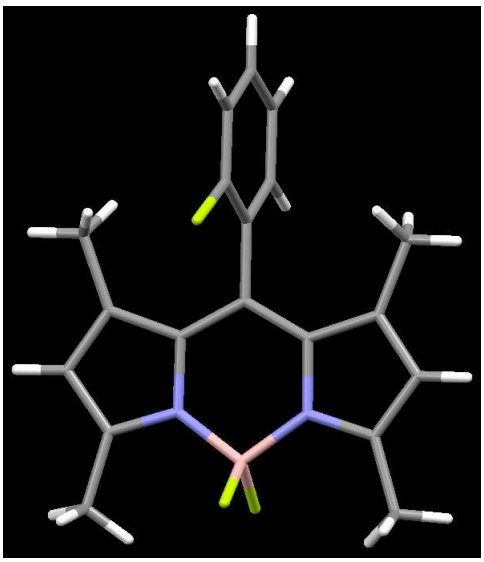

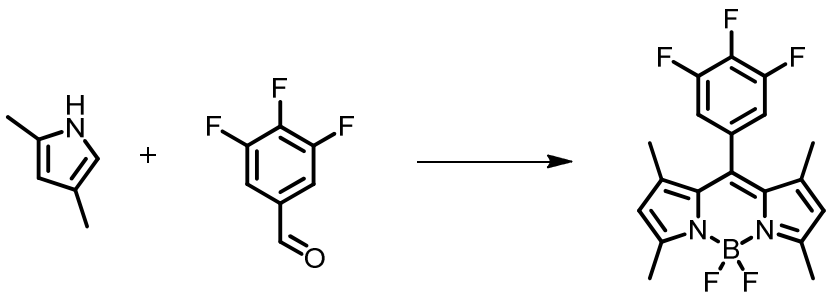

27

A 500 mL round bottomed flask was charged with DCM (250 mL), and purged with N_2 for 1 h. To the flask were added 3,4,5-trifluorobenzoyl chloride (0.3 mL, 2.6 mmol), 2,4-dimethylpyrrole (0.6 mL, 5.5 mmol), TFA (3 drops), and the reaction mixture was stirred at room temperature until all of the acid chloride was consumed. After this time, N,N-diisopropylethylamine (2.1 mL, 12.6 mmol) and $BF_3.Et_2O$ (2.1 mL, 16.8 mmol) were added and the reaction mixture was monitored by tlc until reaction appears complete. The organic solvent mixture was extracted with water (3 x 100 mL) and brine (200 mL). The aqueous layer was backwashed with DCM (100 mL), and the organic portions were combined and dried over $MgSO_4$. After filtration the solvent was removed under reduced pressure. The crude product was purified via column chromatography (silica gel, DCM: petrol [1:1]) to give a red solid, **27**, yield: 243 mg, 0.65 mmol, 25%.

^{1}H NMR ($CDCl_3$, 400 MHz): δ = 6.92 (t, J = 6.9 Hz, 2H), 5.95 (s, 2H), 2.48 (s, 6H), 1.43 (s, 6H).

^{13}C{H} NMR ($CDCl_3$, 100 MHz): δ = 156.85, 150.73, 142.57, 141.73, 141.58, 139.20, 138.89, 137.14, 130.93, 121.93, 113.28, 14.73, 14.67.

^{11}B{^{1}H} NMR ($CDCl_3$, 125 MHz): δ = -0.30 (t, *J* = 32.9 Hz).

^{19}F NMR ($CDCl_3$, 400 MHz): δ = -131.85 (1F), -146.12 (2F), -158.37 (2F).

MP = 181–182 ^{o}C.

MS calc. for $C_{19}H_{16}BF_5N_2$ = 378, found. 378 (M+).

IR = 2929 (C–H), 1550, 1511(C=C, C=N), 1189 cm^{-1} (B–F).

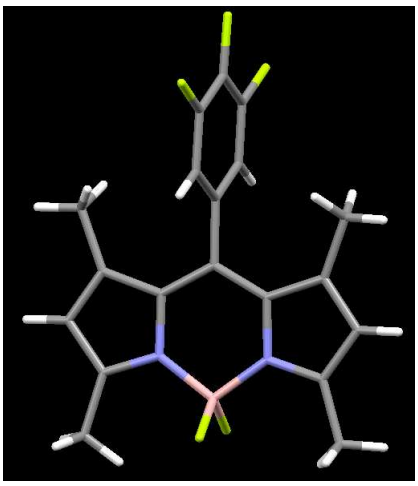

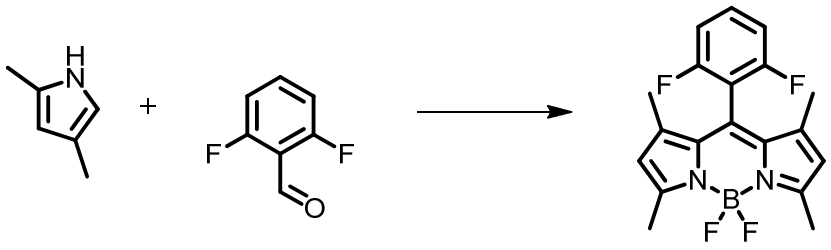

28

A 500 mL round bottomed flask was charged with DCM (250 mL), and purged with N_2 for 1 h. To the flask were added 2,6-difluorobenzaldehyde (0.8 mL, 7.0 mmol), 2,4-dimethyl pyrrole (1.5 mL, 14.8 mmol), TFA (3 drops), and the reaction mixture was stirred at room temperature until all the aldehyde was consumed. Upon completion of the reaction DDQ (1.8 g, 7.7 mmol) was added, and the reaction mixture was stirred at room temperature for 12 h. After this time, N,N-diisopropylethylamine (7.1 mL, 48.3 mmol) and $BF_3.Et_2O$ (7.1 mL, 64.4 mmol) were added and the reaction mixture was monitored by tlc until reaction appears complete. The organic solvent mixture was extracted with water (3 x 100 mL) and brine (200 mL). The aqueous layer was backwashed with DCM (100 mL), and the organic portions were combined and dried over $MgSO_4$. After filtration the solvent was removed under reduced pressure. The crude product was purified via column chromatography (silica gel, DCM: petrol gradient elution) to give a red solid, **28**, yield:, 0.7 mmol, 10%.

^{1}H NMR ($CDCl_3$, 400 MHz): δ = 7.56–7.35 (m, 1H), 7.13–6.94 (m, 2H), 6.00 (s, 2H), 2.55 (s, 6H), 1.54 (s, 6H).

^{13}C{H} NMR ($CDCl_3$, 100 MHz): δ = 161.05, 158.57, 156.55, 142.19, 131.67, 131.57, 131.33, 127.37, 121.66, 112.31, 112.06, 14.76, 13.40.

^{11}B{^{1}H} NMR ($CDCl_3$, 125 MHz): δ = -0.22 (t, J = 31.0 Hz).

^{19}F NMR ($CDCl_3$, 400 MHz): δ = -110.20–112.68 (m, 3F), -146.0 (2F).

MP = 240 ^{o}C.

MS calc. for $C_{19}H_{17}BF_4N_2$ = 360, found. 360 (M+).

IR = 2929 (C–H), 1547, 1508 (C=C, C=N), 1186 cm^{-1} (B–F).

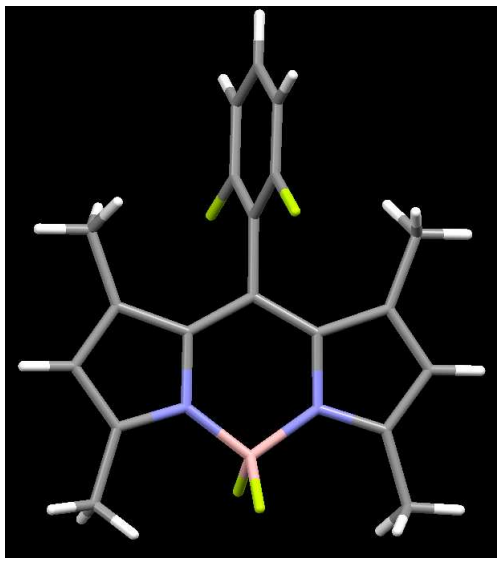

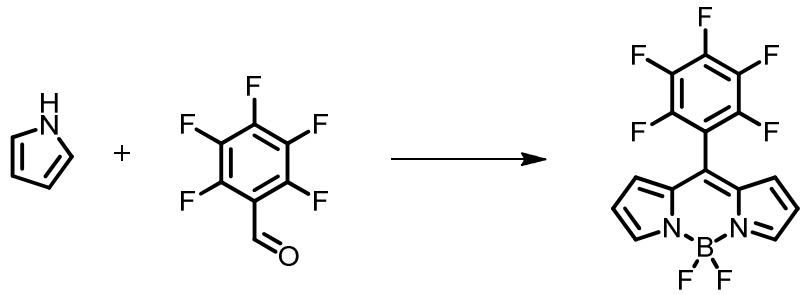

29

Pyrrole (30 mL) was distilled into a 100 mL flask containing 2,3,4,5,6-pentafluorobenzaldehyde (0.6 mL g, 5.1 mmol) and TFA (1 drop). The reaction mixture was then stirred overnight at room temperature. Excess pyrrole was removed via distillation and the residue purified via column chromatography (silica, DCM).

DCM (50 mL), DDQ (1.3 g, 5.6 mmol) was added to the isolated intermediate and the reaction mixture stirred overnight at RT. After this time N,N-diisopropylethylamine (5.0 mL, 30.6 mmol) and $BF_3.Et_2O$ (5.0 mL, 40.8 mmol) were added and the reaction mixture stirred at room temperature until complete. The crude product was extracted using water (3 x 100 mL) and brine (200 mL). The aqueous layer was backwashed with DCM (100 mL) and the organic portions were combined and dried over $MgSO_4$ and the solvent removed under reduced pressure. The product was purified via column chromatography (silica, DCM). The like fractions were combined and the solvent removed under vacuum to give a solid purple/red product, **29** (201 mg, 0.6 mmol, 11%).

^{1}H NMR (500 MHz, $CDCl_3$) δ 7.97 (s, 2H), 6.81 (d, *J* = 4.3 Hz, 2H), 6.69 – 6.47 (m, 2H).

$^{13}C\{^{1}H\}$ NMR (125 MHz, $CDCl_3$) δ 146.75, 145.57, 143.56, 141.51, 138.91, 138.90, 134.97, 134.97, 130.54, 129.46, 119.93, 108.11.

^{19}F NMR (500 MHz, $CDCl_3$) δ -136.33 – -136.83 (m), -144.80 (dd, *J* = 56.4, 28.0 Hz), -149.06 (t, *J* = 28.0 Hz), -158.73 – -159.50 (m).

$^{11}B\{^{1}H\}$ NMR (160 MHz, $CDCl_3$) δ -0.76 (t, *J* = 28.1 Hz).

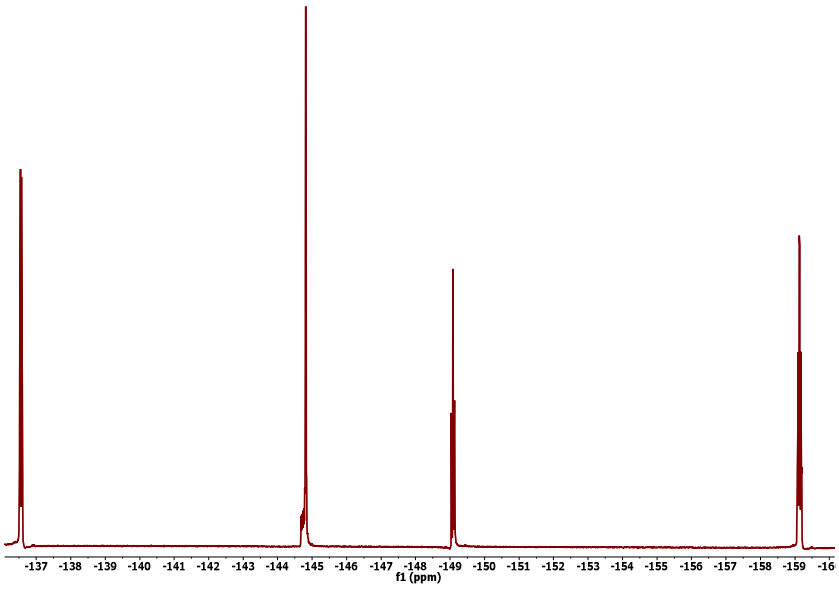

$^{19}F\{^{11}B\}$ NMR spectrum

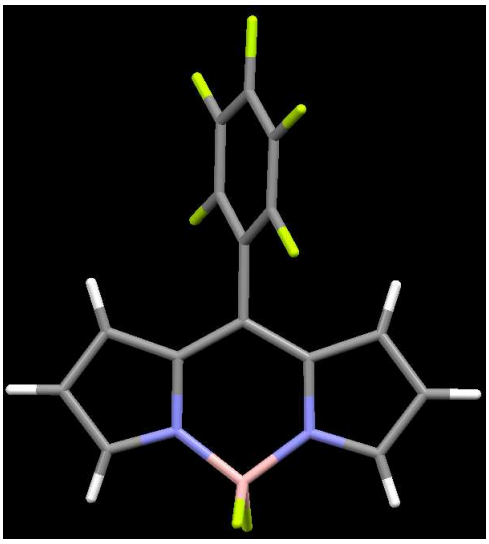

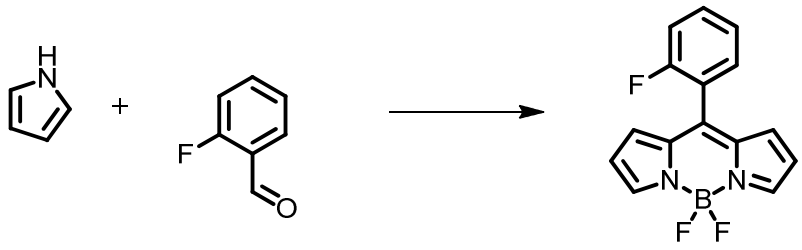

30

Pyrrole (30 mL) distilled into a 100 mL flask containing 2-fluorobenzaldehyde (0.85 g, 8.1 mmol) and TFA (1 drop). The reaction mixture was then stirred overnight at room temperature. Excess pyrrole which remained was removed via distillation.

DCM (50 mL), DDQ (2.0 g, 8.9 mmol) was added to the isolated intermediate and the reaction mixture stirred overnight at RT. After this time N,N-diisopropylethylamine (11.3 mL, 64.8 mmol) and $BF_3.Et_2O$ (11.3 mL, 48.6 mmol) were added and the reaction mixture stirred at room temperature until complete. The crude product was extracted using water (3 x 100 mL) and brine (200 mL). The aqueous layer was backwashed with DCM (100 mL) and the organic portions were combined and dried over $MgSO_4$ and the solvent removed under reduced pressure. The product was purified via column chromatography (silica, DCM). The like fractions were combined and the solvent removed under vacuum to give a solid purple/red product, **30** (230 mg, 0.8 mmol, 10%).

^{1}H NMR (500 MHz, $CDCl_3$) δ 7.93 (s, 1H), 7.60 – 7.50 (m, 1H), 7.45 (td, *J* = 7.3, 1.8 Hz, 1H), 7.33 – 7.28 (m, 1H), 7.25 (td, *J* = 8.8, 8.2, 1.0 Hz, 1H), 6.85 (d, *J* = 4.2 Hz, 1H), 6.56 – 6.49 (m, 1H).

^{19}F NMR (500 MHz, $CDCl_3$) δ -111.22 (q, *J* = 7.4 Hz), -143.48 – -144.96 (m), -145.20 – -146.44 (m).

^{11}B{^{1}H} NMR (160 MHz, $CDCl_3$) δ -0.68 (t, *J* = 28.7 Hz).

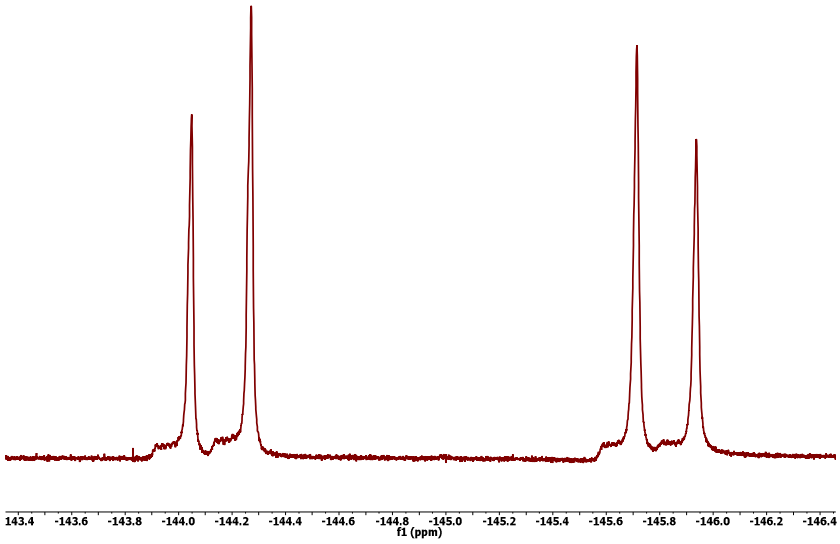

$^{19}F\{^{11}B\}$ NMR spectrum

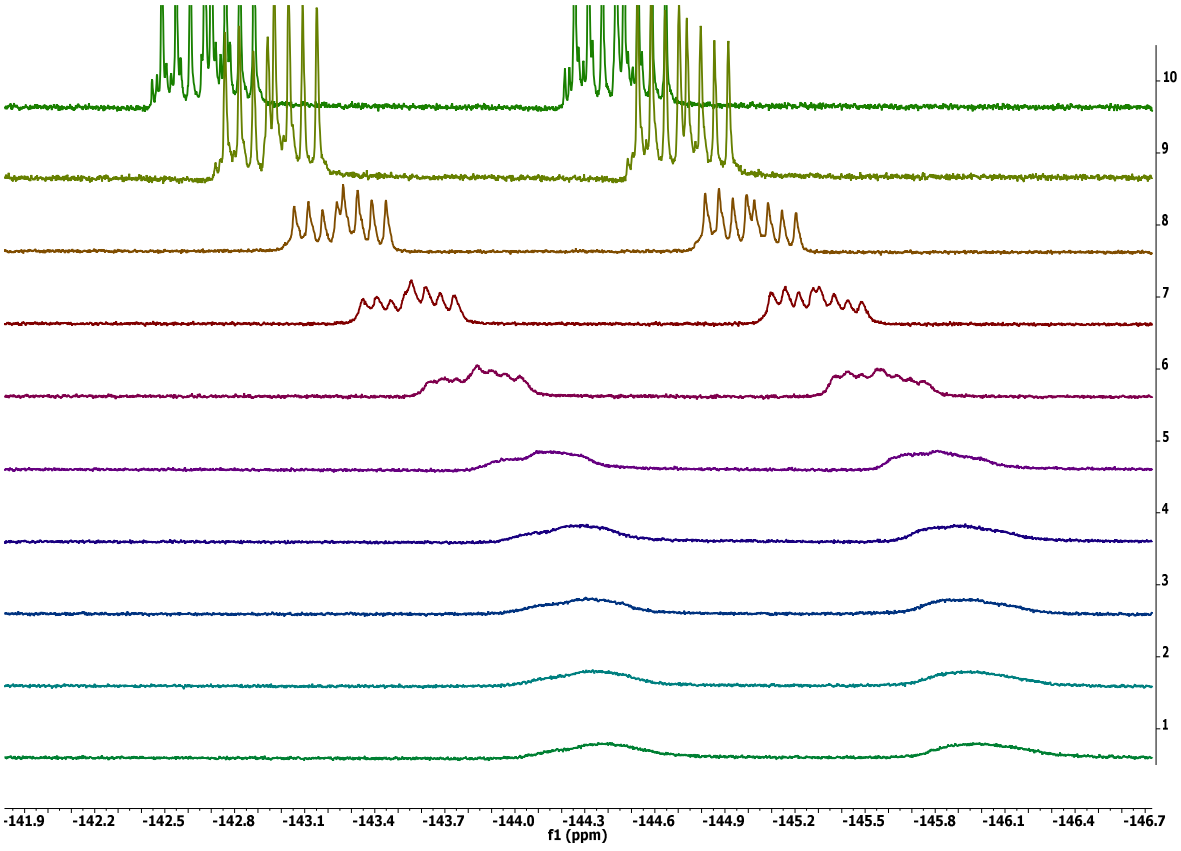

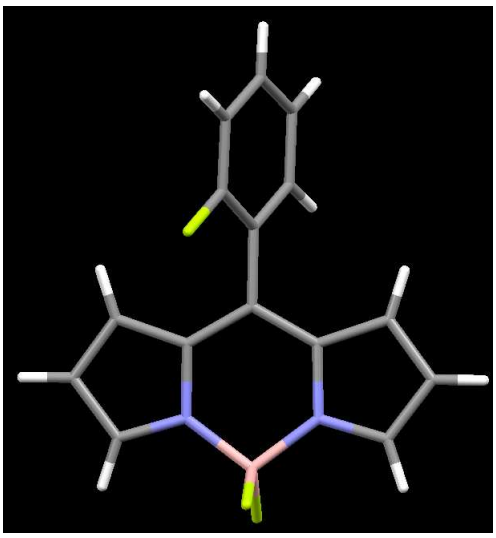

5.4.3. Chapter 4

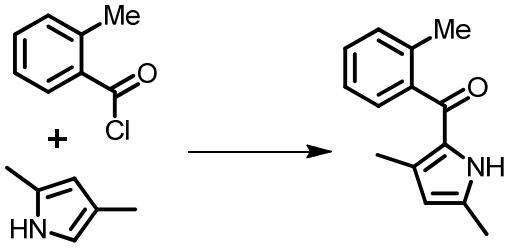

31a

2,4-dimethylpyrrole (2.2 mL, 21.0 mmol) and diethylether (40 mL) was added to a 100 mL round bottomed flask. The reaction vessel was sealed and purged with nitrogen. Ethyl Magnesium Bromide (3.1 mL, 23.0 mmol) was added dropwise to the reaction mixture so as to cause a slight reflux. The reaction mixture was then refluxed for 1 hour, after which time it was allowed to cool to room temperature.

The reaction mixture was transferred to a second RBF containing ether (10 mL) and o-toluoylchloride (3.6 mL, 27.0 mmol) via cannula. The reaction mixture was then stirred at room temperature for 24 hours after which time the crude mixture was extracted using water (3 x 100 mL). The aqueous layer was backwashed with ether (100 mL) and the organic portions were combined and dried over $MgSO_4$ and the solvent removed under reduced pressure. The crude product was purified via column chromatography (silica, DCM: Petrol [1:1] gradient to DCM 100%). The like fractions were combined and the solvent removed under vacuum to give a slightly pink solid, **31a** (2.7g, 12.6 mmol, 60%).

^{1}H NMR ($CDCl_3$, 400 MHz): δ = 9.43 (br s, 1H), 7.40 – 7.30 (m, 1H), 7.30 – 7.24 (m, 3H), 5.86 (d, *J* = 2.7 Hz, 1H), 2.33 (s, 3H), 2.32 (s, 3H), 1.68 (s, 3H)

^{13}C{^{1}H} NMR ($CDCl_3$, 75 MHz): δ = 186.67, 140.63, 136.42, 134.80, 131.79, 130.66, 129.33, 128.46, 126.65, 125.84, 113.10, 19.13, 13.28, 12.96.

MP – 121^{o}C

IR – ~3000 br (N-H), 2968 (C-H Ar), 2816 (C-H), 1674 cm^{-1} (C=O)

r.f. – 0.3 DCM:Pet (1:1)

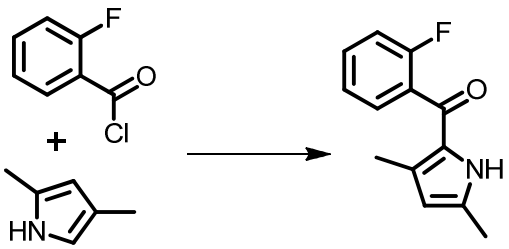

31b

2,4-dimethylpyrrole (3.5 mL, 34.0 mmol) and diethylether (40 mL) was added to a 100 mL round bottomed flask. The reaction vessel was sealed and purged with nitrogen. 3.0 M Ethyl Magnesium Bromide (12.5 mL, 23.0 mmol) was added dropwise to the reaction mixture so as to cause a slight reflux. The reaction mixture was then refluxed for 1 hour, after which time it was allowed to cool to room temperature.

The reaction mixture was transferred to a second RBF containing ether (30 mL) and o-fluorobenzoylchloride (5.4 mL, 44.2 mmol) via cannula. The reaction mixture was then stirred at room temperature for 24 hours after which time the crude mixture was extracted using water (3 x 100 mL). The aqueous layer was backwashed with ether (100 mL) and the organic portions were combined and dried over $MgSO_4$ and the solvent removed under reduced pressure. The crude product was purified trituration using the minimum amount of DCM and adding excess petrol. The solid material was filtered to give a slightly pink solid **31b** (4.9 g, 22.6 mmol, 66%).

^{1}H NMR ($CDCl_3$, 300 MHz): δ = 9.66 (s, 1H), 7.52 – 7.33 (m, 2H), 7.29 – 7.16 (m, 1H), 7.12 (ddd, *J* = 9.3, 8.2, 1.1 Hz, 1H), 5.84 (d, *J* = 2.8 Hz, 1H), 2.28 (s, 3H), 1.80 (d, *J* = 2.8 Hz, 3H).

^{13}C{^{1}H} NMR ($CDCl_3$, 100 MHz) δ = 180.46, 159.17 (d, *J* = 248.9 Hz), 137.04, 132.19, 131.71 (d, *J* = 8.1 Hz), 129.30 (d, *J* = 3.2 Hz), 128.93 (d, *J* = 16.9 Hz), 128.42, 124.43 (d, *J* = 3.2 Hz), 116.15 (d, *J* = 21.4 Hz), 113.42, 13.27, 12.94.

^{19}F NMR (400 MHz, $CDCl_3$) δ = -116.08.

MP – 141^{o}C

IR – 3265 br (N-H), 2919 (C-H Ar), 2850 (C-H), 1578 (C=O), 1288 cm^{-1} (C-F)

MS = calc. for $C_{13}H_{12}FNO$ = 217, found. 218 $(M+H)^{+}$

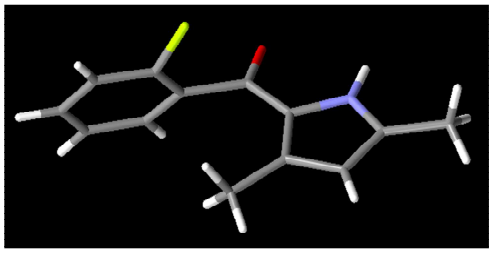

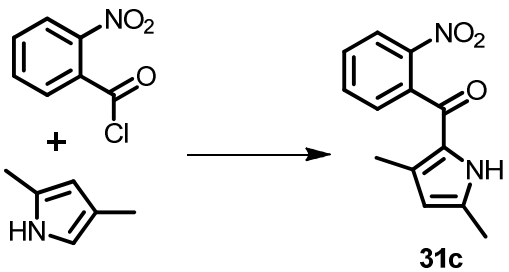

31c

2,4-dimethylpyrrole (2.2 mL, 21.0 mmol) and diethylether (40 mL) was added to a 100 mL round bottomed flask. The reaction vessel was sealed and purged with nitrogen. Ethyl Magnesium Bromide 3.0M (7.7 mL, 23.0 mmol) was added dropwise to the reaction mixture so as to cause a slight reflux. The reaction mixture was then refluxed for 1 hour, after which time it was allowed to cool to room temperature.

The reaction mixture was transferred to a second RBF containing ether (10 mL) and o-nitrobenzoylchloride (3.6 mL, 27.0 mmol) via cannula. The reaction mixture was then stirred at room temperature for 24 hours after which time the crude mixture was extracted using water (3 x 100 mL). The aqueous layer was backwashed with ether (100 mL) and the organic portions were combined and dried over $MgSO_4$ and the solvent removed under reduced pressure. The crude product was purified via column chromatography (silica, DCM: Petrol [1:1] gradient to DCM 100%). The like fractions were combined and the solvent removed under vacuum to give a light yellow solid **31c** (0.8g, 3.3 mmol, 16%).

^{1}H NMR ($CDCl_3$, 400 MHz): δ = 10.50 (br s, 1H), 8.14 (dd, *J* = 8.3, 1.2 Hz, 1H), 7.71 (td, *J* = 7.9, 1.2 Hz, 1H), 7.58 (td, *J* = 7.9, 1.2 Hz, 1H), 7.45 (dd, *J* = 7.5, 1.4 Hz, 1H), 5.80 (d, *J* = 2.6 Hz, 1H), 2.22 (s, 3H), 1.56 (s, 3H).

^{13}C {^{1}H} NMR (100 MHz, $CDCl_3$) δ = 180.98, 146.43, 138.04, 136.97, 134.27, 132.03, 130.19, 128.87, 127.21, 124.75, 113.62, 13.26, 13.01.

MP – 123 ^{o}C

IR – 3257 br (N-H), 2972 (C-H Ar), 1577 (C=O), 1524 (N-O), 1354 cm^{-1} (N-O)

r.f. – 0.5 EtOAc: DCM (1:2)

MS – calc. for $C_{13}H_{12}N_2O_3$ = 244, found. 245 $(M+H)^+$

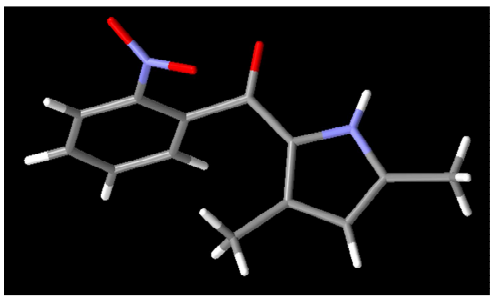

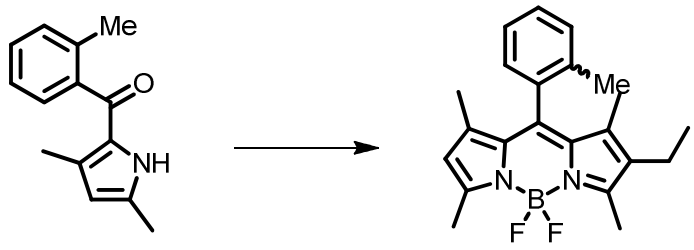

32a

31a (1.4 g, 6.3 mmol) was dissolved in DCM (150 mL) was charged to a 500 mL RBF with stirrer bar and N_2 bleed; this was then degassed for one hour. To this 2,4-dimethyl-3-ethylpyrrole (1.0 mL, 7.6 mmol), TFA (2 drops/ a catalytic amount) were all added to the solvent and the reaction mixture stirred at room temperature until complete. After this time N,N-diisopropylethylamine (6.2 mL, 38.0 mmol) and $BF_3.Et_2O$ (6.2 mL, 50.4 mmol) were added and the reaction mixture stirred until complete. The crude product was extracted using water (3 x 100 mL) and brine (200 mL). The aqueous layer was backwashed with DCM (100 mL) and the organic portions were combined and dried over $MgSO_4$ and the solvent removed under reduced pressure. The crude product was purified via column chromatography (silica, toluene: petrol [1:1]). The like fractions were combined and the solvent removed under vacuum to give a red solid **32a** (0.59 g, 1.6 mmol, 26%).

^{1}H NMR ($CDCl_3$, 400 MHz): δ = 7.38 – 7.32 (m, 1H), 7.31 – 7.26 (m, 2H), 7.14 (dd, *J* = 7.8, 1.4 Hz, 1H), 5.92 (s, 1H), 2.55 (s, 3H), 2.54 (s, 3H), 2.30 (q, *J* = 7.6 Hz, 2H), 2.18 (s, 3H), 1.32 (s, 3H), 1.28 (s, 3H), 0.98 (t, *J* = 7.6 Hz, 3H)

^{13}C{^{1}H} NMR ($CDCl_3$, 100 MHz): δ = 155.42, 153.83, 141.58, 140.64, 139.05, 135.60, 134.94, 133.42, 130.65, 130.51, 129.16, 128.12, 126.85, 120.47, 53.54, 19.36, 17.17, 14.69, 13.73, 12.74, 11.09, 9.48.

^{11}B{^{1}H} NMR ($CDCl_3$, 125 MHz): δ = -0.13 (t, *J* = 33.1 Hz)

^{19}F NMR ($CDCl_3$, 400 MHz): δ = -145.42 – -146.50 (m, 2F)

MS = calc. for $C_{22}H_{25}BF_2N_2$ = 366, found. 367 $(M+H)^+$

MP = 141 ^oC

IR – 2961 (C-H Ar), 2855 (C-H), 1540 (C=C), 1514 (C=N), 1193 cm^{-1} (B-F)

r.f. – 0.4 DCM : petrol (1:1)

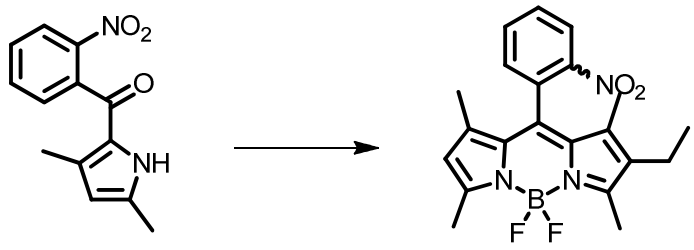

32c

31c (0.8 g, 3.3 mmol) was dissolved in DCM (250 mL) was charged to a 500 mL RBF with stirrer bar and N_2 bleed; this was then degassed for one hour. To this 2,4-dimethyl-3-ethylpyrrole (0.6 g, 3.6 mmol), TFA (2 drops/ a catalytic amount) were all added to the solvent and the reaction mixture stirred at room temperature until complete. After this time N,N-diisopropylethylamine (3.2 mL, 25.9 mmol) and $BF_3.Et_2O$ (3.2 mL, 19.4 mmol) were added and the reaction mixture stirred until complete. The crude product was extracted using water (3 x 100 mL) and brine (200 mL). The aqueous layer was backwashed with DCM (100 mL) and the organic portions were combined and dried over $MgSO_4$ and the solvent removed under reduced pressure. The crude product was purified via column chromatography (silica, DCM: petrol [3:1]). The like fractions were combined and the solvent removed under vacuum to give a red solid **32c** (0.2 g, 0.6 mmol, 18%).

^{1}H NMR ($CDCl_3$, 400 MHz): δ = 8.14 (dd, *J* = 8.2, 1.3 Hz, 1H), 7.76 (td, *J* = 7.6, 1.3 Hz, 1H), 7.67 (td, *J* = 8.2, 1.5 Hz, 1H), 7.42 (dd, *J* = 7.6, 1.5 Hz, 1H), 5.92 (s, 1H), 2.53 (s, 3H), 2.51 (s, 3H), 2.28 (q, *J* = 7.5 Hz, 2H), 1.30 (s, 3H), 1.26 (s, 3H), 0.96 (t, *J* = 7.5 Hz, 3H).

^{13}C{^{1}H} NMR ($CDCl_3$, 100 MHz): δ = 207.17, 156.40, 154.45, 148.54, 140.60, 138.11, 135.57, 134.22, 134.05, 131.28, 130.73, 130.61, 130.23, 125.01, 120.98, 56.54, 31.00, 17.16, 14.59 (t, *J* = 2.2 Hz), 13.80, 12.83 (t, *J* = 2.7 Hz), 11.25.‡‡

^{11}B{^{1}H} NMR ($CDCl_3$, 125 MHz): δ = -0.22 (t, *J* = 32.1 Hz)

^{19}F NMR ($CDCl_3$, 75 MHz): δ = -145.84 (m, 2F)

MS = calc. for $C_{21}H_{22}BF_2N_3O_2$ = 398, found. 398 $(M)^+$

MP = 147^{o}C

‡‡ Splitting of ^{13}C signals has been observed for this compound, resulting in additional peaks being seen.

IR – 2979 (C-H Ar), 2887 (C-H), 1546 (C=C), 1520 (C=N), 1311 (N-O), 1194 cm^{-1} (B-F)

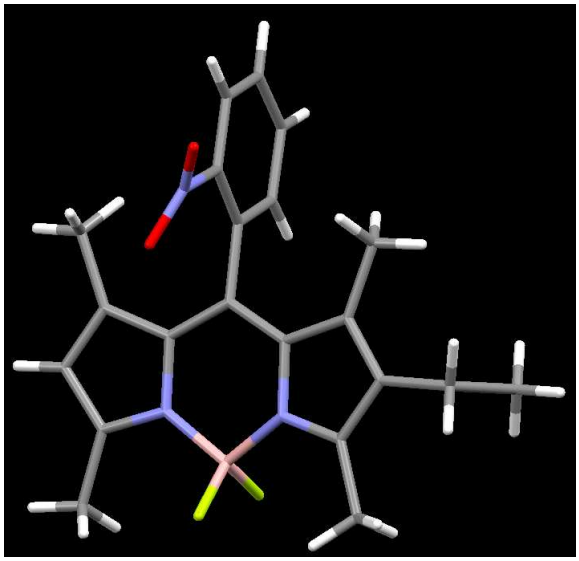

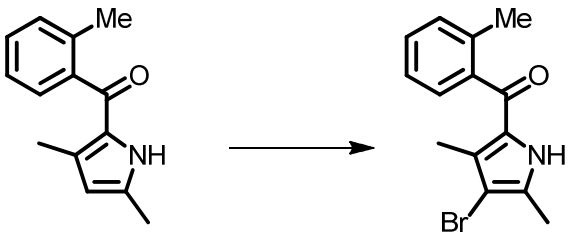

31a **33a**

31a (0.7 g, 3.3 mmol) was dissolved in DCM (100 mL) containing bromine (0.6 g, 3.7 mmol). The reaction mixture was then stirred at room temperature for 24 hours during which time the progress was monitored by TLC. Once the starting material has been used up the reaction mixture was extracted using water (3 x 100 mL). The aqueous layer was backwashed with DCM (100 mL) and the organic portions were combined and dried over $MgSO_4$ and the solvent removed under reduced pressure. The crude product was analysed via NMR and was found to be pure hence no further purification was performed. The product was a purple/brown solid **33a** (1.0 g, 3.3 mmol, 100%).

^{1}H NMR ($CDCl_3$, 300 MHz): δ = 10.99 (br s, 1H), 7.36 (ddd, *J* = 8.0, 5.6, 3.0 Hz, 1H), 7.30 – 7.20 (m, 3H), 2.34 (s, 3H), 2.32 (s, 3H), 1.62 (s, 3H).

^{13}C{^{1}H} NMR ($CDCl_3$, 100 MHz) δ = 186.79, 140.04, 135.91, 135.00, 130.84, 130.22, 129.83, 127.61, 126.97, 125.99, 102.67, 19.27, 12.49, 12.27.

MP – 114^{o}C – 116^{o}C

IR – 3245 (N-H), 2921 (C-H Ar), 2877 (C-H), 1592 cm^{-1} (C=O)

MS –calc. for $C_{13}H_{11}FNOBr$ = 292, found. 292 $(M)^{+}$

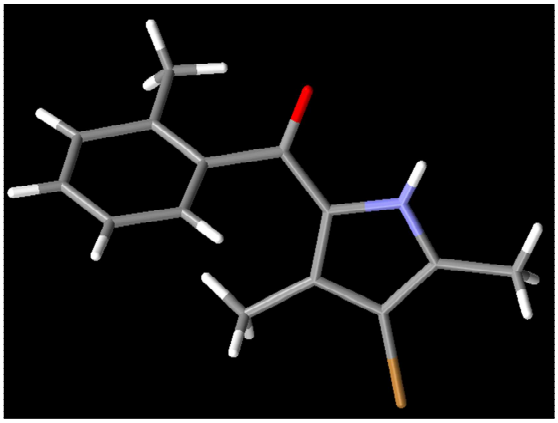

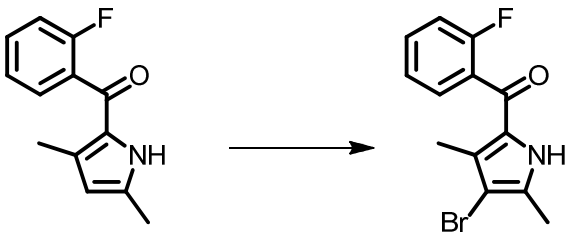

31b **33b**

31b (0.1 g, 4.6 mmol) was dissolved in DCM (100 mL) containing bromine (0.3 mL, 5.1 mmol). The reaction mixture was then stirred at room temperature for 24 hours during which time the progress was monitored by TLC. Once the starting material has been used up the reaction mixture was extracted using water (3 x 100 mL). The aqueous layer was backwashed with DCM (100 mL) and the organic portions were combined and dried over $MgSO_4$ and the solvent removed under reduced pressure. The crude product was analysed via NMR and was found to be pure hence no further purification was performed. The product was a brown crystalline solid **33b** (1.3 g, 4.3 mmol, 95%).

^{1}H NMR (400 MHz, $CDCl_3$) δ = 9.46 (s, 1H), 7.47 (dddd, *J* = 8.3, 7.5, 5.5, 1.8 Hz, 1H), 7.41 (ddd, *J* = 7.5, 5.5, 1.8 Hz, 1H), 7.22 (dt, *J* = 7.5, 1.0 Hz, 1H), 7.14 (ddd, *J* = 9.6, 8.3, 1.0 Hz, 1H), 2.31 (s, 3H), 1.81 (s, 3H).

^{13}C{^{1}H} NMR ($CDCl_3$, 100 MHz) δ = 180.61, 159.28 (d, *J* = 250.1 Hz), 134.85, 132.28 (d, *J* = 8.2 Hz), 129.82, 129.41 (d, *J* = 3.4 Hz), 128.22 (d, *J* = 16.2 Hz), 127.43, 124.56 (d, *J* = 3.4 Hz), 116.28 (d, *J* = 21.4 Hz), 102.82, 12.56, 12.12 (d, *J* = 1.3 Hz).

^{19}F NMR (400 MHz, $CDCl_3$) = δ -115.60 (dt, *J* = 9.6, 5.5 Hz).

MP – 156^{o}C

IR –3253 br (N-H), (C-H Ar) and (C-H) not visible probably due to (N-H) broadness 1595 (C=O) cm^{-1}

MS = calc. for $C_{13}H_{11}FNOBr$ = 295, found. 296 $(M+H)^{+}$

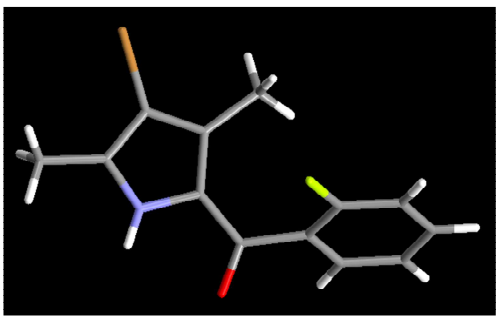

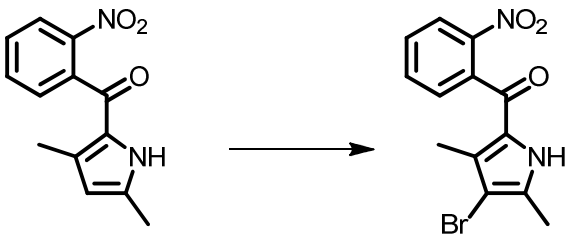

31c **33c**

31c (0.8 g, 3.5 mmol) was dissolved in DCM (100 mL) containing bromine (0.2 mL, 3.9 mmol). The reaction mixture was then stirred at room temperature for 24 hours during which time the progress was monitored by TLC. Once the starting material has been used up the reaction mixture was extracted using water (3 x 100 mL). The aqueous layer was backwashed with DCM (100 mL) and the organic portions were combined and dried over $MgSO_4$ and the solvent removed under reduced pressure. The crude product was analysed via NMR and was found to be pure hence no further purification was performed. The product was a brown crystalline solid **33c** (0.4 g, 1.2 mmol, 36%).

^{1}H NMR (400 MHz, $CDCl_3$) δ = 10.23 & 9.89 (br s, N-H though two forms appear, 1H) 8.21 (dd, *J* = 8.2, 1.1 Hz, 1H), 7.78 – 7.72 (m, 1H), 7.68 – 7.61 (m, 1H), 7.47 – 7.43 (m, 1H), 2.28 (s, 3H), 1.57 (s, 3H).

^{13}C{^{1}H} NMR ($CDCl_3$, 100 MHz) δ = 181.18, 146.46, 136.50, 136.00 (br), 134.37, 130.55, 129.51 (br), 128.73, 126.31, 124.88, 102.88, 12.53, 12.13.

MP – 172-173^{o}C

IR – 3262 br (N-H), (C-H Ar) and (C-H) not visible probably due to (N-H) broadness 1597 (C=O), 1523 (N-O), 1348 (N-O) cm^{-1}

MS - calc. for $C_{13}H_{11}N_2O_3Br$ = 323, found. 323 $(M)^{+}$

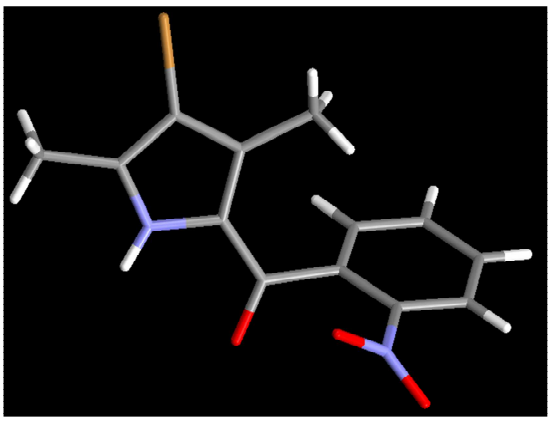

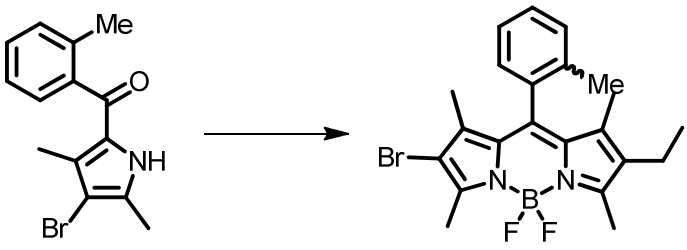

33a **34a**

33a (1.0 g, 3.5 mmol) was dissolved in DCM (150 mL) was charged to a 500 mL RBF with stirrer bar and N_2 bleed; this was then degassed for one hour. To this 2,4-dimethyl-3-ethylpyrrole (0.6 g, 3.6 mmol), TFA (2 drops/ a catalytic amount) were all added to the solvent and the reaction mixture stirred at room temperature until complete. After this time N,N-diisopropylethylamine (3.5 mL, 28.0 mmol) and $BF_3.Et_2O$ (3.5 mL, 21.0 mmol) were added and the reaction mixture stirred until complete. The crude product was extracted using water (3 x 100 mL) and brine (200 mL). The aqueous layer was backwashed with DCM (100 mL) and the organic portions were combined and dried over $MgSO_4$ and the solvent removed under reduced pressure. The crude product was purified via column chromatography (silica, DCM: petrol [1:2]). The like fractions were combined and the solvent removed under vacuum to give a red/ green solid, **34a** (0.7 g, 1.6 mmol, 47%).

^{1}H NMR ($CDCl_3$, 500 MHz): δ = 7.40 – 7.36 (m, 1H), 7.33 – 7.28 (m, 2H), 7.14 – 7.11 (m, 1H), 2.57 (s, 3H), 2.56 (s, 3H), 2.31 (q, *J* = 7.6 Hz, 2H), 2.17 (s, 3H), 1.32 (s, 3H), 1.28 (s, 3H), 0.99 (t, *J* = 7.6 Hz, 3H).

^{13}C{^{1}H} NMR ($CDCl_3$, 125 MHz): δ = 189.76, 158.21, 149.81, 140.62, 137.21, 135.59, 134.59, 134.48, 131.57, 130.78, 129.44, 128.89, 128.04, 126.99, 100.00, 19.36, 17.16, 14.52, 13.45 (t, *J* = 2.5 Hz), 12.97 (t, *J* = 2.5 Hz), 12.68, 11.28.

^{11}B{^{1}H} NMR ($CDCl_3$, 160 MHz): δ = -0.29 (t, *J* = 31.8 Hz)

^{19}F (500 MHz, $CDCl_3$): δ -145.80 (dq, J_{FF} = 110 Hz, J_{BF} = 32.6 Hz, BF), -145.96 (dq, J_{FF} = 110 Hz, J_{BF} = 32.6 Hz, BF)

MS = calc. for $C_{22}H_{24}BF_2N_2Br$ = 444, found. 444 $(M)^+$

MP = 167 ^oC

IR – 2926 (C-H Ar), 2869 (C-H), 1543 (C=C), 1193 cm^{-1} (B-F)

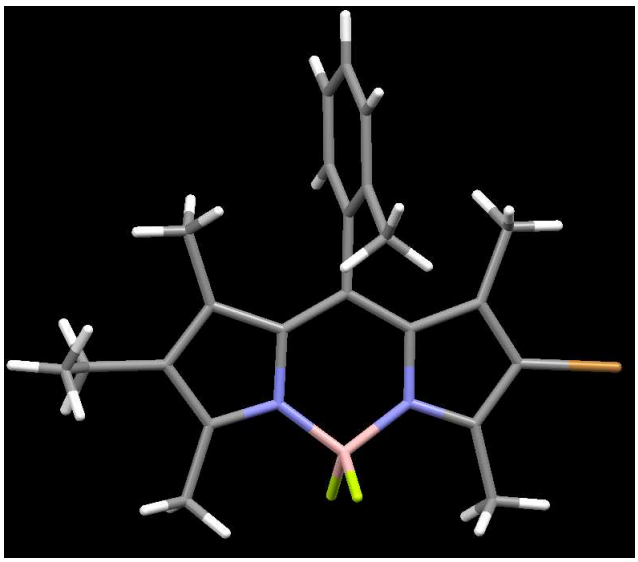

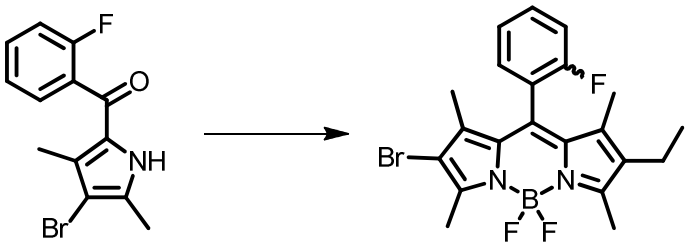

33b **34b**

33b (1.3 g, 4.4 mmol, 1 eq.) was dissolved in DCM (150 mL) was charged to a 500 mL RBF with stirrer bar and N_2 bleed; this was then degassed for one hour. To this 2,4-dimethyl-3-ethylpyrrole (0.6 g, 4.8 mmol, 1.1 eq), TFA (2 drops/ a catalytic amount) were all added to the solvent and the reaction mixture stirred at room temperature until complete. After this time N,N-diisopropylethylamine (4.0 mL, 24.3 mmol, 6 eq.) and $BF_3.Et_2O$ (4.0mL, 32.4 mmol, 8 eq.) were added and the reaction mixture stirred until complete. The crude product was extracted using water (3 x 100 mL) and brine (200 mL). The aqueous layer was backwashed with DCM (100 mL) and the organic portions were combined and dried over $MgSO_4$ and the solvent removed under reduced pressure. The crude product was purified via column chromatography (silica, DCM: petrol [1:1]). The like fractions were combined and the solvent removed under vacuum to give a red solid **34b** (0.7 g, 2.4 mmol, 54%).

^{1}H NMR ($CDCl_3$, 500 MHz): δ 7.53 – 7.46 (m, 1H), 7.32 – 7.26 (m, 1H), 7.26 – 7.17 (m, 2H), 2.57 (s, 3H), 2.56 (s, 3H), 2.31 (q, *J* = 7.6 Hz, 2H), 1.41 (s, 3H), 1.38 (s, 3H), 0.99 (t, *J* = 7.6 Hz, 3H)

^{13}C{^{1}H} NMR ($CDCl_3$, 100 MHz): δ = 160.50, 158.99, 158.04, 150.30, 140.46, 137.09, 134.92, 133.78, 132.12, 131.65, 131.57, 130.51, 130.49, 129.25, 125.22, 122.88, 122.71, 116.61, 116.40, 110.13, 110.09, 17.17, 14.49, 13.49, 13.04, 12.81, 11.37. 6 extra peaks observed due to F-C splitting. These peaks are included in the list of all carbons above. δ 159.27 (d, *J* = 247.2 Hz), 134.98 – 134.85 (m), 134.96 – 134.84 (m), 131.61 (d, *J* = 7.8 Hz), 122.79 (d, *J* = 16.7 Hz), 116.51 (d, *J* = 21.1 Hz), 110.30 – 109.77 (m).

^{11}B{^{1}H} NMR ($CDCl_3$, 160 MHz): δ = -0.33 (t, *J* = 34.2 Hz)

^{19}F NMR ($CDCl_3$, 400 MHz): δ = -114.15 – -114.25 (m, 1F), -145.10 – -146.51 (m, 2F)

MS = calc. for $C_{21}H_{21}BF_3N_2Br$ = 449, found. 449 $(M)^+$

MP = 154 ^{o}C

IR – 2975 (C-H Ar), 2873(C-H), 1547 (C=C), 1197 cm^{-1}(B-F)

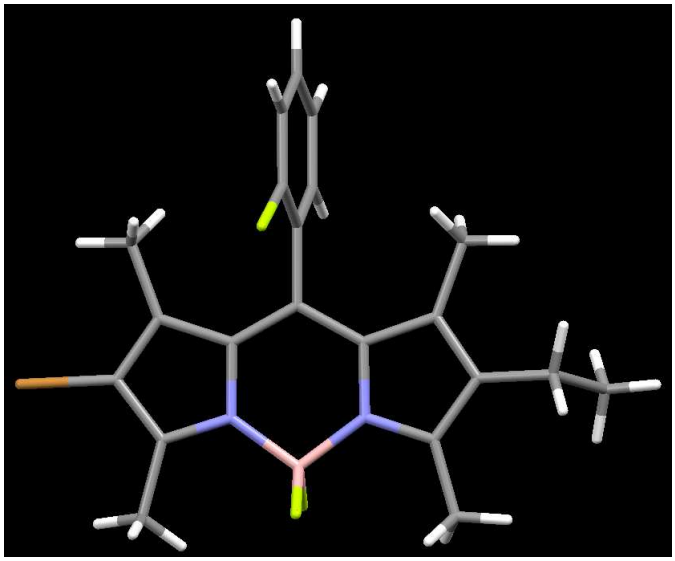

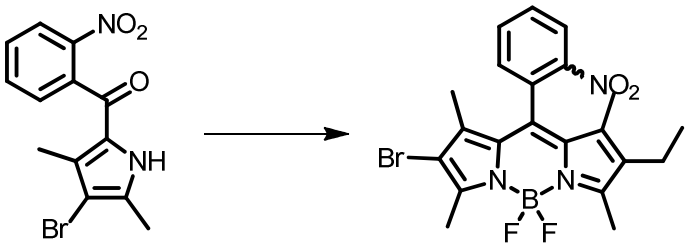

33c **34c**

(4-bromo-3,5-dimethyl-1H-pyrrol-2-yl)(o-nitrophenyl)methanone (0.42 g, 1.4 mmol) was dissolved in DCM (150 mL) was charged to a 250 mL RBF with stirrer bar and N_2 bleed; this was then degassed for one hour. To this 2,4-dimethyl-3-ethylpyrrole (0.25 mL, 1.8 mmol), TFA (2 drops/ a catalytic amount) were all added to the solvent and the reaction mixture stirred at room temperature until complete. After this time N,N-diisopropylethylamine (1.37 mL, 8.3 mmol) and $BF_3.Et_2O$ (1.37 mL, 11.1 mmol) were added and the reaction mixture stirred until complete. The crude product was extracted using water (3 x 100 mL) and brine (200 mL). The aqueous layer was backwashed with DCM (100 mL) and the organic portions were combined and dried over $MgSO_4$ and the solvent removed under reduced pressure. The crude product was purified via column chromatography (silica, DCM: petrol [1:1] to DCM 100%). The like fractions were combined and the solvent removed under vacuum to give a red/ purple solid, **34c** (0.07 g, 0.18 mmol, 13%).

^{1}H NMR ($CDCl_3$, 400 MHz): δ = 8.20 (dd, *J* = 8.3, 1.3 Hz, 1H), 7.79 (td, *J* = 7.5, 1.3 Hz, 1H), 7.71 (td, *J* = 7.8, 1.6 Hz, 1H), 7.44 (dd, *J* = 7.6, 1.5 Hz, 1H), 2.56 (s, 3H), 2.55 (s, 3H), 2.29 (q, *J* = 7.6 Hz, 2H), 1.31 (s, 3H), 1.27 (s, 3H), 0.98 (t, *J* = 7.6 Hz, 3H).

^{13}C{^{1}H} NMR ($CDCl_3$, 100 MHz): δ = 159.27, 150.47, 148.50, 139.49, 136.22, 135.58, 135.17, 134.31, 131.21, 130.82, 130.43, 128.62, 125.18, 17.19, 14.45, 13.52, 13.10, 12.89, 11.42.[§§]

^{11}B{^{1}H} NMR ($CDCl_3$, 160 MHz): δ = -0.36 (t, *J* = 32.1 Hz)

^{19}F NMR ($CDCl_3$, 400 MHz): δ = -145.77 (dq, *J* = 107.1, 32.2 Hz, 2F), -146.44 (dq, *J* = 107.1, 32.2 Hz, 2F)

[§§] Likely overlapping of ^{13}C peaks have obscured two peaks.

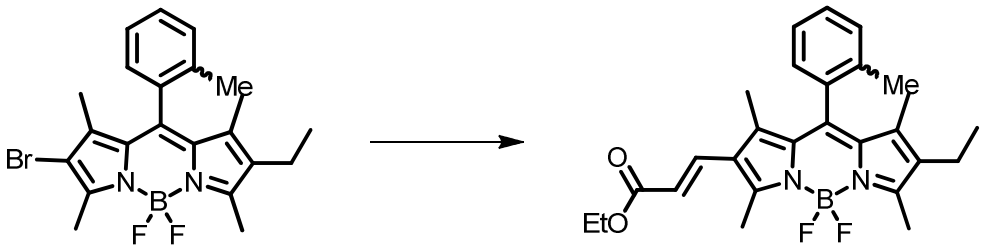

34a **35a**

34a (0.3 g, 0.6 mmol, 1 eq), palladium acetate (0.02 g, 0.08 mmol, 0.1 eq), triphenylphosphine (0.02 g, 0.08 mmol, 0.1 eq), and DMF (5 mL) were added to a clean dry schlenk flask with stirrer bar. The reaction vessel was then purged with nitrogen for 20 minutes after which point ethyl acrylate (0.2 mL, 1.5 mmol, 2.3 eq), triethylamine (0.4 mL, 2.8 mmol, 4.5 eq; in DMF – 6 mL) was added and the reaction stirred at 100^{o}C for 12 hours. After this time the reaction mixture was allowed to cool to room temperature and was separated using DCM (100 mL) and water (3 x 100 mL). The organic layer was then dried over $MgSO_4$ and the slurry filtered and the solvent removed. The crude material was then purified via column chromatography (DCM 100% gradient to DCM: EtOAc; 99:1) to give a red solid **35a** (0.06 g, 0.3 mmol, 46 %).

^{1}H NMR ($CDCl_3$, 400 MHz) δ = 7.60 (d, *J* = 16.2 Hz, 1H), 7.42 – 7.35 (m, 1H), 7.34 – 7.28 (m, 2H), 7.14 (dd, *J* = 7.8, 1.4 Hz, 1H), 6.01 (d, *J* = 16.2 Hz, 1H), 4.21 (q, *J* = 7.1 Hz, 2H), 2.68 (s, 3H), 2.57 (s, 3H), 2.32 (q, *J* = 7.5 Hz, 2H), 2.17 (s, 3H), 1.42 (s, 3H), 1.33 – 1.25 (m, 6H), 0.99 (t, *J* = 7.5 Hz, 3H).

^{13}C{^{1}H} NMR ($CDCl_3$, 100 MHz): δ = 167.79, 158.83, 141.14, 140.75, 138.91, 136.18, 135.65, 135.09, 135.07, 134.61, 132.25, 130.82, 129.70, 129.50, 128.13, 127.05, 124.30, 116.91, 60.36, 19.39, 17.20, 14.50, 14.45, 14.11, 13.05, 11.86, 11.37.

^{11}B{^{1}H} NMR ($CDCl_3$, 160 MHz): δ = -0.18 (t, *J* = 31.6 Hz)

^{19}F NMR ($CDCl_3$, 400MHz): δ = -144.53 (m, 2F)

MS = calc. for $C_{27}H_{31}BF_2N_2O_2$ = 464, found. 464 $(M)^{+}$

MP = 160^{o}C

Rf – 0.10 (DCM)

IR – 2969 (C-H Ar), 2890 (C-H), 1700 (C=N), 1528 (C=C), 1072 cm^{-1} (B-F)

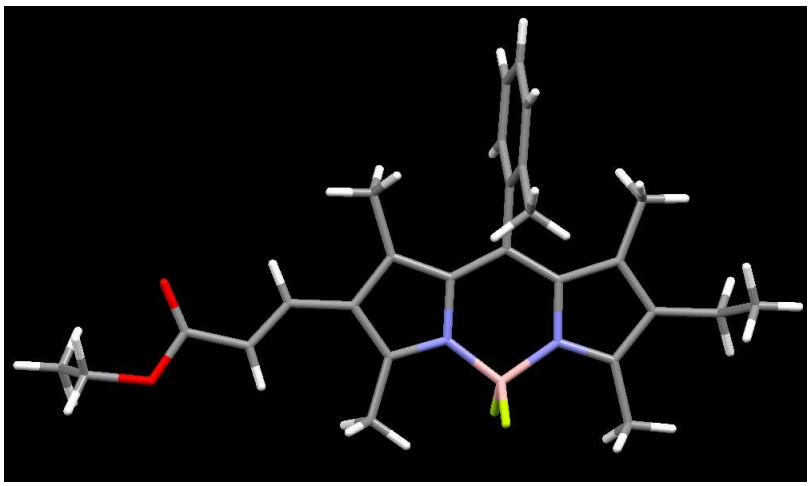

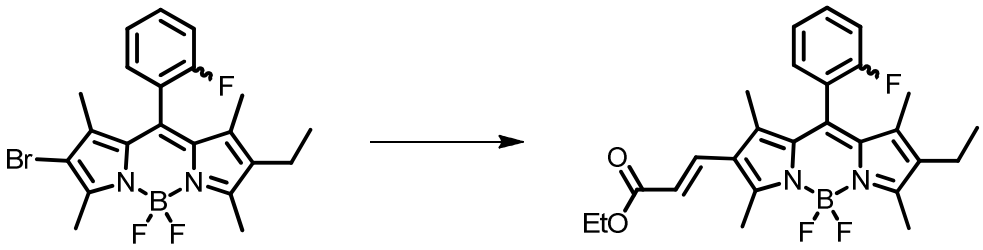

34b **35b**

34b (0.6 g, 1.4 mmol, 1 eq), palladium acetate (0.04 g, 0.2 mmol, 0.1 eq), triphenylphosphine (0.05 g, 0.2 mmol, 0.1 eq), and DMF (25 mL) were added to a clean dry schlenk flask with stirrer bar. The reaction vessel was then purged with nitrogen for 20 minutes after which point ethyl acrylate (0.3 mL, 3.6 mmol, 2.3 eq), triethylamine (0.9 mL, 12.0 mmol, 12.0 eq; in DMF – 10 mL) was added and the reaction stirred at 100^{o}C for 12 hours. After this time the reaction mixture was allowed to cool to room temperature and was separated using DCM (100 mL) and water (3 x 100 mL). The organic layer was then dried over $MgSO_4$ and the slurry filtered and the solvent removed. The crude material was then purified via column chromatography (DCM 100% gradient to DCM: EtOAc; 99:1) to give a red solid **35b** (0.3 g, 0.6 mmol, 45%).

^{1}H NMR ($CDCl_3$, 400 MHz) δ = 7.60 (d, *J* = 16.2 Hz, 1H), 7.50 (dddd, *J* = 8.3, 7.2, 5.2, 1.9 Hz, 1H), 7.30 (td, *J* = 7.2, 1.1 Hz, 1H), 7.24 (td, *J* = 7.2, 1.9 Hz, 1H), 7.21 (td, *J* = 8.3, 1.1 Hz, 1H), 6.01 (d, *J* = 16.2 Hz, 1H), 4.21 (q, *J* = 7.1 Hz, 2H), 2.68 (s, 3H), 2.57 (s, 3H), 2.32 (q, *J* = 7.5 Hz, 2H), 1.51 (s, 3H), 1.38 (s, 3H), 1.29 (t, *J* = 7.1 Hz, 3H), 0.99 (t, *J* = 7.5 Hz, 3H).

^{13}C{^{1}H} NMR ($CDCl_3$, 101 MHz): δ = 167.73, 160.52, 159.61, 158.07, 153.47, 140.57, 138.70, 136.04, 135.48, 134.28, 132.78, 131.72, 131.65, 130.55, 130.53, 130.05, 125.32, 125.29, 124.57, 122.90, 122.73, 117.24, 116.65, 116.44, 60.40, 17.20, 14.45, 14.14, 13.11, 12.00, 11.45.

^{11}B{^{1}H} NMR ($CDCl_3$, 75 MHz): δ = -0.22 (t, *J* = 31.7 Hz)

^{19}F NMR ($CDCl_3$, 75 MHz): δ = -114.16 (d, *J* = 5.2 Hz), -144.23 (dq, *J* = 109.0, 32.0 Hz), -144.83 (dq, *J* = 107.8, 32.0 Hz).

MS = calc. for $C_{26}H_{28}BF_3N_2O_2$ = 468, found. 469 $(M+H)^+$

MP = 177.4 ^{o}C

Rf – 0.06 (EtOAc : Petrol; 1:99)

IR – 2974 (C-H Ar), 2900 (C-H), 1700 (C=N), 1535 (C=C), 1180 cm^{-1} (B-F)